ORFV:
A NOVEL ONCOLYTIC AND IMMUNE STIMULATING PARAPOXVIRUS THERAPEUTIC

By
Julia Rintoul

A thesis submitted to the
Faculty of Graduate and Postdoctoral Studies
in partial fulfillment of the requirements for the degree of
Doctor of Philosophy, specialization in Biochemistry.

Department of Biochemistry, Microbiology, & Immunology
Faculty of Medicine
University of Ottawa

ABSTRACT

Replicating viruses for the treatment of cancer have a number of advantages over traditional therapeutic modalities. They are highly targeted, self-amplifying, and have the added potential to act as both gene-therapy delivery vehicles and oncolytic agents. ORFV, (*Parapoxvirus ovis*, or Orf virus) is the prototypic species of the *Parapoxvirus* genus, causing a benign disease in its natural ungulate host. ORFV possesses a number of unique properties that make it an ideal viral backbone for the development of a cancer therapeutic: it is safe in humans, has the ability to cause repeat infections even in the presence of antibody, and it induces a potent T_h-1 dominated immune response. Here I show for the first time that live replicating ORFV induces an anti-tumour immune response in multiple syngeneic mouse models of cancer that is mediated largely by the potent activation of both cytokine-secreting, and tumouricidal natural killer (NK) cells. I have also highlighted the clinical potential of the virus by demonstration of human cancer cell oncolysis including efficacy in an A549 xenograft model of cancer. The mechanism of ORFV-mediated activation of NK cells has been explored, where I have demonstrated activation via direct *ex vivo* infection of NK cells. I have also highlighted ORFV-mediated activation of dendritic cells (DCs), both *in vivo* and by direct infection *ex vivo*. An *in vivo* DC depletion study demonstrated an indirect mechanism for ORFV NK cell activation, where in the absence of DCs, NK cell activation was diminished, as was the ability of ORFV to clear lung metastases. The ORFV innate immune stimulatory profile has been harnessed for therapeutic application in an experimental surgery model of cancer, where ORFV therapy at the time of surgery reduces the number of cancer metastases. These data highlight the clinical potential of a live, immune stimulating Parapoxvirus therapeutic.

ACKNOWLEDGMENTS

To my supervisor and mentor Dr. John Bell I thank for his continued support, understanding, and infectious passion for science and the pursuit of 'BIG' ideas. To my fellow labmate, and dear friend Chantal – a sincere thank-you for the stimulating scientific discussions, and your refreshing optimism and interest in my project. I would like to thank Marianne, Kelley and Lee for numerous brainstorming coffee sessions, and invaluable insight. To my friends at McMaster University, in particular Brian, Byram, Wan, and Jeanette: your immunology expertise and advice was most valuable. Thank you for your time, patience and enthusiasm for all things ORFV. To Rebbeca and Harry, thank you for the clinical perspective; your excitement and enthusiasm was sincerely appreciated. I am very greatful for our veterinary technicians of the past and present: Lisa, Theresa, and Christiano. I could not have done it without you – thank you for supporting me through the mouse experiment roller coaster(s). To all members of the Bell lab; it has been a true priviledge to share the bench with such a fun, stimulating, successful, and creative group. I will forever cherish our memories both at the bench and beyond.

To my parents, thank you for believing in me. To my father, thank you for teaching me early on the value of education, discipline and drive. To my mother, thank you for encouraging me to following my dreams, and for being my number one cheerleader. To my best friend and partner James, I will never forget your unwavering commitment, patience, and understanding. Thank you once again for allowing me to pursue my dreams.

TABLE OF CONTENTS

LIST OF ABBREVIATIONS

ACT – Adoptive-cell transfer
ATCC – American type culture collection
BCG – Bacilli calmette-guerin
CEA – Carcinoembryonic antigen
CMC – Carboxymethyl cellulose
CPE – Cytopathic effect
CTL – cytotoxic T-lymphocyte
CTLA-4 – Cytotoxic T-lymphocyte antigen 4
DAI – DNA-dependent activator of IFN-regulatory factors
DC – Dendritic cell
DCT – Dopachrome tautomerase
DNA – Deoxyribonucleic acid
DT – Diptheria toxin
DTR – Diptheria toxin receptor
EGFR – Epidermal growth factor receptor
FCS – Fetal calf serum
FDA – Food and drug adminstration
GAG – Glycosaminoglycans
GFP – Green fluorescent protein
GM-CSF – Granulocyte-macrophage colony-stimulating factor
H-60 – minor histocompatibility antigen - 60
HSV – Herpes simplex virus
IDO – Indoleamine-2,3-dioxgenase
IFN – Interferon
ICAM-1 – Intercellular adhersion molecule 1
IL – Interleukin
IP - Intraperitoneal
IT – Intratumoural
ITIM – immunoreceptor tyrosine-based inhibition motif
IV – Intravenous
KIR – Killer cell immunoglobulin-like receptor
LAG3 – Lymphocyte-activation gene 3
MCMV – Murine cyomegalovirus
MDSC – Myeloid-derived suppressor cell
MFI – Mean fluorescence intensity
MHC – Major histocompatibility complex
MOI – Multiplicity of infection
MTD – Maximum tolerable dose
MYXV – Myxoma virus
NDV – Newcastle Disease Virus
NK – Natural killer
NKT – Natural killer T-cell
NX – Nephrectomy
NZ-2 – New Zealand 2

ORFV – Orf virus
OV – Oncolytic virus
PBS – Phosphate buffered saline
Pfu – Plaque forming unit
PKR – Protein kinase R
Poly IC – Polyinosinic:polycytidylic acid
PRR – Pattern recognition receptor
PSA – Prostate-specific antigen
Rae-1 – Retinoic acid early inducible-1
RCNV – Raccoonpoxvirus
RIG-I – Retonoic acid inducible gene I
RNA – Ribonucleic acid
ROS – Reactive oxygen species
SEM – Standard error of the mean
TAA – Tumour associated antigen
TDF – Tumour derived factor
TK – Thymidine kinase
TGF-β - Transforming growth factor-beta
T_h-1 – T helper
TIL – Tumour infiltrating lymphocyte
TLR – Toll like receptor
TNF – Tumour necrosis factor
TRAIL – TNF-related apoptosis-inducing ligand
Treg – Regulatory T-cell
UV – Ultraviolet
VACV – Vaccinia virus
VEGF – Vascular endothelial growth factor
VGF – Vaccinia growth factor
VSV – Vesicular stomatitis virus

LIST OF FIGURES

LIST OF TABLES

CHAPTER 1 INTRODUCTION

1.1 THE HALLMARKS OF CANCER

Cancer is not one disease, but a combination of diseases with a common etiology: the unregulated growth of cells in the body that have the capacity to invade and spread to surrounding tissues. Despite remarkable progress in cancer research, cancer still remains a worldwide epidemic. In 2011, the Canadian Cancer Society estimated that approximately 75,000 Canadians died from cancer, and an additional 200,000 Canadians were diagnosed with cancer.[1] Similar statistics were reported for 2010, and 2009. This is in large part due to the complexity and heterogeneity of neoplastic tissues. The multistep process of tumourigenesis involves a combination of six essential hallmark changes in cell physiology, as described by Hanahan and Weinberg: evasion of apoptosis, self-sufficiency in growth signals, insensitivity to antigrowth signals, sustained angiogenesis, limitless replication potential and invasion and metastasis.[2]

1.1.1 Conventional Cancer Therapy

Surgery still remains the foundation of cancer prevention and treatment as removal of high-risk tissues, or localized disease continues to be an effective anti-cancer strategy. Even when removal of the entire tumour is not possible, doctors often 'debulk' large tumour masses, making subsequent treatment more effective. Besides surgical intervention, traditional radiation and chemotherapy still remain front-line therapy for most cancers. This is in part due to their robustness, and broad applicability across a wide-range of tumour types. These antiproliferative agents target rapidly dividing cells. Therefore this effectiveness comes at the expense of a host of adverse off target effects. These side effects can be acute – like damage to epithelial surfaces, intestinal discomfort, or edema, or they can be late onset

side effects including fibrosis and permanent hair loss, and more severe effects like secondary cancers, heart disease or cognitive decline. These side effects have prompted researchers to develop new therapeutic agents that have a better therapeutic index, coined 'targeted therapy'. These new agents were designed with the goal of targeting one or a small number of molecular targets over-represented in tumours. This new strategy also allows potential for personalized medicine – where the mutational landscape of individual tumours can be determined prior to treatment, thereby ensuring every patient is treated with the appropriate agent. Despite these agents being heralded as the chemotherapy of the future, targeted cancer therapies also have some pitfalls.

The feasibility of personalized medicine for cancer therapy took off following the whole-scale sequencing of cancer genomes.[3] Some of the most important successes in genomic profiling included discovery of recurrent BRAF and PI3K mutations.[3] However, more recent analysis revealed that these mutations are relatively uncommon, and are therefore not likely viable therapeutic targets.[4] In fact, the discovery of predominant therapeutic targets still remains a problem for most epithelial cancers.[3] This raises another caveat to personalized medicine: genomic screening does not consider the functional significance of tumour cell mutations. Clearly the response to a given agent is the best determinant of the functional significance of a particular mutation, however economically there must exist a method to determine functional significance prior to therapy. This raises the concept of driver versus passenger mutations. Genomic screening will identify a number of genomic alterations in tumours, however not all of these are driving tumour formation (passenger mutations).[5] Targeted therapies will only be efficacious if the molecular target is a genetic alteration that is driving tumour progression and survival (driver mutation).[5] For cancers where a driver mutation is not the target of therapy, tumours easily develop

resistance through compensatory signaling networks.[6] The frequency of drug resistance brings to light new challenges and questions the economic feasibility of personalized medicine.

1.2 CANCER THERAPY BY ENHANCING IMMUNE SURVEILLANCE: IMMUNOTHERAPY

The immune surveillance hypothesis has existed for more than a century, however the validity of the concept is only now being fully recognized. Interestingly this has culminated in Hanahan and Weinberg expanding their list of cancer hallmarks to include evasion of immune destruction by tumour cells.[7] The immune hallmarks of cancer are also the topic of a recent review by Cavallo and colleagues, detailing three immune escape mechanisms: ability to thrive in chronic inflammation, evade recognition, and suppress immune reactivity.[8] Exploiting the immune system as a strategy to treat human cancers is an equally old concept, dating back to 1909 when William Coley began treating patients with bacterial material.[9] Although not a widely accepted approach at the time, his treatment had a cure rate of 10% for patients with inoperable sarcomas. These early experiments paved the way for the use of bacilli Calmette-Guerin (BCG) as one of the first immunotherapy treatments in 1976.[10] Although the exact mechanisms of action are not yet known, BCG still remains front-line therapy for bladder cancer.[11] Today, a number of sophisticated strategies have been explored for the development of robust immunotherapies harnessing both innate and adaptive anti-tumour immune responses.

1.2.1 Immune Surveillance

The century long debate of the validity of the immune surveillance hypothesis was rooted in the fact that the hypothesis was not experimentally testable. With the advent of

quality monoclonal antibodies, specific gene targeting, and transgenic mouse models, the concept has now become a widely accepted phenomenon.[12] Evidence supporting a role for the immune system in preventing human cancers is the fact that immunosuppressed transplant patients have a higher incidence of non-viral cancers.[13] As described by Schrieber and colleagues, not only does the immune system protect from tumourigenesis, in doing so, immune surveillance also leads to selection of tumours with lower immunogenicity.[12] This observation has led to a redefining of the immune surveillance hypothesis, where the dual effects of the immune system are now termed 'immunoediting'. Described as the three E's of cancer immunoediting, Schrieber elegantly described how immunoediting occurs in three phases: elimination, equilibrium, and escape.[12] Through a greater understanding of each of these processes, new strategies are being developed to augment natural protection from tumours, identify molecular targets of immunoediting to prevent stabilization of tumour genomes, and molecular strategies to unveil and reverse the immunoediting of poorly immunogenic tumours.[12]

1.2.2 Immune Escape Mechanisms

Despite active immune surveillance, immune competent individuals still develop cancer. The tumours that arise have been 'selected' by the immune system, and are able to thrive as they have reduced immunogenicity. Since both innate and adaptive immune surveillance mechanisms exist, tumours that arise must circumvent both of these defenses. There are two main types of immune escape mechanisms, those that are contact dependent, and those that are contact independent. Contact independent mechanisms of immune escape revolve around the ability of tumours to secrete factors that can facilitate a multitude of downstream cascades. These tumour-derived factors (TDFs) can act directly on the tumour,

or on surrounding cells and include vascular endothelial growth factor (VEGF), interleukin-10 (IL-10), indoleamine-2,3-dioxgenase (IDO), reactive oxygen species (ROS), and transforming growth factor (TGF-β).[14] These agents can act directly on the tumour to increase expression of anti-apoptotic genes, angiogenesis factors, and induce pro-tumourigenic mutations.[14] Release of these factors further creates an immunosuppressive network by recruitment and engagement of immune suppressive cell populations including tumour-associated macrophages, regulatory T-cells (Tregs), natural killer T cells (NKTs), immature DCs, and myeloid-derived suppressor cells (MDSCs).[14] Naturally, Tregs exist to inhibit autoimmune responses, but have also been shown to suppress effector T-cell elimination of tumour cells.[15] Contributing to effector T cell suppression, are the MDSCs. This inhibitory myeloid population has been observed in a number of human cancers,[14] where they act to suppress both $CD8^+$ and $CD4^+$ T cell immune responses through release of TGF-β, ROS, and promotion of tumour angiogenesis.[14]

Tumour cells also escape immune detection through changes in the expression of cell surface molecules required for efficient recognition and destruction by immune effector cells like T cells, and NK cells. Perhaps the most common abnormality of tumours cells is the loss of major histocompatibility complex (MHC) expression. Similarly, many tumours develop mutations in one or more components of the antigen-processing pathway. Without efficient presentation of tumour-associated antigens on the tumour cell surface, these cells can not be seen by the immune system. Unlike most normal cells, tumour cells also fail to express costimulatory molecules required for proper T-cell activation.[14] Furthermore, tumour cells will express cell membrane molecules that deliver negative signals to antigen presenting cells, like CTLA-4 and LAG3. DC engagement of these negative signals prevents DC

maturation, and subsequent effector T cell responses.[14] The importance of this negative feedback immune suppression is evidenced by numerous studies revealing that CTLA-4 blockade leads to enhanced tumour rejection.[16,17] Tumour cells have also been shown to acquire resistance to apoptosis, in part due to aberrant expression of TRAIL, and Fas-ligand, surface molecules involved in mediating T-cell and NK cell death. Tumour cells also evade recognition by NK cells by down-regulation if NKG2D ligands, which are required for engagement of NK cell effector functions.[12]

1.2.3 Harnessing Adaptive Immunity

The most popular approach to cancer immunotherapy is the induction of tumour specific cytotoxic $CD8^+$ T lymphocytes (CTLs), as it is well known that these cells make up the effector arm of the adaptive response to cancer.[18] CTLs can induce a killing of target cells by multiple distinct pathways.[19] Upon recognition of a tumour cell, CTLs can release cytotoxic granules containing perforin and granzymes. These molecules lead to the formation of aqueous channels in the plasma membrane of target cells (perforin), allowing entry of the serine proteases that induce apoptosis through caspase activation (granzymes).[20] Additionally, CTLs can directly induce cell death through cell surface expression of the tumour necrosis family (TNF) member, FAS ligand (FasL). Providing the target tumour cells express death receptor Fas, FasL/receptor interactions trigger apoptosis through the classical caspase cascade.[21] Finally, CTLs can kill target cells by the release of cytokines, like interferon-gamma (IFN-γ) and TNF-α. Release of TNF-α from CTLs can lead to caspase activation, and target-cell apoptosis by engagement of the TNF-α receptor. Release of IFN-γ however, leads to transcriptional activation of Fas and the MHC class I pathway in target

cells, thereby increasing the cell lysis of target cells, and enhanced presentation of endogenous peptides, respectively.[19]

The presence of tumour infiltrating lymphocytes in human tumours has been evidenced as an accurate positive prognostic marker.[22-25] It is not surprising then that researchers are focused on developing new strategies to exploit their natural anti-tumour properties. In 1982, work by van Pel and Boon demonstrated for the first time that the lack of tumour rejection in mice was not caused by the absence of tumour antigens, but instead by failure of the tumour to activate the immune system.[26] The realization that the immune system had the ability to recognize tumours as foreign, led to efforts towards identifying and isolating specific tumour antigens, and the development of a number of vaccine strategies.[27] The initial cancer vaccines did not consider the complexity of successful induction of anti-tumour immune responses however, as it was initially thought that vaccination with antigenic peptides alone would be sufficient to induce anti-tumour T cell responses.[28] It is now well known that the generation of an adaptive immune response first involves DC uptake and presentation of tumour antigens and that the antigen presenting cells must also receive maturation signals upon antigen encounter.

First proposed by Matzinger in 1994, the danger model proposes that in order to elicit an immune response, antigen presenting cells must see antigen in the context of danger signals from injured or dying cells.[29] Some examples of danger signals include DNA, RNA, heat-shock proteins, IFN-α or IL-1β.[30] These signals can be either endogenous, or exogenous, and arise when cells are exposed to physical damage, toxins, or pathogens. Upon encounter of antigen, and an appropriate 'danger signal', DCs induce cell-surface expression of costimulatory signals, and release of pro-inflammatory cytokines, like IL-12.[14]

Importantly, if DCs encounter antigen in the absence of danger signals, and do not supply costimulatory signals, the effector arm of the adaptive immune system may be directed towards induction of immune tolerance by activation of Tregs.[28] For this reason, DCs are known as the key mediators in determining the fate of the T-cell response.

Following lymph node interaction of peptide loaded, costimulatory molecule-expressing DCs with T-cells, these cytotoxic T-cells then must find their way back to the tumour. Despite effective priming and recruitment of tumour specific CTLs to tumours, tumours can still escape destruction by one of the most prevalent tumour escape mechanisms: tumour cell down-regulation of antigen recognition or adhesion molecules.[14] Without efficient T-cell to tumour cell interactions, in particular altered or absent MHC expression, tumour cells can effectively evade CTL-mediated immune recognition and destruction.

1.2.4 Harnessing Innate Immunity

In contrast to the adaptive immune system, the innate immune system is composed of effector cells that can exert rapid anti-tumour function with little or no priming. One of the main effector populations of the innate immune system are NK cells. First described in 1975, these lymphoid cells exert their effector function in the absence of cell-surface antigen-specific receptors, and so named for their capacity to kill virus infected or tumour cells without prior sensitization.[31] Based on the work of Karre and colleagues, the 'missing-self' model was first proposed based on observations that syngeneic tumour cells with low MHC class I expression were eliminated by NK cells.[32] Since nearly all normal cells in the body express MHC class I molecules, missing-self recognition allows for specific elimination of tumour cells, or virally infected cells. The MHC class I-dependent killing mechanism of NK

cells is likely evolutionarily conserved to safeguard against tumour escape from CTL cytotoxicity by insufficient MHC-I expression by tumour cells. The early observations that some tumour cells are still eliminated by NK cells despite normal MHC class I expression, led to a detailed characterization of the regulation of NK cell function.

It is now understood that the NK cell response is regulated by an intricate balance of signals received by an array of cell surface activating and inhibitory receptors.[33] NK cell activating receptors often recognize stress induced ligands on the surface of virus infected, or transformed cells. The best described activating receptor NKG2D is present on murine and human NK cells, and interacts with retinoic acid early inducible-1 (Rae-1), the minor histocompatibility Ag (H-60), in mice, and with MIC in humans.[33] NKG2D ligands are over-expressed during cellular stress, like DNA damage.[31] NK cell inhibitory receptors are used to evaluate the level of 'self' molecules expressed on a target cells and include the lectin-like Ly49 dimers (mouse) and killer cell immunoglobulin-like receptors, or KIRs (humans).[34] These inhibitory receptors mediate their functions through intracellular signaling via a common immunoreceptor tyrosine-based inhibition motif (ITIM).[34] For a detailed list of activating and inhibitory receptors with their respective ligands in both mice and humans, refer to **Figure 1.1**. NK cells also express an array of cytokine receptors that also participate in NK cell development and effector function, such as receptors for IL-15, IL-2 and IL-21.[31]

Upon recognition, NK cells can kill tumour cells via one of several mechanisms. Like $CD8^+$ T cells, one of the major mechanisms of NK cell mediated killing is via granule exocytosis - the release of cytotoxic granules containing perforin and granzymes. NK cells can also directly induce cell death similarly through cell surface expression of members of the tumour necrosis factor and TRAIL death receptor families.[35] Another important feature of NK cells is their ability to secrete a number of effector cytokines, like IFN-γ, and TNF.

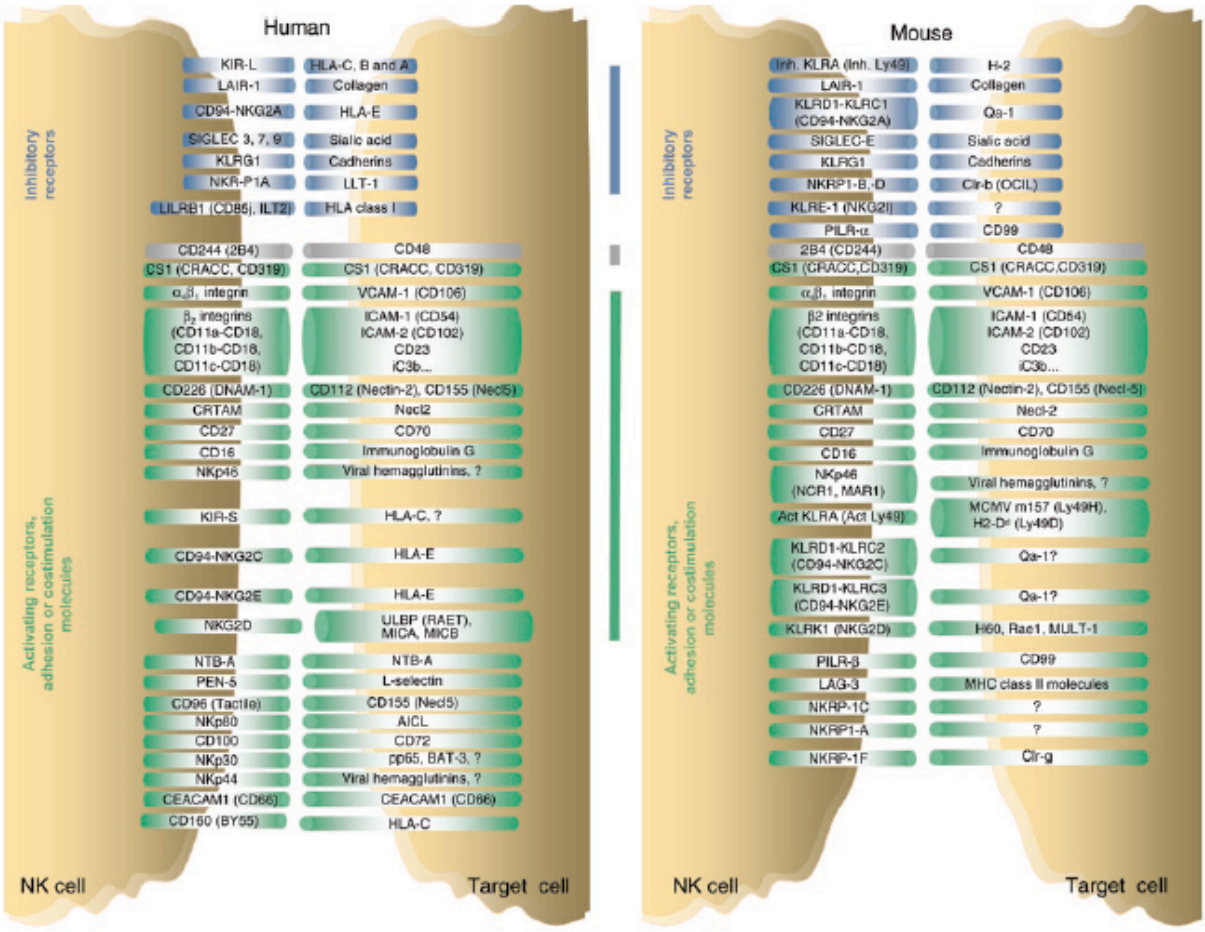
Human
Inhibitory receptors
KIR-L
HLA-C, B and A
LAIR-1
Collagen
CD94-NKG2A
HLA-E
SIGLEC 3, 7, 9
Sialic acid
KLRG1
Cadherins
NKR-P1A
LLT-1
LILRB1 (CD85j, ILT2)
HLA class I
Activating receptors, adhesion or costimulation molecules
CD244 (2B4)
CD48
CS1 (CRACC, CD319)
CS1 (CRACC, CD319)
α4β1 integrin
VCAM-1 (CD106)
β2 integrins (CD11a-CD18, CD11b-CD18, CD11c-CD18)
ICAM-1 (CD54) ICAM-2 (CD102) CD23 iC3b...
CD226 (DNAM-1)
CD112 (Nectin-2), CD155 (Necl5)
CRTAM
Necl2
CD27
CD70
CD16
Immunoglobulin G
NKp46
Viral hemagglutinins, ?
KIR-S
HLA-C, ?
CD94-NKG2C
HLA-E
CD94-NKG2E
HLA-E
NKG2D
ULBP (RAET), MICA, MICB
NTB-A
NTB-A
PEN-5
L-selectin
CD96 (Tactile)
CD155 (Necl5)
NKp80
AICL
CD100
CD72
NKp30
pp65, BAT-3, ?
NKp44
Viral hemagglutinins, ?
CEACAM1 (CD66)
CEACAM1 (CD66)
CD160 (BY55)
HLA-C
NK cell
Target cell
Mouse
Inhibitory receptors
Inh. KLRA (Inh. Ly49)
H-2
LAIR-1
Collagen
KLRD1-KLRC1 (CD94-NKG2A)
Qa-1
SIGLEC-E
Sialic acid
KLRG1
Cadherins
NKRP1-B, -D
Clr-b (OCIL)
KLRE-1 (NKG2I)
?
PILR-α
CD99
Activating receptors, adhesion or costimulation molecules
2B4 (CD244)
CD48
CS1 (CRACC,CD319)
CS1 (CRACC,CD319)
α4β1 integrin
VCAM-1 (CD106)
β2 integrins (CD11a-CD18, CD11b-CD16, CD11c-CD18)
ICAM-1 (CD54) ICAM-2 (CD102) CD23 iC3b...
CD226 (DNAM-1)
CD112 (Nectin-2), CD155 (Necl-5)
CRTAM
Necl-2
CD27
CD70
CD16
Immunoglobulin G
NKp46 (NCR1, MAR1)
Viral hemagglutinins, ?
Act KLRA (Act Ly49)
MCMV m157 (Ly49H), H2-Dd (Ly49D)
KLRD1-KLRC2 (CD94-NKG2C)
Qa-1?
KLRD1-KLRC3 (CD94-NKG2E)
Qa-1?
KLRK1 (NKG2D)
H60, Rae1, MULT-1
PILR-β
CD99
LAG-3
MHC class II molecules
NKRP-1C
?
NKRP1-A
?
NKRP-1F
Clr-g
NK cell
Target cell

Figure 1.1 NK receptors. From Vivier *et al.* with permission from the publisher, (License number 2927121077827): a detailed list of activating/other receptors (green) and inhibitory receptors (blue) with their respective ligands in both mice and humans.[34]

IFN-γ is well known for its ability to suppress infection by viruses, but recent evidence suggests that IFN-γ exerts anti-tumour effector functions directed towards tomour metastases.[36] It is also well established that IFN-γ is capable of killing tumour cells by restricting tumour angiogenesis.[35] Finally, IFN-γ also plays a critical role in regulating downstream immune responses by maturing antigen presenting cells promoting adaptive anti-tumour immunity.

IL-2 was the first growth factor identified to be important for NK cell maturation, cytotoxicity, and cytokine secretion.[37] It is now well established that despite their name, the majority of NK cells isolated from peripheral blood or spleen require priming to become killer cells.[38] Some of the factors involved in the priming of NK cells are natural adjuvants like IL-12, IL-15, IL-18, IFN-α or IFN-β.[39] The priming of naïve NK cells occurs via contact with DCs in draining lymph nodes.[38] Elegant work by Lucas and colleagues delineated a defined cascade of events that must occur for NK cell priming.[40] Referring to **Figure 1.2**, toll-like receptor (TLR) expressing cells must first respond by secretion of Type I interferons. Subsequently, DCs release IL-15 in response to stimulation by the type I IFN, and direct presentation of the IL-15 from the DCs to the NK cells in the lymph node allows for efficient NK cell priming.[38] Indeed the anti-tumour properties of NK cells, including both cytotoxicity and IFN-γ production are dependent upon DC-NK cell-to-cell contact.[41] Not unlike their antigen presenting DC counterparts, NK cells also express a number of TLR's, and *in vitro* exposure of NK cells to TLR ligands does lead to NK cell effector function.[42] However NK cell activation by *in vitro* stimulation by TLR-ligands is more efficient when in the presence of accessory cells, (like DCs) suggesting that the *in vivo* activation of NK cells is still likely an indirect phenomenon.[43]

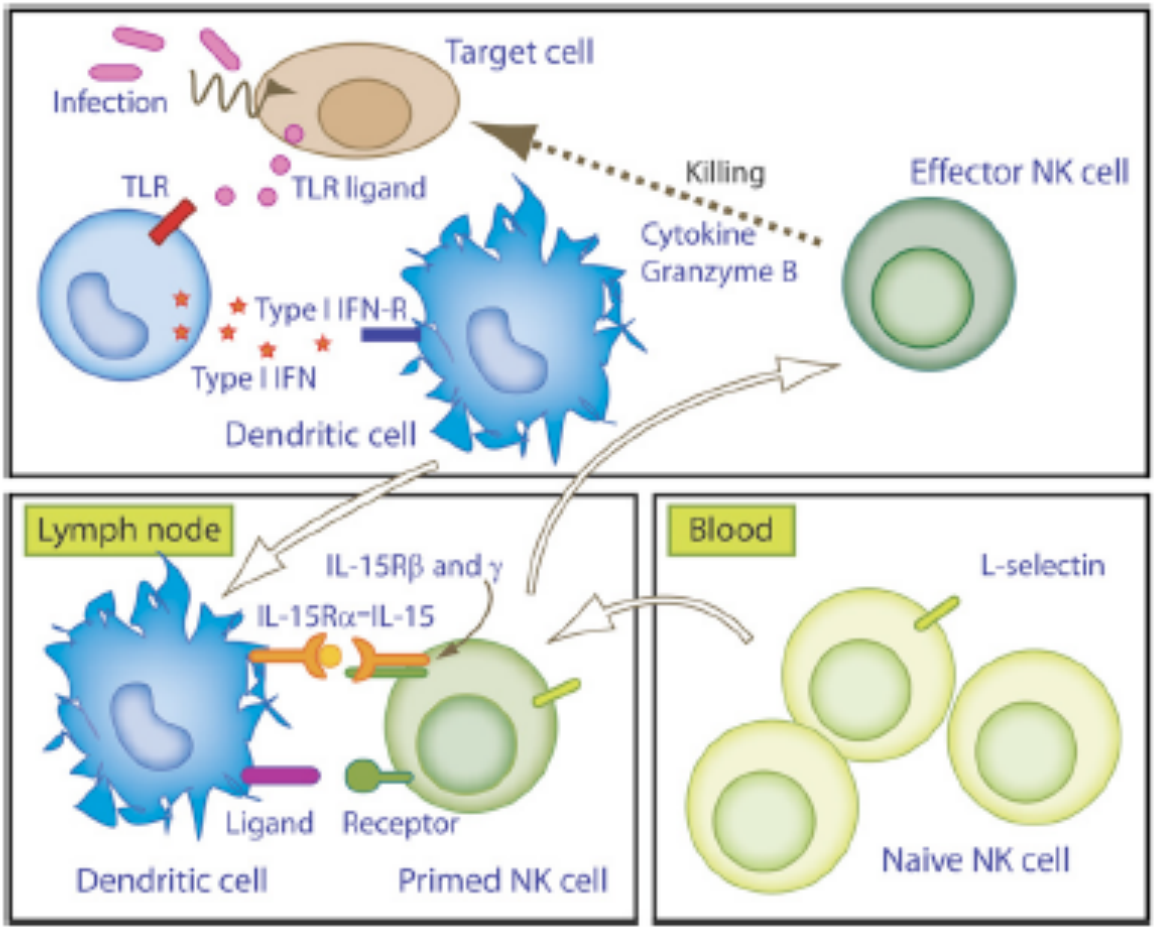
Infection
Target cell
TLR
TLR ligand
Killing
Effector NK cell
Cytokine
Granzyme B
Type I IFN-R
Type I IFN
Dendritic cell
Lymph node
IL-15Rβ and γ
IL-15Rα-IL-15
Ligand
Receptor
Dendritic cell
Primed NK cell
Blood
L-selectin
Naive NK cell

Figure 1.2 Priming of natural killer cells from Long *et al*., 2007 with permission from the publisher (License number 2927130448620). For effective NK cell priming, TLR ligands are first sensed by TLR-expressing cells to promote release of type I IFN. The IFN leads to upregulation of both IL-15 and its cognate receptor by DCs. NK cells migrate to the draining lymph node, where they directly interact with DCs via *trans*-presentation of IL-15.[38,40]

Some of the best evidence to support a role of NK cells in murine tumour immune surveillance was from Schrieber's group, where they demonstrated that the frequency of carcinogen-induced tumours was always higher in mice genetically deficient in key NK cell effector molecules.[44] Due to the rarity of human disease relating to NK cell deficiency, the majority of human data linking a role of NK cells in tumour immune surveillance are correlative in nature. An epidemiological analysis of human NK cell peripheral blood activity discovered a link between low NK cell activity and increased risk of cancer development.[45] The presence of NK cells at tumour sites has also been noted as a positive prognostic marker in various carcinomas.[46] However, the low number of tumour-infiltrating NK cells in most cancers suggests that these cells are not expected to directly impact therapeutic outcome.[46] Nevertheless, a number of strategies have been directed towards increasing the frequency and activity of tumour infiltrating NK cells, like through cytokine mediated activation by IL-2. The first evidence of successful NK cell immunotherapy stems from clinical studies examining the effect of transfer of alloreactive NK cells during the course of stem cell transplantation of leukaemia patients. These studies reported a striking increase in survival and protection from disease recurrence.[46]

1.2.5 Natural Killer cells at the centre of Innate / Adaptive Cross Talk

It is now well established that NK cells play a central regulatory role for subsequent adaptive anti-tumour immune responses. Summarized in **Figure 1.3**, through effector function, and release of chemokines and cytokines, NK cells are central to effective downstream anti-tumour CTL responses. Since NK cells are unique in their capacity to detect and eliminate tumour cells without a requirement for 'danger signals', their effective cross talk to DCs and mediators of the adaptive immune response is crucial for successful

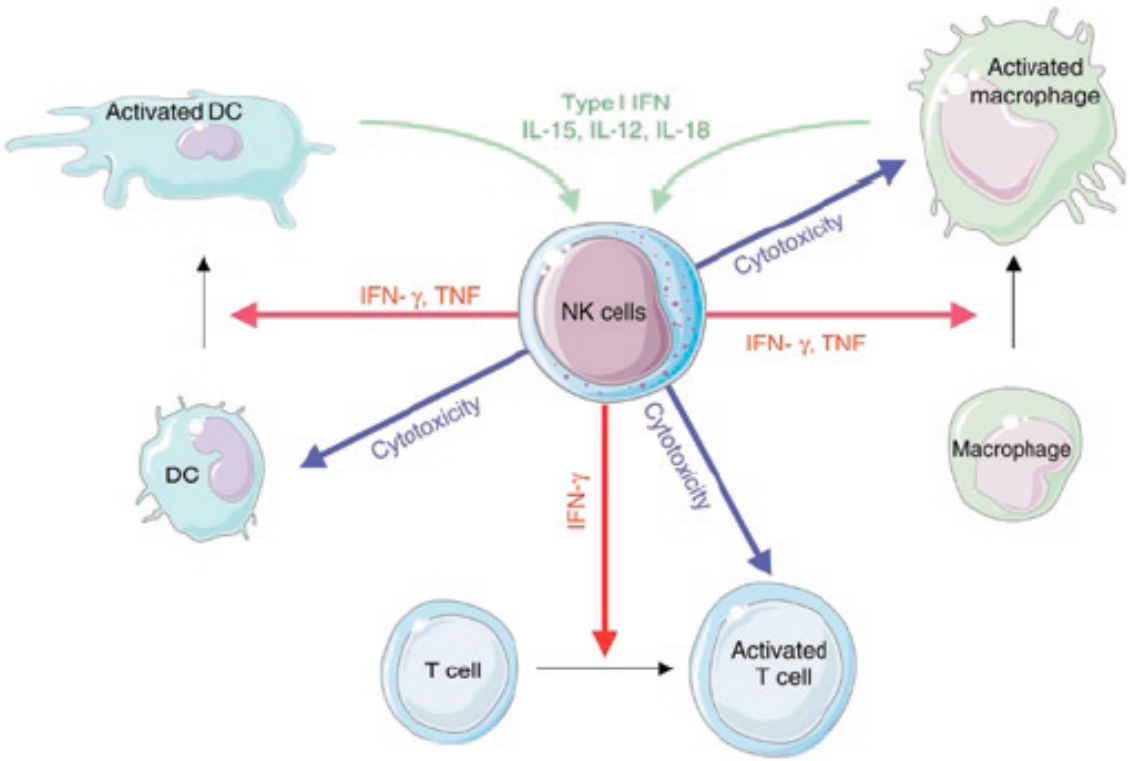
Activated DC
Type I IFN
IL-15, IL-12, IL-18
Activated macrophage
Cytotoxicity
IFN- γ, TNF
NK cells
IFN- γ, TNF
Cytotoxicity
DC
Cytotoxicity
IFN-γ
Macrophage
T cell
Activated T cell

Figure 1.3 NK cell regulatory functions from Vivier *et al*., with permission from the publisher (License number 2927130827289). Once primed by soluble factors (green), NK cells are capable of promoting the maturation of DCs, T-cells, and macrophages (red arrows) by release of cytokines, and expression of cell surface receptors. NK cells are also capable of killing certain subsets of these cell types, if appropriately engaged by lack of self molecules (blue arrows).[34]

adaptive anti-tumour immune responses. Perhaps one of the most important aspects of NK cell regulation is the release of IFN-γ that leads to the recruitment and activation of DCs, T-cells and B cells.[47] This leads to a positive feedback loop, whereby DCs in turn can lead to the activation of NK cells through type I IFN, and cytokines like IL-12 and IL-15.[39] Considering the ability of DCs to recruit NK cells to lymph nodes,[47] it is not surprising that IFN-γ released from NK cells is crucial in priming T helper 1 (Th-1)-biased responses.[48] The importance of NK regulatory functions was highlighted by Mocikat and colleagues, where they demonstated that NK cell priming of DCs was crucial for inducing protective anti-tumour CTL responses.[49]

1.2.6 Current Progress in Immunotherapy

One of the major hurdles in the immunotherapy field has been the development of robust agents that are well tolerated in the clinic. With a better understanding of the complexities of mounting a specific immune response, the vaccine field has progressed to using better peptide formulations. This approach was successful using the melanocyte differentiation antigen gp100 in combination with IL-2 treatment compared to IL-2 treatment alone, resulting in prolonged progression-free survival for melanoma patients.[28] Variations in peptide length, and adjuvant type are current strategies being explored to boost reactivity against the cancer antigen, including the use of viral vectors encoding tumour antigens. New cancer vaccines strategies involving the use of viral vectors have recently shown promise for the treatment of prostate cancer.[28] In a randomized phase II trial, poxvirus expression of the prostate-specific antigen, and adhesion molecules B7-1, LFA-3, and ICAM-1 led to an overall survival benefit.[50] Another strategy involves the use of cell-based vaccines, whereby the entire cancer cell from a patient is used as the source of antigen. The advantage to this

approach is the diversity of antigens; the immune system chooses the peptide. A recent meta-analysis of nearly 200 studies revealed that patients vaccinated with whole tumour antigen had better clinical responses than those vaccinated with a small number of defined antigens.[51] Alternatively, a number of groups have demonstrated advantages of using DC vaccines.[28] DCs are removed from a patient, pulsed with peptide antigens, or whole cell lysates, activated and then re-infused to the patient.

The first FDA approved immunotherapy was the cell-based therapy for prostate cancer called Provenge (sipuleucel-T) by Dendreon.[28] The vaccine was composed of a mix of the patients blood mononuclear cells, granulocyte-colony stimulating factor (GM-CSF) and a tumour differentiation antigen.[28] Although the exact mechanism of action has yet to be defined, Provenge was approved in 2010 based on a 4.1 month improvement in median survival.[28] In order to bypass the need for overcoming tumour immune suppression, Steven Rosenberg created the 'adoptive-cell transfer' (ACT) protocol to directly treat patients with tumouricidal CTLs.[25] This therapy involves the removal of tumour infiltrating lymphocytes (TILs) from a patients tumour, and expansion and selection of these clones *ex vivo*.[25] Prior to administration, the patient receives systemic immunosuppression resulting in lymphodepletion that facilitates engraftment of the transferred T cells.[25] Rosenberg's therapy- although not yet approved, has shown significant responses for patients with metastatic melanoma.[52,53] However, these response rates are associated with serious side effects from the lymphodepletion.[53] Moreover, ACT therapy is also limited by cost, and relies on the availability of TILs as the source of T-cells.

Another approach to increase CTL responses in patients is by taking the 'brakes off' of pre-existing anti-tumour T cell responses. In March of 2011, the FDA granted the approval for the use of the CTLA-4 monoclonal antibody, Ipilimumab for the treatment of

metastatic melanoma.[28] Pioneered by James Allison, extensive pre-clinical studies indentified that blocking the negative regulator of T-cell activation effectively led to the expansion and activation of anti-tumour T-cells.[54,55] However, CTLA-4 blockade was associated with serious inflammation-related adverse events in up to 23% of patients, possibly due to an autoimmune reaction.[28] Nevertherless, the FDA approval of Ipilimumab has reignited the immunotherapy field, as a number of monoclonal antibodies targeted towards activating receptors on T cells (agonistic antibodies) or inhibitory receptors on T-cells (blocking antibodies) are currently being developed.[28]

Although the field has come a long way since the use of Coley's toxin,[9] the average response rates to most of the new agents still remains less than 15%.[56] One solution to ameliorate response rates to immunotherapy regimes might be through combination therapy with established anti-tumour agents. Immunotherapy might be better equipped to induce long term protection from tumours if the patient's tumours have already been partially destroyed. This is especially true if the tumour destruction is causing inflammation, or local danger signals. In collaboration with Allison's group, Bristol-Myers Squibb is conducting a phase III trial whereby an anti-tumour immune response and tumour destruction is first initiated by a single dose of radiation, then followed by treatment with Ipilimumab.[56] This approach may prime the tumour with an *in situ* 'danger signal', allowing even the most immune-suppressed tumours the chance to respond to Ipilimumab.

1.3 REPLICATING VIRUSES FOR THE TREATMENT OF CANCER

Biological therapeutics for cancer constitute an exciting alternative or complement to conventional chemo- and radiotherapies. Oncolytic viruses (OVs) are self-replicating biological agents that can target and kill cancer cells while leaving normal cells unharmed.

Some OVs are naturally occurring, while others must be genetically manipulated to achieve tumour-specific replication. OVs are a unique targeted cancer therapy; instead of targeting a single oncogenic mutation, oncolytic viruses are conveniently addicted to the same common pathways that drive tumour cell growth.[57] One particular example of common pathways dysregulated in tumours that support OV replication are defects in the type I IFN response, (the anti-viral immune response).

OVs have multiple features that can be exploited therapeutically, and therefore offer many benefits to traditional therapies. Oncolytic viruses are self-amplifying at tumour sites, they have a large cloning capacity and can therefore act as gene delivery vehicles and/or vaccines, and as pathogens, OVs inherently activate both innate and adaptive immune responses.

1.3.2 Oncolytic Viruses: History and Overview

The therapeutic application of lytic viruses for the treatment of cancer dates back to the mid-1800s, where doctors reported spontaneous cancer remissions following severe viral infections in patients.[58] A number of different virus strains were subsequently tested for their anti-cancer ability in mouse models in 1952.[59] This spawned a series of human clinical trials in the early 1960s. Although a number of patients experienced durable responses, the use of wild-type virus strains led to a significant number of adverse complications, bringing the field to a halt.[60] With a better understanding of tumour biology, virology and recombinant DNA technology, new oncolytic viruses have been engineered with enhanced safety, and tumour specific replication. The efficacy of engineered viruses for cancer treatment was first evidenced by Martuza *et al.* in 1991.[61] Using mouse models of human glioma, their studies demonstrated reduced toxicity, and anti-tumour efficacy from an attenuated herpes simplex

virus strain. This work paved the way for the development of new, targeted oncolytic viruses. Another approach to reduce the virulence of oncolytic viruses was the search for non-human animal viruses that were non-pathogenic in humans. Newcastle Disease virus (NDV) is an avian virus that in its wild type form is tropic for tumour cells based on defects in their interferon signaling pathways. Early phase clinical trials demonstrated prolonged survival of patients with advanced disease when compared to placebo control treated patients.[62] Another animal virus called vesicular stomatitis virus (VSV) similarly replicates in tumour cells with interferon pathway defects,[63] further demonstrating the potential of animal viruses for the treatment of human cancer.

The resurgence of the oncolytic virus field has led to the clinical development of a number of different virus strains, many of which have been genetically modified for enhanced safety, and increased genetic payload. The first OV approved for use in humans in China was an adenovirus mutant called H101 (similar to ONYX 015) – an E1B-deleted virus strain for the treatment of nasopharyneal carcinoma in combination with cisplatin chemotherapy.[64] A replication competent version of herpes simplex virus (HSV), HSV-1 was modified to contain genetic enhancements relating to its immune stimulatory capacity, and has so far proven to be well tolerated.[65] Called OncoVEX^{GM-CSF}, this oncolytic immune stimulating agent is now entering into phase III multi-national clinical trials, and is forecasted to be the first OV to be approved for human use in North America. A double-stranded RNA virus called Reovirus was also found to have natural tumour-selective replication based on a requirement for an activated Ras signaling cascade.[66] Marketed as Reolysin by Oncolytic Biotech, phase II clinical data of the agent in combination with standard radiation or chemotherapy demonstrated marked responses that have led to the planning of phase III trials targeting head and neck cancer.[65] An oncolytic poxvirus is also in

clinical development in Phase II trials for hepatocellular carcinoma. A San Francisco based company called Jennerex Biotherapeutics has developed this GM-CSF-expressing vaccinia virus oncolytic targeted to tumours based on deletion of its thymidine kinase. The virus has been well tolerated in clinical trial, and has demonstrated tumour selective replication following intravenous administration.[67]

1.3.3 Mechanisms of Action

The primary mechanism of action of most oncolytic agents is the direct oncolysis of tumour cells. In following, one of the main advantages of oncolytic agents is their ability to self-amplify at tumour sites, allowing for spread within large tumours, and the potential for infection of distant tumour metastases. Indeed several pre-clinical studies evaluating the safety and feasibility of intratumoural administration of OVs have discovered that OVs are capable of spreading to uninjected, distant metastases.[68,69] Clinically, intratumoural adminstration of OVs has been associated with shrinkage of uninjected mestastases,[70] however, it was not clear if this shrinkage was caused by tumour infection, or a secondary immunological effect. Nevertheless, this prompted researchers to examine the possibility that these agents might be delivered intravenously. A pivotal study recently published in Nature by Jennerex demonstrated for the first time, successful intravenous delivery of an oncolytic virus to systemic tumour beds.[67] Importantly, these studies were not associated with any serious adverse effects from systemic delivery of the virus.

It is now clear that OVs destroy tumours by a number of additional mechanisms that go beyond direct tumour cell infection and lysis. Some oncolytic agents have demonstrated significant anti-tumour effects mediated through bystander vasculature disruption. Following intravenous delivery of VSV to murine tumours, tumour inflammation caused a catastrophic

loss of blood flow, and subsequent killing of tumour cells.[71] The concept now referred to as 'vasculature shut-down' was also described for oncolytic vaccinia virus, in pre-clinical and clinical models.[71,72] Interestingly, it was later found that the vasculature disruption by VSV was rooted in the virus' ability to directly infect tumour vasculature.[73] Vasculature infection by VSV led to the initiation of fibrin deposition, neutrophil-dependent clot formation, and bystander tumour destruction.[73]

With the advent of recombinant DNA technology, not only can OVs be modified to more specifically target tumour cells, most OVs have a substantial cloning capacity that also allows for insertion of therapeutic transgenes. In this way, OVs are also gene therapy delivery vehicles that by their tumour-targeting nature can significantly increase the genetic payload and therapeutic outcome of OV therapy. A number of groups have examined the benefit of viral expression of immune modulatory molecules like GM-CSF, a cytokine involved in the stimulation of cellular immune responses, like the maturation and recruitment of antigen presenting cells. Phase II treatment with the GM-CSF expressing herpes virus oncolytic (Oncovex$^{GM\text{-}CSF}$) was found to induce significant recruitment of T cells at tumour sites, with reduced prevalence of regulatory cells.[74] A number of the patients in this trial also demonstrated tumour reduction of both primary injected tumours, and uninjected lesions. GM-CSF was also engineered into the oncolytic vaccinia virus, JX-549. In a Phase I trial of intratumoural injection, the GM-CSF cytokine was found to be biologically active.[67] A number of additional strategies to increase the genetic payload of OVs are currently being explored pre-clinically. Some examples include the expression of pro-drugs or suicide genes,[75,76] expression of tumour-associated antigens,[77] or expression of pro-apoptotic genes.[78]

Besides the direct anti-tumour activity of OVs, an increasing body of evidence suggests that the stimulation of an active anti-tumor immune response may be a major contributor to the efficacy achieved by oncolytic viruses. The induction of innate and/or adaptive anti-tumour immune responses is likely triggered by anti-viral immune responses. Highlighted by Prestwich *et al*.,[79] the significant interplay of oncolytic viruses and the immune system highlight the immunotherapy potential of replicating viruses for the treatment of cancer.

1.3.4 Oncolytic Viruses as Immunotherapies

Oncolytic viruses were initially designed to target and lyse tumours cells. In the process however, viral infection of tumours leads to substantial inflammation that arouses both innate and adaptive anti-tumour immune responses. A plethora of evidence now exists demonstrating that most (if not all?) oncolytic viruses are capable of stimulating some form of an anti-tumour immune response.[80] The highly destructive nature of virus infection leads to release of danger signals from cancer cells (danger-associated molecular pattern molecules), and/or from the virus (pathogen-associated molecular pattern molecules).[79] Virus infection of tumour cells has also been reported to increase the uptake of tumour material by antigen-presenting cells.[81] The potent inflammatory response caused by virus infection ultimately overcomes tumour immune suppression, and promotes recruitment of innate immune cells, like macrophages, DCs and NK cells.[79] Oncolytic viruses therefore provide three important components necessary for mounting a specific immune response: an inflammatory storm to overcome immune suppression and recruit innate immune cells, tumour cell death and release of tumour associated antigens, and danger signals to promote

maturation of antigen presenting cells, and downstream adaptive anti-tumour immune responses.

In murine models, oncolytic herpes virus has been shown to enhance DC maturation, and increase tumour infiltrating CTLs and NK cells.[82] These anti-tumour immune responses have been shown to significantly impact therapeutic outcome.[83] In VSV treated mice, there was a strong correlation between therapeutic outcome and NK/CTL responses in a B16ova model.[84] CTL responses were also observed in mice treated with NDV[85] and measles virus.[86] In clinical studies, reovirus treatment led to expansion of effector T cell subsets, as well as NK cells.[87] Similarly a phase I trial of oncolytic measles treatment of cutaneous T cell lymphoma demonstrated increased T cell infiltration and $CD8^+$ T cell expansion.[88] The importance of immune stimulation for OV therapy is further evidenced by the fact that some OVs have demonstrated efficacy independent of viral replication and oncolysis.[84,89,90]

1.3.5 Barriers to OV therapy

Despite their promise in early phase clinical trials, there exist a number of barriers to OV therapy. Summarized in **Fig. 1.4**, in order to successfully reach tumour beds, intravenously delivered OVs must evade elimination by the host at several levels. Within minutes of infection, the liver and spleen absorb most intravenously injected virus.[91] Of the virus particles that emerge from these 'sinks', a series of blood components further react to prevent virus circulation, including neutralizing antibody, complement, or absorption by blood cells. The tumour itself is also considered a hostile environment limiting OV spread, with densely packed tumour cells, extensive extracellular matrix components and high interstitial pressure. Since the immune system has evolved complex mechanisms to restrict the spread and replication of viruses, actively stimulating the immune system during OV

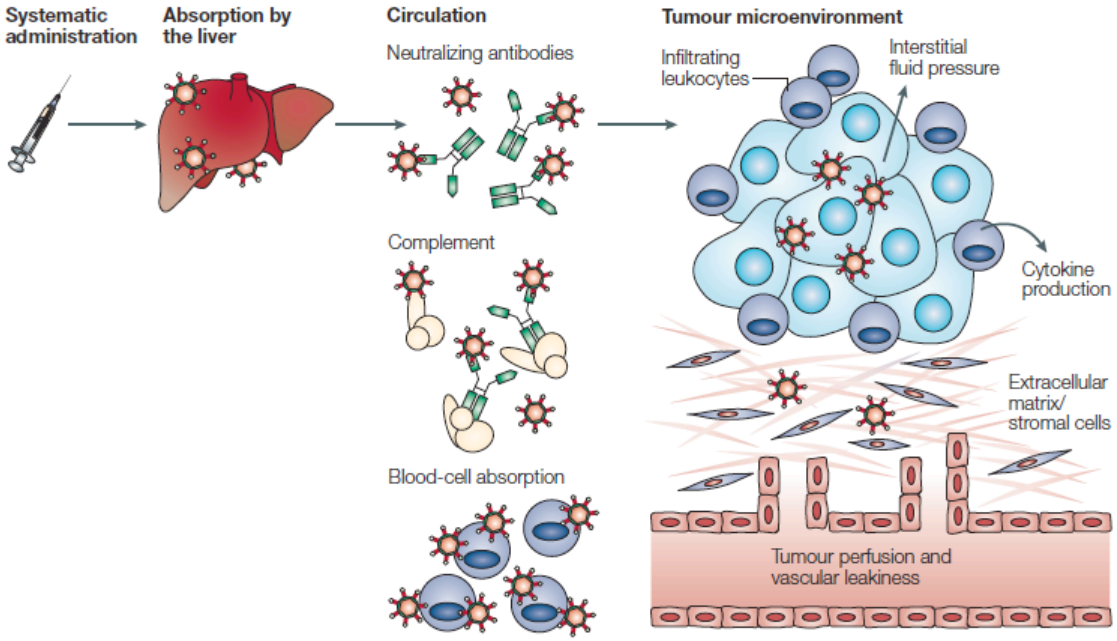
Systematic administration
Absorption by the liver
Circulation
Neutralizing antibodies
Complement
Blood-cell absorption
Tumour microenvironment
Infiltrating leukocytes
Interstitial fluid pressure
Cytokine production
Extracellular matrix/ stromal cells
Tumour perfusion and vascular leakiness

Figure 1.4 Barriers to effective oncolytic virus delivery to tumours, from Parato *et al*. with permission from the publisher (License number 2927140003905).[70] Systemically delivered oncolytic viruses must survive absorption by the liver, and neutralization by blood components prior to reaching tumour beds. At the tumour, OVs must gain access via extravasation from vasculature, and spread within the dense, extracellular-matrix packed tumour microenvironment.

therapy is considered a double edged sword. Indeed the innate immune response has limited viral replication in several animal models,[71,92] and clinical studies.[93] Viral gene products are recognized by specific immunoglobulin surface receptors on B cells, leading to their activation and subsequent production of neutralizing antibodies before the virus even reaches the tumour. Neutralizing antibodies represent a significant barrier to effective OV therapy by VSV, reovirus, and adenoviral vectors.[94-96] Although the relevance has not yet been fully determined in the clinic, previous vaccination programs for some OVs (measles, poliovirus, vaccinia virus) may also prevent effective delivery of these agents.[70] Once OVs reach tumour beds, infiltrating innate immune cells pose an additional barrier to effective OV infection and spread within tumours. VSV persistence has been shown to be sensitive to neutrophils within tumours.[71] Tumour and liver resident macrophages have also been implicated in viral clearence for herpes and adenovirus OVs.[97,98] The anti-viral immune response is further enhanced by release of anti-viral cytokines at the tumour, like type I interferons, IFN-γ, IL-15 and TNF-α. Since most cancer cells lack functional PKR and p53 pathways, anti-viral IFN responses generally do not lead to inhibition of protein translation, or triggering of apoptosis in response to OV therapy. Nevertheless, induction of potent IFN responses has been shown to limit measles replication,[99] and infection by HSV-1.[100]

Best evidenced by an increase in sensitivity to virus infection as a result of NK cell deficiencies,[101] NK cells have long been known for the innate anti-viral effector functions. These defense mechanisms are especially important for protection against lethal herpes virus infections in mice and humans. NK cells can directly recognize virus, through binding of NK TLRs, like TLR-2 association by vaccinia virus.[102] Alternatively, NK cells recognize tumour infected cells by at least three distinct virus-induced changes: recognition of host stress

proteins by activation receptor NKG2D, recognition of modified MHC I molecules by stimulatory receptors, or the direct recognition of cell surface viral products, like m157 from murine cytomegalovirus (MCMV) infection by murine Ly49H receptors.[103] Antibody-mediated depletion of NK cells has allowed for enhanced efficacy by some OVs, like VSV.[104] Dampening of natural killer cell recruitment by cyclophosphamide treatment similarly enhanced the efficacy HSV-1 OV therapy.[92] However, the conclusions drawn from these experiments appear to be model dependent, since other studies demonstrated a dependence on NK cell activity for efficacy of VSV, HSV and reovirus.[89] Since NK cells also exhibit robust anti-tumour effector functions, for the majority of OVs the jury is out as to whether these innate effector cells present as a barrier or ally to effective OV therapy.

1.4 ANTI-CANCER POTENTIAL OF POXVIRUSES

The therapeutic potential of poxviruses was first realized in 1988, after the successful implementation of a vaccination strategy that led to the eradication of smallpox.[105] Stemming from this historical role, the biology and pathogenesis of vaccinia virus has been studied extensively over the years. An appreciation of the virus' behaviour in humans, and its ability to induce long-lasting robust CTL and antibody responses,[106] has led to the development of a number of poxvirus-based therapeutics for a variety of clinical applications.

1.4.1 Poxvirus Biology

Poxviruses constitute a large family of enveloped, double-stranded DNA viruses that replicate entirely in the cytoplasm. Poxvirus virions are large enough to be visualized by light microscopy, averaging in size of approximately 225 nm x 350 nm. Poxvirus genomes are primarily A+T rich, up to 290 kbp in size, encode over 200 genes and are well conserved.[107] Restriction enzyme digestion of DNA from members of the orthopoxvirus

genus showed that the central part of the genomes were conserved, whereas terminal portions varied in both length and restriction size pattern.[108] Genes in the terminal region of the genome- although non-essential for virus replication,[109] encode a number of immune-modulating proteins of complex function involved in viral virulence. Through the cooperative action of virulence factors, poxviruses evade host immune responses and elimination.[110]

Based on its long history, vaccinia virus (VACV) still remains the best-studied member of the poxvirus family. VACV is one of 10 members of the *Orthopoxvirus* genus, which also includes variola virus (smallpox), and cowpox virus. These viruses, as well as all members of the Orthopoxvirus genus, are similar immunologically, which provides the basis for the cross protective nature of smallpox vaccines. The poxvirus virion contains a DNA-protein core that includes all enzymes and factors required for early gene expression.[111] This core is wrapped by a lipid membrane that contains a number of unglycosylated viral proteins.[111] Based on the structure of their membrane, most poxviruses exist in one of two infectious forms: extracellular virion or intracellular virion. These two forms differ in that the extracellular virion contains an additional trans-Golgi derived lipid envelope compared to the intracellular virion.[111]

The mechanism of poxvirus entry into host cells remains controversial, and is thought to be virus strain, and cell-type dependent.[111] It is also dependent on the virion structure. Since intracellular virions are surrounded by a single membrane, the virus core gains entry to cells through fusion of the viral membrane with the plasma membrane.[111] The identity of the receptor(s) by which poxviruses gain entry into host cells also remains controversial, with several refuted claims. Proteins on the surface of intracellular virions are capable of interacting with cell surface glycosaminoglycans (GAGs), and have thus been proposed as

attachment proteins.[112] The binding of extracellular virions is through GAGs, but is complicated by an additional viral lipid membrane. Following binding to host cells, it is thought that the additional membrane is removed by a GAG-dependent, non-fusogenic mechanism.[113]

Poxvirus transcription is divided into 3 stages: early, intermediate, and late. Genes within the virus core are transcribed by the virus-encoded DNA-dependent RNA polymerase. Early mRNAs are synthesized immediately upon entry without the need for host protein synthesis, since the virus encodes an entire transcriptional system.[114] Poxvirus DNA replication occurs within virus factories, within a few hours of expression of early proteins.[114] Virus particle assembly begins in the viral factories, where the viral core emerges with a lipid membrane. By transportation on microtubules, virus particles acquire additional intracellular membranes by association with the trans-Golgi, or endosome compartments, prior to exocytosis through host cell plasma membrane.[115]

1.4.2 Poxviruses as Cancer Therapeutics

Following the eradication of smallpox, a number of different poxvirus species have been developed as live or attenuated anti-viral vaccines. The inherent biological characteristics of poxviruses make them ideal candidates for the development of vectors for therapeutic applications: clear clinical safety, a large cloning capacity, precise virus control of gene expression, lack of genomic integration, high level of immune stimulation, and feasible virus manufacturing procedures.[116] The first generation poxvirus vaccines were wild-type VACV strains, employed during the smallpox eradication. Since the viruses induced significant adverse reactions,[117] new vector vaccines are now primarly constructed from attenuated strains. The most common technique used to attenuate poxviruses involves

sequential passage of the wild-type viruses in tissue culture using cells from an alternative host.[117] This attenuation strategy has been used for almost a century, and has been found to alter virulence, genome composition, and importantly, virus host range.[117] The VACV Ankara strain of VACV was attenuated in the 50s by over 500 passages in chick embryo fibroblast cells. These attenuated strains are replication-defective in most mammalian cells,[118] however, still maintain their ability to express recombinant genes. Alternatively, avipoxviruses like fowlpox and canarypox have a natural host range restriction, as they are only able to replicate in avian cells. Using animal models of viral disease, a number of prophylactic anti-viral poxvirus vaccines have been developed and have shown strong proof-of principle.[119,120] With the discovery of several tumour-associated antigens, several poxvirus vaccine candidates are also being tested in pre-clinical and clinical cancer models directed towards carcinoembryonic antigen (CEA),[121] prostate-specific antigen (PSA),[122] or one of several melanoma-associated antigens.[123]

Through genetic engineering, poxviruses can be specifically attenuated or manipulated by insertion, deletion or disruption of specific target genes. This spawned a new generation of poxvirus cancer therapeutics– poxvirus oncolytics. Poxviruses are the ideal backbone for development of oncolytic agents since they have a broad tumour tropism, they destroy cells rapidly, they do not require defined surface receptor for entry, they have a large cloning capacity, and they replicate entirely in the cytoplasm.[116] Some poxviruses are naturally tumour selective, like the leporipoxvirus Myxoma. The natural tumour selective nature of poxviruses is thought to be attributed to similarities between the hallmarks of cancer,[2] and the optimal replication conditions for poxvirus infection. Myxoma virus is a rabbitpox virus that can replicate in murine tumour cells based on disruption of the type I IFN response,[124] and in human tumour cells with elevated Akt levels.[125] Indeed, a number of

VACV vaccine strains have also demonstrated replication capability in human tumour cells.[126] Recent evidence identified that VACV targets cells with activated EGFR-Ras signaling,[127] yet another common feature of human tumour cells.[2] To ensure optimal safety and a high therapeutic index, some oncolytic poxviruses have been further manipulated genetically. Since tumour cells already harbour genetic mutations that confer the optimal cellular state for virus replication, a number of poxvirus virulence genes become dispensible for poxvirus replication in tumour cells. A number of deletions have been made to oncolytic vaccinia virus, like deletion of viral thymidine kinase (TK). Cellular TK is regulated by E2f transcription factors, and is normally expressed during the S phase during proliferation of normal cells.[128] In cancer cells, TK is constitutively expressed at high levels, irrespective of proliferation status.[129] Another strategy to increase the therapeutic index of oncolytic VACV is the deletion of viral VGF or vaccinia growth factor. VGF is a secreted EGF homologue capable of binding to cellular EGFR.[130] VGF-deletion mutants have increased tumour selectivity as they depend on cancer cell activation of the EGFR pathway.[116]

An oncolytic VACV is currently in Phase II human clinical trials for the treatment of hepatocellular carcinoma. The clinical candidate is termed JX-594, a Wyeth strain engineered with inactivated thymidine kinase, and expressing human GM-CSF.[67] In a Phase I trial of intra-tumoural (IT) treatment of liver tumours, JX-594 was well tolerated and associated with tumour destruction.[131] Recently, JX-594 was shown to infect metastatic tumours in cancer patients following intravenous delivery,[67] demonstrating the tumour targeting capabilities of oncolytic poxviruses. Although VACV is the only poxvirus in clinical development, pre-clinical studies have highlighted the potential of other poxvirus OVs.[125,132]

1.4.3 Parapoxvirus, ORFV

ORFV is the prototypic species of the *Parapoxvirus* genus. ORFV has a worldwide distribution and causes acute dermal infections in its natural ungulate hosts: goat and sheep.[133] The ORFV 139kbp genome has been completely sequenced,[134] and contains 132 putative genes. Although its genome is smaller than that of VACV, their genomes are co-linear in order, spacing and orientation of homologous genes.[134] More than 88 of the ORFV genes share homology with all other *Chordopoxviruses*,[134] and ORFV has at least 31 genes with no homology to any other poxvirus.[135] ORFV infections are initiated and maintained in damaged skin, where the virus replicates in regenerating epidermal cells.[136] ORFV can also cause a benign infection in man if an animal with an infectious lesion on its mouth bites and breaks the skin.

Members of the *Parapoxvirus* genus have a number of unique features that distinguish them from other poxvirus species. By electron microscopy, ORFV particles are ovoid in shape, with a unique criss-cross pattern of spiral tubules wrapped around an inner amorphous core.[137] Unlike most members of the poxvirus family, the *parapoxvirus* genome has an unusually high G+C content, and virions are smaller.[138] These characteristics suggest a significant divergence from other poxvirus genera.[138] *Parapoxvirus* morphogenesis has not been described in detail, however a recent study by Tan *et al*. revealed that not unlike VACV, ORFV particles exist in one of two forms (intracellular versus extracellular virions), where only a minority of virus particles egress from cells as extracellular virions.[137] In search of a receptor that mediated ORFV infection, Scagliarini and colleagues examined heparan binding activity of ORFV surface proteins.[139] These studies revealed that ORFV F1L (homologue to VACV H3L) is capable of binding to cellular heparan sulfate surface receptors. Heparan sulfates are a ubiquitous member of the glycosaminoglycan family, or

GAGs.[140] Since GAGs are exposed on cell surfaces of all mammalian cells, ORFV F1L binding to GAGs via heparan sulfate was proposed to be the mechanism by which ORFV is capable of binding to a wide range of tisses of non-permissive species.[139]

In common with other poxviruses, ORFV expresses a variety of immune-modulating and host range genes. ORFV expresses a homologue of mammalian IL-10, with 80% amino acid identity to the ovine polypeptide.[141] IL-10 is a multi-functional cytokine that is involved in suppressing inflammation, and anti-viral T_h-1 effector functions.[142] In common with *orthopoxviruses* and *leporipoxviruses*, members of the *Parapoxvirus* genus also express a chemokine binding protein.[143] This protein was found to bind to both CC inflammatory cytokines, and C chemokine lymphotactin chemokines.[143] ORFV also expressed a GM-CSF/IL-2 inhibitory factor, which is unique to the *Parapoxvirus* genus.[144] ORFV also expresses virulence factors associated with IFN-resistance[145] and preventing apoptosis.[146] The lesions caused by ORFV infection show an accumulation of vascular endothelial cells that lead to the recruitment of blood vessels at the site of infection. Dr. Mercer at the University of Otago in New Zealand attributed this observation to the virus's expression of vascular endothelial growth factor (VEGF).[147] Expression of VEGF-like factors is unique to members of the *Parapoxvirus* genus. Members of the mammalian VEGF family regulate the formation of new blood vessels and the leakiness of blood vessels.[148] ORFV lesions resulting from infection with a VEGF-deleted ORFV lack extensive dermal vascularization, have a reduced pathology and clear sooner when compared to wild-type lesions.[147] By definition then, ORFV VEGF is a virulence factor. Although naïve to the cancer therapeutic field, the ORFV replicating 'niche' is an isolated regenerative wound with an extensive vasculature, much like a tumour micro-environment.[147]

1.4.4 ORFV as a Potential Cancer Therapeutic

Characterization of ORFV biology and pathogenesis in its natural host has led to a detailed description of the virus' interaction with the host immune system. These studies have revealed that ORFV possesses a number of unique qualities that make it perfectly suited for the development of *parapoxviruses* as anti-viral vaccines. Some of these features include its safety profile, its restricted host-range, and its 'exceptionally strong' induction of inflammation and the innate immune system.[149] Primarily based on the observation that natural infections with ORFV lead to a massive accumulation of DCs within lesions,[150] biotechnology companies became interested in the use of ORFV as an innate immune modulator. These natural characteristics have earned ORFV the nickname -'paraimmunity inducer', and have been harnessed in the biotechnology sector as an inactivated form of ORFV is currently approved in veterinary medicine.[151] A number of recombinant ORFV vaccines have been developed as anti-viral vaccines for a number of veterinary applications, in both permissive and non-permissive hosts.[152,153] Recombinant *parapoxviruses* have demonstrated anti-viral activity against lethal alphaherpes virus infection of swine, and pseudorabies virus infection of mice.[149] Through expression of nucleoprotein p40 from Borna disease virus, recombinant ORFV protected animals from lethal infection in the brain in a non-permissive host species.[154]

The same qualities that make ORFV an ideal anti-viral vector may similarly be harnessed for the development of new cancer biotherapies. In contrast to zoonotic *orthopoxviruses*,[155] human ORFV infections do not lead to serious disease.[156-158] ORFV treatment leads to a potent induction of a T_h-1 dominated immune response involving accumulation of $CD4^+$ and $CD8^+$ T cells, B cells, NK cells, neutrophils, and DCs,[159-161] and cytokines including IL-1β, IL-8, GM-CSF, IL-2, and IFN-γ.[161-163] Interestingly, these robust

immune responses are associated with the viral particle itself, since numerous data have shown immune stimulation by inactivated ORFV in a number of different species,[161,164-166] including humans.[161,167,168] Importantly, the immune stimulation has been compared to other poxviruses, and in all cases the immune stimulatory profile is unique to ORFV.[161,169,170] In addition, in contrast to cytokine therapies, ORFV T_h-1 immune-stimulation is regulated by subsequent up-regulation of T_h-2 cytokines like IL-4 and IL-10.[168,169] An ORFV platform may be superior for development of anti-cancer agents, since *parapoxvirus* researchers have described re-occurring infections in animals as a result of a very short-lived duration of the ORFV-specific immunity.[155,156] Although antibody production after ORFV infection is normal, antibody appears to play little to no role in protection upon re-infection, and neutralizing antibody is rare.[156,171,172] In the context of foreign antigen-expressing ORFV vector vaccines, antigen-specific humoral immunity has been demonstrated even in the face of pre-existing ORFV immunity.[149] This is unique to ORFV, since pre-existing VACV specific immunity often results in poor foreign antigen-specific humoral responses.[173,174] Finally, as a member of the poxvirus family, ORFV may have natural tumour cell replication potential, as has been described for vaccinia, myxoma, and raccoonpoxvirus.[67,132,175]

1.4 RATIONALE, HYPOTHESIS AND OBJECTIVES

Rationale

Replicating viruses for the treatment of cancer offer many benefits to traditional chemotherapeutic or immunotherapeutic drugs: they are targeted, safe, they offer a self-amplifying dose, they are immune-stimulating, and they can be genetically modified to carry therapeutic genes. Poxviruses have a long history as safe and effective vaccine vectors, where some have demonstated natural or engineered capacity for tumour selective

replication. Although naïve to the cancer therapeutic realm, ORFV may have natural tumour targeting abilities, as the ORFV replicative 'niche' is an isolated wound with an extensive vasculature, much like a tumour micro-environment. ORFV as a vector for cancer therapy may have advantages over other anti-cancer therapies, based on ORFV's unique immune stimulation profile, its limited pathogenicity in humans and the fact that the majority of the population has had little to no contact with the virus, and will therefore have no pre-existing immunity to impede its use as a therapeutic.

Hypothesis

ORFV will have natural anti-tumour properties mediated by direct oncolysis of tumour cells and/or induction of an anti-tumour immune response.

Objectives

1. Develop methods and models to test ORFV anti-cancer potential
2. Characterize the *in vitro* and *in vivo* ORFV anti-cancer efficacy
3. Determine the mechanism of ORFV anti-cancer activity

CHAPTER 2 METHODS

Cell lines.

Human and murine cell lines were maintained in Dulbecco's Modified Eagle Medium (DMEM) (HyClone) supplemented with 10% fetal calf serum (FCS) (PAA Laboratories, Etobicoke, Ontario, Canada), and grown at 37°C and 5% CO_2. B16F10-LacZ cells were generated by stable transfection with LacZ complementary DNA, as described earlier.[176]

Human tumour cell lines were from the NCI-60 reference panel: A549, HeLa, M14, OVCAR-8, 91304, PC3, U251, SNB19, MDAMD-435, HCT116, NCI-H23, Caski, SCC25, MCF-7, HT1080, PLC/PRF/5, SF295, SMKEL-3, SKMEL-28, C41, SW620, SF268, ME180, UACC62, SKMEL-2, HOP62, HOP92, U2OS, Cal27, 786-0, HT29, and SCC9. CT26.CL25 (CT26-LacZ), CT26, B16F10, 293T, YAC-1 and OA3.Ts were purchased from ATCC (Manassas, VA). HDFn cells were purchased from Cascade Biologics (Burlington, Canada).

Viruses.

Wild type ORFV strain NZ2 and ΔVEGF-ORFV (VEGF-deleted LacZ-expressing ORFV) strain NZ2[147,177] were obtained from Dr. Andrew Mercer (University of Otago, New Zealand). Oncolytic VAVC, RCNV and MYXV have been described previously.[132] Ad-GFP was kindly provided by Dr. Brian Lichty at McMaster University.[178]

ORFV production, UV inactivation and titering.

Viral stocks were prepared by infection of confluent OA3.Ts at an MOI of 0.05. Cells and supernatants were harvested following a 5 day infection at 37°C, 5% CO_2 by gentle cell scraping. Cell lysates were collected by centrifugation, and re-suspended in 1 mM TRIS pH 9.0, and subjected to 3 freeze-thaw cycles. Cell debris was removed by centrifugation, and lysates dounce homogenized prior to sucrose cushion purification (40%) in a JS-13.1 rotor at 11,500 RPM for 1.5 hours at 4°C. Virus stocks were re-suspended in PBS. Sham infected OA3.Ts were processed as described above, and were used as vehicle control treatments. Inactivation of virus was performed on ORFV preparations at a concentration of 10^8 pfu/mL in PBS using UVC irradiation in the Spectrolinker XL-1000 UV crosslinker (Spectronics Corporation) for 300 seconds. Confirmation of virus inactivation was measured by plaque

assay prior to use. ORFV was titered on confluent monolayers of OA3.Ts using a carboxymethylcellulose (CMC) overlay. Plaques were visualized following a 7-day incubation at 37°C by removal of overlay, and staining with 1% crystal violet (in 80% methanol). VEGF-deleted, LacZ-expressing ORFV (ΔVEGF-ORFV) plaques were visualized using a β-galactosidase-containing stain solution, as described previously.[179]

Animals.

Female 6 to 8 week-old C57Bl/6, Balb/c and CD-1 nude mice were supplied by Charles River Canada (St. Constant, Canada), and were housed in a level 2 biocontainment facility at the Animal Care and Veterinary Services within the University of Ottawa. CD11c-DTR transgenic C57Bl/6 mice have been previously described,[180] and were kindly donated by Dr. Yonghon Wan (McMaster University, Hamilton, Canada). All animal experiments were conducted in accordance with the Animal Care and Veterinary Services standard operating procedures.

***In vitro* viral infections**.

Viability assays were used to compare cell death induced by WT ORFV and ΔVEGF-ORFV at MOIs 0.1 and 1 at 72 hours post infection. Briefly, the indicated tumour cells were prepared in 6-well dishes, and confluent monolayers were infected (or mock-infected) in a 200 μL volume of serum-free medium for 2 hours at 37°C and 5% CO_2 followed by an addition of 2 mL of DMEM containing 10% FBS. At 72 hours post-infection, cells were collected by trypsinization, re-suspended in an equal volume, and the cell viability assessed via Trypan blue exclusion using the Vi-CELL instrument, Beckman Coulter (Mississauga, Canada). Data are presented as the percent viable tumour cells, normalized to the mock-infected control wells for each cell line. The cytotoxicity induced by WT ORFV on B16F10-

LacZ and CT26-LacZ tumour cells was assessed in 96-well plates, using alamarBlue® (AbD Serotec, Raleigh, NC) after a 72 hour infection period. For growth curve analysis, confluent monolayers of cells were infected in a minimal volume of serum free media for 1 hour at 37°C and 5% CO_2. The viral inoculum was then removed, and replaced with DMEM 10% FCS. Cells and supernatants were harvested from wells at 0, 12, 24, 48, 72, and 96 hours post infection. Cell lysates were subjected to 3 freeze-thaw cycles, and titered on OA3.Ts.

***In vivo* tumour models**.

To determine the maximum tolerable dose of WT ORFV and ΔVEGF-ORFV, Balb/c animals were treated once with the indicated virus, at the indicated dose by an intravenous (IV) or intraperitoneal (IP) route of delivery. Animals were monitored for weight loss and signs of distress, and were euthanized at endpoint. For the Balb/c CT26 sub-cutaneous tumour experiment, animals were challenged subcutaneously with $3x10^5$ CT26 cells in the right flank, and were treated intra-tumourally (IT) with 2 doses of 10^7 plaque forming units (pfu) of WT ORFV, ΔVEGF-ORFV or control treated (50 μL of PBS) on days 15 and 20 post tumour implantation. For CD-1 nude xenograft experiments, $2x10^6$ A549 cells were injected subcutaneously into the right flank of mice. At 23 days post-implantation, mice were treated IT with 5 doses of 10^7 ORFV or PBS control. Sub-cutaneous tumours were measured 2-3 times per week using digital calipers. Animals were sacrificed when tumour burden reached a volume of 1500 mm^3. For murine lung models, 10^5 CT26-LacZ cells were injected IV into Balb/c or CD-1 nude mice. Similarly, $3x10^5$ B16F10-LacZ cells were injected IV into C57Bl/6 mice. Mice were then treated IV (unless otherwise indicated) with 1 to 3 doses of ORFV in 100 μL of PBS, or control treated (100 μL of PBS or sham infected lysates), on days 1, 3, and/or 8. Poly IC (Sigma, Oakville, Canada) treatments were delivered IP at a dose

of 150 μg. At 10 days post CT26-LacZ injection, and 14 days post B16F10-LacZ injection, mice were euthanized with Euthanyl, and lungs were harvested and stained with a β-galactosidase solution.[181] The number of lung metastases was determined by separation of lung lobes, and enumeration under a dissection microscope (Leica, Richmond Hill, Canada). For analysis of internal lung metastases, fixed lung tissues were embedded in formalin, sectioned, and stained with hematoxylin and eosin. Internal lung metastases were enumerated in a blinded fashion using an Aperio ScanScope and ImageScope software. Images were captured using Aperio ScanScope (Axiovision Technologies). For lung model survival experiments, animals were treated IV with 3 doses of 10^7 pfu ORFV or 100 μL of PBS, and were monitored for signs of respiratory distress.

Tissue distribution experiments.

Organs were harvested from animals at specified time-points post infection. Tissues were first homogenized, and subjected to 3 freeze/thaw cycles prior to OA3.Ts plaque assay. To allow visualization of plaques at the lowest dilution in the presence of tissue debris, plaques were quantified using an β-galactosidase containing staining solution.[179] The pathology of lung tissues following ORFV therapy was analyzed from CT26-LacZ tumour-bearing Balb/c mice (N=2) treated with PBS or 10^7 ORFV IV at 24 hours. At 72 hours, animals were sacrificed, and lungs isolated, fixed and embedded in paraffin. Hematoxylin and eosin stained sections of lung tissues were examined by a pathologist in a blinded fashion. Images were captured using Aperio ScanScope (Axiovision Technologies) and analyzed using an Aperio ImageScope software.

Cell depletion tumour models.

NK cell depletion experiments were performed using an optimized dose and schedule of Anti-Asialo GM-1 (Cedarlane, Burlington, Canada), or Rat IgG1 κ isotype control (BD Bioscience, Mississauga, Canada): 25 μL IV on days -4, -1, 2, 6, 9, and 13 where cancer cell injection and first ORFV treatment occur on days 0 and 1, respectively. NK cell depletion was confirmed at day 0 (prior to experiment start) in both C57Bl/6 and Balb/c mice. To allow for similar tumour burden in animals treated with the NK depleting antibody, the challenge dose of B16F10-LacZ and CT26-LacZ was reduced in the NK depleted animals to $9x10^4$ and $5x10^4$, respectively. $CD4^+$ and $CD8^+$ T cells were depleted in Balb/c mice using reagents and dose regimes established previously.[182] DC depletion was accomplished by treatment with 100 ng of diphtheria toxin (DT) (Sigma, Mississauga, Canada) IP to CD11c-DTR transgenic C57Bl/6 mice.[180]

Surgical stress model.

C57Bl/6 mice were first treated with PBS, Poly IC or ORFV. At 4 hours post treatment, animals were challenged IV with $3x10^5$ B16F10-LacZ cells. Immediately following tumour challenge, animals were anesthesized for surgery with 2.5% Isofluorance (Baxter Corporation, Mississauga, Canada). Surgical stress was induced by a left nephrectomy. Animals were treated for pain control as per standard procedures established at the University of Ottawa, including doses of bupernorphine (0.05 mg/Kg) administered subcutaneously beginning the morning of surgery, and every 8 hours post surgery. At 3 days post tumour challenge, animals were euthanized, and tissues were processed for flow cytometry (spleen) or evaluation of lung tumour burden (lung).

Flow cytometry.

Murine immune cells were isolated from the spleen, blood, and lung of animals in a similar fashion. Briefly, splenic lymphocytes were isolated by pressure filtration through a 200 μm filter, and red blood cells removed by cell lysis using ACK buffer (0.15 mol/l NH_4Cl, 10 mmol/l $KHCO_3$, 0.1 mmol/l Na_2EDTA) for 5 minutes at room temperature. Saphenous or terminal cardiac puncture were used to isolate blood from mice using EDTA collection tubes. Blood lymphocytes were isolated following 2 cycles of red blood cell lysis with ACK buffer. Lung lymphocytes were isolated by tissue digestion in 10 mL of RPMI 1640 supplemented with 2% FBS, penicillin and streptomycin (Invitrogen, Burlington, Canada), and 10 μg/mL Type IV collagenase (Roche Diagnostics, Montreal, Canada) for 30 minutes at 37°C. Digested lung tissue was then passed through a 40 μM filter, and centrifuged at 300 g for 7 minutes at 4°C. Lung tissues were resuspended in 1 mL of 67.5% Percoll (Sigma, Mississauga, Canada) and transferred to a 15 mL tube. An additional 2 mL of 67.5% Percoll was layered on top of the tissues. An additional 2 mL of 45% Percoll was then overlayed onto the cell suspension. The mixture was centrifuged at 800 g for 15 minutes at room temperature, with the brake and acceleration option at a minimum. Following centrifugation the lymphocyte band was removed, and subjected to a 5 minute red blood cell lysis using ACK buffer. Purified lymphocytes from spleen, blood, or lung were enumerated, and transferred to round bottom, 96-well plates for flow cytometry at a concentration of $2x10^6$ cells per well. For intracellular cytokine analysis, cells were subjected to a GolgiPlug incubation for 5-10 hours, as indicated. (BD Bioscience, Mississauga, Canada). The following antibodies were used to analyze immune cell populations by flow cytometry: CD49b-PE (Clone DX5), CD3-PE (Clone 17A2), CD8-PECy5 (Clone 53-6.7), CD69-FITC (Clone H1.2F3) NK1.1-PE (Clone PK136), Granzyme B-AF700 (Clone GB11), CD11c-

PECy7 (Clone N418), CD80-PE (Clone 16-10A1), CD86-PE (Clone GL-1), CD40-PE-Cy5 (1C10), NK1.1-APC, (PK136), NKG2D-PE (CX5), IL-12-APC (Clone C15.6) and IFNγ-AF647 (Clone XMG1.2) from BD Biosciences, Mississauga, Canada, CD11c-FITC (Clone N418), and TNFα-FITC (Clone MP6-XT22) from eBioscience, San Diego, CA), and CD3-PerCP (Clone 17A2, R&D systems, Minneapolis, MN). Experiments were performed on a Beckman Coulter CyAn and data analyzed using Kaluza software (Beckman Coulter, version 1.1).

NK cytotoxicity assays.

Splenocytes were isolated from tumour naïve ORFV or PBS treated C57Bl/6 mice at time-points post infection. Isolated lymphocytes were pooled, and DX5-sorted (DX5 positive selection Kit, Miltenyi Biotec, Auburn, CA) on an Automacs Pro cell sorter (Miltenyi Biotec). B16F10-LacZ cells were harvested and labeled with Chromium-51 (Perkin Elmer, Waltham, MA) in the form of Na_2CrO_4 at 100 μCi for 60 minutes at 37°C. Sorted NK cells were re-suspended at a concentration of $2.5x10^6$ cells/mL were mixed with target B16F10-LacZ, which were re-suspended at a concentration of $5x10^4$ cells/mL, at different effector to target ratios (50:1, 25:1, 12:1, 6:1). The mixture was incubated for 4 hours prior to analysis of chromium release in the supernatant using a gamma counter (Perkin Elmer).

***Ex vivo* infection of immune cells**.

Natural killer cells were isolated from the spleens of C57Bl/6 mice by negative selection using magnetic sorting and the NK Isolation Kit (Miltenyi Biotec, Auburn, CA). NK cells were supplemented with human recombinant IL-2 at 50 μg/mL (Sigma, Oakville, Canada) and were used immediately in *ex vivo* infection experiments. Bone marrow was isolated from the leg bones of C57Bl/6 mice using procedures described previously.[183] Briefly the femur

and tibia were isolated, and using a 25 gauge needle and 5 mL syringe, the bone marrow was flushed with PBS. Bone marrow was passed through a 40 μM filter, centrifuged at 300 g for 7 minutes at 4°C, and red blood cells removed following a 5 minute ACK lysis. Cells were seeded at a density of $2x10^6$ cells/mL in RPMI 1640 containing 10% FCS, 50 μM 2-mercaptoethanol, (Invitrogen, Burlington, Canada) penicillin and streptomycin. Cells were incubated overnight at 37°C, 5% CO_2. The next day, non-adherent cells were collected, enumerated, and seeded at a density of 10^6 cells/mL in RPMI 1640 containing 50 μM 2-mercaptoethanol, antibiotics, and 10 ng/mL recombinant murine GM-CSF (R & D Systems, Minneapolis, MN). At day 3 of culture, 2 mL of media containing fresh cytokine was added to each 10 cm plate. At day 6 cells, non-adherent and loosely adherent cell clusters were harvested for analysis. NK cells and DCs were plated in 6 well plates, and subjected to ORFV infection at the indicated MOI, for 24 hours prior to analysis by flow cytometry. Alternatively, NK cells were treated with Poly IC (Sigma, Oakville, Canada) at a dose of 50 μg/mL or 200 μg/mL and DCs were treated with CpG ODN 1826 (InvivoGen, Burlington, Canada) at a concentration of 10 μg/mL.

CHAPTER 3 EVALUATING THE ONCOLYTIC POTENTIAL OF A VEGF-DELETED ORFV

3.1 INTRODUCTION

It has been proposed that poxviruses as a class may be naturally designed for tumour selective replication based on their biology and complementing mutations commonly found in cancer cells.[116] The very hallmarks of cancer,[2,7] (blocks in apoptotic signaling, immune evasion and deregulated cell cyle control) bestow cancer cells with the ideal cellular conditions for productive poxvirus infection. Indeed a number of poxviruses have been noted

for their ability to replicate in and lyse tumour cells, including animal viruses like myxoma that have a distinct and limited host range.[124,125] In the literature, it has only been documented that ORFV can productively infect primary cell cultures prepared from normal bovine testis.[147,184] As a member of the poxvirus family, I proposed that in its wild-type form, ORFV may have natural tumour replication potential.

Lesions caused by ORFV infection are always initiated and maintained in wounded skin. Additionally, ORFV expresses a homologue of mammalian vascular endothelial growth factor, (VEGF). Termed VEGF-E, ORFV VEGF has been classified as a unique isoform of the VEGF family, based on its unique receptor recognition: VEGF-E is only bound by VEGFR-2.[148] Members of the VEGF family regulate the formation of new blood vessels via control of angiogenesis, endothelial cell proliferation, and vascular permeability through binding to one of three tyrosine kinase receptors.[185] VEGF-E is only capable of binding VEGFR-2, which is primarly involved in vascular endothelial cell mitogenesis.[185] Driven by the hypoxic tumour microenvironment, angiogenic factors like VEGF and its receptor are often over-expressed in tumours, (reviewed by Goel *et al*.).[186] Angiogenesis is a normal process that is involved in wound healing, where the process is tightly regulated.[187] In tumours however, the desperate need to maintain a blood supply results in highly abnormal vascular networks. By comparison then, Dvorak *et al*. described tumours as "wounds that do not heal".[187] Since ORFV infections are initiated in wounds, where the concentration of growth factors is likely to be high, the ORFV replicative niche is much like a tumour micro-environment. The vascular nature of ORFV lesions therefore provides further evidence that ORFV may naturally target tumours.

Although some wild-type poxviruses have shown tumour selective replication in the absence of toxicity in pre-clinical models,[175] it was unclear if wild-type ORFV would have a

similar safety profile. To test the contribution of VEGF to ORFV virulence in its natural host, a recombinant ORFV was created in which the VEGF gene was deleted. Interestingly, viral replication was similar to lesions caused by wild-type ORFV during early times post infection, but was reduced later in the infection cycle.[147] Importantly, a VEGF-deleted ORFV demonstrated reduced vasculature responses in the lesions of infected sheep compared to wild-type ORFV.[147] These studies implicated VEGF as an ORFV virulence factor. Since it was reported that VEGF expression might be important for maintaining a regenerative response important for sustaining virus replication, I hypothesized that this gene might be dispensable for ORFV replication in tumours. By first establishing methods for the production, and quantification of ORFV, I aimed to identify cancer models that would allow me to evaluate the anti-cancer potential of the virus. These experiments were performed with both wild-type and VEGF-deleted ORFV, to determine which backbone should be chosen for further studies based on their safety profile, and *in vitro* and *in vivo* oncolytic potential.

3.2 RESULTS

ORFV can productively infect HeLa and OA3.T.s cells

Methods were first established for the production and quantification of ORFV. The ability of ORFV to replicate productively in primary goat endothelial cells (OA3.Ts) and human adenocarcinoma cells (HeLa) was determined at both 33°C and 37°C. Multistep growth curve analysis revealed that Wild Type ORFV could productively infect both cell lines, with maximal virus production at 5 days, at 37°C (**Fig. 3.1a**). The amount of virus recovered from HeLa and OA3.Ts cell lysates was determined before and after 2 freeze thaw

a.

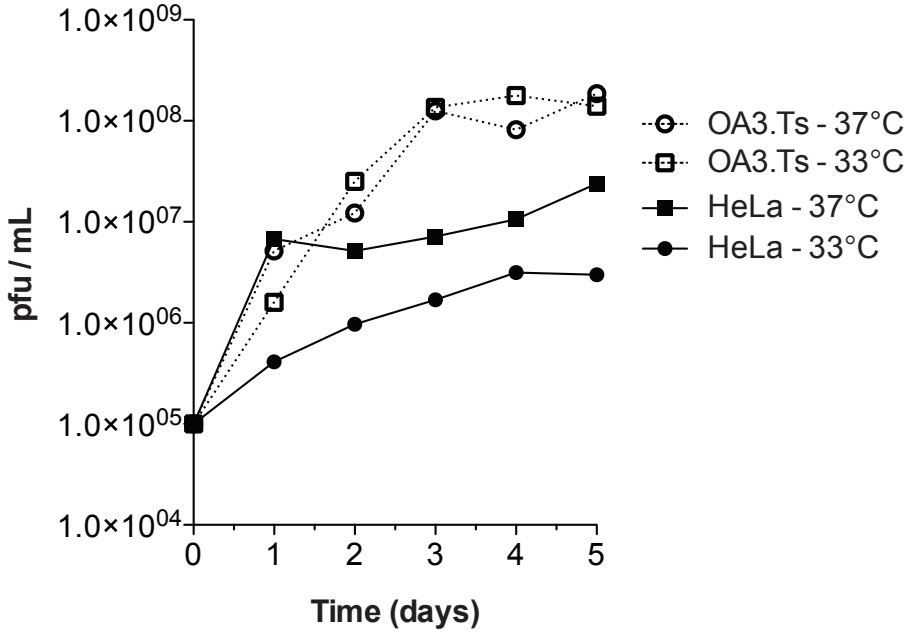
1.0×10^09
1.0×10^08
1.0×10^07
1.0×10^06
1.0×10^05
1.0×10^04
pfu / mL
0
1
2
3
4
5
Time (days)
OA3.Ts - 37°C
OA3.Ts - 33°C
HeLa - 37°C
HeLa - 33°C

b.

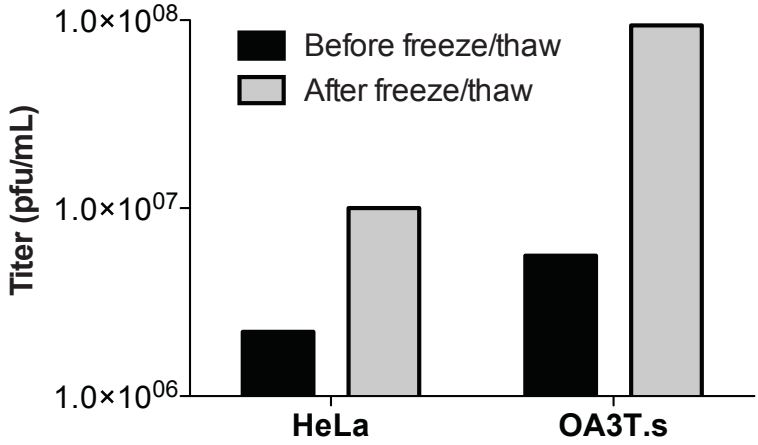
1.0×10^08
1.0×10^07
1.0×10^06
Titer (pfu/mL)
Before freeze/thaw
After freeze/thaw
HeLa
OA3T.s

c.

Figure 3.1 Methods developed for the production, and quantification of ORFV (a) ORFV replication was evaluated on HeLa and OA3.Ts cells at 33°C and 37°C by multistep growth curve analysis at an MOI of 1 (N=1). (**b**) ORFV titer was evaluated before and after two freeze/thaw cycles of HeLa or OA3.Ts ORFV cell lysates, (N=1). (**c**) Crystal violet stained OA3.Ts cells of a log dilustion series ORFV plaque forming assay after a 7-day incubation. pfu, plaque forming unit.

cycles at 5 days post infection. For both cell lines, freeze thaw cycles of infected cell lysates increased the overall ORFV yield (**Fig. 3.1b**). To allow for quantification of ORFV, an OA3.Ts plaque assay was developed, where virus plaques become visible by crystal violet staining following a 7-day incubation (**Fig. 3.1c**).

***In vitro* and *in vivo* comparison of Wild Type and ΔVEGF-ORFV**

The cell killing ability of Wild Type ORFV and ΔVEGF-ORFV was compared *in vitro* on a panel of human cancer cell lines (**Fig. 3.2**). Wild Type and ΔVEGF-ORFV performed similarly across the cell panel, (no significant differences were observed). Although both viruses induced significant cell death at an MOI of 1, very little cytotoxicity was observed at an MOI of 0.1. To evaluate the *in vivo* toxicity of these viruses, maximum tolerable dose (MTD) experiments were performed in a tumour free, Balb/c model (**Fig. 3.3**). The maximum tolerable dose for both viruses was determined to be $2x10^7$ pfu, intraperitoneally, and $1x10^7$ pfu intravenously. The maximum tolerable dose therefore is also the maximum feasible dose. At the MTD dose of Wild Type and ΔVEGF-ORFV, animals showed no sign of weight loss, or fever. To evaluate and compare the *in vivo* anti-tumour potency of Wild Type and ΔVEGF-ORFV, a subcutaneous CT26 tumour model was employed (**Fig. 3.4**). Multistep growth curve analysis revealed that Wild Type ORFV was able to productively infect CT26 cells *in vitro* (**Fig. 3.4a**). However when these cells were implanted into Balb/c animals, 2 intratumoural treatments of virus were not sufficient to significantly extend survival (**Fig. 3.4b**). The persistence of ORFV infection of the CT26 subcutaneous tumours was evaluated when tumors reached a volume of 1500 mm^3. Very little virus was recovered from these tumours (**Fig 3.4c**). An intravenous lung tumour model was also used to evaluate the potential anti-cancer properties of ORFV. A schematic outlining the dose regime is illustrated in **Fig. 3.5a**. Animals were challenged intravenously

a.

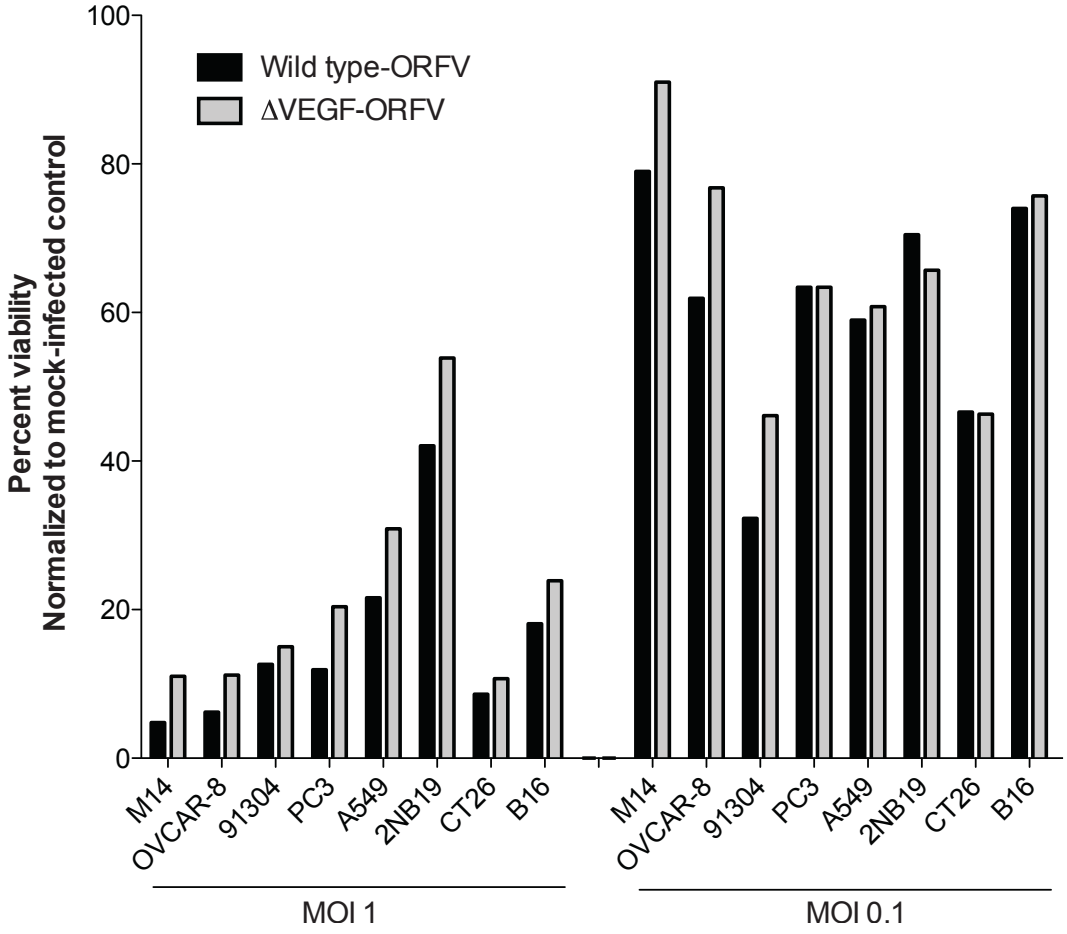
Wild type-ORFV
ΔVEGF-ORFV
Percent viability
Normalized to mock-infected control
100
80
60
40
20
0
M14
OVCAR-8
91304
PC3
A549
2NB19
CT26
B16
M14
OVCAR-8
91304
PC3
A549
2NB19
CT26
B16
MOI 1
MOI 0.1

Figure 3.2 *In vitro* comparison of Wild Type versus ΔVEGF-ORFV tumour cell killing (**a**) Trypan blue dye exclusion was used to evaluate Wild Type and ΔVEGF-ORFV tumour cell killing at 72 hours post infection at an MOI of 1 and 0.1. No significant differences were observed using a two tailed *t*-Test. MOI, multiplicity of infection.

a.

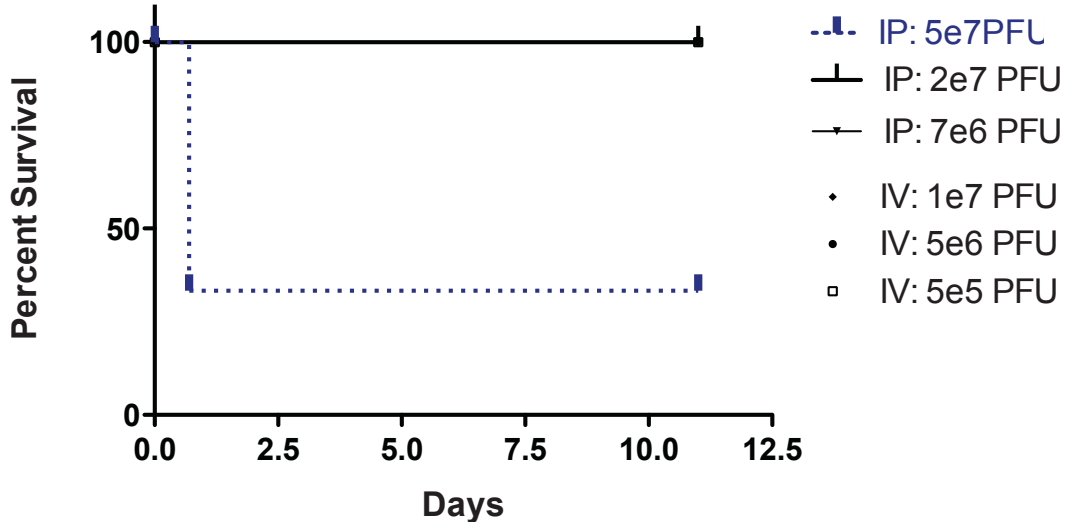
Percent Survival
100
50
0
0.0
2.5
5.0
7.5
10.0
12.5
Days
IP: 5e7PFU
IP: 2e7 PFU
IP: 7e6 PFU
IV: 1e7 PFU
IV: 5e6 PFU
IV: 5e5 PFU

b.

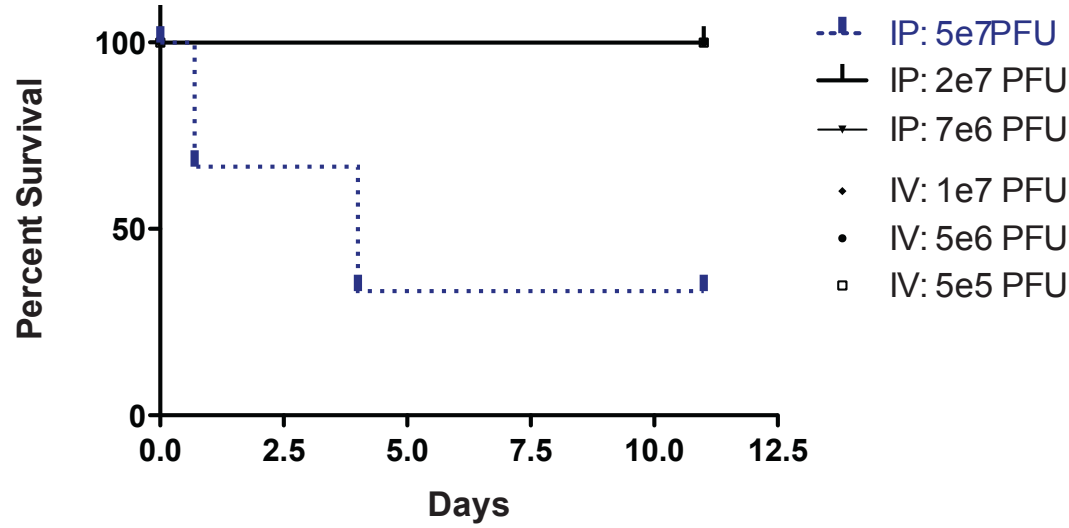
Percent Survival
100
50
0
0.0
2.5
5.0
7.5
10.0
12.5
Days
IP: 5e7PFU
IP: 2e7 PFU
IP: 7e6 PFU
IV: 1e7 PFU
IV: 5e6 PFU
IV: 5e5 PFU

Figure 3.3 *In vivo* comparison of Wild Type versus ΔVEGF-ORFV toxicity (**a**) Evaluation of the maximum tolerable dose of Wild Type ORFV by IP or IV route of delivery, (N=5) (**b**) Evaluation of the maximum tolerable dose of ΔVEGF-ORFV by IP or IV route of delivery, (N=5). IP, intraperitoneal; IV, intravenous.

a.

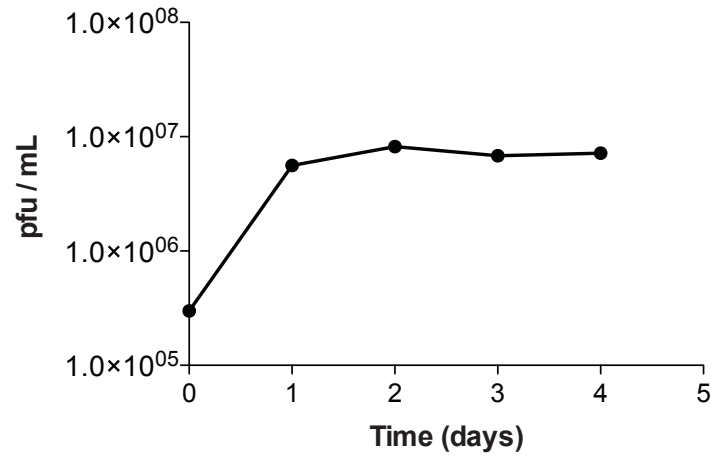
1.0×10^08
1.0×10^07
1.0×10^06
1.0×10^05
pfu / mL
0
1
2
3
4
5
Time (days)

b.

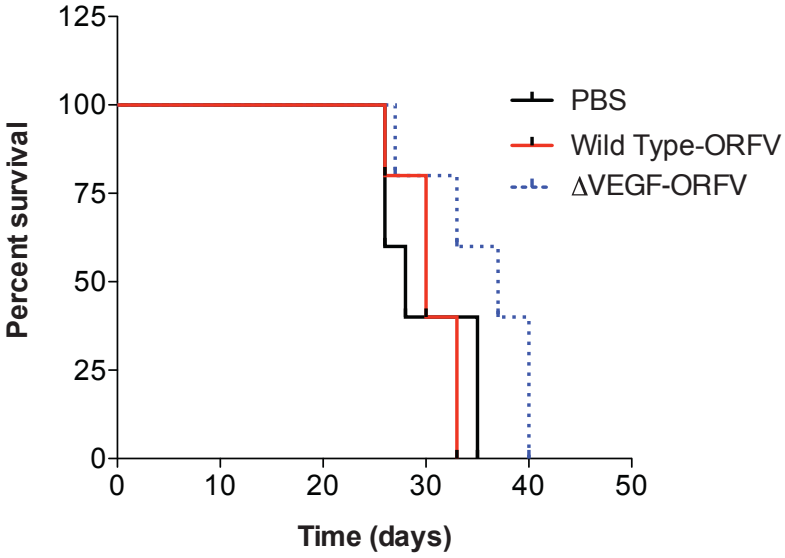
125
100
75
50
25
0
Percent survival
0
10
20
30
40
50
Time (days)
PBS
Wild Type-ORFV
ΔVEGF-ORFV

c.

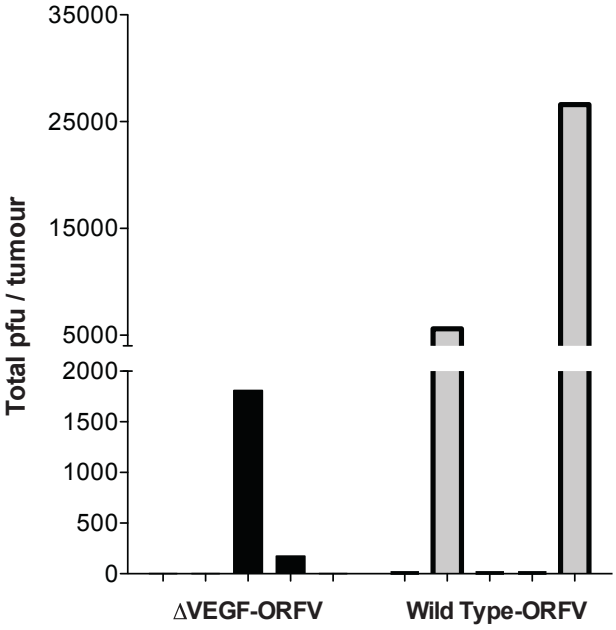
35000
25000
15000
5000
2000
1500
1000
500
0
Total pfu / tumour
ΔVEGF-ORFV
Wild Type-ORFV

Figure 3.4 *In vivo* comparison of Wild Type versus ΔVEGF-ORFV efficacy in a CT26 subcutaneous murine model of cancer (**a**) *In vitro* Wild Type ORFV replication was evaluated on CT26 cells by multistep growth curve analysis at an MOI of 1. (**b**) Percent survival of Balb/c animals challenged with a subcutaneous CT26 tumour was evaluated following 2 intratumoural treatments with 10^7 pfu of Wild Type or ΔVEGF-ORFV, or PBS control. No significant differences were observed following a two-tailed *t*-Test. (**c**) Subcutaneous CT26 tumours were evaluated by plaque assay for the presence of Wild Type or ΔVEGF-ORFV when tumours reached a volume of 1500 mm^3 (N = 5). pfu, plaque forming units; PBS, phosphate buffered saline.

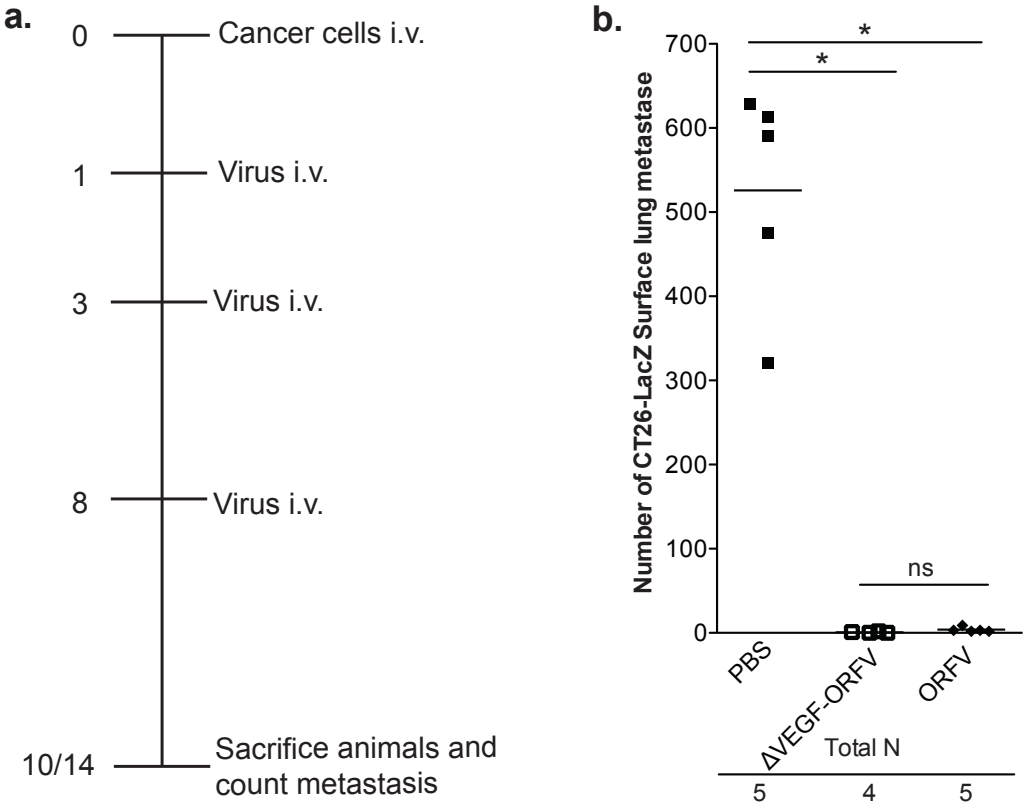
a.
0
Cancer cells i.v.
1
Virus i.v.
3
Virus i.v.
8
Virus i.v.
10/14
Sacrifice animals and count metastasis
b.
Number of CT26-LacZ Surface lung metastase
700
600
500
400
300
200
100
0
*
*
ns
PBS
ΔVEGF-ORFV
ORFV
Total N
5
4
5

Figure 3.5 Comparing ORFV efficacy in a lung model of cancer (**a**) Schematic outlining the treatment schedule (days) for the metastatic lung tumour models. (**b**) The number of surface lung metastases was evaluated from Balb/c animals challenged intravenously with CT26-LacZ cells and treated with 10^7 pfu of Wild Type ORFV, ΔVEGF-ORFV, or PBS control. Bars represent the mean for each group (*P <0.0001, using an unpaired t-Test with Welch's correction).

with CT26-LacZ-labeled tumour cells, and dosed intravenously with ORFV. At 10 days post challenge, lungs were harvested and processed using a β-galactosidase containing stain solution to visualize lung metastases. Surprisingly, both Wild Type, and ΔVEGF-ORFV significantly reduced the number of surface lung metastases in this model (**Fig. 3.5b**).

3.3 DISCUSSION

Since most groups have used primary bovine testis to propagate and titer ORFV,[147,184] I first aimed to establish new methods to efficiently manufacture and quantify the virus. Highlighted in **Figure 3.1**, I have shown that wild-type ORFV can productively infect primary sheep endothelial testis cells (OA3.Ts) and human cervical carcinoma cells (HeLa). Importantly, both of these cell lines are available through ATCC, and easily maintained in culture for up to 10 passages. Not unlike the manufacturing process for VACV, it was found that ORFV virions are cell associated, since freeze thaw cycles of cell lysates significantly increased the viral yield.

The safety and oncolytic potential of wild-type ORFV was compared to a VEGF-deleted ORFV (ΔVEGF-ORFV). In maximal tolerable dose experiments, the maximal tolerable dose was found to be the maximal feasible dose due to manufacturing limitations. Importantly, the same result was obtained for both virus strains, suggesting that neither virus is overly pathogenic to mice. This was not surprising, since several reports have documented ORFV's restricted host range, specifically highlighting mice as a non-permissive host.[149,153] In terms of oncolytic activity, *in vitro* comparison of human tumour infection did not reveal any obvious trends for enhanced activity by either virus. Similarly, *in vivo* comparison of ORFV activity in a sub-cutaneous tumour model demonstrated that despite modest replication in CT26 tumour cells, treatment with either virus was not capable of significantly

impacting overall survival. Based on a 'niche hypothesis', it was anticipated that a VEGF-deleted ORFV might be better suited for tumour infection and spread. Results from CT26 sub-cutaneous tumours revealed however that very little infectious ORFV was present at experiment endpoint, especially for the ΔVEGF-ORFV treated animals.

Interestingly, both wild-type and ΔVEGF-ORFV treatment significantly reduced tumour burden in an intravenous lung metastases model,[132] clearing almost all tumours from the lung. These data suggest that ORFV may have some natural anti-cancer potential, even in its wild-type form. As the first test of intravenous delivery of high-dose ORFV, the lack of pathogenecity in mice was encouraging, as it suggests that wild-type ORFV is a safe backbone for the development of anti-cancer therapeutics. This observation is supported by the fact that in contrast to zoonotic orthopoxviruses,[155] human ORFV infections do not lead to serious disease.[156-158] However, the lack of efficacy in the subcutaneous tumour model suggests that even in its wild-type form, ORFV may lack oncolytic potency. Attenuating ORFV mutations, such as VEGF-deletion may act to further cripple the oncolytic potency of ORFV. Therefore, as a well-tolerated and safe platform, wild type ORFV was chosen as a candidate vector for further characterization.

CHAPTER 4 ORFV: A NOVEL ONCOLYTIC AND IMMUNE STIMULATING PARAPOXVIRUS THERAPEUTIC

4.1 INTRODUCTION

Biological therapeutics for cancer constitute an exciting alternative or complement to conventional chemo- and radiotherapies. Replicating oncolytic viruses are particularly exciting as they have multiple features that can be exploited therapeutically. Although originally selected or engineered to directly infect and destroy cancer cells, there is

accumulating evidence suggesting that OVs are acting via a number of additional mechanisms including tumour vascular disruption,[71,73] and activation of innate[89,90] and/or adaptive anti-tumour immune responses.[188,189] An example of an OV with potent anti-tumour immune stimulating activity is the herpes virus-based OncoVex product that is engineered to express GM-CSF and has recently completed enrollment in a pivotal phase III human clinical trial.[74] The ability to stimulate innate and adaptive anti-tumour immune response has been identified as an important component of the therapeutic activity of several different oncolytic viruses, where some OVs have now demonstrated efficacy even in the absence of oncolytic activity.[84,89,90] These data, combined with the early clinical success of oncolytic viruses[67,74,188] have highlighted the potential impact of replicating viruses for the treatment of cancer. Inactivated preparations of ORFV have demonstrated robust immune stimulation in a number of animal species, including humans.[161,167,168] Interestingly, the anti-viral activity of inactivated ORFV is non-specific, since the immune stimlation does not depend on ORFV expression of viral antigen.[152] Furthermore, the immune stimulation is not restricted by ORFV's limited host range, and is not associated with any signs of inflammation or adverse effects.[152]

Considering ORFV's ability to stimulate the immune system, I sought to evaluate ORFV's anti-cancer potential in immune competent animals. My goal was to evaluate the mechanism of ORFV's anti-cancer activity, by determining the contribution of oncolysis, and immune stimulation. In following, I chose syngeneic murine tumour models that have been used to evaluate both oncolytic, and immunotherapy therapeutics.[132,181,190,191] I aimed to characterize the kinetics of ORFV efficacy, and evaluate its robustness compared to other replicating poxviruses. Since inactivated preparations of ORFV have demonstrated efficacy in a number of anti-viral models,[152,164,165] my goal was to compare live versus inactivated

preparations of ORFV. In this way my experimental approach has allowed me to delineate the mechanisms of ORFV anti-cancer activity and the benefit of using live replicating ORFV.

4.2 RESULTS

ORFV can reduce tumour burden in syngeneic lung models of cancer

The *in vivo* ORFV efficacy was further evaluated in syngeneic lung models of cancer. Using the treatment regime outlined in **Figure 3.5a**, representative images illustrate that ORFV treatment of C57Bl/6 animals leads to a significant reduction in B16F10-LacZ surface lung metastases (**Fig. 4.1a**). Lung tumour burden from animals treated with PBS was quantified and compared to mice treated with 1 dose (on day 1, 3, or 8), or 3 doses of ORFV (**Fig. 4.1b**). I found that even one dose of ORFV as late as day 8-post B16F10-LacZ challenge can significantly reduce tumour burden. Similarly, a Balb/c lung model was also tested and I found that ORFV treatment of CT26-LacZ lung tumour bearing animals led to nearly 100% reduction in tumour burden (**Fig. 4.1c**). Quantification of the number of surface lung metastases demonstrated a significant reduction in tumour burden after either 1 or 3 doses of ORFV (**Fig. 4.1d**). To determine the robustness of ORFV therapy, efficacy was also evaluated in lung model survival experiments (**Fig. 4.2**). Using the 3-dose ORFV treatment regime, virus treatment led to a significant survival advantage in both the C57Bl/6 and Balb/c lung models.

ORFV replication is required for full treatment efficacy

The mechanism of ORFV mediated reduction in tumour burden was analyzed in both models by examining virus amplification *in vitro* in the respective cancer cell lines. Phase contrast

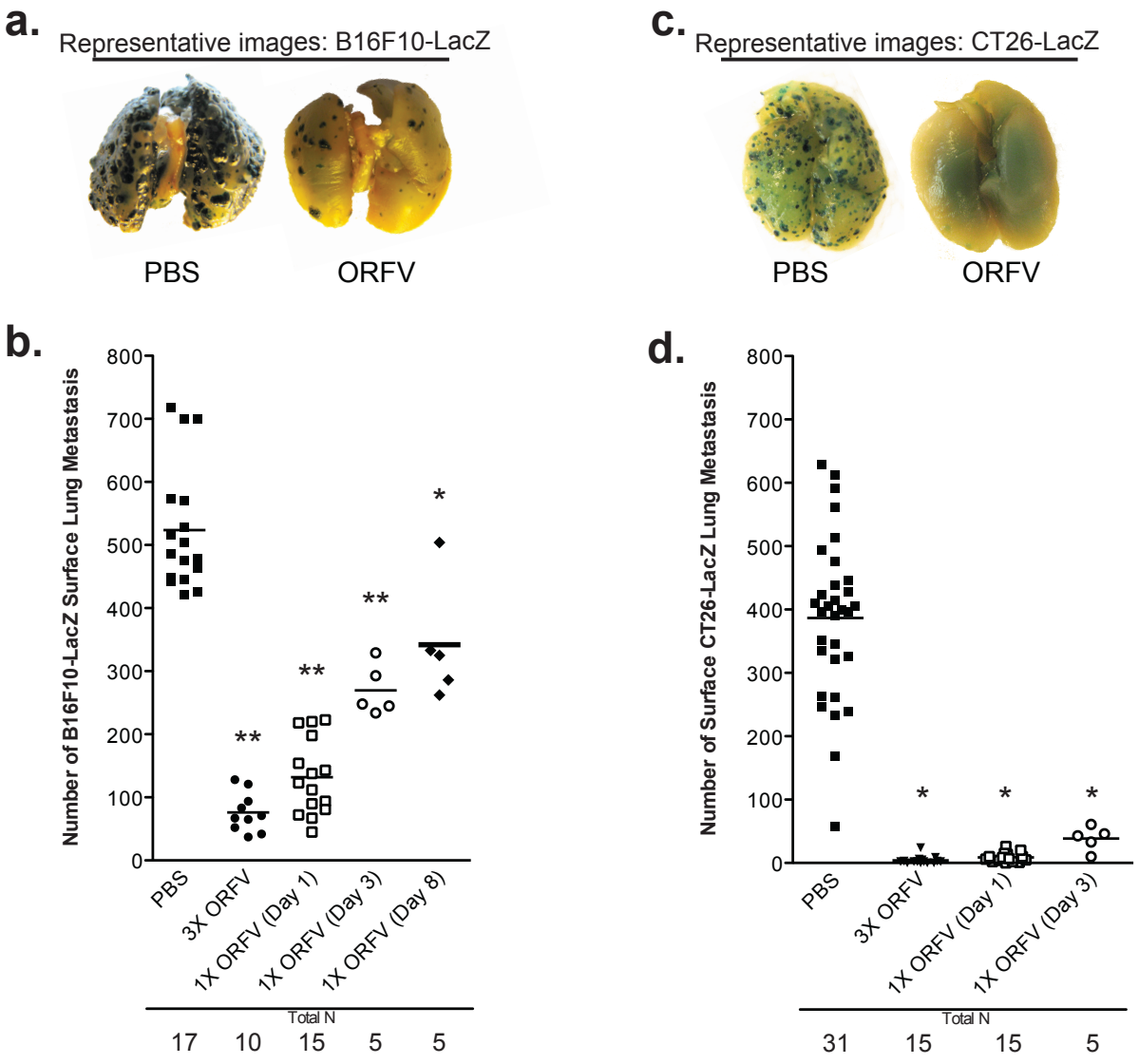
a.
Representative images: B16F10-LacZ
PBS
ORFV
c.
Representative images: CT26-LacZ
PBS
ORFV
b.
Number of B16F10-LacZ Surface Lung Metastasis
800
700
600
500
400
300
200
100
0
**
**
**
*
PBS
3X ORFV
1X ORFV (Day 1)
1X ORFV (Day 3)
1X ORFV (Day 8)
Total N
17
10
15
5
5
d.
Number of Surface CT26-LacZ Lung Metastasis
800
700
600
500
400
300
200
100
0
*
*
*
PBS
3X ORFV
1X ORFV (Day 1)
1X ORFV (Day 3)
Total N
31
15
15
5

Figure 4.1 ORFV can reduce tumor burden in 2 syngeneic mouse models of cancer. C57Bl/6 mice were challenged with $3x10^5$ B16F10-LacZ cells IV, and dosed 1 or 3 times with ORFV (10^7) as indicated. At day 14 after cell injection, lungs were excised and surface metastases were counted. (**a**) Representative images of lungs from animals treated with 3 doses of ORFV, or PBS control are shown. (**b**) The number of surface lung metastases of animals treated as in (**a**); bars represent the mean for each group. (**P* <0.01, ***P* <0.005 using an unpaired *t*-Test with Welch's correction). (**c**) Balb/c mice were challenged with 10^5 CT26-LacZ cells IV, and dosed 1 or 3 times with ORFV (10^7) as indicated. At day 10 after cell injection, mice were sacrificed, their lungs processed as described above. Representative images of lungs from animals treated with 3 doses of ORFV, or PBS are shown. (**d**) The number of surface lung metastases in animals treated as in (**c**); bars represent the mean for each group. (**P* <0.005 using an unpaired, *t*-Test with Welch's correction). PBS, phosphate-buffered saline; 3X ORFV refers to 3 doses of virus (10^7) at days 1, 3 and 8 post cell injection; 1X ORFV refers to 1 dose of virus (10^7) given on the indicated day.

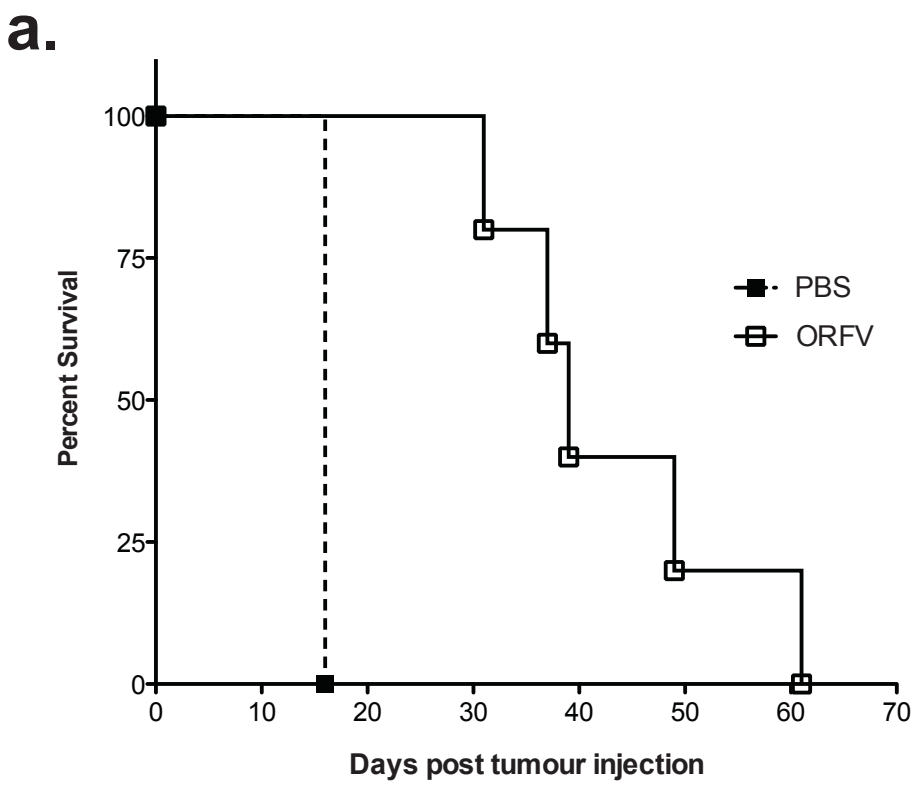
a.
100
75
50
25
0
Percent Survival
0
10
20
30
40
50
60
70
Days post tumour injection
PBS
ORFV

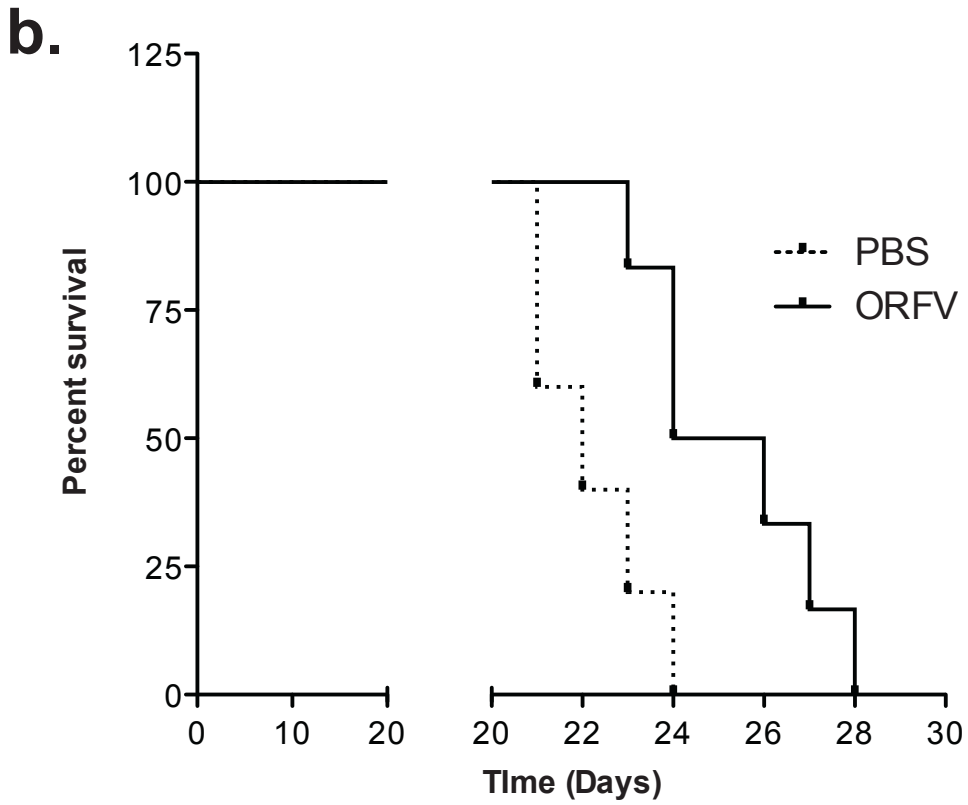
b.
125
100
75
50
25
0
Percent survival
0
10
20
20
22
24
26
28
30
TIme (Days)
PBS
ORFV

Figure 4.2 ORFV can significantly extend survival of mice in 2 lung models of cancer. (**a**) Balb/c mice were challenged with 10^5 CT26-LacZ cells IV, and dosed 3 times with ORFV (10^7) or PBS on days 1, 3 and 8. Animals were monitored for severe respiratory distress, and culled at endpoint. Shown is a Kaplan-Meier survival curve. (N=5, P <0.005 using a log-rank Mantel-Cox test). (**b**) C57Bl/6 mice were challenged with $3x10^5$ B16F10-LacZ cells IV, and dosed 3 times with ORFV (10^7) or PBS on days 1, 3 and 8. Animals were monitored for severe respiratory distress, and culled at endpoint. Shown is a Kaplan-Meier survival curve. (N=5, P <0.05 using a log-rank Mantel-Cox test). PBS, phosphate-buffered saline.

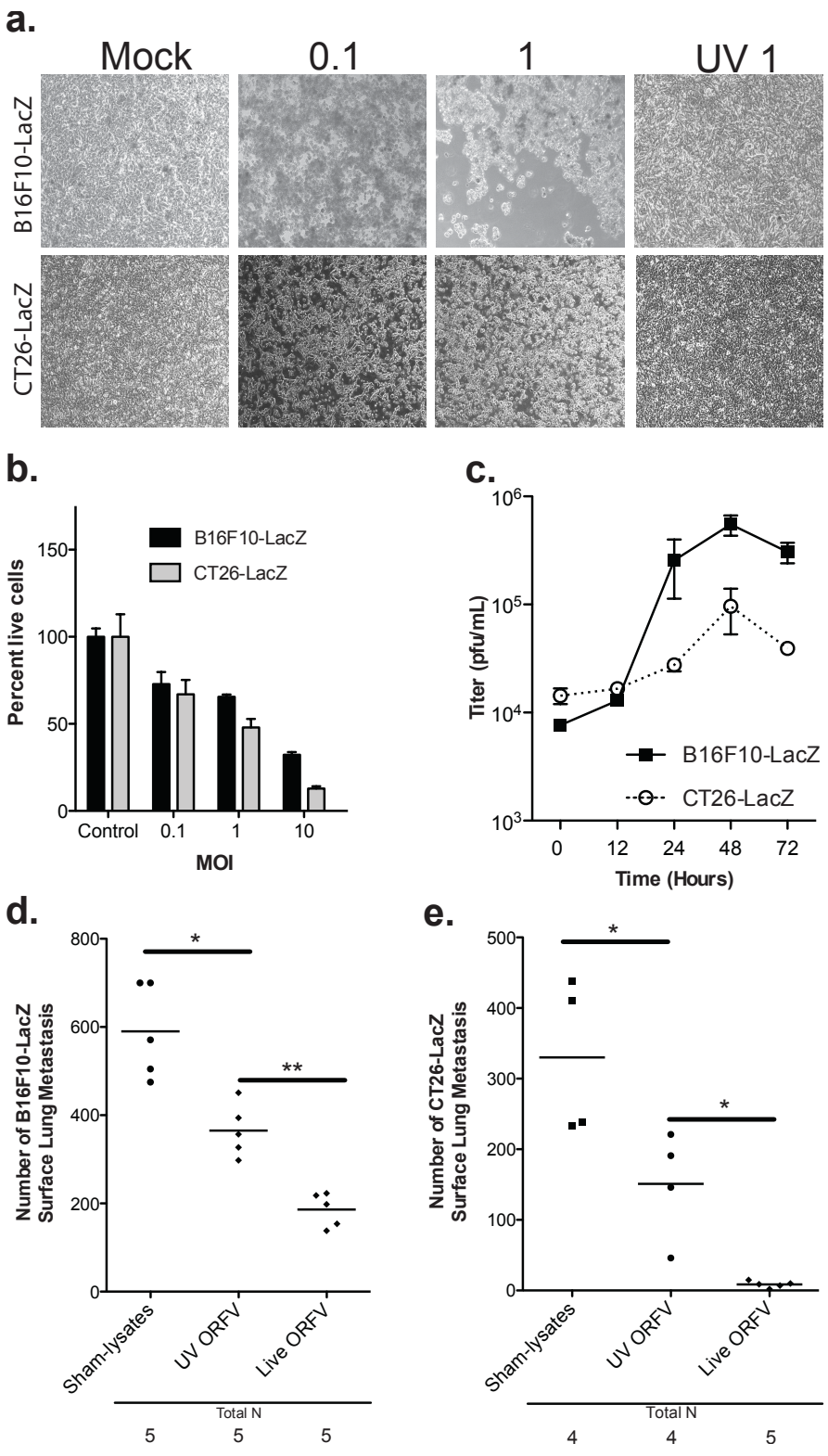
a.
Mock
0.1
1
UV 1
B16F10-LacZ
CT26-LacZ
b.
Percent live cells
150
100
50
0
B16F10-LacZ
CT26-LacZ
Control
0.1
1
10
MOI
c.
Titer (pfu/mL)
10^6
10^5
10^4
10^3
B16F10-LacZ
CT26-LacZ
0
12
24
48
72
Time (Hours)
d.
Number of B16F10-LacZ Surface Lung Metastasis
800
600
400
200
0
*
**
Sham-lysates
UV ORFV
Live ORFV
Total N
5
5
5
e.
Number of CT26-LacZ Surface Lung Metastasis
500
400
300
200
100
0
*
*
Sham-lysates
UV ORFV
Live ORFV
Total N
4
4
5

Figure 4.3 ORFV infection of murine cancer cells. (**a**) Phase contrast images of mock-infected, ORFV infected (MOI of 0.1, and 1) or UV-inactivated ORFV infected (MOI 1) B16F10-LacZ and CT26-LacZ cells at 48 hours post infection at a magnification of 40X. (**b**) Cytotoxicity assays of B16F10-LacZ and CT26-LacZ cells mock-infected (control), or ORFV-infected at the indicated MOI. Percent live cells was determined at 72 hours post-infection by normalization to mock-infected controls. N=4, mean + SEM. (**c**) ORFV growth curves were performed on B16F10-LacZ and CT26-LacZ cell lines at an MOI of 0.3. Cells were infected at time 0, and cell lysates collected and processed by plaque assay at time-points post infection. N=2, mean + SEM. (**d**) C57Bl/6 mice challenged with $3x10^5$ B16F10-LacZ cells IV, and dosed 3 times with sham-infected cell lysates, live or UV-inactivated ORFV (10^7). Day 14 after cell challenge, lungs were isolated and metastases counted. Bars represent the mean for each group. (**P* <0.01, ***P* <0.005 using an unpaired *t*-Test with Welch's correction). (**e**) Balb/c mice challenged with 10^5 CT26-LacZ cells IV, and dosed 3 times with sham-infected cell lysate, live or UV-inactivated ORFV (10^7). Day 10 after cell challenge, lungs were isolated and metastases counted. Bars represent the mean for each group. (**P* <0.05 using an unpaired *t*-Test with Welch's correction). PBS, phosphate-buffered saline; pfu, plaque-forming unit; p.i., post-infection.

images of B16F10-LacZ cells and CT26-LacZ cells at 48 hours post infection showed cell rounding, indicative of a virus induced cytopathic effect (CPE) (**Fig. 4.3a**). The dose dependency of ORFV-induced cell death was quantified (**Fig. 4.3b**) and found to be dependent upon productive infection, since UV inactivated ORFV did not induce CPE in either cell line (**Fig. 4.3a**). The amount of infectious ORFV produced by B16F10-LacZ and CT26-LacZ cancer cells was determined by multi-step growth curve analysis (**Fig. 4.3c**) and revealed that both cell lines could support a modest amount of virus replication. To determine if ORFV replication was important for the *in vivo* efficacy achieved in the C57Bl/6 and Balb/c lung models, efficacy of UV inactivated ORFV was compared to live ORFV (**Fig. 4.3d,e**). Quantification of the number of surface lung metastases in both models indicated that although UV inactivated virus could significantly reduce lung metastases in these models, replicating ORFV was required to achieve maximum efficacy.

Interestingly, despite only modest ORFV replication in murine cancer cell lines, ORFV therapy was as good, or better than oncolytic Vaccinia virus (VACV), Raccoonpox (RCNV) and Myxoma (MYXV) at reducing lung metastases in both lung models (**Fig. 4.4**), even at a log lower dose (**Fig. 4.4b**). From these data, and the observation that UV inactivated virus has some therapeutic activity, I hypothesized that activation of innate or adaptive immune responses by ORFV could be contributing to its anti-cancer activity.

In vivo ORFV infection of lung tumour bearing animals correlates with clearance of lung metastases

A tissue distribution experiment was performed to determine the kinetics of *in vivo* ORFV infection in relation to the kinetics of lung tumour clearance. Tumour bearing C57Bl/6 mice were treated with 10^7 pfu of ORFV IV on day 0, and tissues were harvested at

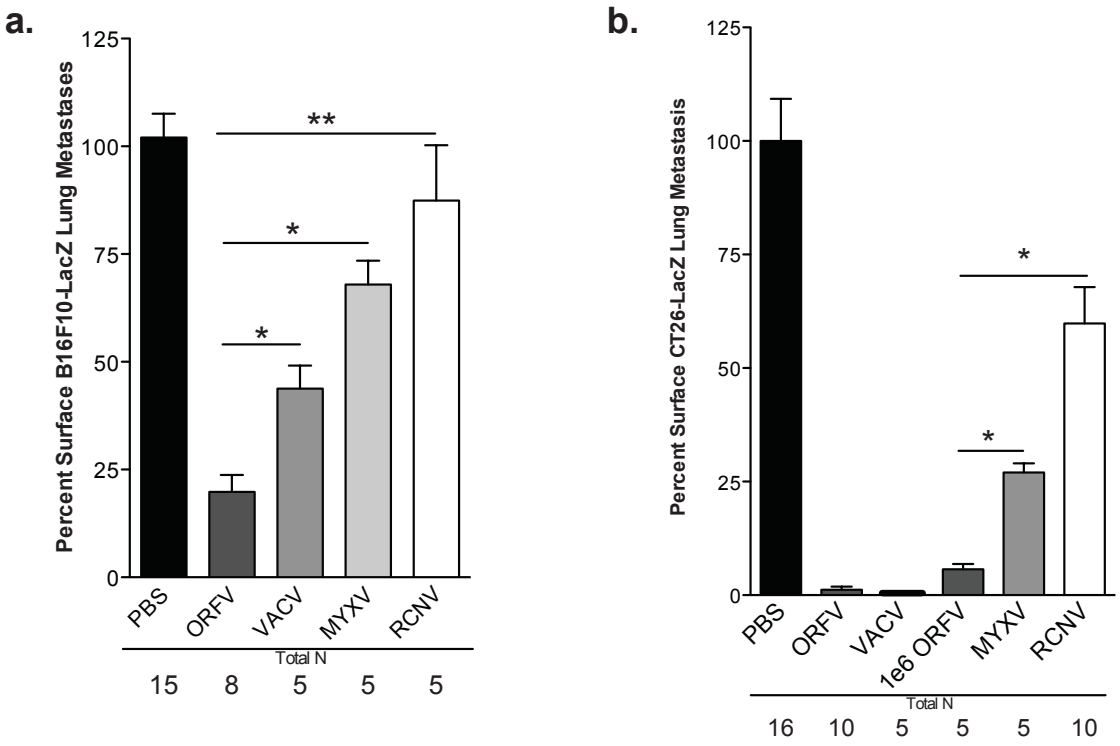
a.
Percent Surface B16F10-LacZ Lung Metastases
125
100
75
50
25
0
**
*
*
PBS
ORFV
VACV
MYXV
RCNV
Total N
15
8
5
5
5
b.
Percent Surface CT26-LacZ Lung Metastasis
125
100
75
50
25
0
*
*
PBS
ORFV
VACV
1e6 ORFV
MYXV
RCNV
Total N
16
10
5
5
5
10

Figure 4.4 ORFV efficacy compared to other oncolytic poxviruses. (**a**) C57Bl/6 mice were challenged with $3x10^5$ B16F10-LacZ cells IV, and dosed 3 times with the indicated virus (10^7), or 100 μL PBS. At day 14 after cell injection, lungs were excised and the percent surface lung metastases was quantified. Bars represent the mean for each group. (**P* <0.01, ***P* <0.0005 using an unpaired *t*-Test with Welch's correction). (**b**) Balb/c mice were challenged with 10^5 CT26-LacZ cells IV, and dosed 3 times with the indicated virus (at 10^7 unless otherwise indicated), or 100 μL of PBS. At day 10 after cell injection, lung metastases were quantified. Bars represent the mean for each group. (**P* <0.0001 using an unpaired, *t*-Test with Welch's correction). PBS, phosphate-buffered saline; VAVC, oncolytic vaccinia virus; MYXV, oncolytic myxoma virus; RCNV, oncolytic raccoonpoxvirus.

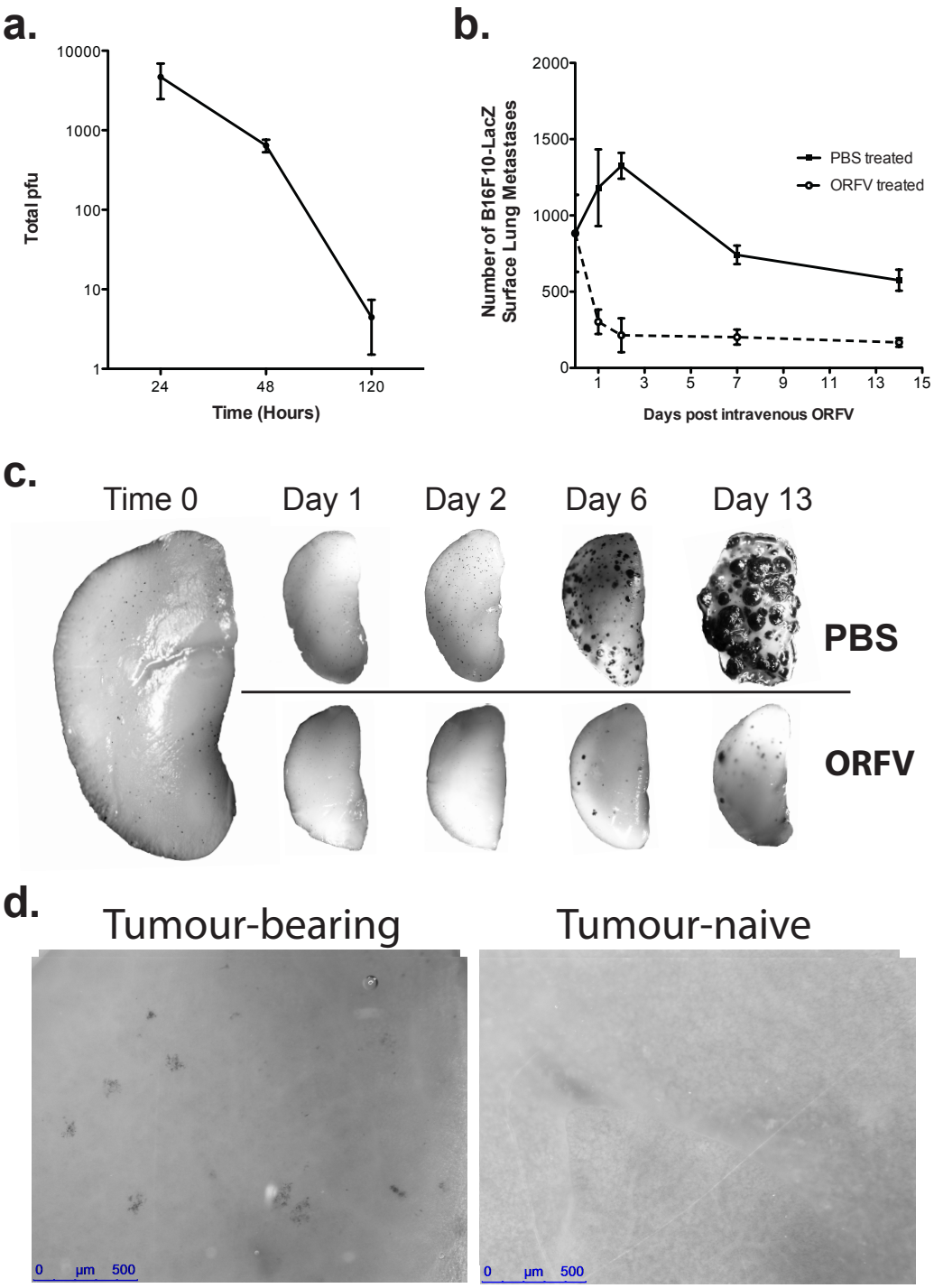
a.
Total pfu
10000
1000
100
10
1
24
48
120
Time (Hours)
b.
Number of B16F10-LacZ Surface Lung Metastases
2000
1500
1000
500
0
1
3
5
7
9
11
13
15
Days post intravenous ORFV
PBS treated
ORFV treated
c.
Time 0
Day 1
Day 2
Day 6
Day 13
PBS
ORFV
d.
Tumour-bearing
Tumour-naive
0 µm 500
0 µm 500

Figure 4.5 Kinetics of *in vivo* ORFV infection and B16F10-LacZ tumour debulking in C57Bl/6 animals. C57Bl/6 mice were challenged with $3x10^5$ B16F10-LacZ cells IV and were treated 24 hours later with ORFV-LacZ (10^7) IV. (**a**) Lung tissues were titered for ORFV at the indicated times post-infection; N=3, mean + SEM. (**b**) C57Bl/6 mice were challenged with $3x10^5$ B16F10-LacZ cells IV and were treated 24 hours later with ORFV (10^7) or PBS IV. Lung tissues were removed at various times post-infection, and the number of surface lung metastases was enumerated; N=3, mean + SEM. (**c**) Representative images of the large lobe of lungs isolated from ORFV or PBS treated animals are shown at time-points post-infection. (**d**) Representative images of lungs from C57Bl/6 mice with and without B16F10 lung tumours (10^6). At day 4, animals were treated with 10^7 ΔVEGF-ORFV. Virus was detected by β-galactosidase staining at 24 hours post infection. PBS, phosphate-buffered saline; pfu, plaque-forming unit.

3 time-points post infection. ORFV was recovered from the lungs at early time-points, and nearly all virus was cleared by day 5 post infection (**Fig. 4.5a**). No virus was recovered from any of the other tissues examined including spleen, liver, kidney, ovary, and brain (data not shown). Lung tumour clearance from ORFV treated animals was found to occur primarily within the first 48 hours post infection, evidenced by both the enumeration of lung metastasis (**Fig. 4.5b**), and representative photographs of the large lobe of lungs from ORFV treated animals (**Fig. 4.5c**). I used a LacZ-expressing version of ORFV (ΔVEGF-ORFV) to determine if virus replication was restricted to the tumour bed. In these experiments, a B16F10 cell line lacking the LacZ transgene was used to initiate tumour formation in mouse lungs and subsequently tumour bearing and tumour free animals were treated with ΔVEGF-ORFV by IV route of delivery. Significant virus infection and spread was only seen in tumour bearing animals (**Fig. 4.5d**).

The tissue distribution experiment was also performed in Balb/c mice to confirm the correlation between *in vivo* ORFV infection and tumour clearance (**Fig. 4.6**). Titer data demonstrate that virus was only recovered from the lungs of animals at day 2 post infection, and was cleared by day 5 (**Fig. 4.6a**). To determine if ORFV infection of the lungs caused any pathology, hematoxylin and eosin stained sections of tumour bearing Balb/c lungs were examined. As seen from **Fig. 4.6b**, ORFV infection demonstrated no pathological effects of the lung. The tumour clearance kinetics following ORFV treatment were also examined in the Balb/c lung model. Similar to the C57Bl/6 model, the clearance of lung metastases occurred primarily within the first 48 hours (**Fig. 4.6c,d)**.

To determine whether the *in vivo* ORFV efficacy was dependent upon IV virus delivery, efficacy was compared in the Balb/c lung model using three routes of delivery: footpad, intraperitoneal, and intravenous ORFV treatment. ORFV was only significantly

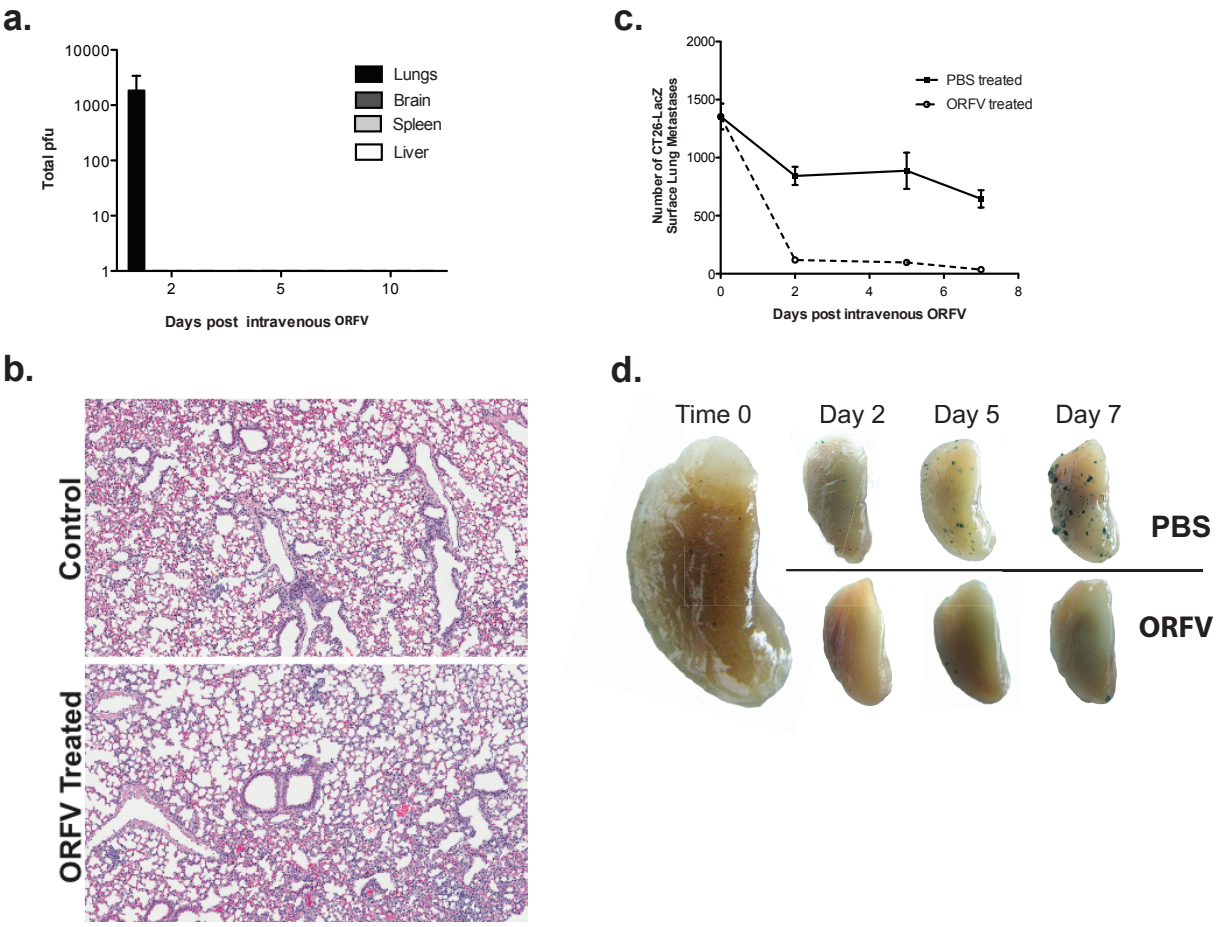
a.
10000
1000
100
10
1
Total pfu
Lungs
Brain
Spleen
Liver
2
5
10
Days post intravenous ORFV
c.
2000
1500
1000
500
0
Number of CT26-LacZ Surface Lung Metastases
PBS treated
ORFV treated
0
2
4
6
8
Days post intravenous ORFV
b.
Control
ORFV Treated
d.
Time 0
Day 2
Day 5
Day 7
PBS
ORFV

Figure 4.6 Kinetics of *in vivo* ORFV infection and CT26-LacZ tumour debulking in Balb/C animals. (**a**) Balb/c mice were challenged with 10^5 CT26-LacZ cells IV and were treated 24 hours later with ORFV-LacZ (10^7) IV. Tissues were titered for ORFV at time-points post-infection and the total amount of virus (total pfu) was plotted over time. N=2, mean + SEM. (**b**) Balb/c mice were challenged with 10^5 CT26-LacZ cells IV, and were treated 24 hours later with 10^7 pfu of ORFV IV or 100μL of PBS. At 72 hours post infection, the lungs were harvested from mice (N=2), fixed, and embedded in paraffin. Hematoxylin and eosin stained sections from a representative PBS treated (top panel) and ORFV treated (bottom panel) lung are shown at a 5X magnification. Images were captured using Aperio ScanScope (Axiovision Technologies) and analyzed using Aperio ImageScope software. Balb/c mice were challenged with 10^5 CT26-LacZ cells IV and were treated 24 hours later with ORFV (10^7) or PBS IV. (**c**) Lung metastases were enumerated at the indicated time-points; N=3, mean + SEM. (**d**) Representative images of the large lobe of lungs isolated from ORFV or PBS treated animals are shown at time-points post-infection. PBS, phosphate-buffered saline; pfu, plaque-forming unit.

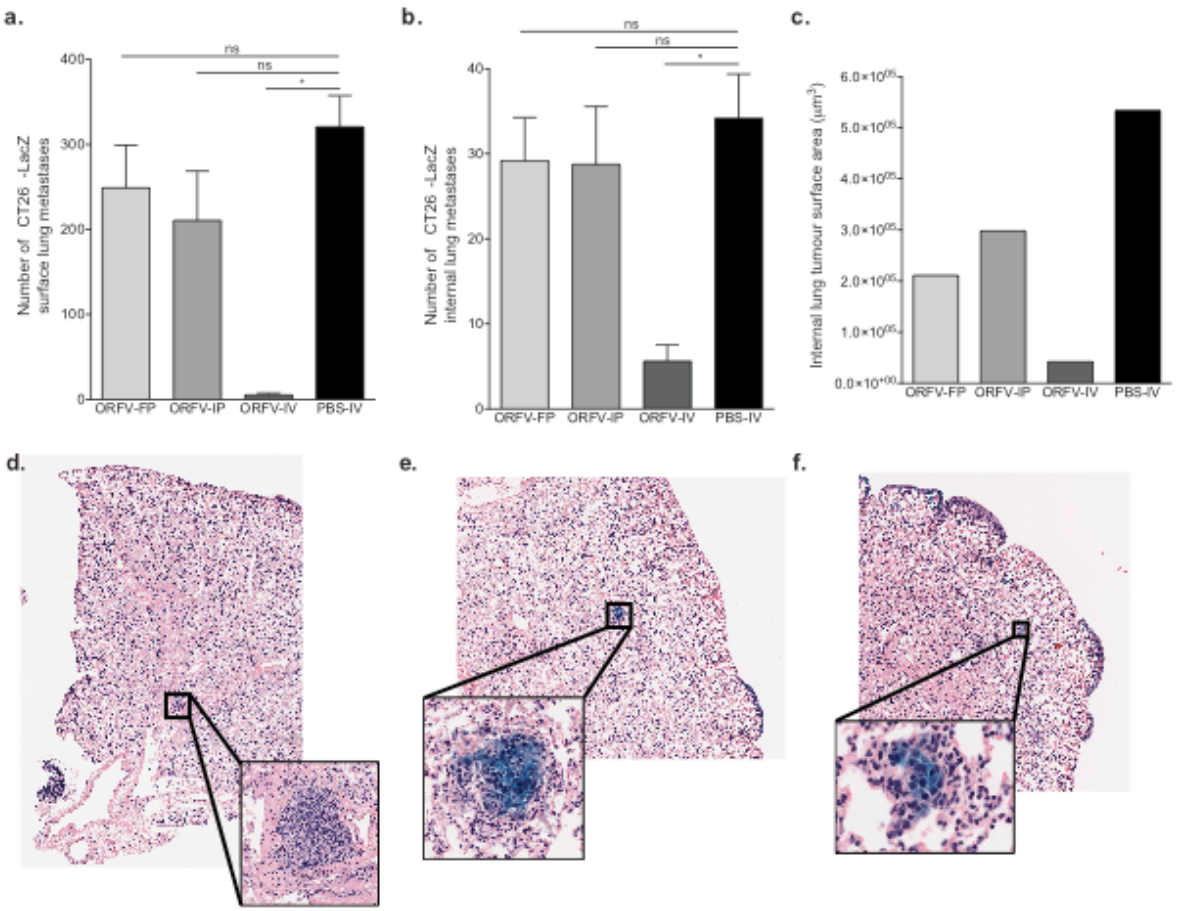
a.
b.
c.
d.
e.
f.
Number of CT26 -LacZ surface lung metastases
Number of CT26 -LacZ internal lung metastases
Internal lung tumour surface area (µm²)
ns
ns
*
ORFV-FP
ORFV-IP
ORFV-IV
PBS-IV

Figure 4.7 ORFV efficacy by different routes of administration. Balb/c mice were challenged with 10^5 CT26-LacZ cells IV and treated once, 24 hours post cell challenge with ORFV (10^7) by footpad, intraperitoneal, or intravenous route of delivery. (**a**) The number of surface lung metastases was compared to PBS treated animals at 10 days post tumour cell challenge. N=5, mean + SEM, (*P <0.001 using an unpaired, t-Test with Welch's correction). (**b**) Paraffin embedded lung tissues were sectioned, stained by H+E, and the number of internal lung metastases were quantified and compared to PBS treated animals at 10 days post tumour cell challenge. N=5, mean + SEM, (*P <0.005 using an unpaired, T-Test with Welch's correction). (**c**) The surface area of internal lung metastases from 1 mouse of ORFV treatment by 3 different routes of administration was compared to PBS treated animals at 10 days post tumour cell challenge. Representative images of H+E stained sections of lungs are shown at 10X magnification, from (**d**) a foot-pad ORFV treated animal, (**e**) an intraperitoneal ORFV-treated animal, and (**f**) a PBS-treated animal. Images were captured using Aperio ScanScope (Axiovision Technologies) and analyzed using Aperio ImageScope software. FP, footpad; IP, intraperitoneal; IV, intravenous; PBS, phosphate-buffered saline.

efficacious at reducing CT26-LacZ surface lung metastases if delivered intravenously (**Fig. 4.7a)**. Analysis of the number and surface area of internal lung metastases following treatment by the different routes of delivery similarly demonstrated a requirement for IV delivery to achieve full treatment benefit (**Fig. 4.7b,c**). Representative images of internal lung metastases are illustrated for footpad, and intraperitoneal ORFV treatments, and PBS treatments, (**Fig. 4.7d,e,f**), respectively.

Flow cytometry and cell depletion studies implicate NK cells in the efficacy achieved by ORFV

To establish the contribution of the immune system in the ORFV-mediated efficacy in the lung models, flow cytometry analysis was performed. Spleens isolated from tumour-bearing Balb/c animals showed dramatic splenomegaly at 5 days post infection with ORFV (**Fig. 4.8a**). The splenomegaly was attributed to expansion in the number of lymphocytes in the spleen, since both the mass and number of splenocytes has increased (**Fig. 4.8b**). Flow cytometry analysis demonstrated a trend towards a disproportionate expansion in innate immune cells (DCs and NK cells) when compared to adaptive immune cells ($CD8^+$ T cells) in the spleen (**Fig. 4.8c**). Expression of the early activation marker CD69 on NK cells from Balb/c splenocytes of tumour bearing animals showed nearly 90% activation at 24 hours post infection compared to PBS treated animals (**Fig. 4.8d**). Splenocytes from tumour-bearing C57Bl/6 animals were analyzed at several time-points post infection where ORFV induced significantly more CD69 expression on NK cells when compared to PBS treated animals (**Fig. 4.8e**).

To determine if the adaptive immune system was required for the ORFV efficacy, CT26-LacZ cells were used to establish lung tumours in athymic, CD-1 nude mice. As seen from **Fig. 4.9a**, three IV doses of ORFV significantly reduced the number of CD26-LacZ

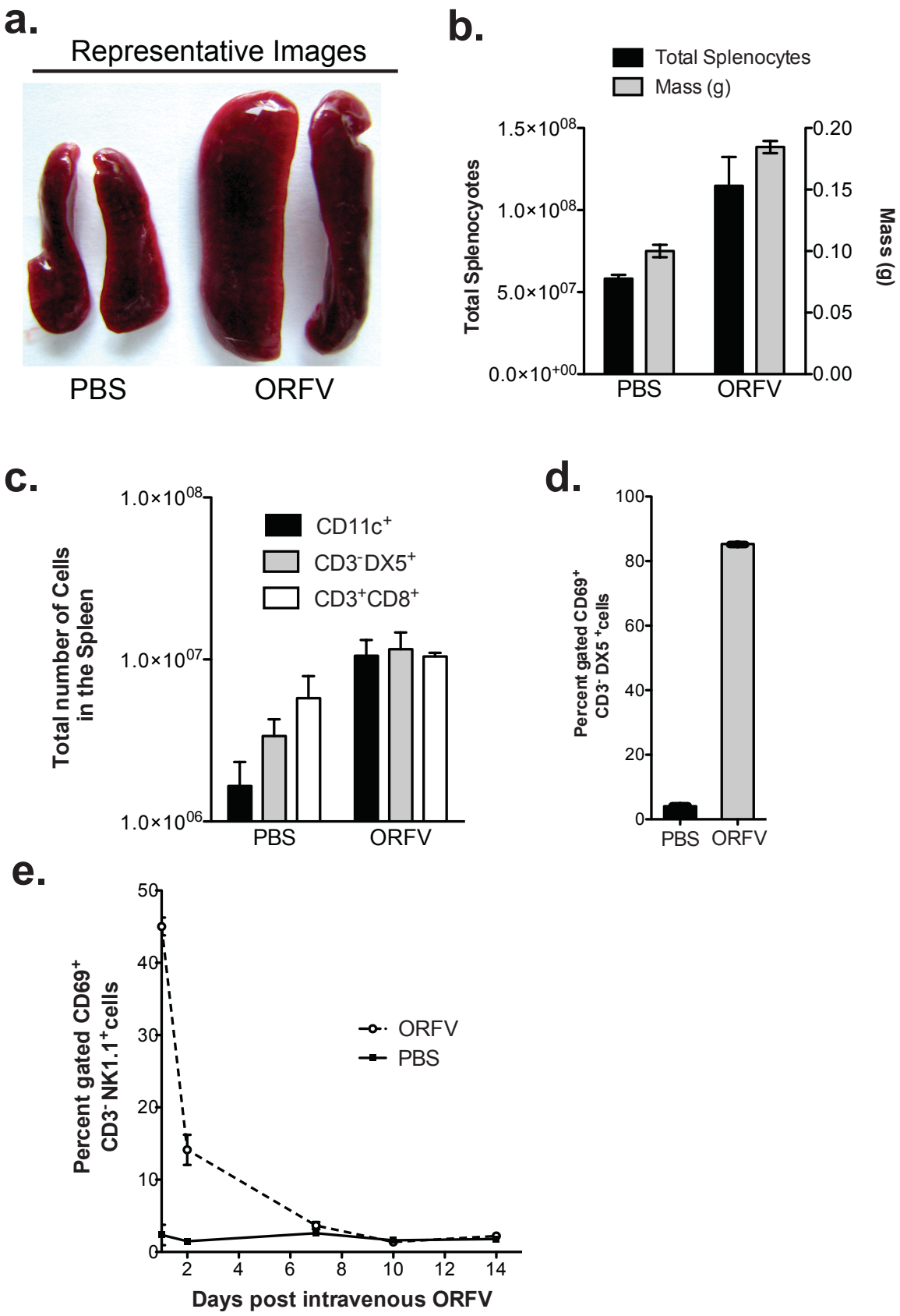
a.
Representative Images
PBS
ORFV
b.
Total Splenocytes
Mass (g)
Total Splenocytes
Mass (g)
1.5×10^08
1.0×10^08
5.0×10^07
0.0×10^+00
0.20
0.15
0.10
0.05
0.00
PBS
ORFV
c.
CD11c+
CD3-DX5+
CD3+CD8+
Total number of Cells in the Spleen
1.0×10^08
1.0×10^07
1.0×10^06
PBS
ORFV
d.
Percent gated CD69+ CD3- DX5 +cells
100
80
60
40
20
0
PBS
ORFV
e.
Percent gated CD69+ CD3- NK1.1+cells
ORFV
PBS
50
40
30
20
10
0
2
4
6
8
10
12
14
Days post intravenous ORFV

Figure 4.8 IV delivery of ORFV leads to expansion and activation of innate immune cells in the spleen. (**a**) Spleens isolated from tumour-bearing Balb/c animals treated with ORFV (10^7) or PBS IV were photographed at 5-days post-infection. (**b**) The mass and total number of splenocytes illustrated in (**a**) were quantified at 5-days post-infection; N=2, mean + SEM. (**c**) The total number of DCs ($CD11c^+$), natural killer cells ($CD3^-DX5^+$) and cytotoxic T cells ($CD3^+CD8^+$) were quantified from spleens isolated from tumour bearing Balb/c mice treated IV with ORFV (10^7) or PBS IV at 5-days post-infection. N=2, mean + SEM. (**d**) CD69 expression was quantified from splenic natural killer cells ($CD3^-DX5^+$) isolated from tumour bearing Balb/c mice 24 hours post ORFV (10^7) or PBS i.v. N=2, mean + SEM. (**e**) CD69 expression was quantified from splenic natural killer cells ($CD3^-NK1.1^+$) isolated from tumour bearing C57Bl/6 mice at time-points post IV ORFV (10^7) or PBS treatment. N=3, mean + SEM. PBS, phosphate-buffered saline.

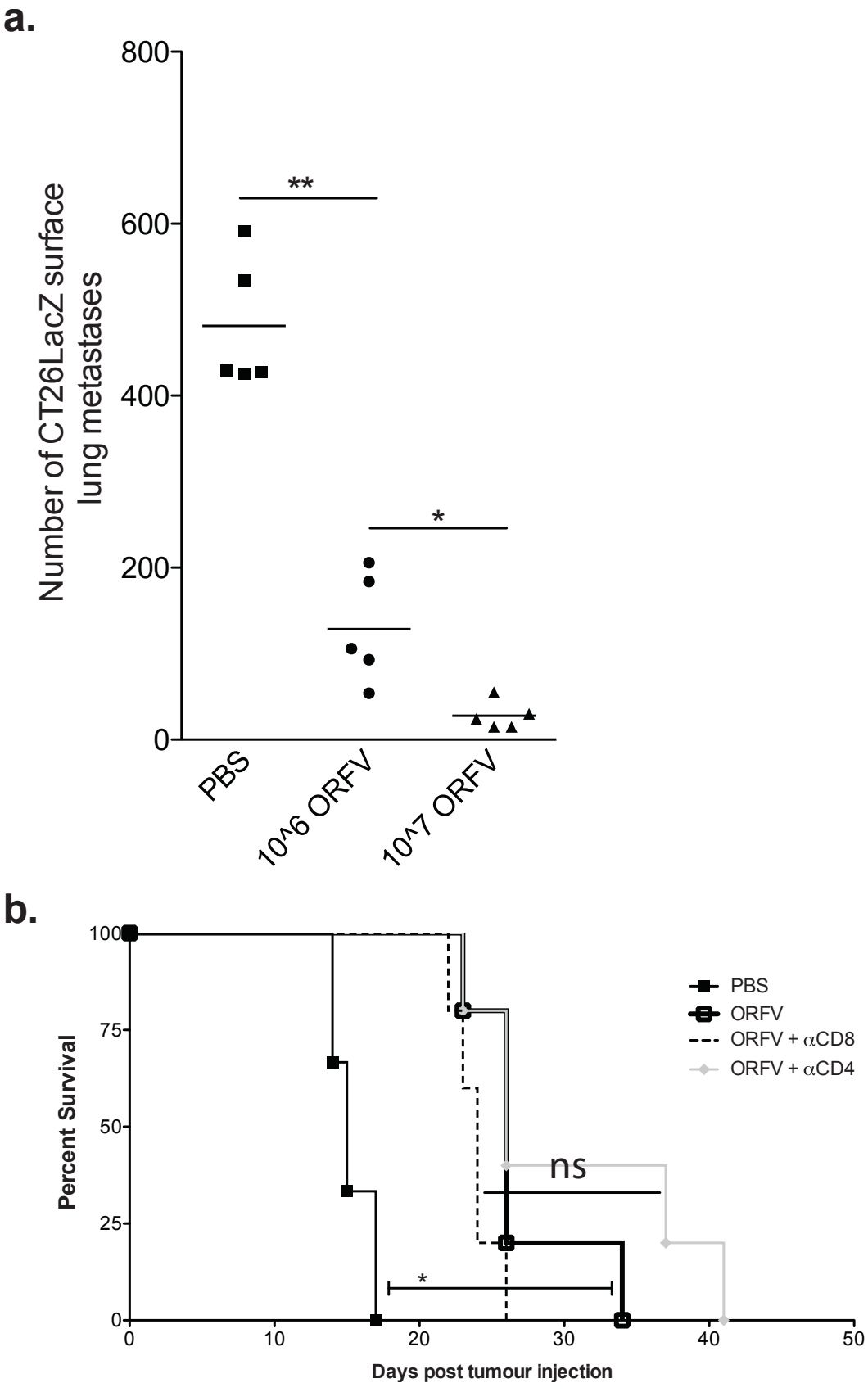
a.
800
600
400
200
0
Number of CT26LacZ surface lung metastases
**
*
PBS
10^6 ORFV
10^7 ORFV
b.
100
75
50
25
0
Percent Survival
0
10
20
30
40
50
Days post tumour injection
PBS
ORFV
ORFV + αCD8
ORFV + αCD4
ns
*

Figure 4.9 *In vivo* ORFV efficacy in the absence of T cells. (**a**) CD-1 nude mice were challenged with 10^5 CT26-LacZ cells IV and treated 3 times IV with ORFV at a dose of 10^7 or 10^6 pfu. The number of surface lung metastases was compared to PBS treated animals at 10 days post tumour cell challenge. N=5, mean + SEM, (*P <0.05, **P <0.0005 using an unpaired student t-Test with Welch's correction). (**b**) Balb/c mice were challenged with 10^5 CT26-LacZ cells IV and treated 3 times IV with ORFV (10^7) (with and without CD4/CD8 depletion) or PBS as a control. Animals were monitored for severe respiratory distress, and culled at endpoint. Shown is a Kaplan-Meier survival curve. N=5 or 6, (P <0.005 using a log-rank Mantel-Cox test). PBS, phosphate-buffered saline.

surface lung metastases, in a dose dependent manner. Furthermore, $CD4^+$ or $CD8^+$ T cells were depleted from ORFV treated animals in a Balb/c CT26-LacZ lung model survival experiment, where ORFV treatment leads to a significant extension in overall survival (**Fig. 4.9b**). I found that neither $CD4^+$ nor $CD8^+$ T cells were required for the ORFV-mediated efficacy in this model. Collectively, these data indicate that ORFV is capable of stimulating an innate immune response, which may be involved in the efficacy achieved in the C57Bl/6 and Balb/c mouse models.

We next examined the contribution of NK cells to ORFV therapy using antibody depletion studies. The dose and schedule of the NK cell depleting anti-body was tested in both C57Bl/6 and Balb/c mice (**Fig. 4.10a,b**) to ensure the depletion was sufficient, and would last for the duration of the experiment. In both the C57Bl/6 and Balb/c lung models, NK cell depletion reduced the ability of live ORFV to clear lung metastases (**Fig. 4.10c,d**). Not surprisingly, UV-inactivated ORFV similarly loses efficacy in the absence of NK cells. NK cell cytotoxicity assays were performed at time-points post-infection from tumour-naïve C57Bl/6 mice treated with live or UV-inactivated ORFV IV (**Fig. 4.10e,f**). At 24-hours post infection, NK cells isolated from spleens from both live and UV-inactivated ORFV-treated animals induced significant cytotoxicity of B16F10-LacZ cells (**Fig. 4.10e**). NK cells isolated from live ORFV-treated animals induced significantly greater B16F10-LacZ cytotoxicity than those isolated from UV-inactivated ORFV-treated animals. At 72 hours post infection, only live ORFV treatment resulted in significant NK cell cytotoxicity of target cells (**Fig. 4.10f**). Thus systemic ORFV treatment induces a potent cytotoxic NK cell response capable of directly killing B16F10-LacZ target cells.

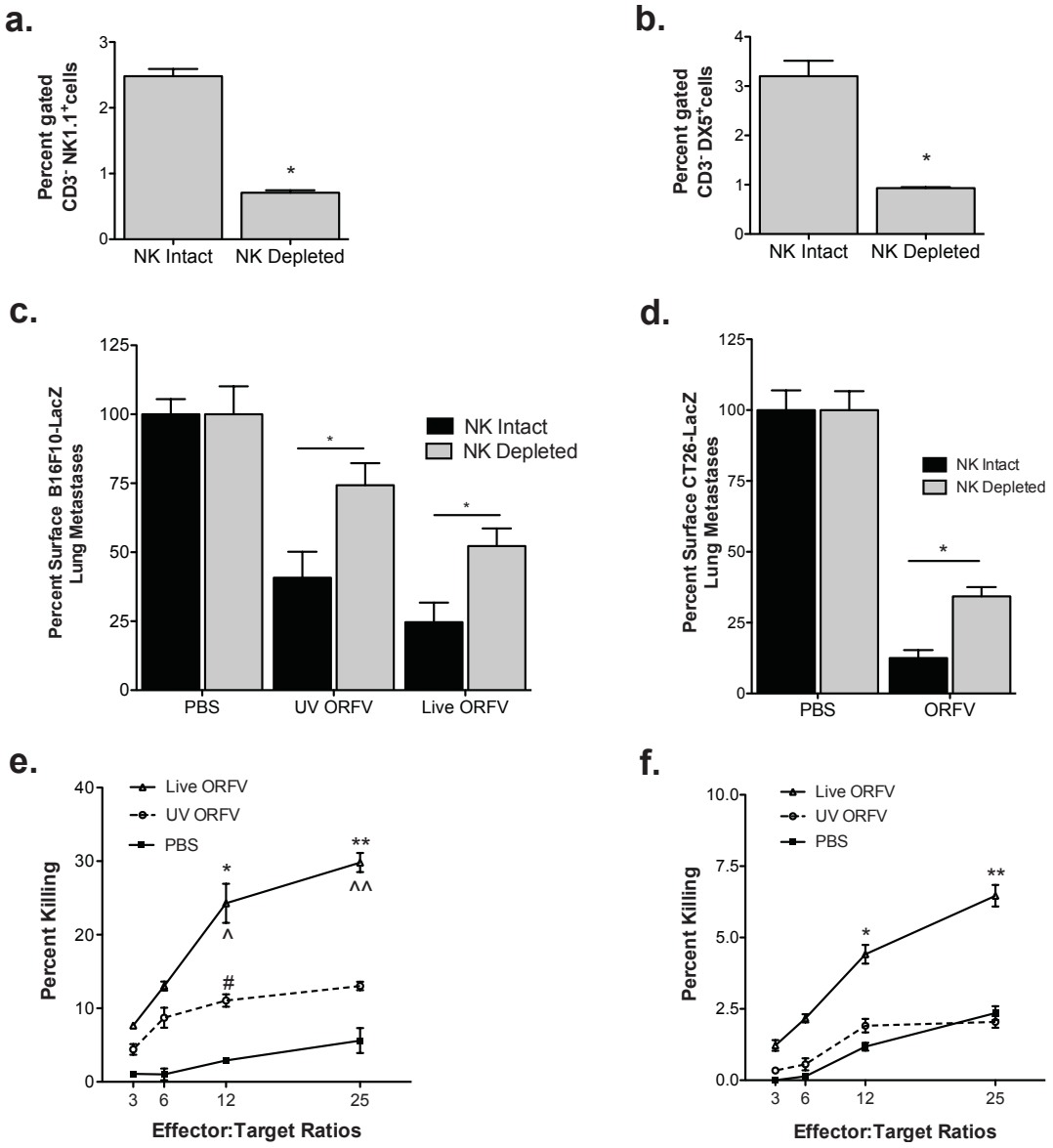
a.
Percent gated CD3- NK1.1+cells
NK Intact
NK Depleted
b.
Percent gated CD3- DX5+cells
NK Intact
NK Depleted
c.
Percent Surface B16F10-LacZ Lung Metastases
NK Intact
NK Depleted
PBS
UV ORFV
Live ORFV
d.
Percent Surface CT26-LacZ Lung Metastases
NK Intact
NK Depleted
PBS
ORFV
e.
Live ORFV
UV ORFV
PBS
Percent Killing
Effector:Target Ratios
f.
Live ORFV
UV ORFV
PBS
Percent Killing
Effector:Target Ratios

Figure 4.10 ORFV activation of NK cells is contributing to efficacy achieved in the lung models. (**a**) Splenocytes from C57Bl/6 animals were analyzed for percent NK cells at day 0. N=6, mean + SEM (**P* <0.0001 using an unpaired student *t*-Test with Welch's correction). (**b**) Splenocytes from Balb/c animals were analyzed for percent NK cells at day 0. N=6, mean + SEM (**P* <0.01 using an unpaired student T-Test with Welch's correction). (**c**) C57Bl/6 animals treated IV with 3 doses of PBS, ORFV or UV inactivated ORFV (10^7) were depleted of NK cells using an optimized dose and schedule of anti-asialo or control IgG antibody. Animals were sacrificed at 14-days post cell injection, and the number of surface lung metastases were quantified. N=5, mean + SEM, (**P* <0.0005 using an unpaired *t*-Test with Welch's correction). (**d**) Balb/c animals treated IV with 3 doses of PBS or ORFV (10^7) were depleted of NK cells using an optimized dose and schedule of anti-asialo IV or control IgG antibody. Animals were sacrificed at 10-days post cell injection, and the number of surface lung metastases were quantified. N=10, mean + SEM, (**P* <0.05 using an unpaired *t*-Test with Welch's correction). *Ex vivo* cytotoxicity assays were performed on NK cells isolated from ORFV or PBS treated C57Bl/6 mice. Spleens were isolated, pooled and enriched for NK cells by $DX5^+$ cell sorting. (**e**) Percent killing of target B16F10-LacZ cells at 24 hours post infection. N=3, mean + SEM, (**P* <0.05, ***P* <0.005 comparing Live ORFV to PBS, ^*P* <0.05, ^^*P* <0.01 comparing Live ORFV to UV ORFV, #*P*<0.05 comparing UV ORFV to PBS, using an unpaired, *t*-Test with Welch's correction). (**f**) Percent killing of target B16F10-LacZ cells at 72 hours post infection. N=3, mean + SEM, (**P* <0.05, ***P* <0.05 using an unpaired *t*-Test with Welch's correction). PBS, phosphate-buffered saline; UV, ultra-violet

ORFV induces potent cytokine expression by NK cells isolated from the spleen, blood and lung To determine the strength and breadth of the ORFV mediated activation of NK cells, tissues from tumour bearing C57Bl/6 animals were analyzed by flow cytometry at 24 hours post ORFV for both granzyme B and IFN-γ expression by NK cells (**Fig. 4.11**). Importantly, these data were collected following a 5-hour GolgiPlug incubation, in the absence of any *ex vivo* stimulation. Representative histograms of lung-derived lymphocytes are illustrated in **Fig. 4.11a**, demonstrating increased expression of both IFN-γ and Granzyme B from NK cells isolated from ORFV treated animals compared to PBS treated animals. Quantification of the percent gated NK cells secreting either granzyme B or IFN-γ from the spleen, blood and lung illustrate significant expression of both cytokines in all tissues isolated from ORFV treated animals (**Fig. 4.11a,b** respectively). In addition, the overall amount of IFN-γ and granzyme B expressed on a per cell basis was quantified (**Fig. 4.11d**), where ORFV treatment also led to significant increases in the mean fluorescence intensity (MFI) of both cytokines from the spleen, blood and lung. Finally, I determined the percent gated NK cells that were expressing *both* IFN-γ and granzyme B (**Fig. 4.11e**). These activated NK cells were only detected in ORFV treated animals, and were identified in all 3 tissues. These data underline ORFV's ability to stimulate a potent, diverse and systemic activation of NK cells.

To evaluate the ability of UV-inactivated ORFV to stimulate *in vivo* cytokine secretion from NK cells, tissues from tumour bearing C57Bl/6 animals were analyzed by flow cytometry at a 24-hour time point. Quantification of the percent gated NK cells secreting either IFN-γ (**Fig. 4.12a**) or granzyme B (**Fig. 4.12b**) from the spleen illustrate significantly more cytokine expression from NK cells isolated from live ORFV treated animals, compared to UV-inactivated ORFV treated animals. Similar results were observed

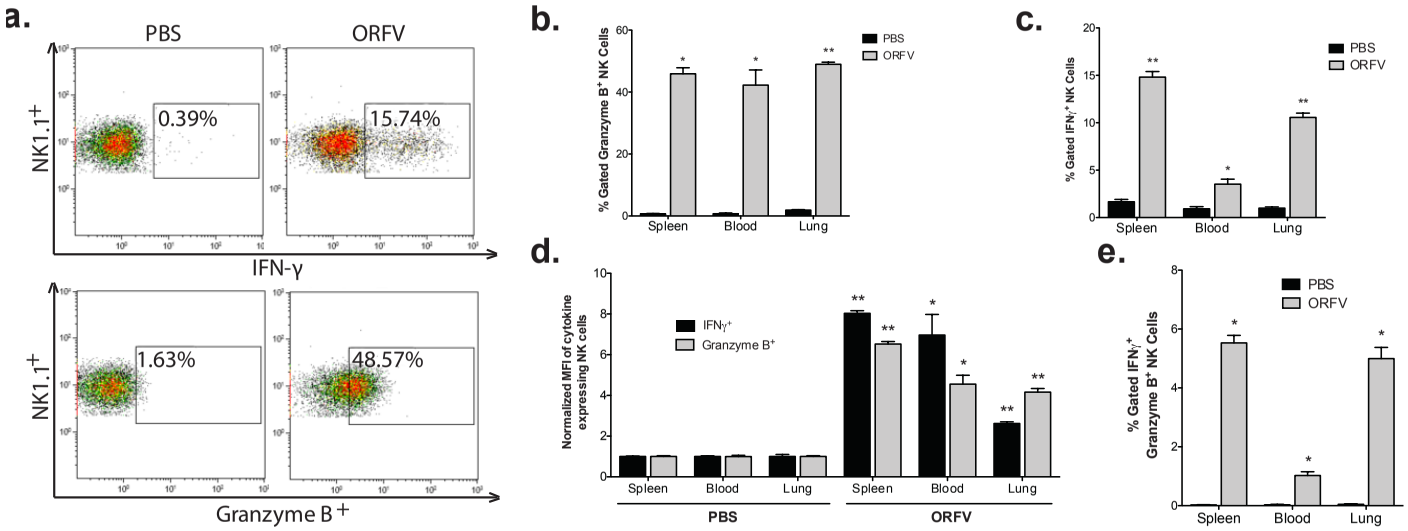
a.
PBS
ORFV
NK1.1+
0.39%
15.74%
IFN-γ
1.63%
48.57%
Granzyme B+
b.
% Gated Granzyme B+ NK Cells
PBS
ORFV
Spleen
Blood
Lung
c.
% Gated IFNγ+ NK Cells
d.
Normalized MFI of cytokine expressing NK cells
IFN-γ+
Granzyme B+
PBS
ORFV
e.
% Gated IFNγ+ Granzyme B+ NK Cells

Figure 4.11 Flow-cytometry analysis of ORFV-activated NK cells. (a) Tumour bearing C57Bl/6 animals were treated IV with (10^7) ORFV, or PBS. At 24 hours post-infection, tissues were harvested from animals, and processed for flow cytometry. Representative histograms are shown of lymphocytes isolated from the lung of animals treated with PBS, or ORFV. (**b**) Percent gated granzyme B expression from NK cells isolated from the spleen, blood, and lung of ORFV and PBS-treated animals is compared. N=4, mean + SEM (**P* <0.005, ***P* <0.0001 using an unpaired T-Test with Welch's correction). (**c**) Percent gated IFN-γ expression from NK cells isolated from the spleen, blood, and lung of ORFV and PBS-treated animals is compared. N=4, mean + SEM (**P* <0.05, ***P* <0.0005 using an unpaired *t*-Test with Welch's correction). (**d**) The amount of granzyme B and IFNγ expressed on a per NK cell basis was determined using the mean fluorescence intensity (MFI). Data are shown as the fold-increase in MFI compared to PBS treated animals. N=4, mean + SEM (**P* <0.01, ***P* <0.0005 using an unpaired T-Test with Welch's correction). (**e**) Percent gated NK cells expressing both granzyme B and IFN-γ was compared for lymphocytes isolated from PBS and ORFV treated animals. N=4, mean + SEM (**P* <0.005). PBS, phosphate-buffered saline; MFI, mean fluorescence intensity.

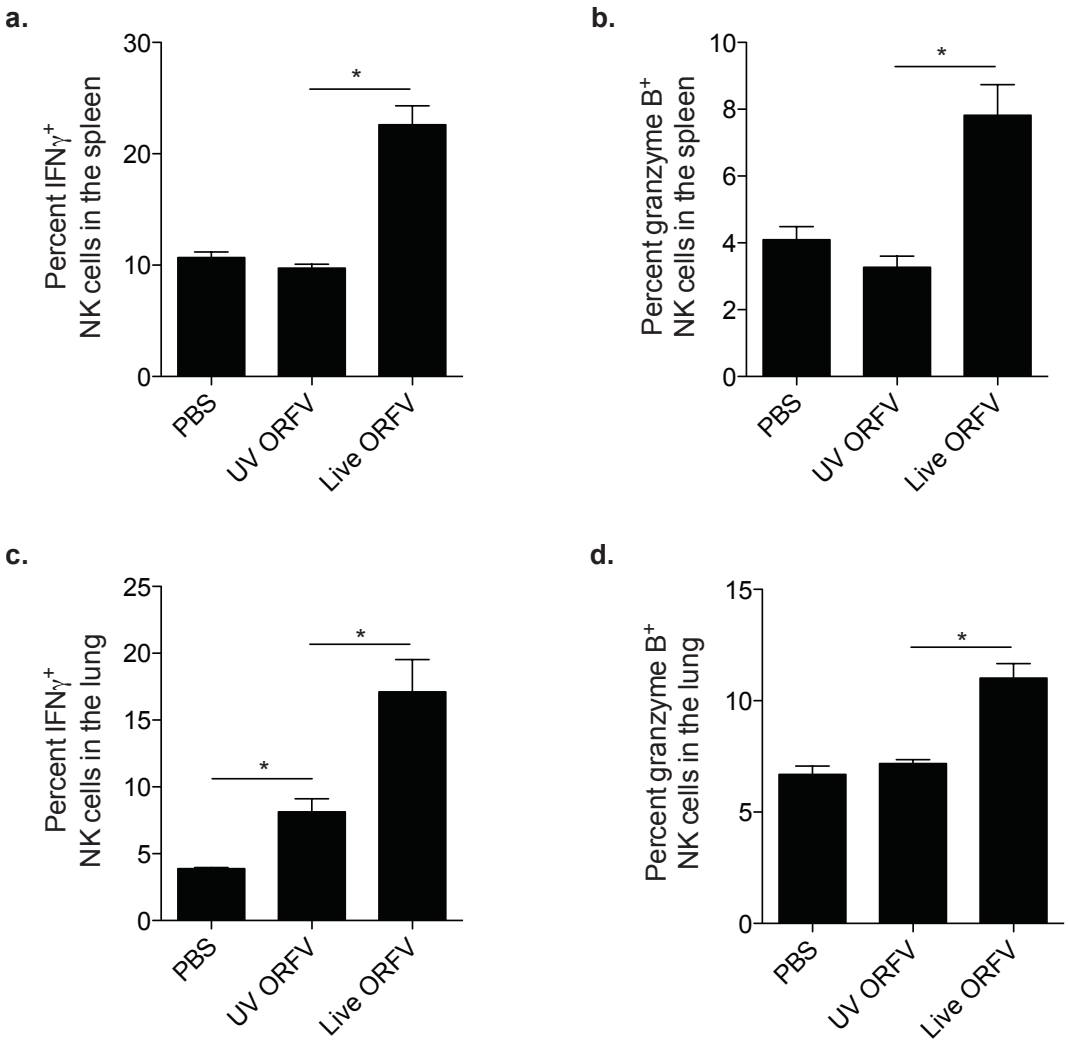
a.
Percent IFNγ+ NK cells in the spleen
30
20
10
0
*
PBS
UV ORFV
Live ORFV
b.
Percent granzyme B+ NK cells in the spleen
10
8
6
4
2
0
*
PBS
UV ORFV
Live ORFV
c.
Percent IFNγ+ NK cells in the lung
25
20
15
10
5
0
*
*
PBS
UV ORFV
Live ORFV
d.
Percent granzyme B+ NK cells in the lung
15
10
5
0
*
PBS
UV ORFV
Live ORFV

Figure 4.12 Flow-cytometry analysis comparing live ORFV to UV inactivated ORFV *in vivo* stimulation of NK cells. Lung tumour-bearing C57Bl/6 animals were treated IV with (10^7) UV-ORFV, Live ORFV, or PBS. At 24 hours post-infection, tissues were harvested from animals, and processed for flow cytometry. (**a**) Percent gated IFN-γ^+ NK cells in the spleen was compared. (**b**) Percent gated granzyme B^+ NK cells in the spleen was compared. (**c**) Percent gated IFN-γ^+ NK cells in the lungs was compared. (**d**) Percent gated granzyme B^+ NK cells in the lungs was compared. N=3, mean + SEM (*P <0.05, using an unpaired t-Test with Welch's correction).

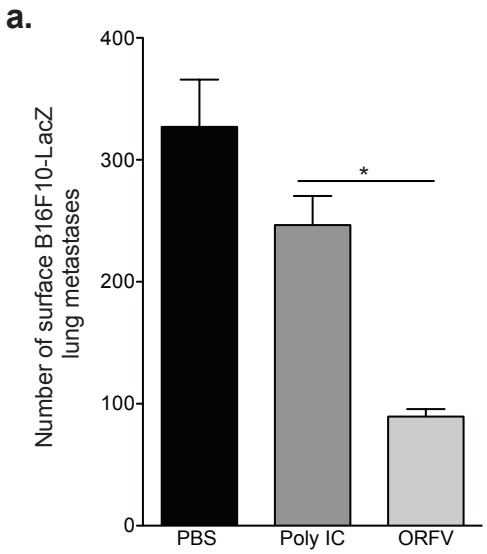
a.
Number of surface B16F10-LacZ lung metastases
400
300
200
100
0
*
PBS
Poly IC
ORFV

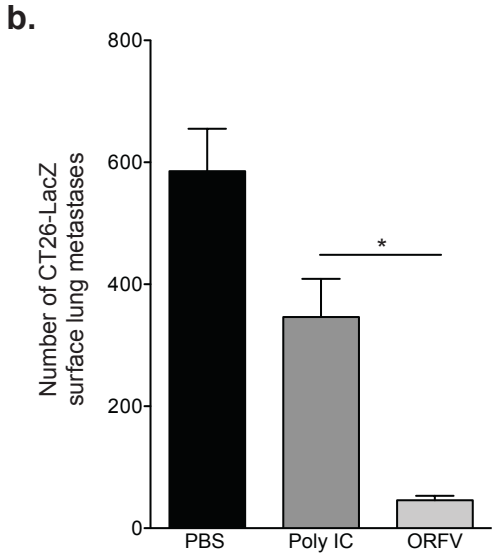
b.
Number of CT26-LacZ surface lung metastases
800
600
400
200
0
*
PBS
Poly IC
ORFV

Figure 4.13 Comparing ORFV efficacy to TLR-3 agonist, Poly IC. The number of surface lung metastases was evaluated from animals challenged intravenously with cancer cells, and treated with three doses of 10^7 pfu of ORFV IV, 150 μg of Poly IC, or 100 μL of PBS IV. (**a**) The number of B16F10-LacZ surface lung metastases from C57Bl/6 animals was compared at 14 days post cell challenge. N=5, mean + SEM, (**P* <0.05 using an unpaired, *t*-Test with Welch's correction). (**b**) The number of CT26-LacZ surface lung metastases from Balb/c animals was compared at 10 days post cell challenge. N=5, mean + SEM, (**P* <0.05 using an unpaired, *t*-Test with Welch's correction).

for NK cells isolated from the lungs (**Fig. 4.12c,d** for IFN-γ and granzyme B, respectively). To evaluate the robustness of ORFV therapy, I compared *in vivo* efficacy in both lung models to the TLR-3 agonist, Poly IC. At therapeutically relevant doses of Poly IC, ORFV performed significantly better in both lung models (**Fig. 4.13**).

ORFV therapy reduces tumour burden in an A549 xenograft model of cancer

To evaluate the virus' clinical potential, *in vitro* growth curve analysis was performed on a panel of human cancer cells lines, and the fold increase in virus production was determined (**Table 4.1**). Using a 10-fold increase as the cut-off for productive infection, ORFV was able to productively infect 16 of the 31 cell lines tested, with over 3-log output in A549 lung adenocarcinoma cells. ORFV growth curve analysis of infected A549 cancer cells and normal human dermal fibroblast cells (nHDF) highlights the preferential cytotoxicity and amplification in cancer cells (**Fig. 4.14a,b**). To test ORFV *in vivo*, CD-1 nude mice were engrafted with A549 cells subcutaneously, and mice were treated intra-tumourally with 5 doses of ORFV (10^7) or PBS vehicle control. ORFV was able to significantly reduce A549 tumour burden as illustrated by tumour volume measurements (**Fig. 4.14c**). Collectively, these data highlight ORFV's potential as a replicating therapeutic for the treatment of human cancer.

4.3 DISCUSSION

I have identified and characterized the anti-cancer properties of a new poxvirus platform and show for the first time that ORFV treatment of both immune competent and xenograft human tumour models leads to significant anti-tumour acitivity. My results implicate NK cells in the ORFV-mediated reduction in tumour burden (**Fig. 4.8,4.10,4.11,4.12**). In earlier studies, inactivated ORFV particles on their own where shown

Cell Line	Cell Origin	Permissive	Fold Increase	Day
MDAMB-435	Breast carcinoma	+	19	1
U251	Glioblastoma	+	8	1
Cal27	Head and Neck squamous cell carcinoma	-	3	1
HCT116	Colon carcinoma	-	3	1
NCI-H23	Adeno lung carcinoma	-	0	1
Caski	Epidermoid carcinoma	-	0	1
SCC25	Head and Neck squamous cell carcinoma	-	0	1
HT1080	Fibrosarcoma	+	207	2
PLC/PRF/5	Renal carcinoma	+	88	2
MCF-7	Breast cancer	+	10	2
M14	Melanoma	+	10	2
OVCAR-8	Ovarian carcinoma	-	8	2
SNB19	CNS carcinoma	-	7	2
SCC9	Head and Neck squamous cell carcinoma	-	4	2
SKMEL-28	Melanoma	-	3	2
C41	Cervical carcinoma	-	3	2
SW620	Colon carcinoma	-	3	2
786-0	Renal carcinoma	-	3	2
SF268	CNS sarcoma	-	2	2
HT29	Colon carcinoma	-	2	2
HeLa	Cervical carcinoma	+	551	3
SF295	Glioblastoma	+	54	3
SKMEL-3	Melanoma	+	37	3
HOP92	Lung carcinoma	+	32	3
ME180	Cervical carcinoma	+	26	3
UACC62	Melanoma	+	21	3
SKMEL-2	Melanoma	+	15	3
HOP-62	Non-small cell lung carcinoma	-	3	3
A549	Lung adenocarcinoma	+	1090	4
U2OS	Osteosarcoma	+	16	4
PC3	Prostate carcinoma	+	12	4

Table 4.1 ORFV infection of human cancer cell lines. ORFV growth curves were performed on a panel of human cancer cell lines at an MOI of 1. Cells were infected at time 0, and cell lysates collected and processed for virus by OA3.Ts plaque assay at time-points post infection. Virus titer was compared to input titers at the indicated time point post infection to calculate the fold increase in ORFV.

a.

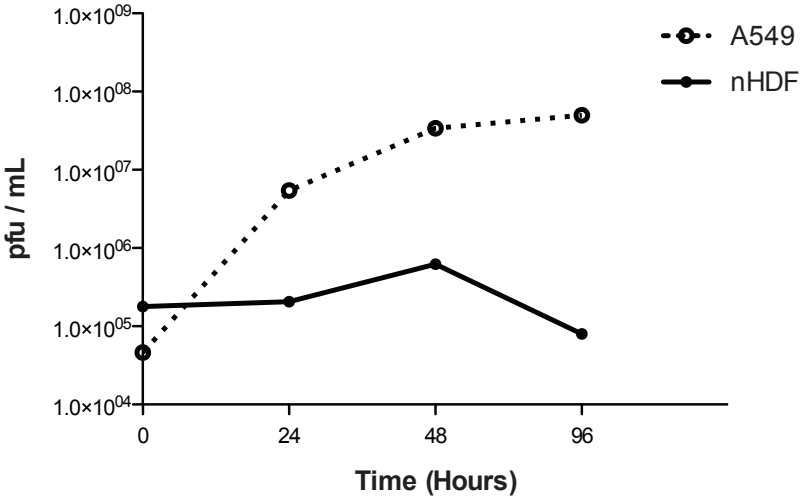
1.0×10^09
1.0×10^08
1.0×10^07
1.0×10^06
1.0×10^05
1.0×10^04
pfu / mL
A549
nHDF
0
24
48
96
Time (Hours)

b.

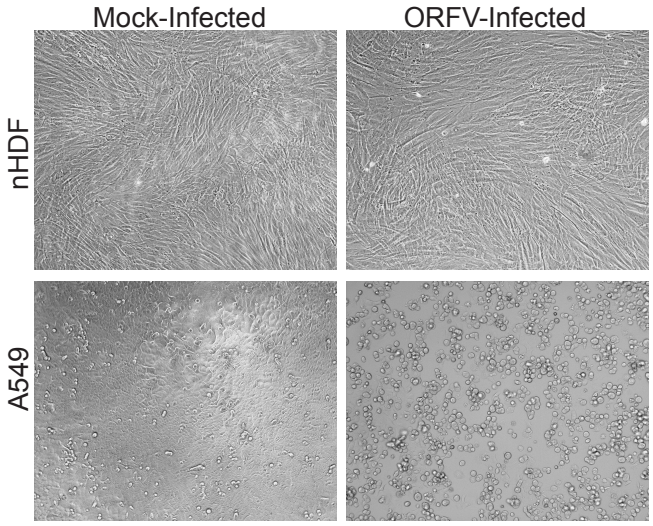
Mock-Infected
ORFV-Infected
nHDF
A549

c.

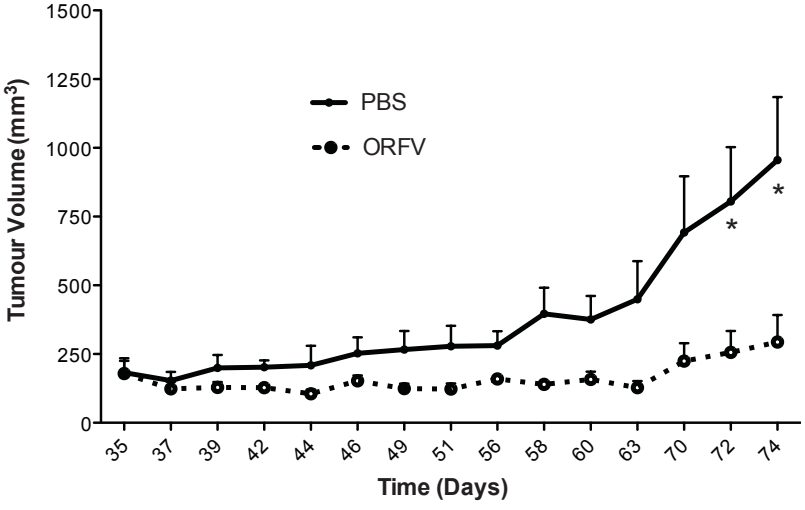
1500
1250
1000
750
500
250
0
Tumour Volume (mm3)
PBS
ORFV
*
*
35
37
39
42
44
46
49
51
56
58
60
63
70
72
74
Time (Days)

Figure 4.14 ORFV therapy reduces tumor burden in an A549 xenograft model of cancer. (**a**) Representative ORFV growth curves on A549 and nHDF cells at an MOI of 1. Cells were infected at time 0, and cell lysates collected and processed for virus by OA3.Ts plaque assay at time-points post infection. (**b**) Phase contrast images of mock-infected, and ORFV infected A549 and nHDF cells at an MOI of 0.05, at 72 hours post infection at a magnification of 40X. (**c**) Human A549 cells ($2x10^6$) were seeded sub-cutaneously into the right flank of CD-1 nude mice. ORFV (10^7) or PBS treatments were given intra-tumorally on days 24, 27, 29, 31 and 34-post tumour implantation. Mouse tumour volume was monitored over time. N=5, mean + SEM, (*P <0.05 using an unpaired T-Test with Welch's correction). A549, human lung adenocarcinoma cells; nHDF neonatal human dermal fibroblast cells; PBS, phosphate-buffered saline; pfu, plaque-forming unit; MOI, multiplicity of infection.

to stimulate a T_h-1 dominated immune response,[161,164,165] and so it was not surprising that UV inactivated ORFV had a significant impact in the metastatic lung models (**Fig. 4.3**). Replicating ORFV however has a significantly greater impact in the lung models; possibly due to its induction of more potent cytokine and cytotoxic NK cell responses (**Fig. 4.10,4.12**), coupled with its oncolytic activity in the murine cancer cells (**Fig. 4.3**).

My finding that ORFV treatment was only efficacious in the lung models if delivered intravenously, suggests that tumour clearance was dependent upon the presence of ORFV in the lungs. Previous work has established that OV delivered by footpad injection[192] does not migrate to the lungs. Since ORFV only significantly reduces tumour burden by intravenous delivery (**Fig. 7**), it is likely that ORFV must be present at the tumour site for effective priming of anti-tumour NK cell responses.

A number of oncolytic viruses have been shown to induce potent adaptive anti-tumour immune responses (reviewed by Melcher *et al*.),[80] but only a select few have been shown to stimulate anti-tumour NK cell responses.[89,90,183] Since cytokine production by NK cells supports T_h-1 immunity,[48] the induction of IFN-γ secreting NK cells suggests that ORFV treatment could lead to adaptive anti-tumour immune responses. Interestingly, several reports have now indicated that human[193] and mouse[194] NK cells can be divided into two phenotypically distinct subsets: poorly cytotoxic, cytokine producing NK cells, and highly cytotoxic, poor cytokine producing NK cells. Interestingly, I have shown that ORFV is capable of stimulating NK cells of both phenotypes (**Fig. 4.10,4.11**).

In my pre-clinical studies, I observed significant increases in the size of spleens in ORFV treated mice and this could present as a potential site for an adverse reaction. However, the splenomegaly was transient since immune cell populations returned to their

normal proportions within 8 days post treatment. Kinetic studies have found that the ORFV-induced pro-inflammatory immune response is balanced with subsequent induction of an anti-inflammatory response.[168,169] I believe that the unique biology of ORFV that allows for self-regulation of inflammatory responses can be exploited for safe an effect therapeutic benefit as I describe herein.

From a clinical perspective, I are encouraged that ORFV efficacy in murine lung tumour models was comparable or better than 2 other oncolytic poxviruses (**Fig. 4.4**), and that ORFV was able to infect a panel of human cancer cell lines (**Table 4.1**). In the parapoxvirus literature, it has only ever been documented that ORFV can productively infect primary cell cultures prepared from bovine testis.[125,147,184] My findings that a number of human tumour cell lines are permissive for ORFV replication is reminiscent of the earlier studies with myxoma virus that had documented a restricted host range of the virus, and later found myxoma to replicate well in human cancer cells.[125] Indeed I show here that ORFV can replicated in A549 cells and when engrafted into nude mice, has readily apparent anti-tumour activity *in vivo* (**Fig. 4.14**). These data emphasize ORFV's potential as a multi-modality viral therapy for humans, where the virus could have both an oncolytic impact, and potentially induce even greater immune responses than those reported here in murine models. I was also encouraged that ORFV performed better than the TLR-3 agonist Poly IC in both lung metastasis models (**Fig. 4.13**). TLR agonists like Poly IC have been tested as anti-cancer agents in clinical trial, however their lack of potency combined with serious adverse reactions has limited their application.[195]

ORFV's potent activation of NK cells, and human cancer cell oncolysis highlight the novel anti-cancer potential of the virus. Since antibody has been reported to be a barrier to OV therapy,[94-96] it is advantageous that the majority of the population has had limited

exposure to ORFV, and that antibody does not prevent re-occurring infections in animals.[155,156,171,172] These characteristics, combined with the unique biology of the ORFV virion and its limited pathogenicity in humans make it an attractive platform for the development of new anti-cancer biotherapeutics.

CHAPTER 5: MECHANISM AND THERAPEUTIC APPLICATION OF ORFV INNATE IMMUNE STIMULATION

5.1 INTRODUCTION

Several reports have documented ORFV's immune stimulating capacity in a number of different species, including humans. The exact mechanism by which ORFV stimulates the immune system however is not yet known, but both TLR-dependent and independent mechanisms have been described, including signaling via CD14.[168,169] CD14 is a pattern recognition receptor (PRR) that acts as a coreceptor for the activation of TLRs.[168] The TLR family consists of at least 12 distinct members that are primarily expressed by innate sentinel cells, like DCs and macrophages.[196] Another group of PRR are the RNA helicases involved in intracellular recognition of double stranded RNA: RIG-I and MDA-5. These viral sensing molecules have been implicated in the recognition of Epstein-Barr virus,[197] influenza virus,[198] and measles virus.[199] Although it was found that VACV recognition by DCs was mediated by both TLR-2[200] and TLR-4,[201] these TLRs do not contribute to ORFV activation of DCs.[202] Since other members of the poxvirus family have been reported to activate DCs via TLR-independent pathways,[203] it is possible that ORFV recognition occurs via similar TLR-independent recognition, by perhaps as of yet unidentified intracellular receptors.

Inactivated ORFV treatment of monocytes has been well documented in both human[168,169] and mouse[202] immune cells, where treatment leads to release of type I IFN, and

T_h-1 cytokines like IL-12 and IL-18. The release of both IL-12 and IL-18 cytokines was shown to be required for subsequent production of IFN-γ by either T cells or NK cells.[168] In the context of viral infection, after sensing pathogens, DCs mature by increasing expression of MHC, costimulatory molecules and importantly, by release of inflammatory cytokines.[204] The production of IL-12 from DCs can further induce NK cell production of IFN-γ and/or lead to enhanced cytotoxic capacity.[205] The direct contact between DCs and NK cells has also proven to be critical for DC-mediated activation of NK cells.[204]

A number of viruses have been noted for their ability to directly engage NK cells. Upon infection of mice with MCMV, NK cell activating receptor Ly49H is capable of recognizing the MCMV m157 gene that is expressed on the surface of infected cells.[206] In humans, influenza infection leads to NK activation via activating receptor NKp46 binding to virus hemagglutinin on the surface of infected cells.[207] Recent evidence suggests that NK cells express a number of TLRs, and are therefore capable of directly sensing viral pathogens.[102] NK cells have also been noted as important mediators in protection from poxvirus infection.[102,208] Interestingly, VACV was found to directly activate murine NK cells via recognition by TLR-2.[102] These experiments also demonstrated that UV-inactivated VACV was capable of activating NK cells via TLR-2,[102] thereby suggesting recognition of VACV particles was independent of newly synthesized viral gene products.

DC-based vaccination strategies are a novel anti-cancer therapy, that have been shown to induce both innate and adaptive anti-tumour effector function.[192,209] Importantly, recent clinical evidence from DC vaccine trials have demonstrated that NK cell responses were a better correlative for positive patient outcome than T cell responses.[210] Considering the evidence supporting DC-NK crosstalk,[39,192,209] virus-induced activation of DCs is an

attractive anti-cancer strategy. Indeed a number of viruses have already been noted for their ability to activate NK cells via DCs.[192,211] For example, NK cell responses induced by herpes virus infection of mice were diminished following *in vivo* ablation of CD11c-positive DCs.[211] The relevance of DC mediated activation of tumouricidal NK cells is further evidenced by the work of Wan and colleagues, where they have highlighted the potential of VSV infected DCs as an effective anti-tumour strategy.[192]

A number of studies have described ORFV activation of DCs using inactivated preparations of the virus. In the context of oncolytic therapy, I first aimed to confirm ORFV's ability to activate DCs *in vivo*. Using *ex vivo* infection models, I next evaluated ORFV's capacity to directly activate NK cells or DCs. The importance of ORFV activated DCs for ORFV anti-tumour efficacy was further evaluated in a murine DC-depletion model. Finally, a surgery model of cancer was employed to demonstrate the clinical applicability of a replicating, immune stimulating parapoxvirus therapeutic for the treatment of cancer.

5.2 RESULTS

ORFV is capable of directly activating NK cells and DCs

To first determine if ORFV could directly activate NK cells, naïve untreated C57Bl/6 animals were sacrificed, and their spleens used to isolate purified, untouched $NK1.1^+$ cells. Following *in vitro* stimulation with IL-2, NK cells were infected with ORFV at an MOI of 3, or treated with the TLR-3 agonist Poly IC at either 50 μg/mL or 200 μg/mL (**Fig. 5.1a**) NK cells were then harvested at 24 hours, and examined by flow cytometry for activation status. Representative flow cytometry dot plots illustrate that ORFV treatment led to an increase in CD69 expression compared to levels expressed from naive NK cells (**Fig. 5.1b**). The percentage of NK1.1 positive cells expressing the early activation marker CD69 was

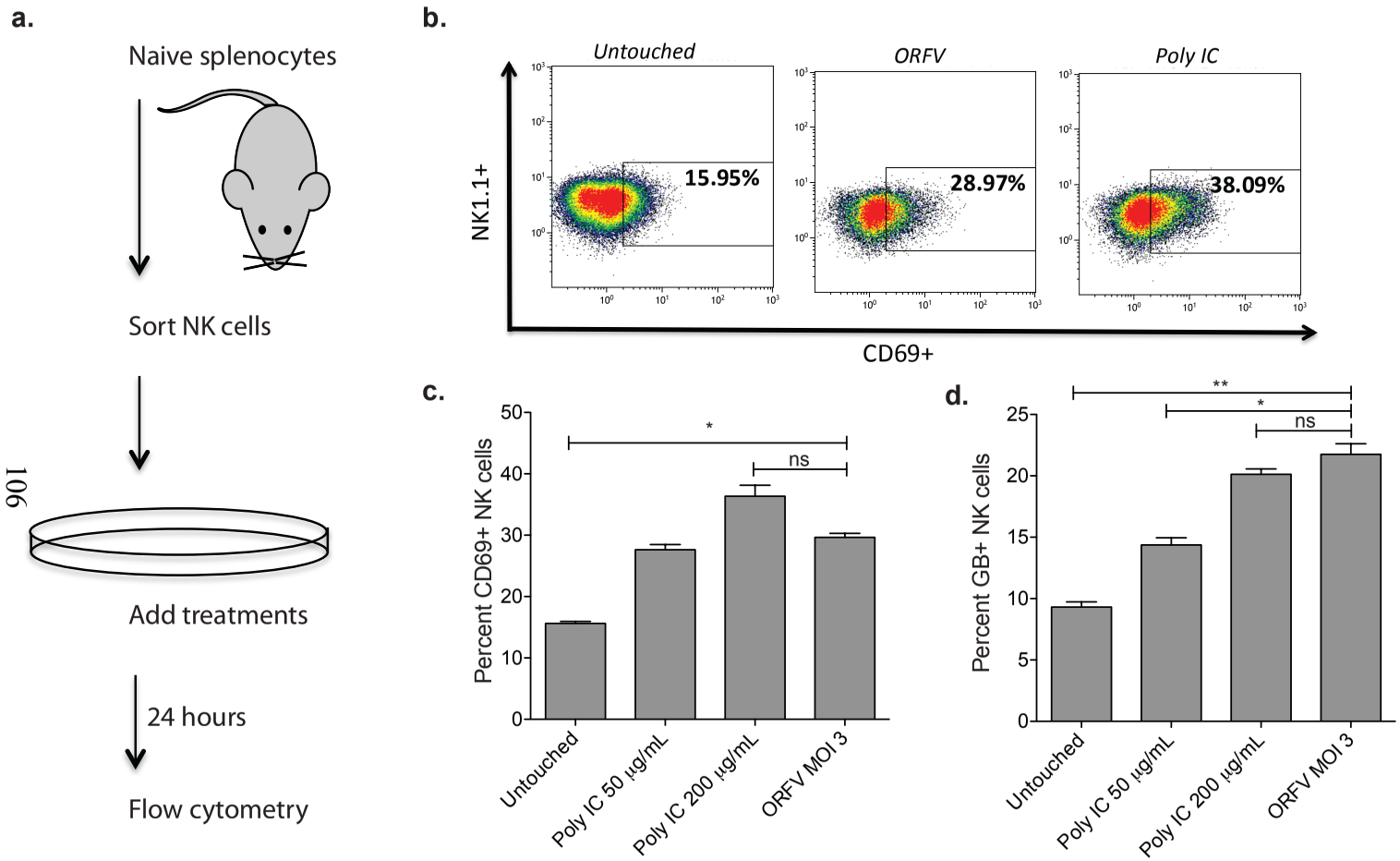
a.
Naive splenocytes
Sort NK cells
10^6
Add treatments
24 hours
Flow cytometry
b.
Untouched
ORFV
Poly IC
15.95%
28.97%
38.09%
NK1.1+
CD69+
c.
Percent CD69+ NK cells
50
40
30
20
10
0
*
ns
Untouched
Poly IC 50 μg/mL
Poly IC 200 μg/mL
ORFV MOI 3
d.
Percent GB+ NK cells
25
20
15
10
5
0
**
*
ns
Untouched
Poly IC 50 μg/mL
Poly IC 200 μg/mL
ORFV MOI 3

Figure 5.1 *Ex vivo* ORFV infection of NK cells. (**a**) A schematic outlining the NK isolation and treatment schedule for *ex vivo* infections. (**b**) Representative flow-cytometry dot plots of percent gated NK cells ($NK1.1^+$ cells) versus percent gated $CD69^+$ cells for the indicated treatments. (**c**) The percent gated $CD69^+$ NK cell population was quantified for each treatment group. N=2, mean + SEM (**P* < 0.005 using an unpaired, *t*-Test with Welch's correction). (**d**) The percent gated granzyme B^+ NK cell population was quantified for each treatment group. N=2, mean + SEM (**P* < 0.01, ***P* <0.05 using an unpaired, *t*-Test with Welch's correction). GB, granzyme B.

quantified (**Fig. 5.1c**). ORFV stimulation of NK cells led to a significant increase in CD69 expression that was comparable to the high dose of Poly IC. The intracellular expression of granzyme B was also quantified (**Fig. 5.1d**), where ORFV stimulation was found to significantly increase granzyme B expression from NK cells compared to naïve untreated controls. Interestingly, ORFV induced more granzyme B expression from NK cells than did 50 μg/mL of Poly IC.

In the context of the B16F10-LacZ C57Bl/6 lung model, the *in vivo* activation status of DCs was evaluated (**Fig. 5.2**). Tissues from tumour bearing C57Bl/6 animals treated with PBS or ORFV were analyzed by flow cytometry for CD11c expression, and corresponding expression of co-stimulatory molecules and cytokines at 24 hours post IV ORFV. There were significantly more $CD11c^+$ cells in the lung and blood of ORFV treated animals compared to PBS treated animals (**Fig. 5.2a**). DC expression of co-stimulatory molecules CD80 and CD86 were elevated in the blood and lung, and spleen, respectively (**Fig. 5.2b,c**). ORFV treatment also led to significantly more TNFα and IL-12 cytokine expression from DCs in the lung (**Fig. 5.2d,e**).

To evaluate the ability of UV-inactivated ORFV to stimulate *in vivo* co-stimulatory molecule or cytokine expression by DCs, tissues from tumour bearing C57Bl/6 animals were analyzed by flow cytometry at a 24-hour time point. Quantification of the percent gated $CD11c^+$ cells expressing CD86 was evaluated in the spleen, illustrating significantly more co-stimulatory molecule expression from live ORFV treated animals, compared to UV-inactivated ORFV treated animals (**Fig. 5.3a**). Similar results were observed in the blood and lung for $CD11c^+$ cells expressing CD80 (**Fig. 5.3c,d**). DCs isolated from the spleen of live

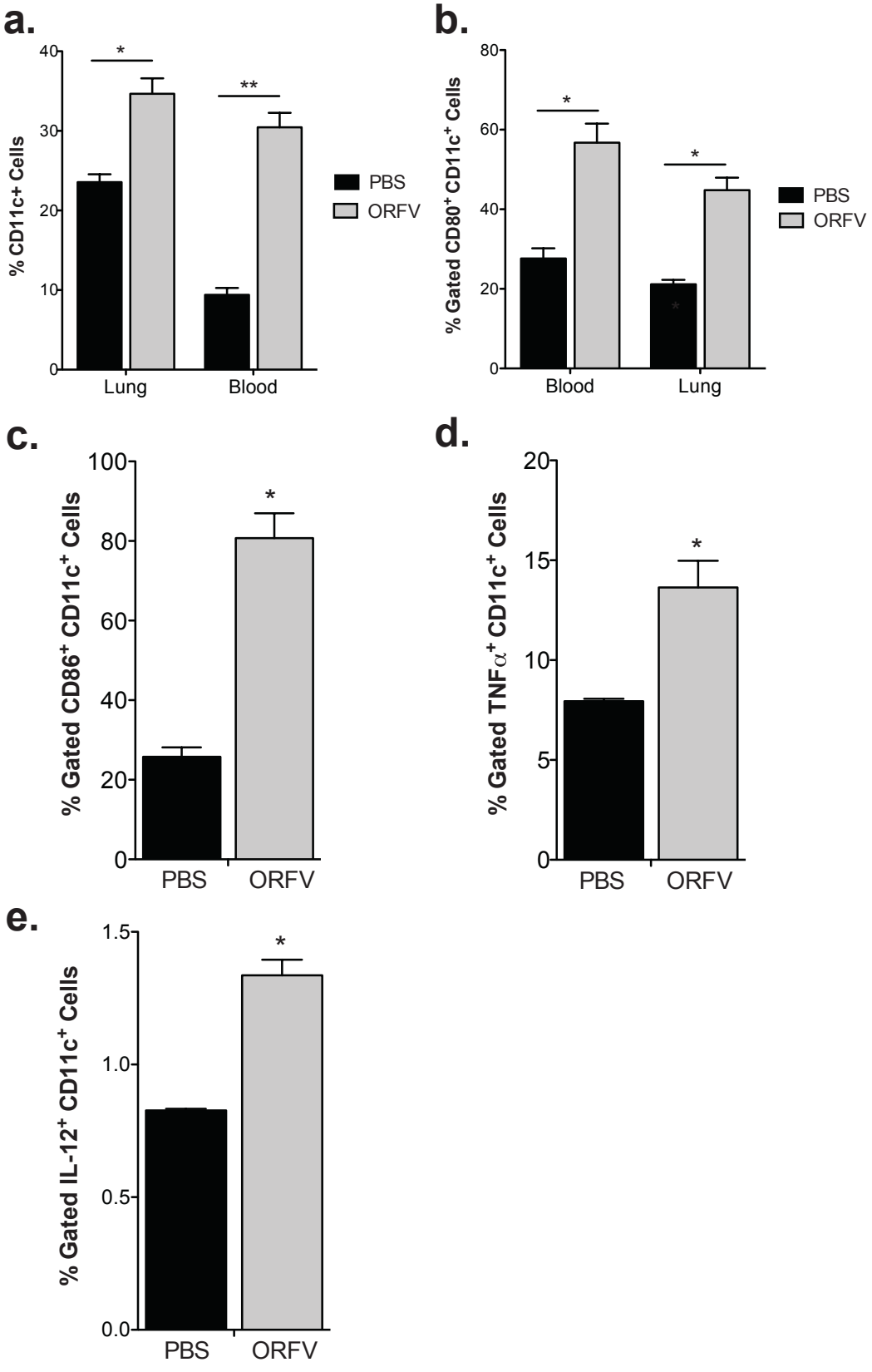
a.
% CD11c+ Cells
40
30
20
10
0
*
**
PBS
ORFV
Lung
Blood
b.
% Gated CD80+ CD11c+ Cells
80
60
40
20
0
*
*
PBS
ORFV
Blood
Lung
c.
% Gated CD86+ CD11c+ Cells
100
80
60
40
20
0
*
PBS
ORFV
d.
% Gated TNFα+ CD11c+ Cells
20
15
10
5
0
*
PBS
ORFV
e.
% Gated IL-12+ CD11c+ Cells
1.5
1.0
0.5
0.0
*
PBS
ORFV

Figure 5.2 Flow-cytometry analysis of ORFV-activated DCs. (**a**) Tumour bearing C57Bl/6 animals were treated IV with (10^7) ORFV, or PBS. At 24 hours post-infection, tissues were harvested from animals, and processed by flow cytometry. The percent total $CD11c^+$ cells in the lung and blood was compared. (**b**) Percent gated $CD80^+$ expression from $CD11c^+$ cells isolated from the blood, and lung of ORFV and PBS-treated animals is compared. (**c**) Percent gated $CD86^+$ expression from $CD11c^+$ cells isolated from the spleen of ORFV and PBS-treated animals is compared. (**d**) Percent gated $TNF\alpha^+$ expression from $CD11c^+$ cells isolated from the lung of ORFV and PBS-treated animals is compared. (**e**) Percent gated $IL\text{-}12^+$ expression from $CD11c^+$ cells isolated from the lung of ORFV and PBS-treated animals is compared. N=3, mean + SEM (*P <0.05, **P <0.01 using an unpaired t-Test with Welch's correction). PBS, phosphate buffered saline.

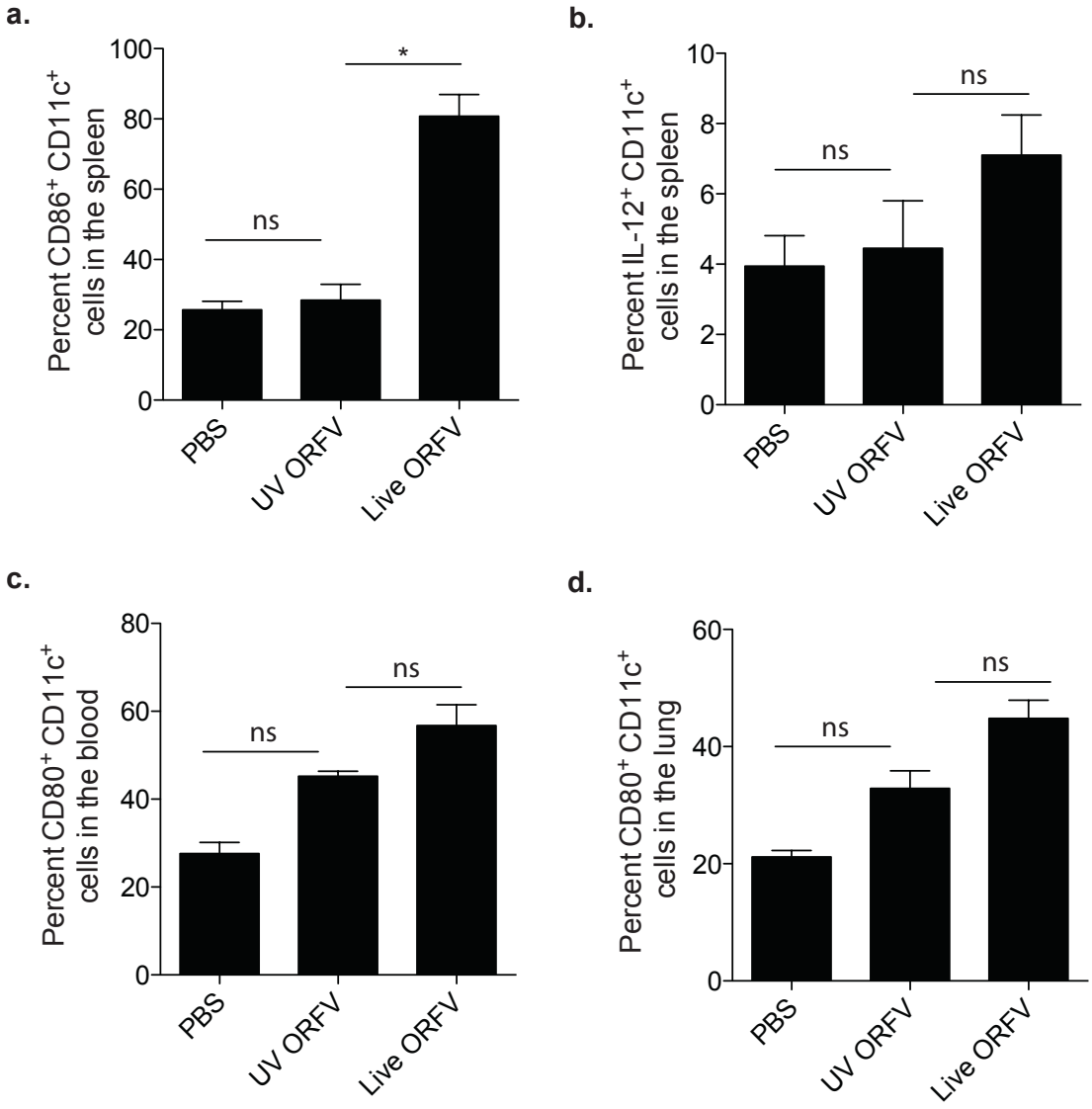
a.
Percent CD86+ CD11c+ cells in the spleen
100
80
60
40
20
0
ns
*
PBS
UV ORFV
Live ORFV
b.
Percent IL-12+ CD11c+ cells in the spleen
10
8
6
4
2
0
ns
ns
PBS
UV ORFV
Live ORFV
c.
Percent CD80+ CD11c+ cells in the blood
80
60
40
20
0
ns
ns
PBS
UV ORFV
Live ORFV
d.
Percent CD80+ CD11c+ cells in the lung
60
40
20
0
ns
ns
PBS
UV ORFV
Live ORFV

Figure 5.3 Flow-cytometry anlysis comparing live ORFV to UV inactivated ORFV *in vivo* stimulation of DCs. Lung tumour-bearing C57Bl/6 animals were treated IV with (10^7) UV-ORFV, Live ORFV, or PBS. At 24 hours post-infection, tissues were harvested from animals, and processed for flow cytometry. (**a**) Percent gated $CD86^+$ $CD11c^+$ cells in the spleen was compared. N=3, mean + SEM (*P <0.01, using an unpaired *t*-Test with Welch's correction). (**b**) Percent gated IL-12^+ $CD11c^+$ cells in the spleen was compared. (**c**) Percent gated $CD80^+$ $CD11c^+$ cells in the blood was compared. (**d**) Percent gated $CD80^+$ $CD11c^+$ cells in the lung was compared. (N=3, mean + SEM, no significant differences as measured by a unpaired *t*-Test with Welch's correction).

ORFV treated animals also secreted more IL-12 than DCs isolated from UV-inactivated ORFV treated animals (**Fig. 5.3b**).

To evaluate if ORFV was capable of directly activating DCs, bone marrow was isolated from naïve untreated C57Bl/6 animals, and DCs were isolated following a 6-day GM-CSF maturation period. In a similar fashion as experiments performed for NK cells (**Fig. 5.1a**), DCs were infected with ORFV at an MOI of 3, treated with the TLR-9 agonist CpG at 10 μg/mL or remained treatment free (**Fig. 5.4**). At an 18-hour time point, DCs were harvested and examined by flow cytometry for cell surface expression of co-stimulatory molecules CD86 and CD40. ORFV infection of DCs led to an increase in both CD86 and CD40 expression compared to naïve, untouched DCs as visualized from the flow cytometry histograms in **Fig. 5.4a,d**, respectively. The amount of co-stimulatory molecule expressed on a per cell basis was quantified, and represented as the mean fluorescence intensity (MFI). ORFV infection of DCs significantly increased the MFI of CD86 and CD40, (**Fig. 5.4b,e**). The amount of CD86 expressed per ORFV treated cell was equivalent to the amount expressed per CpG treated cell. Finally, the percent $CD86^{+}CD11c^{+}$ cells was also compared, and it was found that ORFV treatment resulted in significantly more positive cells than untreated, and CpG treated DCs (**Fig. 5.4c**). The percent $CD40^{+}CD11c^{+}$ cells was also significantly higher in ORFV treated samples compared to naïve, untouched samples (**Fig. 5.4f**).

To further evaluate if ORFV was capable of directly activating murine DCs, cytokine expression was examined by flow cytometry at 24 hours post infection with live ORFV, Ad-GFP, or CpG positive control (**Fig. 5.5a,b,c** - respectively). ORFV treated DCs induced significant expression of TNF-α, with some expression of cytokine IL-12. This is contrast to

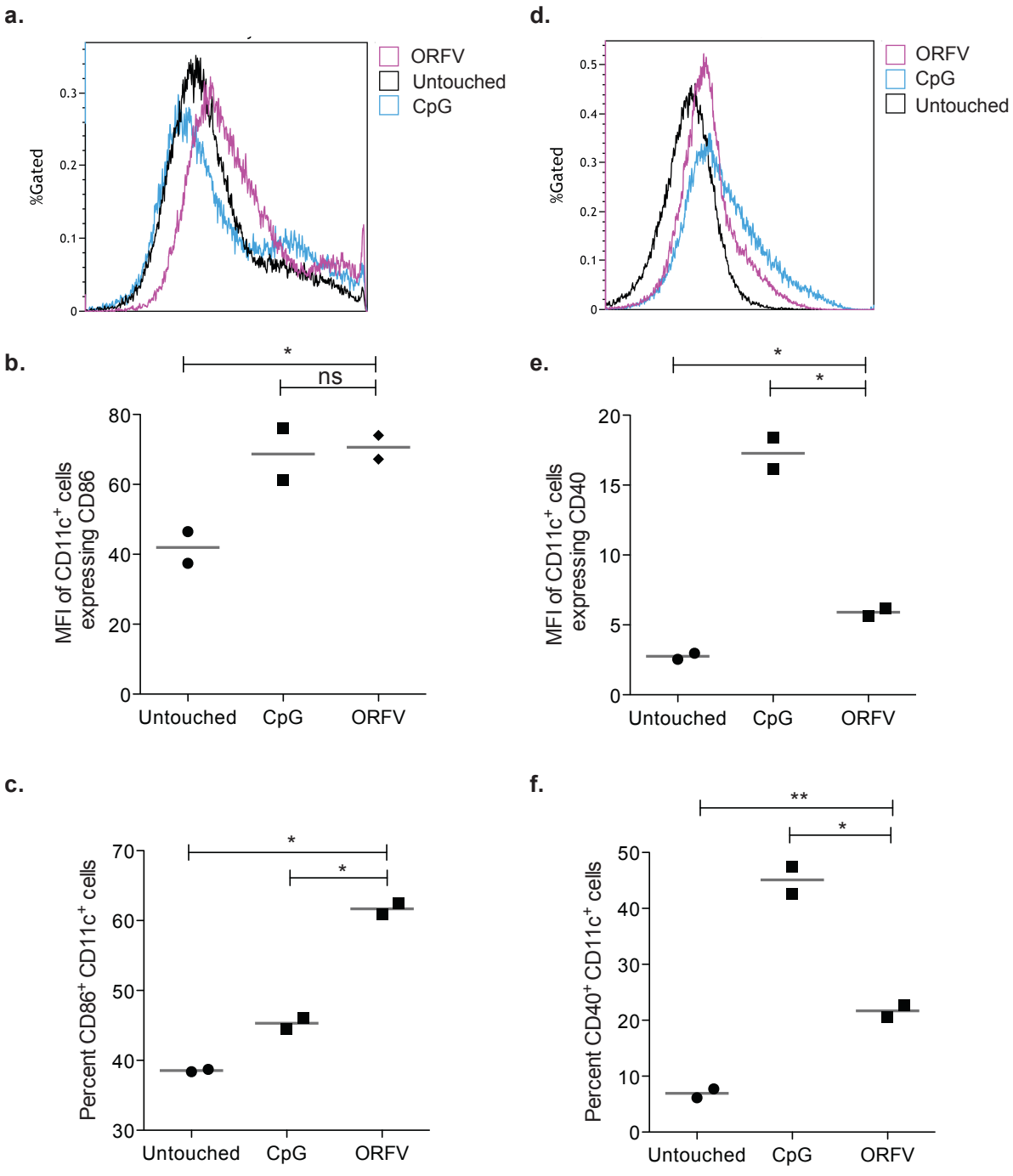
a.
ORFV
Untouched
CpG
%Gated
0
0.1
0.2
0.3
d.
ORFV
CpG
Untouched
%Gated
0
0.1
0.2
0.3
0.4
0.5
b.
*
ns
MFI of CD11c+ cells expressing CD86
0
20
40
60
80
Untouched
CpG
ORFV
e.
*
*
MFI of CD11c+ cells expressing CD40
0
5
10
15
20
Untouched
CpG
ORFV
c.
*
*
Percent CD86+ CD11c+ cells
30
40
50
60
70
Untouched
CpG
ORFV
f.
**
*
Percent CD40+ CD11c+ cells
0
10
20
30
40
50
Untouched
CpG
ORFV

Figure 5.4 *Ex vivo* ORFV infection of DCs and flow cytometry analysis of co-stimulatory molecule expression. (**a**) Representative flow-cytometry histogram overlay comparing CD86 expression by DCs untreated, or infected with ORFV (MOI 3) or CpG (10 μg/mL). (**b**) Quantification of the amount of CD86 being expressed per $CD11c^+$ cell, represented as the mean fluorescence intensity (MFI). N=2, mean + SEM (*$P < 0.05$ using an unpaired *t*-Test with Welch's correction). (**c**) The percent gated $CD86^+$ $CD11c^+$ cells was quantified and compared. N=2, mean + SEM (*P <0.005 using an unpaired *t*-Test with Welch's correction). (**d**) Representative flow-cytometry histogram overlay comparing CD40 expression by DCs untreated, or treated with ORFV (MOI 3) or CpG (10 μg/mL). (**e**) Quantification of the amount of CD40 being expression per $CD11c^+$ cell, represented as the mean fluorescence intensity (MFI). N=2, mean + SEM (*$P < 0.05$ using an unpaired *t*-Test with Welch's correction). (**f**) The percent gated $CD40^+$ $CD11c^+$ cells was quantified and compared. N=2, mean + SEM (*P <0.05, **P <0.01 using an unpaired *t*-Test with Welch's correction). MFI, mean fluorescence intensity.

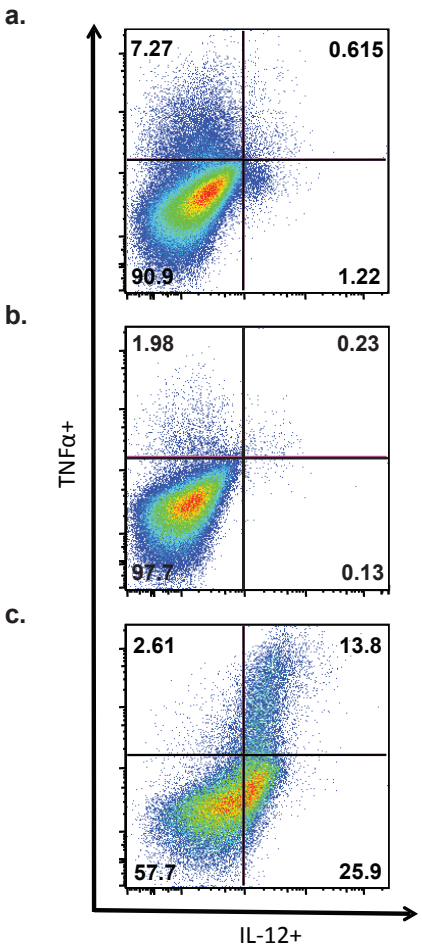
a.
7.27
0.615
90.9
1.22
b.
1.98
0.23
97.7
0.13
c.
2.61
13.8
57.7
25.9
TNFα+
IL-12+

Figure 5.5 *Ex vivo* ORFV infection of DCs and flow cytometry analysis of cytokine expression. Representative flow-cytometry dot plots of DC expression of cytokines TNF-α and IL-12 following *ex vivo* infection of DCs with (**a**) ORFV at an MOI of 3 or (**b**) Ad-GFP at an MOI of 100 or (**c**) CpG at 10 μg/mL. TNF-α, tumour necrosis factor alpha; IL-12, interleukin-12.

a.

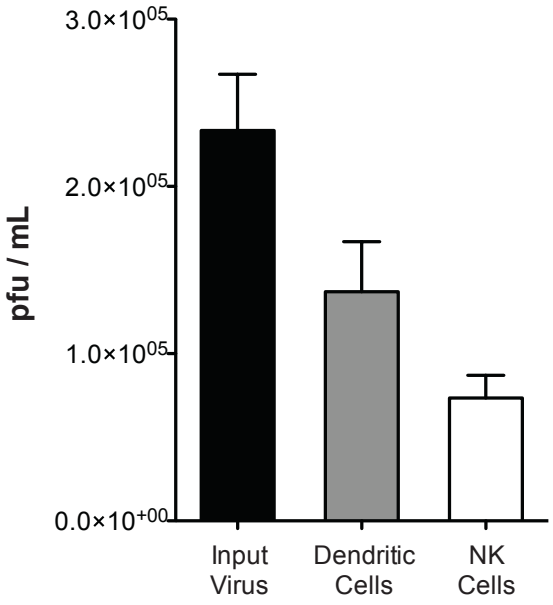
3.0×10^05
2.0×10^05
1.0×10^05
0.0×10^+00
pfu / mL
Input Virus
Dendritic Cells
NK Cells

Figure 5.6 ORFV infection of NK cells and DCs. (**a**) ORFV titer of infected DCs and NK cells at 24 hours post infection at an MOI of 1, compared to input virus. PBS, phosphate-buffered saline.

DCs stimulated with CpG that showed significant expression of both cytokines. Interestingly, ORFV treatment induced greater cytokine expression than Ad-GFP treated DCs. To rule out virus amplification in murine NK cells and DCs, ORFV infection of both subsets was also analyzed by plaque assay (**Fig. 5.6**). At 24 hours post infection, neither cell type supported productive ORFV infection.

Cell depletion studies implicate DCs in the activation of NK cells, and clearance of lung metastases

To evaluate the contribution of DCs in mediating the *in vivo* activation of NK cells, DC depletion was accomplished by diptheria toxin treatment of CD11c-DTR transgenic C57Bl/6 mice. As outlined in **Fig. 5.7**, CD11c-DTR animals were challenged with B16F10-LacZ cells, and 8 hours later, half of the animals were treated with diptheria toxin (DT) to deplete DCs. Animals were divided into 4 groups: PBS + DT, PBS alone, virus + DT, and virus alone. At 15 hours, animals were treated with virus, or PBS. At 24 hours, animals were sacrificed, and their spleens and lungs evaluated for immune function and tumour burden, respectively. The total number of cells isolated from the spleen of each mouse was quantified (**Fig. 5.7b**), and no significant differences were observed. To confirm depletion of DCs, flow cytometry was used to quantify the number of $CD11b^{+}CD11c^{+}$ (DCs) in the spleen of each mouse (**Fig. 5.7c**). In both PBS treated and virus treated groups, DT successfully depleted DCs from the spleen.

To determine how DC depletion impacted the activation of NK cells, flow cytometry was used to evaluate the level of CD69 expression on NK cells (**Fig. 5.8**). As seen from the histogram in **Fig. 5.8a**, ORFV induced significant CD69 expression on NK cells compared to naïve, PBS treated animals. Conversely, the level of CD69 expression on NK cells from DC-depleted animals was much lower, despite treatment with ORFV. The amount of CD69

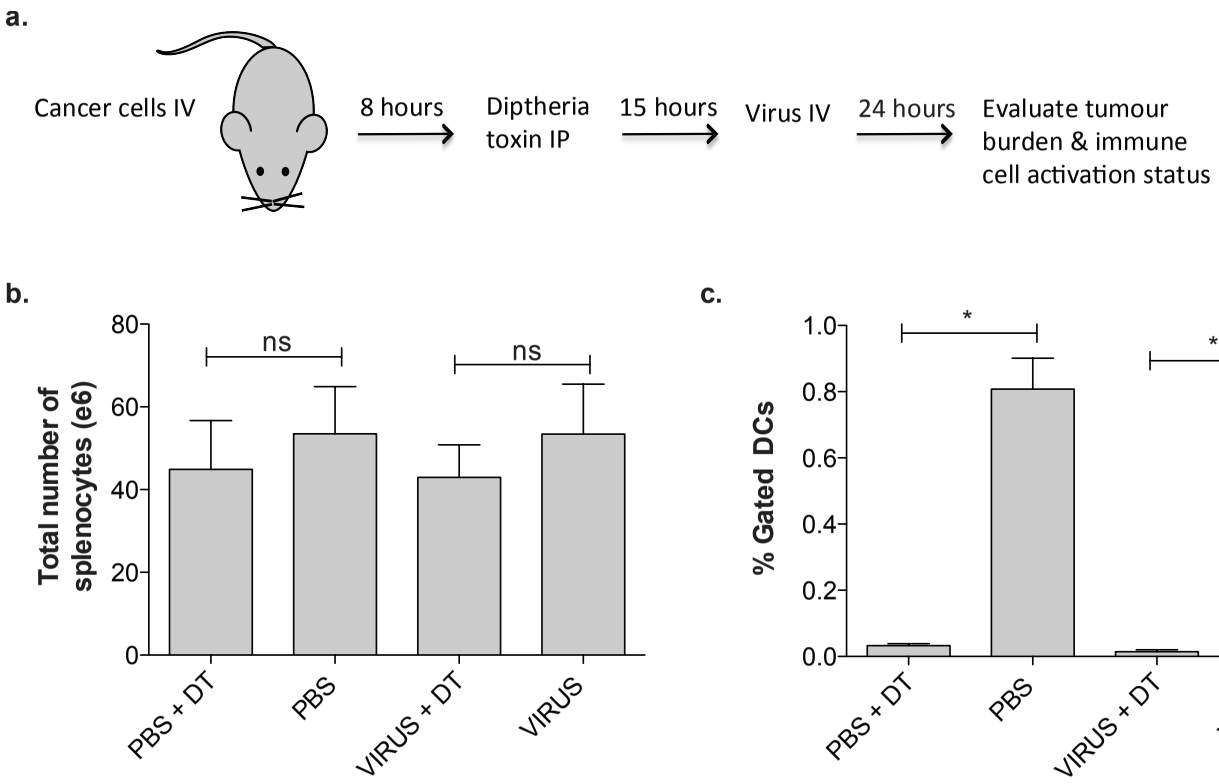
a.
Cancer cells IV
8 hours
Diptheria toxin IP
15 hours
Virus IV
24 hours
Evaluate tumour burden & immune cell activation status
b.
Total number of splenocytes (e6)
80
60
40
20
0
ns
ns
PBS + DT
PBS
VIRUS + DT
VIRUS
c.
% Gated DCs
1.0
0.8
0.6
0.4
0.2
0.0
*
*
PBS + DT
PBS
VIRUS + DT
VIRUS

Figure 5.7 *In vivo* DC depletion and experiment outline. (**a**) A schematic outlining the treatment schedule for DC depetion of C57Bl/6 CD11c-DTR transgenic mice. (**b**) The total number of splenocytes from mice at experiment endpoint. N=8, mean + SEM (**c**) The percent gated DCs was determined by flow cytometry from the spleen of mice at experiment endpoint. N=8, mean + SEM (*P <0.0001, using an unpaired t-Test with Welch's correction). DT, diptheria toxin; IV, intravenous; IP, intraperitoneal; PBS, phosphate buffered saline.

a.

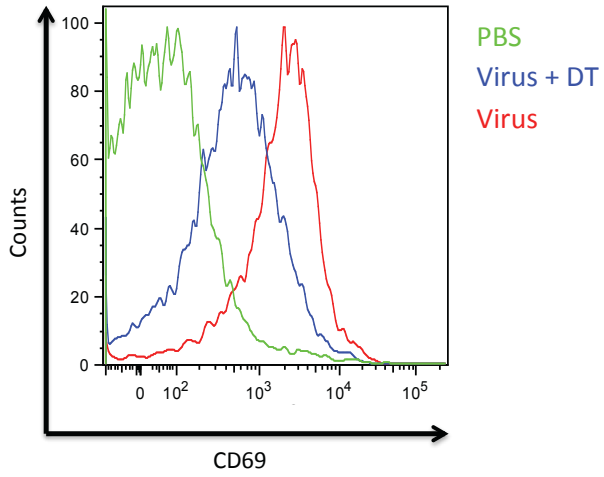
PBS
Virus + DT
Virus
Counts
CD69
100
80
60
40
20
0
0
10^2
10^3
10^4
10^5

b.

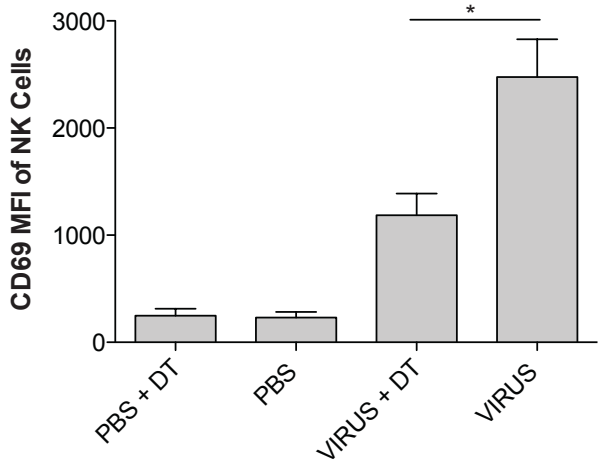
CD69 MFI of NK Cells
3000
2000
1000
0
*
PBS + DT
PBS
VIRUS + DT
VIRUS

c.

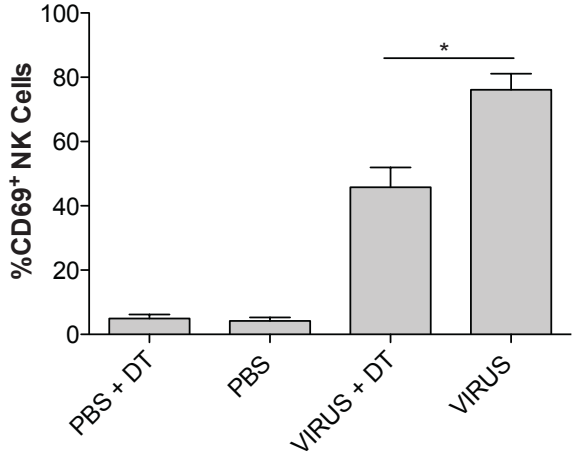
%CD69+ NK Cells
100
80
60
40
20
0
*
PBS + DT
PBS
VIRUS + DT
VIRUS

Figure 5.8 Flow-cytometry analysis of ORFV-activated NK cells in the absence of DCs. Splenocytes were isolated from C57Bl/6 CD11c-DTR transgenic animals at experiment endpoint, and were processed for flow cytometry. (**a**) Representative histogram of NK cell expression of CD69 for PBS treated animals (PBS), ORFV treated animals with DC depletion (Virus + DT), and ORFV treated animals (Virus). (**b**) A quantification of the amount of CD69 expressed on a per NK cell basis from splenocytes isolated from mice at experiment endpoint determined using the mean fluorescence intensity (MFI) (**c**) Percent gated CD69 expression from NK cells isolated from the spleen at experiment endpoint. N=8, mean + SEM. (**P* <0.0001, using an unpaired *t*-Test with Welch's correction). DT, diptheria toxin; MFI, mean fluorescence intensity; PBS, phosphate buffered saline.

expressed per NK cell was quantified, and the mean fluorescence intensity was found to be significantly reduced in animals depleted of DCs and treated with ORFV, compared to DC-intact ORFV treated animals (**Fig. 5.8b**). Similar trends were observed for the quantification of percent NK cells expressing CD69 (**Fig. 5.8c**). The number of surface lung metastases was also quantified and compared (**Fig. 5.9**). Consistent with the NK depletion studies (**Fig. 4.10**), DC depletion led to a significant reduction in ORFV efficacy.

ORFV activation of NK cells is independent of tumour cell infection

To rule out the possibility that the ORFV mediated activation of NK cells was not in part facilitated through NK cell recognition of ORFV-infected tumour cells, NK cell activation was evaluated *in vivo* in the presence and absence of tumour cells. Briefly, CT26-LacZ tumour-bearing or tumour naïve Balb/c mice were treated with ORFV, or remained treatment naïve. At a 24-hour time point, both the lungs, and spleen were evaluated for CD69 expression by NK cells. The number of NK cells detected in the lungs of animals was equivalent between tumour bearing virus naïve animals, tumour-naïve virus treated animals and tumour-bearing ORFV treated animals (**Fig. 5.10a**). As expected, the percent gated $CD69^+$ NK cells was significantly higher in the lungs of ORFV treated animals than virus naïve animals (**Fig. 5.10b**). However, there was no difference in CD69 expression between tumour-bearing, and tumour-naïve ORFV treated groups. Similar results were observed in the spleen (**Fig. 5.10c,d**).

Since it is well known that cytokine expression by DCs can lead to upregulation of NK cell activation receptors, the expression of NKG2D by NK cells was evaluated in tumour-naïve ORFV treated C57Bl/6 mice (**Fig. 5.11**). In both the blood and spleen, the percentage of NK cells expressing NKG2D was significantly higher than NK cells isolated from PBS treated animals.

a.

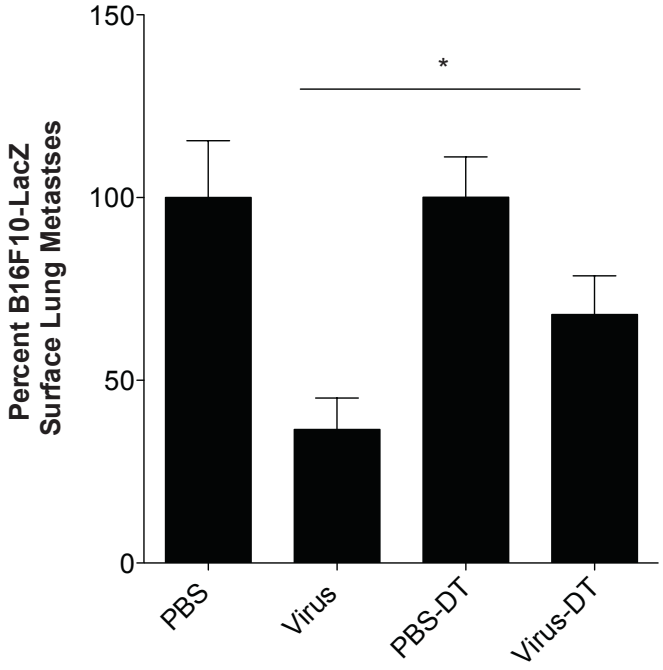
Percent B16F10-LacZ Surface Lung Metastses
150
100
50
0
*
PBS
Virus
PBS-DT
Virus-DT

Figure 5.9 *In vivo* ORFV efficacy in the absence of DCs. (**a**) Lungs were isolated from C57Bl/6 CD11c-DTR transgenic animals at experiment endpoint, and the number of B16F10-LacZ surface lung metastases were quantified and compared. N=8, mean + SEM, (*P <0.05 using an unpaired t-Test with Welch's correction). DT, diptheria toxin; PBS, phosphate buffered saline.

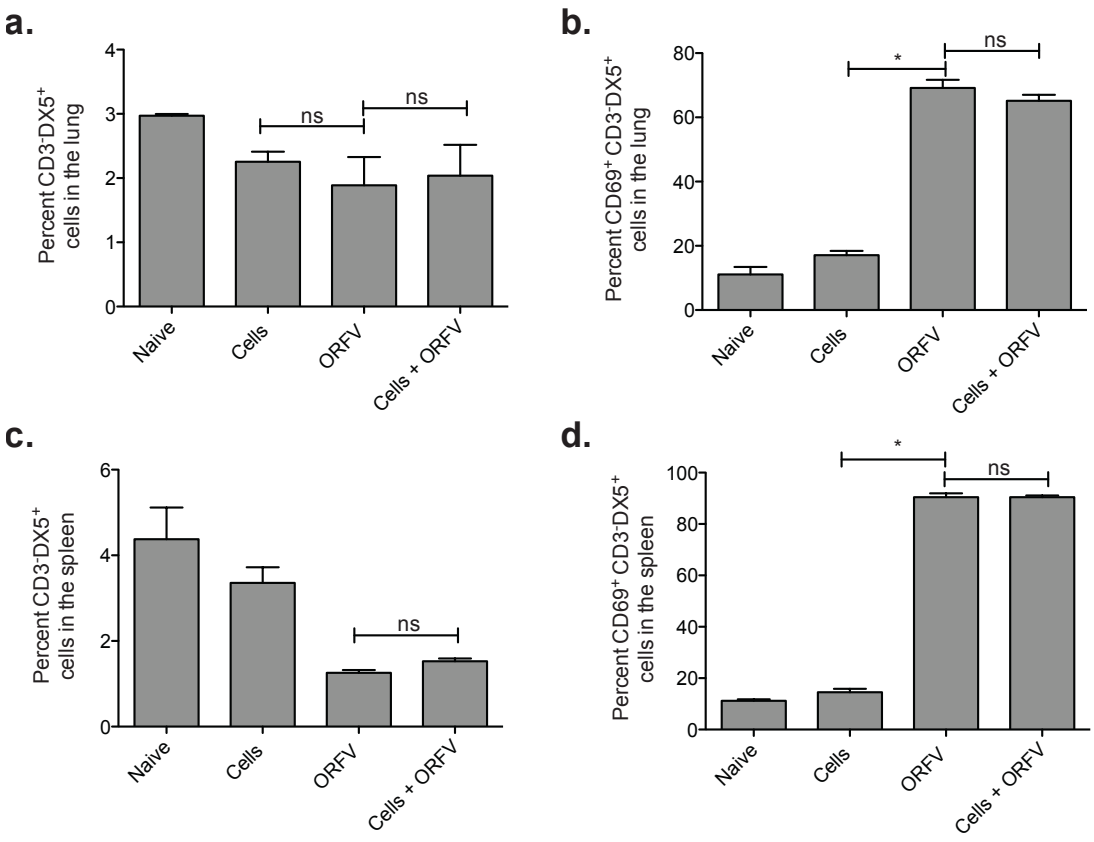
a.
Percent CD3-DX5+ cells in the lung
4
3
2
1
0
ns
ns
Naive
Cells
ORFV
Cells + ORFV
b.
Percent CD69+ CD3-DX5+ cells in the lung
80
60
40
20
0
*
ns
Naive
Cells
ORFV
Cells + ORFV
c.
Percent CD3-DX5+ cells in the spleen
6
4
2
0
ns
Naive
Cells
ORFV
Cells + ORFV
d.
Percent CD69+ CD3-DX5+ cells in the spleen
100
80
60
40
20
0
*
ns
Naive
Cells
ORFV
Cells + ORFV

Figure 5.10 Comparing *in vivo* ORFV activation of NK cells in the presence and absence of tumour. Balb/c animals were divided into 4 groups: naïve, tumour-bearing (cells), ORFV treated (ORFV) or tumour-bearing, ORFV treated (cells + ORFV). Balb/c animals were challenged with 10^5 CT26-LacZ tumour cells IV. At 24 hours, animals received ORFV treatment IV (10^7). At 48 hours, animals were sacrificed, and their lungs, and spleens were processed and analyzed by flow cytometry. (**a**) The percent gated NK cells in the lung was quantified. (**b**) Percent gated CD69 expression from NK cells isolated from the lung. (**c**) The percent gated NK cells in the spleen was quantified. (**d**) Percent gated CD69 expression from NK cells isolated from the spleen. N=2, mean + SEM (*P <0.05, using an unpaired T-Test with Welch's correction).

a.

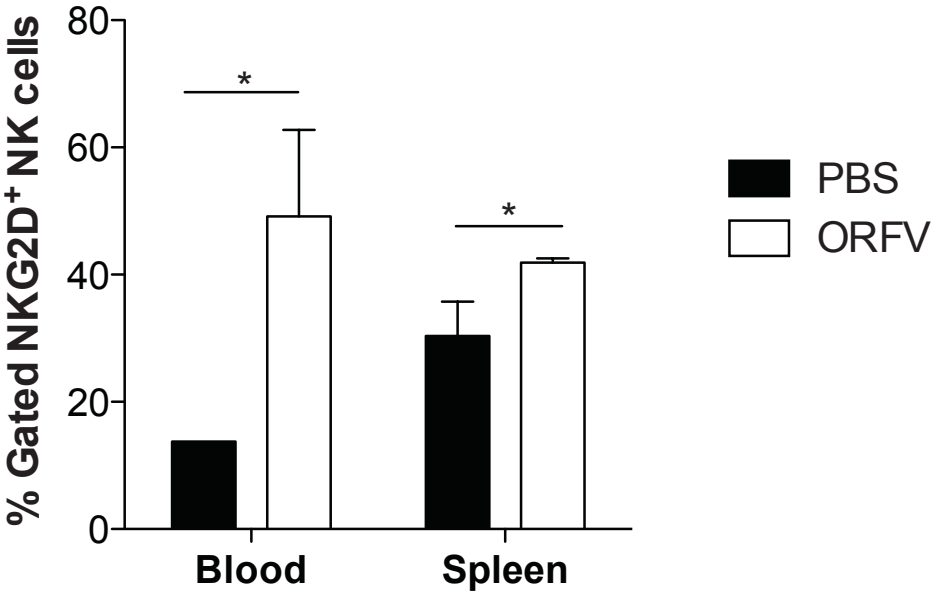

Figure 5.11 Flow-cytometry analysis of NK activation receptor, NKG2D. (**a**) C57Bl/6 animals were treated with ORFV (10^7) or PBS IV. At 24 hours animals were sacrificed and the blood and spleen processed for flow cytometry. Percent gated NKG2D expression by NK cells isolated from the blood, and spleen of ORFV and PBS-treated animals is compared. N=3, mean + SEM (*P <0.05, using an unpaired t-Test Welch's correction). PBS, phosphate-buffered saline.

To determine if ORFV could prevent the seeding of lung tumour mestastases in a prophylactic lung model, ORFV was delivered intravenously to Balb/c animals 2 days prior to CT26-LacZ IV tumour cell challenge (**Fig. 5.12**). To completely rule out the effects of virus amplification, and persistence in the lungs UV-inactivated ORFV was used. Interestingly, UV-inactivated ORFV was capable of significantly reducing CT26-LacZ lung metastases in the prophylactic setting.

ORFV can significantly reduce tumour mestastases in a model of surgery

Since ORFV was capable of stimulating NK cells up to 2 days prior to therapy, even in the absence of tumour cells, I hypothesized that the virus might act as an effective immune modulator to counteract the formation of tumour metastases that form as a result of surgical stress during the perioperative period. The surgical stress model is depicted in **Fig. 5.13a**. Briefly, 4 hours after animals are treated with an immune modulator, they are challenged with tumour cells intravenously followed immediately by anesthesia and partial nephrectomy. At a 3-day timepoint, animals were euthanized, and lungs were evaluated for tumour burden. The effect of surgical stress can be seen from the quantification of lung metastases from PBS treated animals (**Fig. 5.13b**, left), where there is significantly more tumour burden in animals subjected to surgery. Interestingly, ORFV is able to completely rescue the NK related effects of surgery, and significantly reduce the number of lung metastases in the surgical group.

To evaluate the contribution of NK cells in mediating the immune suppression caused by surgical stress, cytotoxicity assays were performed. As seen in **Fig. 5.14a**, NK cells isolated from animals that underwent surgery have limited cytotoxicity towards the YAC-1 target cells compared to naïve, no surgery treated animals. In contrast, NK cells isolated from

a.

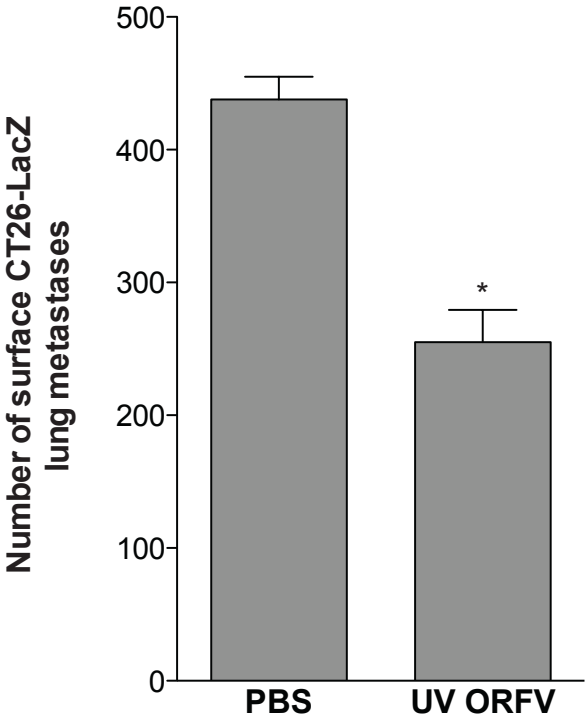
Number of surface CT26-LacZ lung metastases
500
400
300
200
100
0
*
PBS
UV ORFV

Figure 5.12 ORFV as an immunotherapy. (**a**) Balb/c animals were treated with UV-inactivated ORFV (10^7) or PBS IV, and 2 days later challenged with 10^5 CT26-LacZ cells IV. Animals were sacrificed at 10-days post cell injection, lungs were isolated and processed, and the number of surface lung metastases was compared. N=5, mean + SEM, (**P* <0.001 using an unpaired *t*-Test with Welch's correction). PBS, phosphate-buffered saline; UV, ultra-violet.

a.

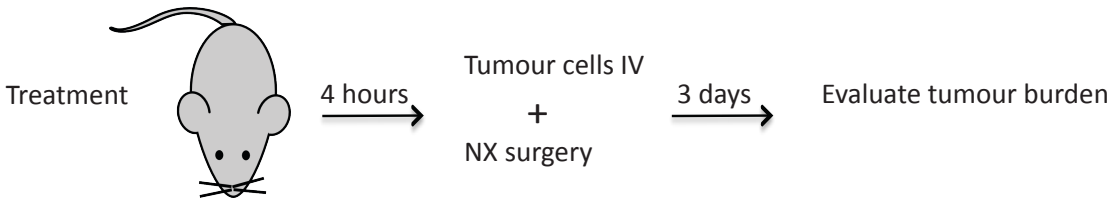
Treatment
4 hours
Tumour cells IV
+
NX surgery
3 days
Evaluate tumour burden

b.

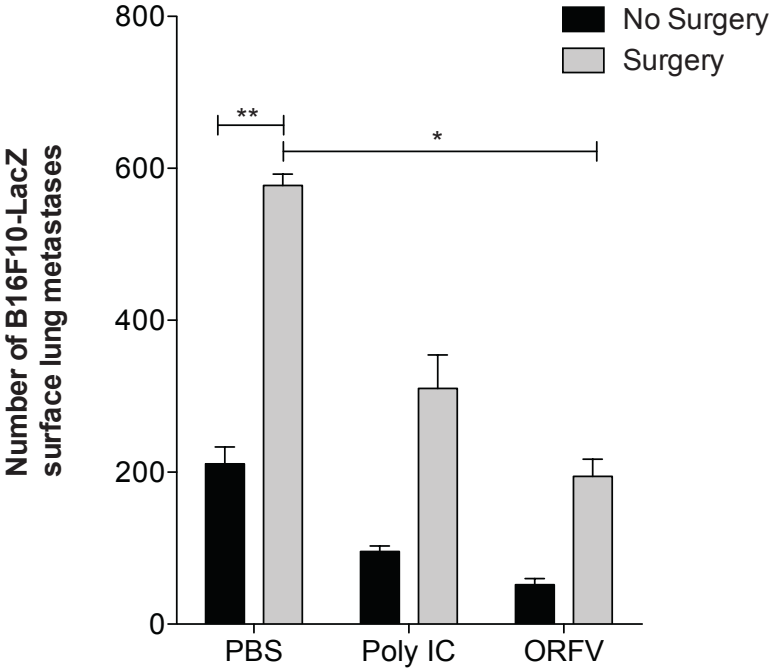
No Surgery
Surgery
Number of B16F10-LacZ surface lung metastases
800
600
400
200
0
**
*
PBS
Poly IC
ORFV

Figure 5.13 ORFV as an immunotherapy in a surgery model of cancer. (**a**) A schematic outlining the treatment schedule for the model of surgical stress. (**b**) The number of surface B16F10-LacZ lung metastases from C57Bl/6 animals treated as (**a**) were quantified and compared. N=4, mean + SEM, (*$P <$ 0.05, **$P < 0.0005$ using an unpaired *t*-Test with Welch's correction). nx, surgery by nephrectomy; PBS, phosphate buffered saline; Poly IC, polyinosinic:polycytidylic acid.

a.

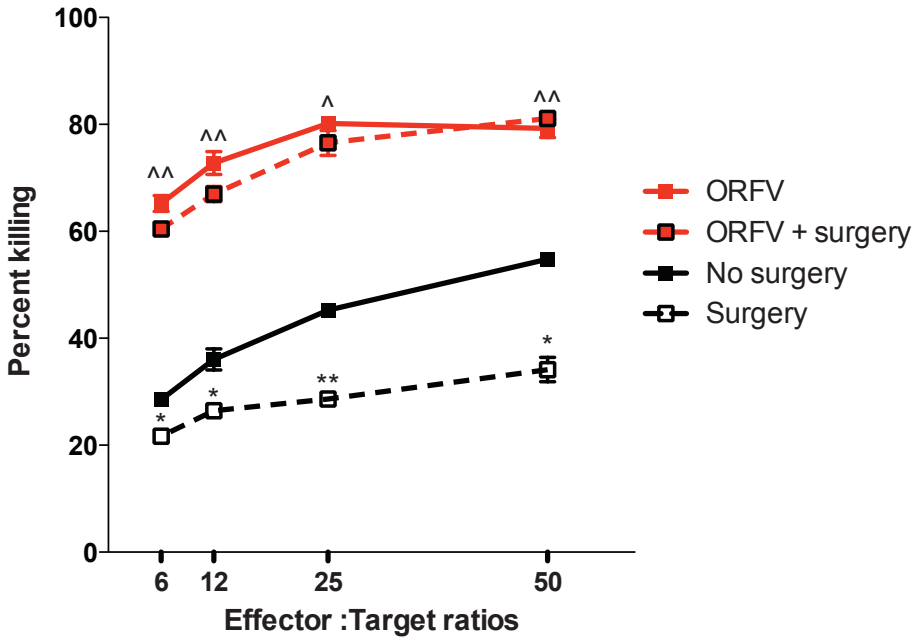
100
80
60
40
20
0
Percent killing
^^
^^
^
^^
*
*
**
*
6
12
25
50
Effector :Target ratios
ORFV
ORFV + surgery
No surgery
Surgery

b.

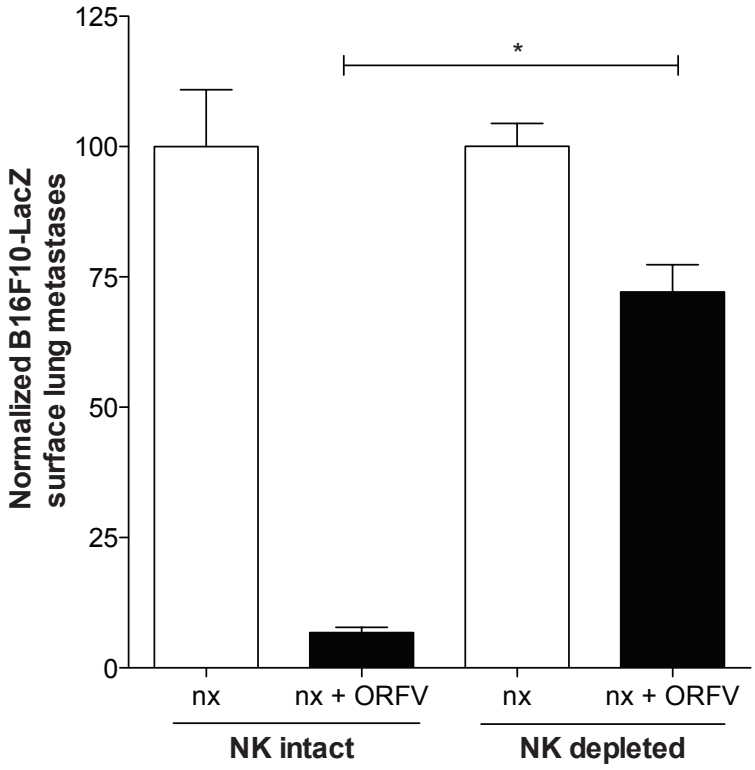
125
100
75
50
25
0
Normalized B16F10-LacZ surface lung metastases
*
nx
nx + ORFV
nx
nx + ORFV
NK intact
NK depleted

Figure 5.14 ORFV rescues the NK cell impairment imposed by surgical stress. (**a**) *Ex vivo* cytotoxicity assays were performed on NK cells isolated from C57Bl/6 mice from 4 treatment groups: surgery with PBS treatment (Surgery), no surgery with PBS treatment (No surgery), surgery with ORFV treatment (ORFV + surgery), and no surgery with ORFV treatment (ORFV). Spleens were isolated, pooled and enriched for NK cells by $DX5^+$ cell sorting. NK cells were then mixed with chromium labeled YAC-1 target cells in triplicate, at different effector:target ratios. Shown is the percent killing of target YAC-1 cells at 24 hours post infection. N=3, mean + SEM, (**P* <0.05, ***P* <0.01 comparing surgery to no surgery, ^*P* <0.01, ^^*P* <0.001 comparing ORFV surgery to no surgery using an unpaired, *t*-Test with Welch's correction). (**b**) C57Bl/6 animals were depleted of NK cells by treatment with 3 25 μL doses of anti-asialo antibody (or IgG control) IV on days -3, and -1 and 2. Animals were treated with ORFV (10^7) or PBS with surgery by nephrectomy. Animals were sacrificed at 3-days post cell injection, lungs were isolated and processed, and the number of surface lung metastases was compared. N=5, mean + SEM, (**P* <0.0005 using an unpaired *t*-Test with Welch's correction). nx, surgery by nephrectomy.

ORFV treated animals induced significant cytotoxicity of target cells. Additionally, ORFV treatment completely rescued the NK cell impairment caused by surgical stress.

Finally, to determine the contribution of ORFV activated NK cells in the surgery model, C57Bl/6 mice were depleted of NK cells in the context of surgery (**Fig. 5.14b**). The ability of ORFV to reduce surgical stress-induced tumour metastases was compared in the presence and absence of NK cells. With NK cells intact, ORFV reduced lung metastases by nearly 90%, whereas in the absence of NK cells, ORFV only reduced lung metastases by approximately 25%. This significant difference in ORFV activity highlights the importance of immune modulation for ORFV efficacy.

A model of ORFV anti-tumour activity

The mechanism of ORFV anti-cancer activity is highlighted in **Fig. 5.15**. ORFV has demonstrated direct oncolysis of tumour cells. ORFV has also demonstrated robust activation of cytokine-secreting, cytotoxic NK cells. NK cell mediated killing of tumour cells appears to be the primary anti-tumour mechanism in the lung models. ORFV activated NK cells secrete significant amounts of both granzyme B, and IFN-γ - both capable of inducing tumour cell death. The activation of NK cells may be direct, through *in vitro* activation of NK cell surface PRR, or indirect via DC activation. DC activation by ORFV leads to cytokine secretion, which in turn may lead to robust NK cell activation *in vivo*. Cytokine secretion by DCs may also explain how *in vivo* ORFV therapy leads to increased NKG2D activating receptor expression by NK cells.

5.3 DISCUSSION

The mechanism of ORFV immune stimulation has been the focus of a number of recent reports.[168,169,202] Using inactivated ORFV, these studies highlighted the importance of

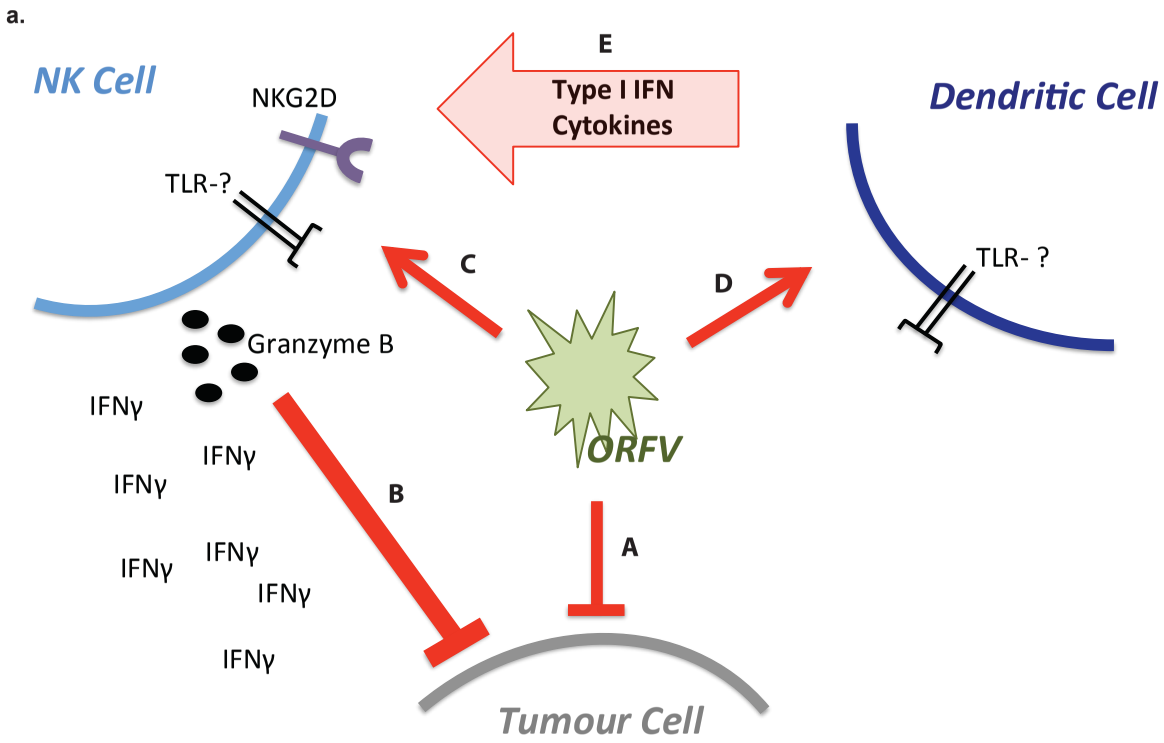
a.
NK Cell
NKG2D
TLR-?
E
Type I IFN
Cytokines
Dendritic Cell
TLR- ?
C
D
Granzyme B
IFNγ
IFNγ
IFNγ
IFNγ
IFNγ
IFNγ
IFNγ
B
A
ORFV
Tumour Cell

Figure 5.15 Mechanistic model of ORFV anti-tumour activity. ORFV anti-tumour activity can be both direct, through oncolysis of tumour cells (**a**), or indirect via activation of immune cell anti-tumour effector functions (**b**). ORFV activated NK cells can kill tumours via cytokine secretion of granzyme B and IFN-γ, or direct cytotoxicity of cancer cells. The activation of NK cells may be direct, through stimulation of an unknown TLR (**c**), or indirect via DC activation (**d**). ORFV activated DCs release cytokines capable of activating NK cells (**e**). DC cytokine expression has also been found to increase expression of NKG2D on NK cells. TLR, toll-like receptor; IFN-γ, interferon-gamma.

the ORFV virion, and expression of proteins for the unique immune stimulatory profile. The mechanism of immune stimulation was found to include both TLR dependent and independent mechanisms resulting in cytokine secretion from monocytes or antigen presenting cells.[168] I aimed to determine if oncolytic ORFV could have similar effects on murine DCs, and whether ORFV activation of DCs was the primary mechanism of NK cell activation. Our studies indicate that ORFV may be able to directly activate NK cells (**Fig. 5.1**). NK cells have been shown to express a number of TLRs, including TLR-3,7,8 and 9.[102] Although the PRR responsible for recognizing ORFV has yet to be determined, it is possible that the virions are recognized directly by NK cells. Indeed it was recently discovered that VACV particles (live and UV inactivated virions) directly activate NK cells via TLR-2.[102]

In the context of the lung metastasis model, I have also confirmed that ORFV infection leads to significant activation of $CD11c^+$ DCs (**Fig. 5.2**). Through *ex vivo* infection, I have verified that live ORFV is capable of directly activiating DCs (**Fig. 5.4, 5.5**). Using the CD11c-DTR transgenic C57Bl/6 mice, I demonstrated that DC depletion reduces the level of NK cell activation, and the ability of ORFV to clear lung metastases. Indeed several reports have highlighted the importance of DC/NK cross talk,[183,192,211] and so it was not surprising that the ORFV activated DCs are at least partially responsible for ORFV-mediated NK cell activation. Interestingly, quantifiation of lung metastases (**Fig. 5.9**) demonstrated approximately 50% loss of efficacy, similar to results found for the NK cell depletion experiments (**Fig. 4.10**). Since the DC depletion was efficacious (**Fig. 5.7**), these data could suggest that the ORFV oncolysis is still an important component to efficacy. Alternatively, ORFV immune stimulation may lead to activation of other anti-tumour effector populations, like macrophages. ORFV has been shown to activate macrophages,[212] and under certain conditions these cells have demonstrated anti-tumour effector functions.[213] It was however

curious that DC depletion resulted in a 50% loss of efficacy *and* a 50% loss in NK cell activation (**Fig. 5.8**). These data highlight the possibility that direct ORFV-activation of NK cells may also be contributing to the immune stimulation.

I have demonstrated in Chapter 4 that a live replicating ORFV is more efficacious at *in vivo* activation of NK cells than UV inactivated ORFV (**Fig. 4.10, 4.12**). I have also demonstrated that live ORFV is more efficacious at activating DCs *in vivo* (**Fig. 5.3**). Recently, Friebe and colleagues created a VACV/ORFV expression library to identify a number of candidate ORFV open reading frames responsible for the immune stimulation.[169] They found several, most of which were related to virion structure. Although it is possible that the quantitative difference in immune stimulation by live and UV-inactivated ORFV is attributed to additional PRR engagement by a protein expressed late in the ORFV infection, extensive characterization of ORFV immune stimulation would suggest that this is not the case.[168,169,202] The difference in *in vivo* immune stimulation therefore may be attributed to persistence and amplification of replicating ORFV. An active infection is likely to cause more inflammation, recruit more immune cells, *and* has potential to cause more cell death. Active infection therefore would cause a greater 'danger signal' than UV-inactivated ORFV. Interestingly, Weber and colleagues reported that both live, and inactivated ORFV was capable of inducing apoptosis in murine monocytes.[214] I have demonstrated that ORFV does not productively infect NK cells or DCs (**Fig. 3.6**), however I have not ruled out the possibility that ORFV may be killing these cells. Since I have demonstrated an increase in the percentage of $CD11c^+$ cells in the lung and blood following ORFV treatment, it is unlikely that this is the case. Further evidence dismissing the possibility of ORFV-induced apoptosis of immune populations is the study by Siegemund and colleagues, where they

reported no signs of apoptosis from murine bone marrow derived DCs cultured with inactivated ORFV.[202]

Virus induced NK cell killing of target cells can occur via one of several mechanisms (reviewed in Chapter 1.3.5). Some poxviruses have been noted for their ability to decrease cellular MHC I expression on infected cells so as to evade elimination by T cells.[215] Decrease in MHC I expression makes these cells inherently sensitive to NK cell killing. My studies clearly illustrated however that NK cell activation by ORFV was not dependent on cancer cell infection, since NK cells were activated to the same extent in tumour naïve animals (**Fig. 5.10**). Prophylactic treatment with UV-inactivated ORFV also demonstrated a reduction in lung metasases (**Fig. 5.12**). Furthermore, NK cells removed from a tumour naive, ORFV-treated mouse were still capable of inducing NK cell cytotoxicity (**Fig. 4.10**). Together, these data indicate that NK cell effector function following ORFV treatment is independent of cancer cell infection.

Other studies have highlighted a requirement for natural cytotoxicity receptors in the recognition of vaccinia virus infected cells,[216] however the mechanisms underlying NK cell responses to poxvirus infection remain largely unknown. I have shown here that *in vivo* ORFV infection leads to an increase in NKG2D expression (**Fig. 5.11**). The NK cell NKG2D activation receptor has been implicated as having an important role in anti-tumour responses, primarily serving as a receptor for NK cell cytotoxicity via granule exocytosis.[35] Murine NKG2D has been shown to recognize two MHC I related molecules: retinoic acid early Rae-1 gene products, and H-60.[217] These ligands have been shown to stimulate cytotoxicity and IFN-γ production by NK cells.[217] These ligands are not expressed by normal cells, but are found up-regulated on numerous tumour cells. Curiously, B16 melanoma cells and CT26

colon carcinoma cells were shown to express very low, to undetectable levels of these NKG2D ligands.[217,218] Unless there exists as of yet unidentified NKG2D ligands, NKG2D receptor ligation may not be the positive signal for NK cell cytotoxicity of B16F10-LacZ and CT26-LacZ cells. Since B16F10-LacZ tumour cells have demonstrated very low levels of MHC I expression (Bell laboratory, unpublished data), it is likely that even a very weak stimulation via an NK cell activation receptor could trigger B16F10-LacZ killing. Further studies examining the expression of NK cell activation receptors following ORFV treatment will be required to determine the positive signal for initiation of NK cytotoxicity of the murine cancer cells.

In addition to direct stimulation via activation receptor-ligand interactions, NK cells are also activated via cytokine release from infected cells, or from activated DCs.[219] Considering the decrease in NK cell activation following DC depletion, ORFV activated DCs are likely contributing to NK cell release of IFN-γ and TNF-α. Indeed I have shown that DCs express IL-12 upon ORFV infection, which has been shown to be an important mediator of NK cell activation and subsequent cytokine expression (**Fig. 5.2, 5.5**).[219]

Surgical intervention is still considered front line therapy for a number of cancers. The surgical removal of tumours is known however, to disrupt tumour beds and associated vasculature, leading to release of tumour cells into circulation.[220] Surgery also leads to release of growth factors that are suspected to promote metastasis locally, and at distant sites.[221] Not suprising, the physical stress of surgery has been associated with the induction of an immune suppressive state during the perioperative period.[222] Although the exact mechanims underlying immune suppression during the perioperative period remain largely undefined, a number of studies in animals and humans have described dramatic suppression

of cell-mediated immunity as a result of surgery, correlating to the degree of tissue damage caused by the surgery.[222] Since NK cells have a prominent role in immune surveillance, I hypothesized that by activation of NK cells during the perioperative period, I may be able to reduce the frequency of tumour metastases. Indeed, using a model of surgical stress I demonstrated that the ORFV-mediated activation of the innate immune system could be harnessed to reduce the amount of tumour seeding caused by surgical stress (**Fig. 5.13**). Interestingly, not only did ORFV rescue the NK cell immune suppression caused by surgical stress, NK cells isolated from ORFV treated animals demonstrated no immune dampening effect from surgery (**Fig. 5.14a**). The efficacy of ORFV prophylactic treament during surgery was demonstrated to be NK cell mediated (**Fig. 5.14b**) since NK cell depletion abrogated 75% of the tumour clearing capacity of the virus.

I have created a model to summarize the mechanism of ORFV anti-cancer activity (**Fig. 5.15**), including the oncolytic and immune stimulating capacity of the virus. I have demonstrated that ORFV has the capacity to directly kill, and productively infect human and mouse cancer cells. I have also demonstrated that live, replicating ORFV infection of mice leads to robust activation of NK cells by both direct and indirect stimulation via DC activation. To more precisely delineate the mechanism of NK cell activation, future experiments might include *ex vivo* infection of NK-DC cocultures. The NK cell activation could be evaluated by flow cytometry when cultured alone, or in combination with bone marrow derived DCs. To rule out the possibility that live, replicating ORFV could be stimulating cells via additional PRR, these experiments should be conducted with both live and UV inactivated ORFV. Since there is conflicting evidence as to whether ORFV is capable of killing immune cells,[202,214] these experiments should also examine the ability of live and UV inactivated ORFV to cause apoptosis in both DC and NK cells. To further study

the ORFV immune stimulation, in particular the PRR(s) involved in initiation of cytokine release, *ex vivo* infection of DC-NK cocultures in the presence of TLR neutralizing antibodies could identify TLR-dependent signaling. ORFV has so far eluded researchers in the identification of the responsible PRR, with evidence suggesting that ORFV is unqiue from VACV and ectromelia virus in not requiring TLR-2 or TLR-4.[202] Friebe and colleagues had proposed TLR-7 as the PRR responsible for ORFV immune stimulation.[168] Although the natural TLR-7 ligand(s) remain to be identified, stimulation of TLR-7 with the anti-viral agent imiquimod results in release of IL-12, IFN-γ, and TNF-α - similar to effects induced by ORFV.[223] ORFV has also been shown to activate monocytes via TLR-independent mechanisms, with a specific requirement for IRF7, but not IRF3.[202] These data suggest that ORFV may activate monocytes via novel DNA-sensing pathways. The recent discovery of a new cytoplasmic DNA receptor, DAI (DNA-dependent activator of IFN-regulatory factors)[224] suggests that there may exist even more as of yet unidentified intracellular viral sensing pathways.

CHAPTER 6: FUTURE DIRECTIONS

6.1 INCREASE THE ONCOLYTIC POTENCY OF ORFV

ORFV offers many benefits over current viral therapeutics including its limited pathogenicity in humans and its unique immune stimulatory profile. Not unlike most of the *Parapoxvirus* genus however, ORFV has a restricted host range primarily infecting ungulates. Evaluation of ORFV's oncolytic capacity in a panel of human tumour cells demonstrated that, unlike VACV, ORFV was only capable of productively infecting a fraction of the cells (**Table 4.1**). To increase the cancer cell tropism and oncolytic potency of

ORFV, it will be important to determine the molecular signature that permits productive ORFV infection. This could be accomplished through data-mining current databases providing gene signatures of cell lines in the NCI-60 panel, or through microarray analysis. Using ORFV infected cells that are either permissive or restrictive to ORFV infection, a comparison of the transcriptional signatures may identify pathways that either facilitiate or prevent ORFV productive infection. With this knowledge, and the capacity to easily genetically manipulate poxvirus genomes, an enhanced oncolytic ORFV could be developed as a broadly applicable cytolytic anti-cancer agent.

One explanation for ORFV's restricted host range is the fact that unlike most poxvirus species, ORFV lacks a number of host range genes like C7L, K1L, and K3L.[225] Deletion of any one of these host range genes from VACV leads to severe replication defects.[226] Furthermore, expression of host range genes C7L and K1L alone are capable of complementing the replication defects of attenuated VACV strains, like MVA.[226] These data suggest that simple expression of VACV host range genes by ORFV may increase the host range of the virus, allowing the virus to more productively infect cancer cells. Preliminary data suggest that ORFV expression of VACV E3L (a viral inhibitor of PKR) allows for increased ORFV potency in selected cancer cell lines (Komar, Laporte, Rintoul *et al*. unpublished data).

An alternative approach to increasing the oncolytic potency of ORFV is the sequential passage of the virus in tumour cells. Poxvirus genomes are sensitive to genomic recombination if under the appropriate selection pressure, evidenced by the successful creation of attenuated VACV strains.[118] Parapoxviruses are likely not immune to genomic instability in the context of continuous selection pressure, evidenced by the genetic diversity and sequence variation between individual field isolates.[134] The sequential passage of wild

type ORFV on human tumour cells may lead to generation of natural variants, which could be selected based on one of several desirable traits like increased spread, increased lytic capacity, or increased virus output.

The OV field has come a long way from their 'virocentric' roots. It is now well understood that OVs are multi-modality therapeutics that elicit their anti-tumour efficacy via mechanisms beyond direct lysis of tumour cells. In fact, several well-known oncolytic viruses have now demonstrated efficacy even in the absence of oncolysis,[74,79,90] stressing the importance of OV induced anti-tumour immune responses. With these data in mind, the OV field has now rejected the original hypothesis that OV efficacy is solely due to oncolysis of tumour cells. What is not clear however, is whether a fast, potent, lytic OV is more efficacious at systemic tumour debulking than a slow, non-lytic OV. With the creation of new ORFV strains developed with enhanced oncolysis capacity, it will be interesting to compare their *in vivo* efficacy, immune stimulatory capacity, and their dependence on anti-tumour immune-mediated elimination of tumours.

6.2 DEVELOP ORFV AS A ONCOLYTIC VACCINE

With a better understanding of OV mechanism of action, a number of groups are now exploring the anti-tumour vaccine potential of these agents, through generation of tumour associated antigen (TAA) expressing viruses. The obvious advantage to this approach is the expression of relevant TAAs at the tumour site during an inflammatory reaction. Vigil and colleagues demonstrated pre-clinical benefit of an oncolytic NDV expressing the model antigen β-galactosidase.[85] TAA-expressing OVs would be especially beneficial for tumour types that express foreign antigens like viral proteins, as is the case for some liver and cervical cancers. Indeed a study using oncolytic vaccinia virus for the treatment of liver

cancer found, even without antigen-expression, patients undergoing treatment had reduced hepatitis B viral load.[227] These data suggest that OV treatment of viral-associated tumours could allow for generation of anti-viral, and in addition, anti-tumour immune responses. Recent work by Bridle and colleagues highlighted an elegant heterologous prime boost strategy using the B16 melanoma antigen, dopachrome tautomerase (DCT).[189] Using a non-replicating adenovirus vector expressing DCT as a prime, systemic administration of VSV-DCT led to durable cures in a B16 brain tumour model. Using this heterologous prime boost strategy, the authors demonstrated that 40% of the T-cells were directed towards DCT, and immune response to the VSV vector was reduced when compared to treatment with VSV-DCT alone.

In the context of anti-viral vaccines, ORFV has proven to be the ideal vaccine vector based on its safety profile, and the very short-lived duration of the ORFV-specific immunity.[155,156] Importantly, foreign antigen expression by ORFV vector vaccines, has been demonstrated even in the face of pre-existing ORFV immunity.[149] This is unique to ORFV, since pre-existing VACV specific immunity often results in poor foreign antigen-specific humoral responses.[173,174] I have demonstrated the recruitment and activation of DCs and robust anti-tumour effector activity by NK cells, including secretion of IFN-γ. Indeed, several studies have identified the importance of NK cell release of IFN-γ for T-cell recruitment, and activation.[48] ORFV's unique capacity to stimulate the immune system, without evidence of vector specific immunity suggests that an oncolytic, TAA-expressing ORFV may be the ideal tumour vaccination strategy. I have engineered a DCT-expressing ORFV that is currently being tested at McMaster University using the prime boost strategy in

a B16 lung model. The ORFV-DCT oncolytic activity, innate immune stimulation and potential adaptive immune responses may allow for more durable and efficacious treatment.

6.3 ORFV IN COMBINATION WITH OTHER ANTI-CANCER TREATMENTS

I have highlighted the potential for ORFV combination therapy in the context of surgery. Surgery is still a required step in the treatment of most solid tumours, however complete resection of tumours does not protect patients from recurrence, and metastatic disease. Treatment with an oncolytic innate immune stimulator just prior to surgery may help to reduce the occurrence of metastatic disease. To ensure the safety of ORFV treament of surgery patients however, the virus may require attenuation by means of its VEGF virulence gene. Since the ORFV replicative niche is an isolated wound with extensive vasculature, not only would ORFV stimulate the immune system, there is a risk that the virus might also replicate in the regenerating surgical wound. I have demonstrated significant efficacy in the murine lung models using a VEGF-deleted ORFV, suggesting that this backbone could be a suitable candidate vector for treatment of surgical patients.

A number of OVs have demonstrated increased efficacy when used in combination with other front-line therapies, like chemo- and radiotherapy. Recent pre-clinical evidence with oncolytic HSV demonstrated synergistic anti-tumour activity against glioblastoma when combined with the alkylating agent temozolomide.[228] A recent phase I/II clinical trial with patients with advanced, treatment refractory disease substantiated pre-clinical data suggesting that oncolytic reovirus performs better when used in combination with carboplatin or paclitaxel.[229] Since ORFV heavily relies on the immune system for anti-tumour efficacy, not unlike most immunotherapy regimes, ORFV treatment will be most efficacious when treating patients with minimal residual disease. Since large tumours have

established immune tolerance and escape mechanisms, treating tumours with a broadly applicable chemotherapy may not only debulk tumours, but also turn the table on immune suppression. In its current form ORFV is not the most robust cytolytic OV, therefore combination treatment with cytotoxic agents prior to ORFV therapy may result in increased anti-tumour efficacy.

A number of tumour vasculature-targeting agents have been developed for the treatment of cancer. Avastin is a monoclonal antibody that inhibits angiogenesis through competitive binding to the VEGF receptor. A number of receptor tyrosine kinase inhibitors capable of blocking angiogensis signaling have also been developed. Marketed as Sutent, this receptor tyrosine kinase inhibitor was approved by the FDA in 2006 for the treatment of renal cell carcinoma.[230] Recent studies have demonstrated that an additional mechanism of OV efficacy can involve the targeted destruction of tumour vasculature by direct infection,[73] or through by-stander immune mechanisms.[71] The OV field has recently begun testing various combination strategies with vasculature-targeting agents. Some of these studies have highlighted that VEGF blockade *or* treatment of murine tumours allows for enhanced delivery[231] and/or infection of tumour endothelium by OVs.[232] These observations may be attributed to the fact that successful systemic delivery of OVs to tumours requires that the tumour is vascularized, and that vessels are sufficiently permeable to allow efficient extravasation of viral particles.[233] Interestingly, wild type ORFV expresses a variant of VEGF that is fully functional on human endothelial cells.[148] Despite their clear dependence on tumour vasculature for delivery, and in some cases anti-tumour efficacy, to date- OV researchers have not examined the potential of an OV expressing a vascular targeting agent like VEGF. ORFV VEGF might be the best candidate isoform for such experiments, as VEGF-E has specific VEGFR specificity that is unique: it only targets VEGFR-2.[148] Since

VEGFR-2 is the receptor that mediates mitotic activity of endothelial cells and vascular permeability, OV expression of VEGF-E might allow for increase delivery and anti-tumour efficacy. To examine the effects of ORFV expression of VEGF at tumour sites, future experiments should develop a model to characterize tumour vasculature following wild type ORFV treatment, compared to VEGF-deleted ORFV treatment. Such a model would be useful for evaluating the benefit of combination strategies. A VEGF-expressing ORFV might be most beneficial as a method to prime tumours for intravenous delivery of subsequent doses of ORFV, or other OVs – in particular, OVs that benefit from the VEGF 'burst' effect described by Vile and colleagues.[232] Similarly, although vasculature-targeting agents have been associated with toxicity and minimal therapeutic benefit,[230] they may serve as an excellent springboard for combination therapies with OVs like ORFV. If ORFV infection of tumours leads to increased vascular sprouting and angiogenesis, these tumours may be more sensitive to subsequent treatment with vasculature disrupting agents.

6.4 CONCLUDING REMARKS

Despite the development of new, targeted anti-cancer agents, the incidence of treatment related toxicities and cancer deaths over the last decade has been less than encouraging.[1] Oncolytic viruses offer a new hope for cancer patients, as they offer the robustness of chemo- and radiotherapies, with minimal treatment-related toxicities. With a number of human clinical trials underway, OVs may soon be an improved treatment for human disease. Once approved, the path to clinical implementation will be paved and viral therapy of cancer may eventually become the new standard of care. In the mean time, pre-clinical development and characterization of new OVs with unique mechanism of action is of utmost importance. I have identified for the first time the anti-cancer potential of a wild-type

parapoxvirus, ORFV. Even in its wild type form, ORFV has an excellent safety profile and natural anti-tumour potential. An ORFV platform, through additional manipulation, or combination strategies, may be a superior backbone for the development of new anti-cancer agents. In summary, these studies highlight the promise of novel parapoxviruses for the treatment of cancer that may one day be added to the growing armamentarium of cancer therapeutics.

REFERENCES

1. Canadian Cancer Society, Canadian Cancer Statistics 2011. Viewed March 12 2012 at http://www.cancer.ca/~/media/CCS/Canada%20wide/Files%20List/English20files%20heading/PDF%20%20Policy%20%20Canadian%20Cancer%20Statistics%20%20English/Canadian%20Cancer%20Statistics%202011%20%20English.ashx, 2011.

2. Hanahan, D, and Weinberg, RA (2000). The hallmarks of cancer. *Cell* **100**: 57-70.

3. Haber, DA, Gray, NS, and Baselga, J (2011). The evolving war on cancer. *Cell* **145**: 19-24.

4. Beroukhim, R, Mermel, CH, Porter, D, Wei, G, Raychaudhuri, S, Donovan, J *et al.* (2010). The landscape of somatic copy-number alteration across human cancers. *Nature* **463**: 899-905.

5. Ashworth, A, Lord, CJ, and Reis-Filho, JS (2011). Genetic interactions in cancer progression and treatment. *Cell* **145**: 30-38.

6. Johannessen, CM, Boehm, JS, Kim, SY, Thomas, SR, Wardwell, L, Johnson, LA *et al.* (2010). COT drives resistance to RAF inhibition through MAP kinase pathway reactivation. *Nature* **468**: 968-972.

7. Hanahan, D, and Weinberg, RA (2011). Hallmarks of cancer: the next generation. *Cell* **144**: 646-674.

8. Cavallo, F, De Giovanni, C, Nanni, P, Forni, G, and Lollini, PL (2011). 2011: the immune hallmarks of cancer. *Cancer Immunol Immunother* **60**: 319-326.

9. Coley, WB (1989). The treatment of inoperable sarcoma with the mixed toxins of erysipelas and bacillus prodigiosus: immediate and final results in one hundred and forty cases. *Journal amer med assoc* **31**: 389-395.

10. Morales, A, and Eidinger, D (1976). Bacillus Calmette-Guerin in the treatment of adenocarcinoma of the kidney. *J Urol* **115**: 377-380.

11. Kamat, AM, and Lamm, DL (2001). Immunotherapy for bladder cancer. *Curr Urol Rep* **2**: 62-69.

12. Dunn, GP, Old, LJ, and Schreiber, RD (2004). The three Es of cancer immunoediting. *Annu Rev Immunol* **22**: 329-360.

13. Birkeland, SA, Storm, HH, Lamm, LU, Barlow, L, Blohme, I, Forsberg, B *et al.* (1995). Cancer risk after renal transplantation in the Nordic countries, 1964-1986. *Int J Cancer* **60**: 183-189.

14. Stewart, TJ, and Abrams, SI (2008). How tumours escape mass destruction. *Oncogene* **27**: 5894-5903.

15. Gallimore, A, and Sakaguchi, S (2002). Regulation of tumour immunity by CD25+ T cells. *Immunology* **107**: 5-9.

16. Leach, DR, Krummel, MF, and Allison, JP (1996). Enhancement of antitumor immunity by CTLA-4 blockade. *Science* **271**: 1734-1736.

17. Phan, GQ, Yang, JC, Sherry, RM, Hwu, P, Topalian, SL, Schwartzentruber, DJ *et al.* (2003). Cancer regression and autoimmunity induced by cytotoxic T lymphocyte-associated antigen 4 blockade in patients with metastatic melanoma. *Proc Natl Acad Sci U S A* **100**: 8372-8377.

18. Castelli, C, Rivoltini, L, Andreola, G, Carrabba, M, Renkvist, N, and Parmiani, G (2000). T-cell recognition of melanoma-associated antigens. *J Cell Physiol* **182**: 323-331.

19. Andersen, MH, Schrama, D, Thor Straten, P, and Becker, JC (2006). Cytotoxic T cells. *J Invest Dermatol* **126**: 32-41.

20. Trapani, JA, and Smyth, MJ (2002). Functional significance of the perforin/granzyme cell death pathway. *Nat Rev Immunol* **2**: 735-747.

21. Nagata, S (1996). Fas-mediated apoptosis. *Adv Exp Med Biol* **406**: 119-124.

22. Clark, WH, Jr., Elder, DE, Guerry, Dt, Braitman, LE, Trock, BJ, Schultz, D *et al.* (1989). Model predicting survival in stage I melanoma based on tumor progression. *J Natl Cancer Inst* **81**: 1893-1904.

23. Zhang, L, Conejo-Garcia, JR, Katsaros, D, Gimotty, PA, Massobrio, M, Regnani, G *et al.* (2003). Intratumoral T cells, recurrence, and survival in epithelial ovarian cancer. *N Engl J Med* **348**: 203-213.

24. Naito, Y, Saito, K, Shiiba, K, Ohuchi, A, Saigenji, K, Nagura, H *et al.* (1998). CD8+ T cells infiltrated within cancer cell nests as a prognostic factor in human colorectal cancer. *Cancer Res* **58**: 3491-3494.

25. Dudley, ME, and Rosenberg, SA (2003). Adoptive-cell-transfer therapy for the treatment of patients with cancer. *Nat Rev Cancer* **3**: 666-675.

26. Van Pel, A, and Boon, T (1982). Protection against a nonimmunogenic mouse leukemia by an immunogenic variant obtained by mutagenesis. *Proc Natl Acad Sci U S A* **79**: 4718-4722.

27. Rosenberg, SA (1999). A new era for cancer immunotherapy based on the genes that encode cancer antigens. *Immunity* **10**: 281-287.

28. Mellman, I, Coukos, G, and Dranoff, G (2011). Cancer immunotherapy comes of age. *Nature* **480**: 480-489.

29. Matzinger, P (1994). Tolerance, danger, and the extended family. *Annu Rev Immunol* **12**: 991-1045.

30. Matzinger, P (2002). The danger model: a renewed sense of self. *Science* **296**: 301-305.

31. Vivier, E, Raulet, DH, Moretta, A, Caligiuri, MA, Zitvogel, L, Lanier, LL *et al.* (2011). Innate or adaptive immunity? The example of natural killer cells. *Science* **331**: 44-49.

32. Karre, K, Ljunggren, HG, Piontek, G, and Kiessling, R (1986). Selective rejection of H-2-deficient lymphoma variants suggests alternative immune defence strategy. *Nature* **319**: 675-678.

33. Lanier, LL (2005). NK cell recognition. *Annu Rev Immunol* **23**: 225-274.

34. Vivier, E, Tomasello, E, Baratin, M, Walzer, T, and Ugolini, S (2008). Functions of natural killer cells. *Nat Immunol* **9**: 503-510.

35. Hayakawa, Y, and Smyth, MJ (2006). NKG2D and cytotoxic effector function in tumor immune surveillance. *Semin Immunol* **18**: 176-185.

36. Street, SE, Cretney, E, and Smyth, MJ (2001). Perforin and interferon-gamma activities independently control tumor initiation, growth, and metastasis. *Blood* **97**: 192-197.

37. Trinchieri, G (1989). Biology of natural killer cells. *Adv Immunol* **47**: 187-376.

38. Long, EO (2007). Ready for prime time: NK cell priming by dendritic cells. *Immunity* **26**: 385-387.

39. Smyth, MJ, Hayakawa, Y, Takeda, K, and Yagita, H (2002). New aspects of natural-killer-cell surveillance and therapy of cancer. *Nat Rev Cancer* **2**: 850-861.

40. Lucas, M, Schachterle, W, Oberle, K, Aichele, P, and Diefenbach, A (2007). Dendritic cells prime natural killer cells by trans-presenting interleukin 15. *Immunity* **26**: 503-517.

41. Fernandez, NC, Lozier, A, Flament, C, Ricciardi-Castagnoli, P, Bellet, D, Suter, M *et al.* (1999). Dendritic cells directly trigger NK cell functions: cross-talk relevant in innate anti-tumor immune responses in vivo. *Nat Med* **5**: 405-411.

42. Sivori, S, Falco, M, Della Chiesa, M, Carlomagno, S, Vitale, M, Moretta, L *et al.* (2004). CpG and double-stranded RNA trigger human NK cells by Toll-like receptors: induction of cytokine release and cytotoxicity against tumors and dendritic cells. *Proc Natl Acad Sci U S A* **101**: 10116-10121.

43. Hart, OM, Athie-Morales, V, O'Connor, GM, and Gardiner, CM (2005). TLR7/8-mediated activation of human NK cells results in accessory cell-dependent IFN-gamma production. *J Immunol* **175**: 1636-1642.

44. Shankaran, V, Ikeda, H, Bruce, AT, White, JM, Swanson, PE, Old, LJ *et al.* (2001). IFNgamma and lymphocytes prevent primary tumour development and shape tumour immunogenicity. *Nature* **410**: 1107-1111.

45. Imai, K, Matsuyama, S, Miyake, S, Suga, K, and Nakachi, K (2000). Natural cytotoxic activity of peripheral-blood lymphocytes and cancer incidence: an 11-year follow-up study of a general population. *Lancet* **356**: 1795-1799.

46. Levy, EM, Roberti, MP, and Mordoh, J (2011). Natural killer cells in human cancer: from biological functions to clinical applications. *J Biomed Biotechnol* **2011**: 676198.

47. Degli-Esposti, MA, and Smyth, MJ (2005). Close encounters of different kinds: dendritic cells and NK cells take centre stage. *Nat Rev Immunol* **5**: 112-124.

48. Martin-Fontecha, A, Thomsen, LL, Brett, S, Gerard, C, Lipp, M, Lanzavecchia, A *et al.* (2004). Induced recruitment of NK cells to lymph nodes provides IFN-gamma for T(H)1 priming. *Nat Immunol* **5**: 1260-1265.

49. Mocikat, R, Braumuller, H, Gumy, A, Egeter, O, Ziegler, H, Reusch, U *et al.* (2003). Natural killer cells activated by MHC class I(low) targets prime dendritic cells to induce protective CD8 T cell responses. *Immunity* **19**: 561-569.

50. Kantoff, PW, Schuetz, TJ, Blumenstein, BA, Glode, LM, Bilhartz, DL, Wyand, M *et al.* (2010). Overall survival analysis of a phase II randomized controlled trial of a Poxviral-based PSA-targeted immunotherapy in metastatic castration-resistant prostate cancer. *J Clin Oncol* **28**: 1099-1105.

51. Neller, MA, Lopez, JA, and Schmidt, CW (2008). Antigens for cancer immunotherapy. *Semin Immunol* **20**: 286-295.

52. Rosenberg, SA, Restifo, NP, Yang, JC, Morgan, RA, and Dudley, ME (2008). Adoptive cell transfer: a clinical path to effective cancer immunotherapy. *Nat Rev Cancer* **8**: 299-308.

53. Dudley, ME, Yang, JC, Sherry, R, Hughes, MS, Royal, R, Kammula, U *et al.* (2008). Adoptive cell therapy for patients with metastatic melanoma: evaluation of intensive myeloablative chemoradiation preparative regimens. *J Clin Oncol* **26**: 5233-5239.

54. Hodi, FS, O'Day, SJ, McDermott, DF, Weber, RW, Sosman, JA, Haanen, JB *et al.* (2010). Improved survival with ipilimumab in patients with metastatic melanoma. *N Engl J Med* **363**: 711-723.

55. Chambers, CA, Kuhns, MS, Egen, JG, and Allison, JP (2001). CTLA-4-mediated inhibition in regulation of T cell responses: mechanisms and manipulation in tumor immunotherapy. *Annu Rev Immunol* **19**: 565-594.

56. Couzin-Frankel, J (2010). Immune Therapy Steps Up the Attack. *Science* **330**: 440-443.

57. Kim, M, Williamson, CT, Prudhomme, J, Bebb, DG, Riabowol, K, Lee, PW *et al.* (2010). The viral tropism of two distinct oncolytic viruses, reovirus and myxoma virus, is modulated by cellular tumor suppressor gene status. *Oncogene* **29**: 3990-3996.

58. Dock (1904). The influence of complicating diseases upon leukaemia. *Am J Med Sci* **127**: 561-592.

59. Moore, AE (1952). Viruses with oncolytic properties and their adaptation to tumors. *Ann N Y Acad Sci* **54**: 945-952.

60. Kelly, E, and Russell, SJ (2007). History of oncolytic viruses: genesis to genetic engineering. *Mol Ther* **15**: 651-659.

61. Martuza, RL, Malick, A, Markert, JM, Ruffner, KL, and Coen, DM (1991). Experimental therapy of human glioma by means of a genetically engineered virus mutant. *Science* **252**: 854-856.

62. Csatary, LK, Eckhardt, S, Bukosza, I, Czegledi, F, Fenyvesi, C, Gergely, P *et al.* (1993). Attenuated veterinary virus vaccine for the treatment of cancer. *Cancer Detect Prev* **17**: 619-627.

63. Stojdl, DF, Lichty, B, Knowles, S, Marius, R, Atkins, H, Sonenberg, N *et al.* (2000). Exploiting tumor-specific defects in the interferon pathway with a previously unknown oncolytic virus. *Nat Med* **6**: 821-825.

64. Garber, K (2006). China approves world's first oncolytic virus therapy for cancer treatment. *J Natl Cancer Inst* **98**: 298-300.

65. Eager, RM, and Nemunaitis, J (2011). Clinical development directions in oncolytic viral therapy. *Cancer Gene Ther* **18**: 305-317.

66. Hashiro, G, Loh, PC, and Yau, JT (1977). The preferential cytotoxicity of reovirus for certain transformed cell lines. *Arch Virol* **54**: 307-315.

67. Breitbach, CJ, Burke, J, Jonker, D, Stephenson, J, Haas, AR, Chow, LQ *et al.* (2011). Intravenous delivery of a multi-mechanistic cancer-targeted oncolytic poxvirus in humans. *Nature* **477**: 99-102.

68. Taki, M, Kagawa, S, Nishizaki, M, Mizuguchi, H, Hayakawa, T, Kyo, S *et al.* (2005). Enhanced oncolysis by a tropism-modified telomerase-specific replication-selective adenoviral agent OBP-405 ('Telomelysin-RGD'). *Oncogene* **24**: 3130-3140.

69. Campadelli-Fiume, G, De Giovanni, C, Gatta, V, Nanni, P, Lollini, PL, and Menotti, L (2011). Rethinking herpes simplex virus: the way to oncolytic agents. *Rev Med Virol* **21**: 213-226.

70. Parato, KA, Senger, D, Forsyth, PA, and Bell, JC (2005). Recent progress in the battle between oncolytic viruses and tumours. *Nat Rev Cancer* **5**: 965-976.

71. Breitbach, CJ, Paterson, JM, Lemay, CG, Falls, TJ, McGuire, A, Parato, KA *et al.* (2007). Targeted inflammation during oncolytic virus therapy severely compromises tumor blood flow. *Mol Ther* **15**: 1686-1693.

72. Kirn, DH, Wang, Y, Le Boeuf, F, Bell, J, and Thorne, SH (2007). Targeting of interferon-beta to produce a specific, multi-mechanistic oncolytic vaccinia virus. *PLoS Med* **4**: e353.

73. Breitbach, CJ, De Silva, NS, Falls, TJ, Aladl, U, Evgin, L, Paterson, J *et al.* (2011). Targeting tumor vasculature with an oncolytic virus. *Mol Ther* **19**: 886-894.

74. Kaufman, HL, Kim, DW, DeRaffele, G, Mitcham, J, Coffin, RS, and Kim-Schulze, S (2010). Local and distant immunity induced by intralesional vaccination with an oncolytic herpes virus encoding GM-CSF in patients with stage IIIc and IV melanoma. *Ann Surg Oncol* **17**: 718-730.

75. Leveille, S, Samuel, S, Goulet, ML, and Hiscott, J (2011). Enhancing VSV oncolytic activity with an improved cytosine deaminase suicide gene strategy. *Cancer Gene Ther* **18**: 435-443.

76. Zaoui, K, Bossow, S, Grossardt, C, Leber, MF, Springfeld, C, Plinkert, PK *et al.* (2012). Chemovirotherapy for head and neck squamous cell carcinoma with EGFR-targeted and CD/UPRT-armed oncolytic measles virus. *Cancer Gene Ther* **19**: 181-191.

77. Galanis, E, Hartmann, LC, Cliby, WA, Long, HJ, Peethambaram, PP, Barrette, BA *et al.* (2010). Phase I trial of intraperitoneal administration of an oncolytic measles virus strain engineered to express carcinoembryonic antigen for recurrent ovarian cancer. *Cancer Res* **70**: 875-882.

78. Jin, J, Liu, H, Yang, C, Li, G, Liu, X, Qian, Q *et al.* (2009). Effective gene-viral therapy of leukemia by a new fiber chimeric oncolytic adenovirus expressing TRAIL: in vitro and in vivo evaluation. *Mol Cancer Ther* **8**: 1387-1397.

79. Prestwich, RJ, Harrington, KJ, Pandha, HS, Vile, RG, Melcher, AA, and Errington, F (2008). Oncolytic viruses: a novel form of immunotherapy. *Expert Rev Anticancer Ther* **8**: 1581-1588.

80. Melcher, A, Parato, K, Rooney, CM, and Bell, JC (2011). Thunder and lightning: immunotherapy and oncolytic viruses collide. *Mol Ther* **19**: 1008-1016.

81. Moehler, MH, Zeidler, M, Wilsberg, V, Cornelis, JJ, Woelfel, T, Rommelaere, J *et al.* (2005). Parvovirus H-1-induced tumor cell death enhances human immune response in vitro via increased phagocytosis, maturation, and cross-presentation by dendritic cells. *Hum Gene Ther* **16**: 996-1005.

82. Benencia, F, Courreges, MC, Fraser, NW, and Coukos, G (2008). Herpes virus oncolytic therapy reverses tumor immune dysfunction and facilitates tumor antigen presentation. *Cancer Biol Ther* **7**: 1194-1205.

83. Sobol, PT, Boudreau, JE, Stephenson, K, Wan, Y, Lichty, BD, and Mossman, KL (2011). Adaptive antiviral immunity is a determinant of the therapeutic success of oncolytic virotherapy. *Mol Ther* **19**: 335-344.

84. Galivo, F, Diaz, RM, Thanarajasingam, U, Jevremovic, D, Wongthida, P, Thompson, J *et al.* (2010). Interference of CD40L-mediated tumor immunotherapy by oncolytic vesicular stomatitis virus. *Hum Gene Ther* **21**: 439-450.

85. Vigil, A, Martinez, O, Chua, MA, and Garcia-Sastre, A (2008). Recombinant Newcastle disease virus as a vaccine vector for cancer therapy. *Mol Ther* **16**: 1883-1890.

86. Gauvrit, A, Brandler, S, Sapede-Peroz, C, Boisgerault, N, Tangy, F, and Gregoire, M (2008). Measles virus induces oncolysis of mesothelioma cells and allows dendritic cells to cross-prime tumor-specific CD8 response. *Cancer Res* **68**: 4882-4892.

87. White, CL, Twigger, KR, Vidal, L, De Bono, JS, Coffey, M, Heinemann, L *et al.* (2008). Characterization of the adaptive and innate immune response to intravenous oncolytic reovirus (Dearing type 3) during a phase I clinical trial. *Gene Ther* **15**: 911-920.

88. Heinzerling, L, Kunzi, V, Oberholzer, PA, Kundig, T, Naim, H, and Dummer, R (2005). Oncolytic measles virus in cutaneous T-cell lymphomas mounts antitumor immune responses in vivo and targets interferon-resistant tumor cells. *Blood* **106**: 2287-2294.

89. Prestwich, RJ, Errington, F, Diaz, RM, Pandha, HS, Harrington, KJ, Melcher, AA *et al.* (2009). The case of oncolytic viruses versus the immune system: waiting on the judgment of Solomon. *Hum Gene Ther* **20**: 1119-1132.

90. Apostolidis, L, Schirrmacher, V, and Fournier, P (2007). Host mediated anti-tumor effect of oncolytic Newcastle disease virus after locoregional application. *Int J Oncol* **31**: 1009-1019.

91. Smith, E, Breznik, J, and Lichty, BD (2011). Strategies to enhance viral penetration of solid tumors. *Hum Gene Ther* **22**: 1053-1060.

92. Fulci, G, Breymann, L, Gianni, D, Kurozomi, K, Rhee, SS, Yu, J *et al.* (2006). Cyclophosphamide enhances glioma virotherapy by inhibiting innate immune responses. *Proc Natl Acad Sci U S A* **103**: 12873-12878.

93. Chiocca, EA, Abbed, KM, Tatter, S, Louis, DN, Hochberg, FH, Barker, F *et al.* (2004). A phase I open-label, dose-escalation, multi-institutional trial of injection with an E1B-Attenuated adenovirus, ONYX-015, into the peritumoral region of recurrent malignant gliomas, in the adjuvant setting. *Mol Ther* **10**: 958-966.

94. Bessis, N, GarciaCozar, FJ, and Boissier, MC (2004). Immune responses to gene therapy vectors: influence on vector function and effector mechanisms. *Gene Ther* **11 Suppl 1**: S10-17.

95. Hirasawa, K, Nishikawa, SG, Norman, KL, Coffey, MC, Thompson, BG, Yoon, CS *et al.* (2003). Systemic reovirus therapy of metastatic cancer in immune-competent mice. *Cancer Res* **63**: 348-353.

96. Willmon, C, Harrington, K, Kottke, T, Prestwich, R, Melcher, A, and Vile, R (2009). Cell carriers for oncolytic viruses: Fed Ex for cancer therapy. *Mol Ther* **17**: 1667-1676.

97. Fulci, G, Dmitrieva, N, Gianni, D, Fontana, EJ, Pan, X, Lu, Y *et al.* (2007). Depletion of peripheral macrophages and brain microglia increases brain tumor titers of oncolytic viruses. *Cancer Res* **67**: 9398-9406.

98. Shashkova, EV, Doronin, K, Senac, JS, and Barry, MA (2008). Macrophage depletion combined with anticoagulant therapy increases therapeutic window of systemic treatment with oncolytic adenovirus. *Cancer Res* **68**: 5896-5904.

99. Haralambieva, I, Iankov, I, Hasegawa, K, Harvey, M, Russell, SJ, and Peng, KW (2007). Engineering oncolytic measles virus to circumvent the intracellular innate immune response. *Mol Ther* **15**: 588-597.

100. Kurozumi, K, Hardcastle, J, Thakur, R, Yang, M, Christoforidis, G, Fulci, G *et al.* (2007). Effect of tumor microenvironment modulation on the efficacy of oncolytic virus therapy. *J Natl Cancer Inst* **99**: 1768-1781.

101. Biron, CA, Byron, KS, and Sullivan, JL (1989). Severe herpesvirus infections in an adolescent without natural killer cells. *N Engl J Med* **320**: 1731-1735.

102. Martinez, J, Huang, X, and Yang, Y (2010). Direct TLR2 signaling is critical for NK cell activation and function in response to vaccinia viral infection. *PLoS Pathog* **6**: e1000811.

103. Lee, SH, Miyagi, T, and Biron, CA (2007). Keeping NK cells in highly regulated antiviral warfare. *Trends Immunol* **28**: 252-259.

104. Altomonte, J, Wu, L, Chen, L, Meseck, M, Ebert, O, Garcia-Sastre, A *et al.* (2008). Exponential enhancement of oncolytic vesicular stomatitis virus potency by vector-mediated suppression of inflammatory responses in vivo. *Mol Ther* **16**: 146-153.

105. Fenner, F, Henderson, DA, Aria, I, Jezek, Z, & Ladnyi, ID (1988). Small pox and its eradication. *(World Health Organization, Geneva)*.

106. Miller, JD, van der Most, RG, Akondy, RS, Glidewell, JT, Albott, S, Masopust, D *et al.* (2008). Human effector and memory CD8+ T cell responses to smallpox and yellow fever vaccines. *Immunity* **28**: 710-722.

107. Goebel, SJ, Johnson, GP, Perkus, ME, Davis, SW, Winslow, JP, and Paoletti, E (1990). The complete DNA sequence of vaccinia virus. *Virology* **179**: 247-266, 517-263.

108. Esposito, JJ, and Knight, JC (1985). Orthopoxvirus DNA: a comparison of restriction profiles and maps. *Virology* **143**: 230-251.

109. Gubser, C, Hue, S, Kellam, P, and Smith, GL (2004). Poxvirus genomes: a phylogenetic analysis. *J Gen Virol* **85**: 105-117.

110. Seet, BT, Johnston, JB, Brunetti, CR, Barrett, JW, Everett, H, Cameron, C *et al.* (2003). Poxviruses and immune evasion. *Annu Rev Immunol* **21**: 377-423.

111. Moss, B (2006). Poxvirus entry and membrane fusion. *Virology* **344**: 48-54.

112. Chung, CS, Hsiao, JC, Chang, YS, and Chang, W (1998). A27L protein mediates vaccinia virus interaction with cell surface heparan sulfate. *J Virol* **72**: 1577-1585.

113. Law, M, Carter, GC, Roberts, KL, Hollinshead, M, and Smith, GL (2006). Ligand-induced and nonfusogenic dissolution of a viral membrane. *Proc Natl Acad Sci U S A* **103**: 5989-5994.

114. Broyles, SS (2003). Vaccinia virus transcription. *J Gen Virol* **84**: 2293-2303.

115. Smith, GL, Vanderplasschen, A, and Law, M (2002). The formation and function of extracellular enveloped vaccinia virus. *J Gen Virol* **83**: 2915-2931.

116. Kirn, DH, and Thorne, SH (2009). Targeted and armed oncolytic poxviruses: a novel multi-mechanistic therapeutic class for cancer. *Nat Rev Cancer* **9**: 64-71.

117. Jacobs, BL, Langland, JO, Kibler, KV, Denzler, KL, White, SD, Holechek, SA *et al.* (2009). Vaccinia virus vaccines: past, present and future. *Antiviral Res* **84**: 1-13.

118. McCurdy, LH, Larkin, BD, Martin, JE, and Graham, BS (2004). Modified vaccinia Ankara: potential as an alternative smallpox vaccine. *Clin Infect Dis* **38**: 1749-1753.

119. Smith, GL, Mackett, M, and Moss, B (1983). Infectious vaccinia virus recombinants that express hepatitis B virus surface antigen. *Nature* **302**: 490-495.

120. Boyle, DB, and Coupar, BE (1988). Construction of recombinant fowlpox viruses as vectors for poultry vaccines. *Virus Res* **10**: 343-356.

121. Hodge, JW, Poole, DJ, Aarts, WM, Gomez Yafal, A, Gritz, L, and Schlom, J (2003). Modified vaccinia virus ankara recombinants are as potent as vaccinia recombinants in diversified prime and boost vaccine regimens to elicit therapeutic antitumor responses. *Cancer Res* **63**: 7942-7949.

122. Eder, JP, Kantoff, PW, Roper, K, Xu, GX, Bubley, GJ, Boyden, J *et al.* (2000). A phase I trial of a recombinant vaccinia virus expressing prostate-specific antigen in advanced prostate cancer. *Clin Cancer Res* **6**: 1632-1638.

123. Smith, CL, Dunbar, PR, Mirza, F, Palmowski, MJ, Shepherd, D, Gilbert, SC *et al.* (2005). Recombinant modified vaccinia Ankara primes functionally activated CTL specific for a melanoma tumor antigen epitope in melanoma patients with a high risk of disease recurrence. *Int J Cancer* **113**: 259-266.

124. Wang, F, Ma, Y, Barrett, JW, Gao, X, Loh, J, Barton, E *et al.* (2004). Disruption of Erk-dependent type I interferon induction breaks the myxoma virus species barrier. *Nat Immunol* **5**: 1266-1274.

125. Wang, G, Barrett, JW, Stanford, M, Werden, SJ, Johnston, JB, Gao, X *et al.* (2006). Infection of human cancer cells with myxoma virus requires Akt activation via

interaction with a viral ankyrin-repeat host range factor. *Proc Natl Acad Sci U S A* **103**: 4640-4645.

126. Thorne, SH, Hwang, TH, O'Gorman, WE, Bartlett, DL, Sei, S, Kanji, F *et al.* (2007). Rational strain selection and engineering creates a broad-spectrum, systemically effective oncolytic poxvirus, JX-963. *J Clin Invest* **117**: 3350-3358.

127. Katsafanas, GC, and Moss, B (2004). Vaccinia virus intermediate stage transcription is complemented by Ras-GTPase-activating protein SH3 domain-binding protein (G3BP) and cytoplasmic activation/proliferation-associated protein (p137) individually or as a heterodimer. *J Biol Chem* **279**: 52210-52217.

128. Bello, LJ (1974). Regulation of thymidine kinase synthesis in human cells. *Exp Cell Res* **89**: 263-274.

129. Hengstschlager, M, Knofler, M, Mullner, EW, Ogris, E, Wintersberger, E, and Wawra, E (1994). Different regulation of thymidine kinase during the cell cycle of normal versus DNA tumor virus-transformed cells. *J Biol Chem* **269**: 13836-13842.

130. Buller, RM, Chakrabarti, S, Moss, B, and Fredrickson, T (1988). Cell proliferative response to vaccinia virus is mediated by VGF. *Virology* **164**: 182-192.

131. Park, BH, Hwang, T, Liu, TC, Sze, DY, Kim, JS, Kwon, HC *et al.* (2008). Use of a targeted oncolytic poxvirus, JX-594, in patients with refractory primary or metastatic liver cancer: a phase I trial. *Lancet Oncol* **9**: 533-542.

132. Evgin, L, Vaha-Koskela, M, Rintoul, J, Falls, T, Le Boeuf, F, Barrett, JW *et al.* (2010). Potent oncolytic activity of raccoonpox virus in the absence of natural pathogenicity. *Mol Ther* **18**: 896-902.

133. Haig, D, McInnes, C, Deane, D, Lear, A, Myatt, N, Reid, H *et al.* (1996). Cytokines and their inhibitors in orf virus infection. *Vet Immunol Immunopathol* **54**: 261-267.

134. Mercer, AA, Ueda, N, Friederichs, SM, Hofmann, K, Fraser, KM, Bateman, T *et al.* (2006). Comparative analysis of genome sequences of three isolates of Orf virus reveals unexpected sequence variation. *Virus Res* **116**: 146-158.

135. Xing, K, Deng, R, Wang, J, Feng, J, Huang, M, and Wang, X (2006). Genome-based phylogeny of poxvirus. *Intervirology* **49**: 207-214.

136. McKeever, DJ, Jenkinson, DM, Hutchison, G, and Reid, HW (1988). Studies of the pathogenesis of orf virus infection in sheep. *J Comp Pathol* **99**: 317-328.

137. Tan, JL, Ueda, N, Mercer, AA, and Fleming, SB (2009). Investigation of orf virus structure and morphogenesis using recombinants expressing FLAG-tagged envelope

structural proteins: evidence for wrapped virus particles and egress from infected cells. *J Gen Virol* **90**: 614-625.

138. Delhon, G, Tulman, ER, Afonso, CL, Lu, Z, de la Concha-Bermejillo, A, Lehmkuhl, HD *et al.* (2004). Genomes of the parapoxviruses ORF virus and bovine papular stomatitis virus. *J Virol* **78**: 168-177.

139. Scagliarini, A, Gallina, L, Dal Pozzo, F, Battilani, M, Ciulli, S, and Prosperi, S (2004). Heparin binding activity of orf virus F1L protein. *Virus Res* **105**: 107-112.

140. Kjellen, L, and Lindahl, U (1991). Proteoglycans: structures and interactions. *Annu Rev Biochem* **60**: 443-475.

141. Fleming, SB, McCaughan, CA, Andrews, AE, Nash, AD, and Mercer, AA (1997). A homolog of interleukin-10 is encoded by the poxvirus orf virus. *J Virol* **71**: 4857-4861.

142. Moore, KW, de Waal Malefyt, R, Coffman, RL, and O'Garra, A (2001). Interleukin-10 and the interleukin-10 receptor. *Annu Rev Immunol* **19**: 683-765.

143. Seet, BT, McCaughan, CA, Handel, TM, Mercer, A, Brunetti, C, McFadden, G *et al.* (2003). Analysis of an orf virus chemokine-binding protein: Shifting ligand specificities among a family of poxvirus viroceptors. *Proc Natl Acad Sci U S A* **100**: 15137-15142.

144. Deane, D, McInnes, CJ, Percival, A, Wood, A, Thomson, J, Lear, A *et al.* (2000). Orf virus encodes a novel secreted protein inhibitor of granulocyte-macrophage colony-stimulating factor and interleukin-2. *J Virol* **74**: 1313-1320.

145. McInnes, CJ, Wood, AR, and Mercer, AA (1998). Orf virus encodes a homolog of the vaccinia virus interferon-resistance gene E3L. *Virus Genes* **17**: 107-115.

146. Kwon, JA, and Rich, A (2005). Biological function of the vaccinia virus Z-DNA-binding protein E3L: gene transactivation and antiapoptotic activity in HeLa cells. *Proc Natl Acad Sci U S A* **102**: 12759-12764.

147. Savory, LJ, Stacker, SA, Fleming, SB, Niven, BE, and Mercer, AA (2000). Viral vascular endothelial growth factor plays a critical role in orf virus infection. *J Virol* **74**: 10699-10706.

148. Ogawa, S, Oku, A, Sawano, A, Yamaguchi, S, Yazaki, Y, and Shibuya, M (1998). A novel type of vascular endothelial growth factor, VEGF-E (NZ-7 VEGF), preferentially utilizes KDR/Flk-1 receptor and carries a potent mitotic activity without heparin-binding domain. *J Biol Chem* **273**: 31273-31282.

149. Fischer, T, Planz, O, Stitz, L, and Rziha, HJ (2003). Novel recombinant parapoxvirus vectors induce protective humoral and cellular immunity against lethal herpesvirus challenge infection in mice. *J Virol* **77**: 9312-9323.

150. Lear, A, Hutchinson, G, Reid, H, Norval, M, and Haig, D (1996). Phenotypic characterisation of the dendritic cells accumulating in ovince dermis following primary and secondary orf virus infections. *Eur. J. Dermatol.* **6**: 135-140.

151. Buttner, M (1993). Principles of paramunization. Option and limits in veterinary medicine. *Comp Immunol Microbiol Infect Dis* **16**: 1-10.

152. Weber, O, Siegling, A, Friebe, A, Limmer, A, Schlapp, T, Knolle, P *et al.* (2003). Inactivated parapoxvirus ovis (Orf virus) has antiviral activity against hepatitis B virus and herpes simplex virus. *J Gen Virol* **84**: 1843-1852.

153. Rziha, HJ, Henkel, M, Cottone, R, Meyer, M, Dehio, C, and Buttner, M (1999). Parapoxviruses: potential alternative vectors for directing the immune response in permissive and non-permissive hosts. *J Biotechnol* **73**: 235-242.

154. Henkel, M, Planz, O, Fischer, T, Stitz, L, and Rziha, HJ (2005). Prevention of virus persistence and protection against immunopathology after Borna disease virus infection of the brain by a novel Orf virus recombinant. *J Virol* **79**: 314-325.

155. Czerny, CP, Zeller-Lue, C, Eis-Hubinger, AM, Kaaden, OR, and Meyer, H (1997). Characterization of a cowpox-like orthopox virus which had caused a lethal infection in man. *Arch Virol Suppl* **13**: 13-24.

156. Haig, DM, and Mercer, AA (1998). Ovine diseases. Orf. *Vet Res* **29**: 311-326.

157. Robinson, AJ, and Petersen, GV (1983). Orf virus infection of workers in the meat industry. *N Z Med J* **96**: 81-85.

158. Lederman, ER, Green, GM, DeGroot, HE, Dahl, P, Goldman, E, Greer, PW *et al.* (2007). Progressive ORF virus infection in a patient with lymphoma: successful treatment using imiquimod. *Clin Infect Dis* **44**: e100-103.

159. Jenkinson, DM, Hutchinson, G, and Reid, H (1992). The B and T cell responses to orf virus infection. *Vet. Dermatol.* **3**: 57-64

.

160. Jenkinson, DM, McEwen, PE, Onwuka, SK, Moss, VA, Elder, HY, Hutchinson, G *et al.* (1990). The pathological changes and polymorphonuclear and mast cell responses in the skin of spcific pathogen-free lambs following primary and secondary challenge with orf virus. *Vet. Dermatol.* **2**: 1-9.

161. Buttner, M, Czerny, CP, Lehner, KH, and Wertz, K (1995). Interferon induction in peripheral blood mononuclear leukocytes of man and farm animals by poxvirus vector candidates and some poxvirus constructs. *Vet Immunol Immunopathol* **46**: 237-250.

162. Haig, DM, and McInnes, CJ (2002). Immunity and counter-immunity during infection with the parapoxvirus orf virus. *Virus Res* **88**: 3-16.

163. Haig, D, Deane, D, Percival, A, Myatt, N, Thomson, J, Inglis, L *et al.* (1996). The cytokine response of afferent lymph following orf virus reinfection of sheep. *Vet. Dermatol.* **7**: 11-20.

164. Schutze, N, Raue, R, Buttner, M, and Alber, G (2009). Inactivated parapoxvirus ovis activates canine blood phagocytes and T lymphocytes. *Vet Microbiol* **137**: 260-267.

165. Fachinger, V, Schlapp, T, Strube, W, Schmeer, N, and Saalmuller, A (2000). Poxvirus-induced immunostimulating effects on porcine leukocytes. *J Virol* **74**: 7943-7951.

166. Mayr, A, Buttner, M, Wolf, G, Meyer, H, and Czerny, CP (1989). Experimenteller Nachweis paraspezifischer Wirkung von gereinigten und inaktivierten Pockenviren. *J. Vet. Med.* **36**: 81-99.

167. Yirrell, DL, Vestey, JP, and Norval, M (1994). Immune responses of patients to orf virus infection. *Br J Dermatol* **130**: 438-443.

168. Friebe, A, Siegling, A, Friederichs, S, Volk, HD, and Weber, O (2004). Immunomodulatory effects of inactivated parapoxvirus ovis (ORF virus) on human peripheral immune cells: induction of cytokine secretion in monocytes and Th1-like cells. *J Virol* **78**: 9400-9411.

169. Friebe, A, Friederichs, S, Scholz, K, Janssen, U, Scholz, C, Schlapp, T *et al.* (2011). Characterization of immunostimulatory components of orf virus (parapoxvirus ovis). *J Gen Virol* **92**: 1571-1584.

170. Sullivan, JT, Mercer, AA, Fleming, SB, and Robinson, AJ (1994). Identification and characterization of an orf virus homologue of the vaccinia virus gene encoding the major envelope antigen p37K. *Virology* **202**: 968-973.

171. Buddle, BM, Dellers, RW, and Schurig, GG (1984). Contagious ecthyma virus-vaccination failures. *Am J Vet Res* **45**: 263-266.

172. Czerny, CP, Waldmann, R, and Scheubeck, T (1997). Identification of three distinct antigenic sites in parapoxviruses. *Arch Virol* **142**: 807-821.

173. Kundig, TM, Kalberer, CP, Hengartner, H, and Zinkernagel, RM (1993). Vaccination with two different vaccinia recombinant viruses: long-term inhibition of secondary vaccination. *Vaccine* **11**: 1154-1158.

174. Perkus, ME, Piccini, A, Lipinskas, BR, and Paoletti, E (1985). Recombinant vaccinia virus: immunization against multiple pathogens. *Science* **229**: 981-984.

175. Lun, X, Yang, W, Alain, T, Shi, ZQ, Muzik, H, Barrett, JW *et al.* (2005). Myxoma virus is a novel oncolytic virus with significant antitumor activity against experimental human gliomas. *Cancer Res* **65**: 9982-9990.

176. Kirstein, JM, Graham, KC, Mackenzie, LT, Johnston, DE, Martin, LJ, Tuck, AB *et al.* (2009). Effect of anti-fibrinolytic therapy on experimental melanoma metastasis. *Clin Exp Metastasis* **26**: 121-131.

177. Wise, LM, Savory, LJ, Dryden, NH, Whelan, EM, Fleming, SB, and Mercer, AA (2007). Major amino acid sequence variants of viral vascular endothelial growth factor are functionally equivalent during Orf virus infection of sheep skin. *Virus Res* **128**: 115-125.

178. Damjanovic, D, Zhang, X, Mu, J, Medina, MF, and Xing, Z (2008). Organ distribution of transgene expression following intranasal mucosal delivery of recombinant replication-defective adenovirus gene transfer vector. *Genet Vaccines Ther* **6**: 5.

179. Chakrabarti, S, Brechling, K, and Moss, B (1985). Vaccinia virus expression vector: coexpression of beta-galactosidase provides visual screening of recombinant virus plaques. *Mol Cell Biol* **5**: 3403-3409.

180. Jung, S, Unutmaz, D, Wong, P, Sano, G, De los Santos, K, Sparwasser, T *et al.* (2002). In vivo depletion of CD11c+ dendritic cells abrogates priming of CD8+ T cells by exogenous cell-associated antigens. *Immunity* **17**: 211-220.

181. Stanford, MM, Shaban, M, Barrett, JW, Werden, SJ, Gilbert, PA, Bondy-Denomy, J *et al.* (2008). Myxoma virus oncolysis of primary and metastatic B16F10 mouse tumors in vivo. *Mol Ther* **16**: 52-59.

182. Ohashi, PS, Oehen, S, Buerki, K, Pircher, H, Ohashi, CT, Odermatt, B *et al.* (1991). Ablation of "tolerance" and induction of diabetes by virus infection in viral antigen transgenic mice. *Cell* **65**: 305-317.

183. Boudreau, JE, Stephenson, KB, Wang, F, Ashkar, AA, Mossman, KL, Lenz, LL *et al.* (2011). IL-15 and type I interferon are required for activation of tumoricidal NK cells by virus-infected dendritic cells. *Cancer Res* **71**: 2497-2506.

184. Balassu, TC, and Robinson, AJ (1987). Orf virus replication in bovine testis cells: kinetics of viral DNA, polypeptide, and infectious virus production and analysis of virion polypeptides. *Arch Virol* **97**: 267-281.

185. Stacker, SA, and Achen, MG (1999). The vascular endothelial growth factor family: signalling for vascular development. *Growth Factors* **17**: 1-11.

186. Goel, S, Duda, DG, Xu, L, Munn, LL, Boucher, Y, Fukumura, D *et al.* (2011). Normalization of the vasculature for treatment of cancer and other diseases. *Physiol Rev* **91**: 1071-1121.

187. Dvorak, HF (1986). Tumors: wounds that do not heal. Similarities between tumor stroma generation and wound healing. *N Engl J Med* **315**: 1650-1659.

188. Mastrangelo, MJ, Maguire, HC, Jr., Eisenlohr, LC, Laughlin, CE, Monken, CE, McCue, PA *et al.* (1999). Intratumoral recombinant GM-CSF-encoding virus as gene therapy in patients with cutaneous melanoma. *Cancer Gene Ther* **6**: 409-422.

189. Bridle, BW, Hanson, S, and Lichty, BD (2010). Combining oncolytic virotherapy and tumour vaccination. *Cytokine Growth Factor Rev* **21**: 143-148.

190. Wang, M, Bronte, V, Chen, PW, Gritz, L, Panicali, D, Rosenberg, SA *et al.* (1995). Active immunotherapy of cancer with a nonreplicating recombinant fowlpox virus encoding a model tumor-associated antigen. *J Immunol* **154**: 4685-4692.

191. Epaulard, O, Toussaint, B, Quenee, L, Derouazi, M, Bosco, N, Villiers, C *et al.* (2006). Anti-tumor immunotherapy via antigen delivery from a live attenuated genetically engineered Pseudomonas aeruginosa type III secretion system-based vector. *Mol Ther* **14**: 656-661.

192. Boudreau, JE, Bridle, BW, Stephenson, KB, Jenkins, KM, Brunelliere, J, Bramson, JL *et al.* (2009). Recombinant vesicular stomatitis virus transduction of dendritic cells enhances their ability to prime innate and adaptive antitumor immunity. *Mol Ther* **17**: 1465-1472.

193. Cooper, MA, Fehniger, TA, and Caligiuri, MA (2001). The biology of human natural killer-cell subsets. *Trends Immunol* **22**: 633-640.

194. Silva, A, Andrews, DM, Brooks, AG, Smyth, MJ, and Hayakawa, Y (2008). Application of CD27 as a marker for distinguishing human NK cell subsets. *Int Immunol* **20**: 625-630.

195. Krown, SE, Kerr, D, Stewart, WE, 2nd, Field, AK, and Oettgen, HF (1985). Phase I trials of poly(I,C) complexes in advanced cancer. *J Biol Response Mod* **4**: 640-649.

196. Trinchieri, G, and Sher, A (2007). Cooperation of Toll-like receptor signals in innate immune defence. *Nat Rev Immunol* **7**: 179-190.

197. Samanta, M, Iwakiri, D, Kanda, T, Imaizumi, T, and Takada, K (2006). EB virus-encoded RNAs are recognized by RIG-I and activate signaling to induce type I IFN. *EMBO J* **25**: 4207-4214.

198. Le Goffic, R, Pothlichet, J, Vitour, D, Fujita, T, Meurs, E, Chignard, M *et al.* (2007). Cutting Edge: Influenza A virus activates TLR3-dependent inflammatory and RIG-I-dependent antiviral responses in human lung epithelial cells. *J Immunol* **178**: 3368-3372.

199. Gitlin, L, Barchet, W, Gilfillan, S, Cella, M, Beutler, B, Flavell, RA *et al.* (2006). Essential role of mda-5 in type I IFN responses to polyriboinosinic:polyribocytidylic acid and encephalomyocarditis picornavirus. *Proc Natl Acad Sci U S A* **103**: 8459-8464.

200. Zhu, J, Martinez, J, Huang, X, and Yang, Y (2007). Innate immunity against vaccinia virus is mediated by TLR2 and requires TLR-independent production of IFN-beta. *Blood* **109**: 619-625.

201. Hutchens, MA, Luker, KE, Sonstein, J, Nunez, G, Curtis, JL, and Luker, GD (2008). Protective effect of Toll-like receptor 4 in pulmonary vaccinia infection. *PLoS Pathog* **4**: e1000153.

202. Siegemund, S, Hartl, A, von Buttlar, H, Dautel, F, Raue, R, Freudenberg, MA *et al.* (2009). Conventional bone marrow-derived dendritic cells contribute to toll-like receptor-independent production of alpha/beta interferon in response to inactivated parapoxvirus ovis. *J Virol* **83**: 9411-9422.

203. Waibler, Z, Anzaghe, M, Ludwig, H, Akira, S, Weiss, S, Sutter, G *et al.* (2007). Modified vaccinia virus Ankara induces Toll-like receptor-independent type I interferon responses. *J Virol* **81**: 12102-12110.

204. Andoniou, CE, van Dommelen, SL, Voigt, V, Andrews, DM, Brizard, G, Asselin-Paturel, C *et al.* (2005). Interaction between conventional dendritic cells and natural killer cells is integral to the activation of effective antiviral immunity. *Nat Immunol* **6**: 1011-1019.

205. Orange, JS, and Biron, CA (1996). An absolute and restricted requirement for IL-12 in natural killer cell IFN-gamma production and antiviral defense. Studies of natural killer and T cell responses in contrasting viral infections. *J Immunol* **156**: 1138-1142.

206. Brown, MG, Dokun, AO, Heusel, JW, Smith, HR, Beckman, DL, Blattenberger, EA *et al.* (2001). Vital involvement of a natural killer cell activation receptor in resistance to viral infection. *Science* **292**: 934-937.

207. Mandelboim, O, Lieberman, N, Lev, M, Paul, L, Arnon, TI, Bushkin, Y *et al.* (2001). Recognition of haemagglutinins on virus-infected cells by NKp46 activates lysis by human NK cells. *Nature* **409**: 1055-1060.

208. Parker, AK, Parker, S, Yokoyama, WM, Corbett, JA, and Buller, RM (2007). Induction of natural killer cell responses by ectromelia virus controls infection. *J Virol* **81**: 4070-4079.

209. van den Broeke, LT, Daschbach, E, Thomas, EK, Andringa, G, and Berzofsky, JA (2003). Dendritic cell-induced activation of adaptive and innate antitumor immunity. *J Immunol* **171**: 5842-5852.

210. Di Nicola, M, Zappasodi, R, Carlo-Stella, C, Mortarini, R, Pupa, SM, Magni, M *et al.* (2009). Vaccination with autologous tumor-loaded dendritic cells induces clinical and immunologic responses in indolent B-cell lymphoma patients with relapsed and measurable disease: a pilot study. *Blood* **113**: 18-27.

211. Kassim, SH, Rajasagi, NK, Zhao, X, Chervenak, R, and Jennings, SR (2006). In vivo ablation of CD11c-positive dendritic cells increases susceptibility to herpes simplex virus type 1 infection and diminishes NK and T-cell responses. *J Virol* **80**: 3985-3993.

212. Haig, DM, Thomson, J, McInnes, CJ, Deane, DL, Anderson, IE, McCaughan, CA *et al.* (2002). A comparison of the anti-inflammatory and immuno-stimulatory activities of orf virus and ovine interleukin-10. *Virus Res* **90**: 303-316.

213. Kohchi, C, Inagawa, H, Hino, M, Oda, M, Nakata, K, Yoshida, A *et al.* (2004). Utilization of macrophages in anticancer therapy: the macrophage network theory. *Anticancer Res* **24**: 3311-3320.

214. Kruse, N, and Weber, O (2001). Selective induction of apoptosis in antigen-presenting cells in mice by Parapoxvirus ovis. *J Virol* **75**: 4699-4704.

215. Boshkov, LK, Macen, JL, and McFadden, G (1992). Virus-induced loss of class I MHC antigens from the surface of cells infected with myxoma virus and malignant rabbit fibroma virus. *J Immunol* **148**: 881-887.

216. Chisholm, SE, and Reyburn, HT (2006). Recognition of vaccinia virus-infected cells by human natural killer cells depends on natural cytotoxicity receptors. *J Virol* **80**: 2225-2233.

217. Diefenbach, A, Jamieson, AM, Liu, SD, Shastri, N, and Raulet, DH (2000). Ligands for the murine NKG2D receptor: expression by tumor cells and activation of NK cells and macrophages. *Nat Immunol* **1**: 119-126.

218. Zhou, H, Luo, Y, Lo, JF, Kaplan, CD, Mizutani, M, Mizutani, N *et al.* (2005). DNA-based vaccines activate innate and adaptive antitumor immunity by engaging the NKG2D receptor. *Proc Natl Acad Sci U S A* **102**: 10846-10851.

219. French, AR, and Yokoyama, WM (2003). Natural killer cells and viral infections. *Curr Opin Immunol* **15**: 45-51.

220. Eschwege, P, Dumas, F, Blanchet, P, Le Maire, V, Benoit, G, Jardin, A *et al.* (1995). Haematogenous dissemination of prostatic epithelial cells during radical prostatectomy. *Lancet* **346**: 1528-1530.

221. Hofer, SO, Molema, G, Hermens, RA, Wanebo, HJ, Reichner, JS, and Hoekstra, HJ (1999). The effect of surgical wounding on tumour development. *Eur J Surg Oncol* **25**: 231-243.

222. Ben-Eliyahu, S (2003). The promotion of tumor metastasis by surgery and stress: immunological basis and implications for psychoneuroimmunology. *Brain Behav Immun* **17 Suppl 1**: S27-36.

223. Hemmi, H, Kaisho, T, Takeuchi, O, Sato, S, Sanjo, H, Hoshino, K *et al.* (2002). Small anti-viral compounds activate immune cells via the TLR7 MyD88-dependent signaling pathway. *Nat Immunol* **3**: 196-200.

224. Takaoka, A, Wang, Z, Choi, MK, Yanai, H, Negishi, H, Ban, T *et al.* (2007). DAI (DLM-1/ZBP1) is a cytosolic DNA sensor and an activator of innate immune response. *Nature* **448**: 501-505.

225. Meng, X, Chao, J, and Xiang, Y (2008). Identification from diverse mammalian poxviruses of host-range regulatory genes functioning equivalently to vaccinia virus C7L. *Virology* **372**: 372-383.

226. Najera, JL, Gomez, CE, Garcia-Arriaza, J, Sorzano, CO, and Esteban, M (2010). Insertion of vaccinia virus C7L host range gene into NYVAC-B genome potentiates immune responses against HIV-1 antigens. *PLoS One* **5**: e11406.

227. Liu, TC, Hwang, T, Park, BH, Bell, J, and Kirn, DH (2008). The targeted oncolytic poxvirus JX-594 demonstrates antitumoral, antivascular, and anti-HBV activities in patients with hepatocellular carcinoma. *Mol Ther* **16**: 1637-1642.

228. Kanai, R, Rabkin, SD, Yip, S, Sgubin, D, Zaupa, CM, Hirose, Y *et al.* (2012). Oncolytic virus-mediated manipulation of DNA damage responses: synergy with chemotherapy in killing glioblastoma stem cells. *J Natl Cancer Inst* **104**: 42-55.

229. Karapanagiotou, EM, Roulstone, V, Twigger, K, Ball, M, Tanay, M, Nutting, C *et al.* (2012). Phase I/II Trial of Carboplatin and Paclitaxel Chemotherapy in Combination

with Intravenous Oncolytic Reovirus in Patients with Advanced Malignancies. *Clin Cancer Res*.

230. Powles, T, Chowdhury, S, Jones, R, Mantle, M, Nathan, P, Bex, A *et al.* (2011). Sunitinib and other targeted therapies for renal cell carcinoma. *Br J Cancer* **104**: 741-745.

231. Tseng, JC, Granot, T, DiGiacomo, V, Levin, B, and Meruelo, D (2010). Enhanced specific delivery and targeting of oncolytic Sindbis viral vectors by modulating vascular leakiness in tumor. *Cancer Gene Ther* **17**: 244-255.

232. Kottke, T, Hall, G, Pulido, J, Diaz, RM, Thompson, J, Chong, H *et al.* (2010). Antiangiogenic cancer therapy combined with oncolytic virotherapy leads to regression of established tumors in mice. *J Clin Invest* **120**: 1551-1560.

233. Harrington, K, Alvarez-Vallina, L, Crittenden, M, Gough, M, Chong, H, Diaz, RM *et al.* (2002). Cells as vehicles for cancer gene therapy: the missing link between targeted vectors and systemic delivery? *Hum Gene Ther* **13**: 1263-1280.

CONTRIBUTIONS OF COLLABORATORS

The following colleagues are recognized as contributing to the work detailed in this thesis. Dr. Marianne Stanford provided some of the data highlighted in Figure 4.6. Dr. Lee-Hwa Tai and Christiano De Souza provided some technical expertise for the chromium release assays depicted in Figure 4.10, panels e and f. Dr. Lee-Hwa Tai also undertook the experiments illustrated in Figure 5.14. The experiments depicted in Figures 5.5, 5.7, 5.8 and 5.9 were performed by myself at McMaster University in Hamilton Ontario in collaboration with Dr. Brian Lichty and Dr. Yonhong Wan's groups. Dr. Byram Bridle and Dr. Jeanette Boudreau offered technical expertise at McMaster University.

APPENDICES

APPENDIX I: PREVENTING POSTOPERATIVE METASTATIC DISEASE BY INHIBITING SURGERY INDUCED NATURAL KILLER CELL DYSFUNCTION

Lee-Hwa Tai, Christiano Tanese de Souza, Simon Belanger, Lundi Ly, Julia L. Rintoul, Abhirami A. Ananth, Tiffany Lam, Theresa Falls, John C. Bell, Andrew P. Makrigiannis, and Rebecca A. Auer

Contribution:

Manufactured, purified, and quantified ORFV for all experiments. Assisted in the design, and execution of oncolytic virus flow cytometry experiments. Assisted in the execution of animal experiments.

Submitted: *Under Review, Cancer Research, May 30th 2012*

Running Title: Oncolytic virus inhibits surgery induced NK cell dysfunction

Preventing postoperative metastatic disease by inhibiting surgery induced natural killer cell dysfunction

Lee-Hwa Tai[1], Christiano Tanese de Souza[1], Simon Bélanger[2], Lundi Ly[1,2], Julia Rintoul[1,2], Abhirami A. Ananth[1,2], Tiffany Lam[1], Theresa Falls[1], John C. Bell[1,2], Andrew P. Makrigiannis[2], and Rebecca A. Auer[1,3]

[1]Centre for Innovative Cancer Research, Ottawa Hospital Research Institute, Ottawa, ON, Canada

[2]Department of Biochemistry, Microbiology, and Immunology, University of Ottawa, Ottawa,

Running Title: Oncolytic virus inhibits surgery induced NK cell dysfunction

ABSTRACT

Natural killer cell clearance of tumor cell emboli following surgery is thought to be vital in preventing postoperative metastases. Using a mouse model of surgical stress, we transferred surgically stressed NK cells into NK-deficient mice and observed enhanced lung metastases in these tumor-bearing mice compared to recipient mice who received untreated NK cells, establishing that NK cells play a crucial role in mediating tumor clearance following surgery. Accordingly, *in vivo* splenocyte/tumor rejection and *in vitro* target cell killing by NK cells were significantly reduced in surgically stressed mice. Surgery markedly reduced NK cell total numbers in the spleen and affected NK cell migration. NK cell expression of NKG2D, KLRG1, CD62L and CD11b was diminished following surgery. Furthermore, perioperative administration of novel oncolytic ORFV and vaccinia virus can reverse NK cell suppression following surgery and this correlates with a reduction in the postoperative formation of metastases. In human studies, postoperative cancer surgery patients had reduced NK cell cytoxicity and we demonstrate for the first time that oncolytic vaccinia virus markedly increases NK cell activity in cancer patients. These data provide direct *in vivo* evidence that surgical stress impairs global NK cell function. Perioperative cancer therapies aimed at targeting the mechanisms responsible for the prometastatic effects of surgery will reduce metastatic recurrence and improve survival in surgical cancer patients.

Running Title: Oncolytic virus inhibits surgery induced NK cell dysfunction

INTRODUCTION

Surgeons have long suspected that surgery, a necessary step in the treatment of solid cancers, facilitates the metastatic process. Despite the initial observation of this phenomenon in 1913 (1) it remains an area of unresolved inquiry. Numerous animal studies using implanted and spontaneous tumor models have clearly demonstrated that surgery promotes the formation of metastatic disease (2, 3) and the number of metastatic deposits that develop is directly proportional to the magnitude of surgical stress (2). In clinical studies, a complicated postoperative course corrresponds to an increase in physiologic surgical stress. This has been shown to correlate with an inferior cancer survival and an increased incidence of metastatic disease (4, 5).

A number of perioperative changes have been proposed to explain the promotion of metastases formation following surgery including dissemination of tumor cells during the surgical procedure (6, 7), local and systemic release of growth factors (8, 9), and cellular immune suppression. Intraoperative circulating tumor cells have been detected in patients with a variety of metastatic cancers and may be a valuable prognostic marker (10, 11). The cellular immune suppression following major surgery appears to peak at 3 days (12) following surgery, but may persist for weeks (12, 13).

Natural Killer (NK) cells are cytotoxic lymphocytes that constitute a major component of the innate immune system. Immunosurveillance of the host by NK cells for malignant and virally-infected cells results in direct cytotoxicity and the production of cytokines and chemokines to enhance the immune response. NK cells are able to distinguish normal cells from unhealthy cells by monitoring for surface expression of a variety of molecules (14). NK cell dysfunction following surgery has been documented in both human patients (13, 15, 16) and

animal models (17, 18). Postoperative NK cell suppression correlates with increased metastases in animal models of spontaneous (3) and implanted (19, 20) metastases, while in human studies low NK activity during the perioperative period is associated with a higher rate of cancer recurrence and mortality in a number of different cancer types (21, 22).

The perioperative period represents not only a window of opportunity for cancer cells to form metastases but also a therapeutic window in which to intervene in the metastatic process. Traditional cancer therapies, such as chemotherapy, are considered too toxic to be administered to patients recovering from a major surgery as they impair wound healing (23). Alternatively, immune therapies are ideal candidates for perioperative administration. The perioperative administration of recombinant cytokines has been explored in early phase clinical trials (24, 25). These studies have demonstrated that perioperative administration prevent the supression of NK cell activity that occurs following surgery (26, 27).

We recently reported on oncolytic vaccinia virus to selectively infect, replicate and express a transgene in cancer tissue of human patients following an intravenous infusion (28). This exciting clinical data is a landmark in the development of oncolytic viruses (OV) as a novel biotherapeutic platform. OV have several demonstrated mechanisms of action including direct tumour cell cytotoxicity, tumour-specific vascular shutdown, and induction of innate and adaptive immune responses (29). We have also recently demonstrated that another OV- ORFV, has a profound effect on NK cells following i.v. delivery and that this NK cell activation is the main mechanism by which ORFV exerts its anti-tumour effect (30). The compelling pre-clinical and clinical data with OV has led us to hypothesize that perioperative treatment with OV could improve recurrence-free survival following surgical resection.

Running Title: Oncolytic virus inhibits surgery induced NK cell dysfunction

While the detrimental impact of surgery on NK cell function has clearly been addressed, the direct *in vivo* role of NK cells in clearing tumor metastases following surgery has yet to be demonstrated. In this study, the function of NK cells in surgically stressed mice was rigorously characterized and the first use of novel OV to recover this defect is provided.

RESULTS

Surgical stress results in more experimental lung metastases and NK cells are important mediators of this effect.

We have developed a reproducible mouse model of surgical stress that results in the dramatic enhancement of pulmonary metastases. At 3d post-abdominal nephrectomy and B16F10lacZ tumor inoculation, lungs were harvested and visualized for metastases. Surgery clearly increases the amount of pulmonary metastases compared to no surgery control mice by 2-fold (Figure 1A, NK cell intact). In addition, our findings indicate that this prometastatic effect seen following surgery is not mouse strain, cell-type, anesthesia/analgesia or surgery specific (unpublished data).

Previous studies have demonstrated that NK cells play an important role in clearing tumor cells in the vasculature (31, 32). To determine if this mechanism is operating in the postoperative period, the surgical stress experiment was repeated following pharmacological depletion of NK cells using anti-asialo GM1 serum. In mice depleted of NK cells, both no surgery control and surgically stressed mice developed increased lung tumor burden. More importantly, surgery did not result in an increased number of lung metastases over and above the no surgery controls, suggesting a preventive role for NK cells in the postoperative formation of metastases (Figure 1A, NK cell depleted). These findings were further confirmed by reproducing the same results in transgenic mice deficient in NK cells (IL2γR-KO, NK-deficient

mice) (Figure 1B). Thus, the underlying mechanism of surgical stress resulting in increased metastases appears to involve NK cells.

Surgery suppresses NK cell function and prevents them from removing experimental lung metastases

To corroborate that NK cells indeed facilitate the removal of lung tumor metastases, we adoptively transfered purified splenic $DX5^+$ NK cells from surgically stressed and no surgery control mice into NK-deficient mice. To establish experimental lung metastases, 3e5 B16lacZ cells were injected into NK-deficient mice 1h after NK cell transfer. At 3d post treatment, we found significantly increased lung tumor burden in NK-deficient mice that received surgically stressed NK cells compared to those that received NK cells from no surgery control animals (Figure 1C). As an added control, we transfered the negative immune cell population post NK cell enrichment and observed complete abrogation of the effect of surgery on pulmonary metastases (Figure 1C), further eliminating potential roles played by T cells and macrophages in our surgical stress model. By transfering surgically stressed NK cells and recreating the effect of surgery on the formation of metastases, we have definitively established that the prometastatic effect of surgery is mediated by NK cells.

Defective killing of tumor cells by surgically stressed NK cells *in vitro*

Since surgical stress resulted in dysfunctional NK cell clearance of tumor cells *in vivo*, we questioned whether NK cell cytotoxicity was impaired by performing an *in vitro* NK cell cytotoxicity assay. Various chromium-labeled tumor target cells were incubated with $DX5^+$ purified NK cells from no surgery control and surgically stressed mice 18 h post-surgery (Figure 2). It was found that against all tumor targets tested (NKG2D ligand bearing YAC-1, MHC-I-deficient B16F10lacZ and RMA-S), surgically stressed NK cells were significantly inhibited in

their ability to kill tumor cells (2A-C). Interestingly, the killing of Thy1.2 labeled EL-4 target cells was found to be similarly impaired by surgically stressed NK cells in an antibody dependent cellular cytotoxicity (ADCC) assay (Figure 2D). This data strongly suggests that surgical stress impairs various NK cell activating receptors and causes a generalized NK cell cytotoxicity defect.

Defective killing of hematopoietic and tumor cells by surgically stressed NK cells *in vivo*

Healthy NK cells have the ability to reject transplanted hematopoeitic cells from mice deficient in β2m, which is necessary for normal MHC-I surface expression (33). The rejection of $\beta2m^{-/-}$ splenocytes is mediated by NK cells as shown by pre-treatment of mice with NK cell-depleting antibody (34). To determine if surgically stressed NK cells effectively immunosurvey for the expression of MHC-I on peripheral cells *in vivo*, a $\beta2m^{-/-}$ splenocyte rejection assay was performed. Approximately, 70% of $\beta2m^{-/-}$ splenocytes were rejected by no surgery control mice. However, surgically stressed mice displayed only half as much rejection (Figure 3A). Next, the rejection by surgically stressed mice of tumor cells deficient in MHC-I molecules was tested. The rejection of RMA-S cells has also been shown to be due to NK cells by serum-mediated NK cell depletion (35). Similar to the rejection of MHC-I splenocytes, the rejection of RMA-S by surgically stressed mice (55%) was significantly lower than no surgery controls (80%) (Figure 3B). These results corroborate our *in vitro* NK cell killing data and demonstrate that surgically stressed NK cells have defective *in vivo* cytotoxicity.

Surgically stressed NK cells display abnormal NK cell migration and markers

The dysfunctional cytotoxic responses of surgically stressed NK cells raises the question of how other facets of NK cell function is affected by surgery. We examined NK cell frequencies in the spleen, blood and lungs by flow cytometry and they were found to be similar in no surgery

control and surgically stressed mice (Figure 4A). Other immune cell populations were also assessed in the spleen and no differences were detected (Supplemental Figure 1A). However, total NK cell numbers in spleen were reduced by half in surgically stressed mice and were similar in blood and lungs (Figure 4B). Given this significant decrease, we assessed various lymph nodes (LN) for accumulation of NK cells and detected no differences between surgery and untreated groups (Supplemental Figure 1B). Since, spleen NK cells did not appear to migrate to LN post-surgery, we assessed for their presence elsewhere (peritoneal cavity, peripheral blood, lungs) through splenocyte transfer. We observed an increase in $CFSE^+$ cells in the peritoneum of surgically stressed mice, but not at other sites (Figure 4C). This suggests that following surgery, spleen NK cells migrate preferentially to sites of surgical trauma (abdominal nephrectomy is performed in the peritoneal cavity). Next, we addressed the question of NK cell viability. We observed comparable high percentages of live cells (PI^-/Annexin V^-) in both surgically stressed and no surgery control splenic NK cells. These results demonstrate that the dysfunction in NK cells observed is not due to cell viability (Supplemental Figure 1C). A panel of NK cell markers (NKG2D, KLRG1, CD62L and CD11b) were further tested on splenic NK cells (Figure 4E) and found to show decreased expression following surgery. The reduction in the expression of NKG2D corroborates with defective NK cell killing observed in surgically stressed NK cells against YAC-1 tumors (Figure 2A) as YAC-1 tumors express multiple ligands for the activating NKG2D NK cell receptor (36). KLRG1 is a marker of NK cell activation/maturation and its decrease likely reflects impaired NK cell function post-surgery. CD62L is a cell adhesion molecule that binds to selectins for NK cell migration and CD11b is a complement receptor. Decreased expression of CD62L and CD11b by surgically stressed NK cells also explains the altered splenic NK cell numbers and migration observed post-surgery. By

comparison, NK cell surface expression of NK1.1, CD122, DX5, NKp46, NKRP1C, LFA-1, B220, CD27 and Ly49D were assessed and no significant difference was detected between treatment groups (data not shown).

Novel anti-cancer OV as perioperative therapy against immune suppressive effects of surgery

Given the suppressive effects of surgery on NK cell function, we employed perioperative treatments to enhance NK cell function and attenuate the formation of metastatic disease following surgery. First, we used poly(I:C), a synthetic dsRNA agonist for Toll-Like Receptor-3 and a well established activator of NK cells (37). At 3d post-Poly(I:C) and surgery, a striking decrease in tumor metastases was observed compared to surgery alone. In parallel, a dramatic increase in NK cell cytoxicity was observed following surgery at two different doses of poly(I:C) (15ug, 150ug) (Supplemental Figure 2). This strongly indicates that NK cell suppression seen following surgery is reversible and that further evaluation of candidate NK cell activators as perioperative cancer treatments is warranted.

Currently, there are a number of novel OV candidates in our lab under assessment. These include Parapoxvirus Ovis (ORFV) in preclinical development and an attentuated vaccinia virus strain that contains the immune modulating gene GM-CSF (JX-594) in clinical development. First, we determined whether perioperative OV can attenuate the formation of metastatic disease following surgery in our mouse model. At 3d post-treatment with therapeutic doses of ORFV or JX-594-GFP^{+}/βgal^{-}, a dramatic attenuation of experimental metastases was observed in surgically stressed mice compared to surgically stressed mice that did not receive OV therapy, suggesting that both viruses mediate tumor metastases removal (Figure 5A,B). Next, we determined whether the decrease in metastases was a virus-induced NK cell-mediated

"tumoricidal" effect or OV-mediated "viral oncolysis" effect. When NK cells were depleted, we observed for both viruses, approximately 1/3 less metastases in the surgery + OV group (Figure 5C,D) compared to the surgery alone group with NK depletion. This data suggests that tumor metastases removal in our surgical stress model is mainly mediated through OV viral activation of NK cells and subsequent NK cell mediated tumor lysis. This does not rule out a partial and important role of OV-mediated killing of tumors. This data is supported by our previous findings of the strong NK stimulating abilities of ORFV (30). The extent of JX-594-GFP^{+}/βgal^{-} on NK cell activation is currently being assessed in our lab. To further characterize NK cell function following perioperative administration of OV, we examined NK cell cytotoxicity and IFNγ secretion. We observed a significant surgery induced defect in NK cell killing along with a dramatic recovery of NK killing following perioperative administration of both OV compared to surgery alone (Figure 5E,F). Similarly, we observed increased IFNγ secretion from surgically stressed mice receiving perioperative OV compared to surgery alone (Figure 5G-J). Lastly, we observed a complete rescue of $\beta_2m^{-/-}$ splenocyte rejection post-surgery with ORFV or JX-594-GFP^{+}/βgal^{-}treatments (Figure 5K), showing that the effect by both OV is due to NK cell activation. Taken together these results demonstrate that we can successfully treat perioperative NK cell suppression with novel OV therapy.

Surgery suppresses and intravenous infusion of oncolytic vaccinia virus enhances NK cell function in human cancer patients

To understand and prevent postoperative NK cell suppression in human patients, we collected blood from cancer patients as part of two different protocols: Ottawa Hospital cancer surgery patients enrolled in the Perioperative Blood Collection Program and in the neoadjuvant JX-594 Phase 2a clinical trial. Blood is collected at different time points including

preoperatively, on postoperative day (POD) 1, POD 3 (±1) and POD 28 (±14) for the first study and at preOV, postOV D3, postOV D14 and postOV D49 for the second trial. As part of the first study, we observed a decrease in the NK cell cytotoxicity at POD 1 and 3 and a return to baseline at POD 28(±14) in 2 human patients studied so far (Figure 6A). In the neoadjuvant JX-594 trial, NK cell cytotoxicity improves in the setting of JX-594 compared to baseline control blood for 2 enrolled patients (Figure 6B).

DISCUSSION

In this study, we have clearly demonstrated that the innate NK cell responses triggered by OV are a vital component of successful perioperative treatment, capable of overcoming immunosuppressive post-surgery microenvironments and clearing metastatic disease. We, therefore, propose the perioperative stimulation of the immune system with OV as a way to avoid the NK suppressive effects of cancer surgery. The early postoperative period is an ideal window for immune-based anticancer therapies because the tumor burden is at its absolute lowest immediately following resection of the primary tumor. There is strong evidence in the animal setting that a whole host of agents that broadly stimulate the immune system are effective in significantly reducing the incidence of metastatic disease after surgery. Perioperative administration of recombinant IL-2 and IFN-α has been explored in early phase clinical trials demonstrating their potential to prevent postoperative NK cell suppression and enhance progression-free survival (24-27, 38-42). Other non-conventinal immunomodulators have been evaluated for their ability to boost cellular immunity in the perioperative period including cimetidine (43) mistletoe extract (44) and GM-CSF (45). Despite the paucity of data, it is promising that perioperative treatment strategies, aimed at NK cell stimulation, improve cancer outcomes. This is an area that evidently warrants further study.

We clearly demonstrate that an analogous mechanism of surgery induced NK cell cyototoxic suppression is occuring in human patients following surgery. Our human data confirms that NK cell activity is indeed suppressed following surgery, but returns to baseline at POD 28(±14). As part of the neoadjuvant JX-594 trial, NK cell cytotoxicity improves in the setting of OV treatment compared to baseline control blood and no adverse events were reported. These results show the feasibility of administering OV perioperatively to cancer patients.

In addition to our research interests in developing OV as direct oncolytic agents, we want to explore the potential for OV to trigger innate and adaptive immune responses. This will maximize the potential clinical impact of this virotherapy. It is very likely that stimulation of NK cells play an important role in the therapeutic effect of many OV, not only by enhancing NK cell mediated killing of tumor target cells but also by triggering a robust, T-cell mediated, antitumor immune response (46). Our preliminary evidence suggests that preoperative tumor vaccines may be an effective means of establishing specific immune responses against the tumor before resection. The combination of nonspecific perioperative immune up-regulation and preoperative tumor vaccines could provide the patient with the ability to kill tumor cells in the immediate postoperative period through specific and innate immune responses. Ongoing work in our lab is focused on understanding the molecular mechanism of surgery-mediated NK cell suppression in the preclinical and clinical setting along with investigating the efficacy of a preoperative tumor vaccine strategy in our preclinical surgery model.

Surgical removal of solid primary tumors is an essential component of cancer treatment. However, we and others has clearly demonstrated surgery induced suppression of immune cells, in particular we have demonstrated NK cell dysfunction leading to impaired clearing of experimental metastases. There are currently no standard perioperative anti-cancer therapies

given to cancer surgery patients. Research into neoadjuvant immune therapy is clearly warranted to prevent immune dysfunction following surgery and to eradicate micrometastatic disease. Understanding the mechanisms of perioperative NK cell suppression and stimulation with novel cancer therapies will permit the rational design of perioperative therapeutics aimed at preventing metastatic cancer recurrence following complete surgical resection.

MATERIALS AND METHODS

Mice - C57BL/6 (B6), IL2γR-KO (NK-deficient), and β-2-microglobulin-deficient ($\beta 2m^{-/-}$) mice were purchased from The Jackson Laboratory. Animals were housed in pathogen-free conditions at the Animal Care Veterinary Service facility of the University of Ottawa (Ontario) in accordance with institutional guidelines. All studies and manipulations performed on animals were in accordance with university guidelines and approved by the Animal Care Committee at the University of Ottawa.

Establishment of murine surgical stress model – Mice were subjected to 2.5% Isofluorane (Baxter Corp) for induction and maintenance of anesthesia. Routine perioperative care for mice was conducted as per standard protocols at the University of Ottawa including pain control using Buprenorphine (0.05mg/kg) administered subcutaneously (s.c.) the day d of surgery and every 8h for 2 d postoperatively. Surgical stress was induced in mice by an abdominal laparotomy (3cm midline incision) and left nephrectomy preceded by an i.v. challenge of 3e5 B16lacZ cells to establish pulmonary metastases. Animals were euthanized at 18 h or 3 d following tumor cell injection and their harvested lungs were stained with X-gal (Bioshop) as described previously (47). Total number of surface visible metastases was determined on the largest lung lobe (left lobe) using a stereomicroscope (Leica Microsystems). This analysis correlates well with the total number of lung metastases on all 5 lobes and was therefore used for the current study. For

rescue of tumor cell clearance assays, 150ug Poly(I:C), 1e7 PFU of ORFV and 1e7 PFU of oncolytic vaccinia virus was injected into mice 2 h and 3e5 B16lacZ cell 1h, respectively, before surgery.

Cell lines and viruses – B16F10LacZ melanoma cell line was obtained from Dr K Graham (LRCP, Ontario) and maintained in cDMEM. Cells were resuspended in DMEM without serum for i.v. injection through the lateral tail vein. 3e5 cells at >95% viability were injected in a 0.1ml volume/mouse. RMA (thymoma) and RMA-S (MHC-deficient variant of RMA) were a kind gift from Dr. Andre Veillette (IRCM, Quebec). YAC-1 and K562 leukemia cell line was purchased from ATCC and maintained in cRPMI. All cell lines were verified to be mycoplasma free and show appropriate microscopic morphology at time of use. Wild type ORFV (strain NZ2) was obtained from Dr. Andrew Mercer (University of Otago, New Zealand) and was injected and titred as previously described (48). Oncolytic vaccinia virus JX-594-GFP^{+}/βgal^{-} was prepared as previously described (49).

Antibodies and FACS analysis. - To analyze splenic, blood and lung lymphocyte populations, organs were removed from mice and RBCs lysed using ACK lysis buffer. The following mAbs were used: anti-TCRβ (H57-597), anti-CD62L (MEL-14), anti-CD11b (M1/70), anti-CD122 (TM-beta1), anti-NKG2D (CX5), and anti-KLRG1 (2F1) were purchased from eBiosciences. PI/Annexin V stains and Isotype controls were purchased from BD Biosciences. Spleen NK cell IFNγ secretion was examined following a 5h GolgiPlug (BD Bioscience) incubation using the following Abs: CD3-PerCP (clone 17A2, R&D systems), NK1.1-PE (PK136) and IFNγ-AF647 (XMG1.2) all from BD Bioscience. Flow cytometry acquisitions were performed on a CyAN-ADP using Summit software (Beckman Coulter). Data was analyzed with Kaluza software.

Evaluation of the role of NK cells in postoperative tumor metastases - NK cells were depleted using α-asialoGM1 antibody (Cedarlane) as previously described (30). The lung tumor burden was quantified at 3d post-surgery.

NK cell adoptive transfer experiments – For NK cell transfer experiments, splenocytes were isolated from no surgery control or 18 post-surgery from B6 mice, enriched for NK cells with $DX5^+$ microbeads on an AutomacsPro cell sorter (Miltenyi Biotec). 1e6 $DX5^+$ NK cells as determined by flow cytometry were injected via the lateral tail vein into NK-deficient mice. For all transfers, 3e5 B16lacZ tumor cells were injected i.v. 1h post immune cell transfer. 3d post immune and tumor cell injection, lungs of NK-deficient mice were isolated and quantified with Xgal (as above). For CFSE labeled whole splenocyte transfers, bulk splenocytes were processed and labeled with 10uM of CFSE (Invitrogen). 10e6 $CFSE^+$ splenocytes were injected i.v. into mice that received surgery 2h prior. 18 h post splenocyte transfer – lung, peripheral blood and peritoneal lavage cells were processed and analyzed by flow cytometry for $CFSE^+$ cells.

***In vitro* NK cell assays** - The chromium release assay was performed as previously described (50). Briefly, splenocytes were isolated from surgically stressed and control mice at 18 h post-surgery. Pooled and sorted NK cells were re-suspended at a concentration of $2.5x10^6$ cells/ml and then mixed with chromium labelled target cells (YAC-1, B16F10LacZ, RMA-S and EL-4), which were re-suspended at a concentration of $3x10^4$ cells/ml at different effector to target ratios (E:T) (50:1, 25:1, 12:1, 6:1). The cell mixture was incubated for 4 h prior to analysis of ^{51}Cr release in the supernatant using a gamma counter (Perkin Elmer). For ADCC, after ^{51}Cr-labelling, target cells were incubated in the presence of 10 μg/ml of anti-Thy1.2 mAb or Isotype control Ab for 30 min and then washed before co-incubation with effector cells. For rescue of

NK cell impairment assays, Poly(I:C), ORFV and JX-594-GFP$^+$/βgal$^-$ was injected into mice 4 h before surgery.

***In vivo* NK cell assays** - The splenocyte rejection assay was performed as previously described (50). Briefly, splenocytes from MHC-deficient and sufficient mice were isolated and labeled with 5 μM and 0.5 μM CFSE, respectively. A mixture of 3e6 splenocytes of each population were injected in the tail vein of recipient mice treated with surgery (4 h prior). After 16 h, spleens from recipient mice were harvested and analyzed for the presence of CFSE-labeled donor cells by flow cytometry. For rescue of NK cell impairment assays, ORFV and JX-594-GFP$^+$/βgal$^-$ was injected into mice 2 h before surgery. For tumor rejection assays MHC-I positive (RMA) and MHC-I-negative (RMA-S) tumor cells were differentially labeled with CFSE. A mixture of 1e6 cells of each type was injected intra-peritoneal into B6 recipient mice treated with surgery (4 h prior). After 18h, peritoneal cells were harvested with PBS-2mM EDTA and analyzed for the presence of CFSE-labeled tumor cells by flow cytometry.

Human PBMC cytotoxicity assay

Human whole blood was collected (Perioperative blood collection program = OHREB#2011884, Neoadjuvant JX-594 clinical trial NCT01329809) and processed immediately for PBMC using Ficoll-Paque (Stemcell). PBMC were resuspended at a concentration of $7.5x10^6$ in freezing media (RPMI with 12.5% Human Serum Albumin and 10% DMSO). 1mL aliquots were frozen in cryovials overnight at -80°C and transferred to liquid N_2 for long term storage. K562 were harvested and labelled with ^{51}Cr as described for YAC-1 cells. PBMC were re-suspended at a concentration of $5x10^6$ cells/ml and then mixed with target K562 which were re-suspended at a concentration of $5x10^4$ cells/ml at different E:T ratios. Assessment of PBMC killing was determined as above.

Statistical analysis - Statistical significance was determined by student t test with a cutoff P value of 0.05. Data is presented as +/- SD.

REFERENCES

1. Tyzzer EE. Factors in the Production and Growth of tumor Metastases. J Med Res 1913; 28: 309-32 1.
2. Tsuchiya Y, Sawada S, Yoshioka I, et al. Increased surgical stress promotes tumor metastasis. Surgery 2003; 133: 547-55.
3. Glasner A, Avraham R, Rosenne E, et al. Improving survival rates in two models of spontaneous postoperative metastasis in mice by combined administration of a beta-adrenergic antagonist and a cyclooxygenase-2 inhibitor. J Immunol 2010; 184: 2449-57.
4. Lerut T, Moons J, Coosemans W, et al. Postoperative Complications After Transthoracic Esophagectomy for Cancer of the Esophagus and Gastroesophageal Junction Are Correlated With Early Cancer Recurrence: Role of Systematic Grading of Complications Using the Modified Clavien Classification. Ann Surg 2009.
5. Eberhardt JM, Kiran RP, Lavery IC. The impact of anastomotic leak and intra-abdominal abscess on cancer-related outcomes after resection for colorectal cancer: a case control study. Dis Colon Rectum 2009; 52: 380-6.
6. Fortner JG. Inadvertent spread of cancer at surgery. J Surg Oncol 1993; 53: 191-6.
7. Yamaguchi K, Takagi Y, Aoki S, Futamura M, Saji S. Significant detection of circulating cancer cells in the blood by reverse transcriptase-polymerase chain reaction during colorectal cancer resection. Ann Surg 2000; 232: 58-65.
8. Belizon A, Balik E, Feingold DL, et al. Major abdominal surgery increases plasma levels of vascular endothelial growth factor: open more so than minimally invasive methods. Ann Surg 2006; 244: 792-8.
9. Pera M, Nelson H, Rajkumar SV, Young-Fadok TM, Burgart LJ. Influence of postoperative acute-phase response on angiogenesis and tumor growth: open vs. laparoscopic-assisted surgery in mice. J Gastrointest Surg 2003; 7: 783-90.
10. Paterlini-Brechot P, Benali NL. Circulating tumor cells (CTC) detection: clinical impact and future directions. Cancer Lett 2007; 253: 180-204.
11. Karl A, Tritschler S, Hofmann S, Stief CG, Schindlbeck C. Perioperative search for circulating tumor cells in patients undergoing radical cystectomy for bladder cancer. Eur J Med Res 2009; 14: 487-90.
12. Coffey JC, Wang JH, Smith MJ, Bouchier-Hayes D, Cotter TG, Redmond HP. Excisional surgery for cancer cure: therapy at a cost. Lancet Oncol 2003; 4: 760-8.
13. Espi A, Arenas J, Garcia-Granero E, Marti E, Lledo S. Relationship of curative surgery on natural killer cell activity in colorectal cancer. Dis Colon Rectum 1996; 39: 429-34.
14. Lanier LL. NK cell recognition. Annu Rev Immunol 2005; 23: 225-74.
15. Pollock RE, Lotzova E, Stanford SD. Mechanism of surgical stress impairment of human perioperative natural killer cell cytotoxicity. Arch Surg 1991; 126: 338-42.
16. Pollock RE, Lotzova E, Stanford SD. Surgical stress impairs natural killer cell programming of tumor for lysis in patients with sarcomas and other solid tumors. Cancer 1992; 70: 2192-202.
17. Page GG, Blakely WP, Ben-Eliyahu S. Evidence that postoperative pain is a mediator of the tumor-promoting effects of surgery in rats. Pain 2001; 90: 191-9.
18. Ben-Eliyahu S, Page GG, Yirmiya R, Shakhar G. Evidence that stress and surgical interventions promote tumor development by suppressing natural killer cell activity. Int J Cancer 1999; 80: 880-8.

19. Benish M, Bartal I, Goldfarb Y, et al. Perioperative use of beta-blockers and COX-2 inhibitors may improve immune competence and reduce the risk of tumor metastasis. Ann Surg Oncol 2008; 15: 2042-52.
20. Goldfarb Y, Sorski L, Benish M, Levi B, Melamed R, Ben-Eliyahu S. Improving postoperative immune status and resistance to cancer metastasis: a combined perioperative approach of immunostimulation and prevention of excessive surgical stress responses. Ann Surg 2011; 253: 798-810.
21. Tartter PI, Steinberg B, Barron DM, Martinelli G. The prognostic significance of natural killer cytotoxicity in patients with colorectal cancer. Arch Surg 1987; 122: 1264-8.
22. Fujisawa T, Yamaguchi Y. Autologous tumor killing activity as a prognostic factor in primary resected nonsmall cell carcinoma of the lung. Cancer 1997; 79: 474-81.
23. Guillot B, Bessis D, Dereure O. Mucocutaneous side effects of antineoplastic chemotherapy. Expert Opin Drug Saf 2004; 3: 579-87.
24. Klatte T, Ittenson A, Rohl FW, Ecke M, Allhoff EP, Bohm M. Perioperative immunomodulation with interleukin-2 in patients with renal cell carcinoma: results of a controlled phase II trial. Br J Cancer 2006; 95: 1167-73.
25. Oosterling SJ, van der Bij GJ, Mels AK, et al. Perioperative IFN-alpha to avoid surgically induced immune suppression in colorectal cancer patients. Histol Histopathol 2006; 21: 753-60.
26. Deehan DJ, Heys SD, Ashby J, Eremin O. Interleukin-2 (IL-2) augments host cellular immune reactivity in the perioperative period in patients with malignant disease. Eur J Surg Oncol 1995; 21: 16-22.
27. Houvenaeghel G, Bladou F, Blache JL, et al. Tolerance and feasibility of perioperative treatment with interferon-alpha 2a in advanced cancers. Int Surg 1997; 82: 165-9.
28. Breitbach CJ, Burke J, Jonker D, et al. Intravenous delivery of a multi-mechanistic cancer-targeted oncolytic poxvirus in humans. Nature; 477: 99-102.
29. Kirn DH, Thorne SH. Targeted and armed oncolytic poxviruses: a novel multi-mechanistic therapeutic class for cancer. Nat Rev Cancer 2009; 9: 64-71.
30. Rintoul JL, Lemay CG, Tai LH, et al. ORFV: A Novel Oncolytic and Immune Stimulating Parapoxvirus Therapeutic. Mol Ther.
31. Gorelik E, Wiltrout RH, Okumura K, Habu S, Herberman RB. Role of NK cells in the control of metastatic spread and growth of tumor cells in mice. Int J Cancer 1982; 30: 107-12.
32. Hanna N. The role of natural killer cells in the control of tumor growth and metastasis. Biochim Biophys Acta 1985; 780: 213-26.
33. Liao NS, Bix M, Zijlstra M, Jaenisch R, Raulet D. MHC class I deficiency: susceptibility to natural killer (NK) cells and impaired NK activity. Science 1991; 253: 199-202.
34. Lakshmikanth T, Burke S, Ali TH, et al. NCRs and DNAM-1 mediate NK cell recognition and lysis of human and mouse melanoma cell lines in vitro and in vivo. J Clin Invest 2009; 119: 1251-63.
35. Dong Z, Cruz-Munoz ME, Zhong MC, Chen R, Latour S, Veillette A. Essential function for SAP family adaptors in the surveillance of hematopoietic cells by natural killer cells. Nat Immunol 2009; 10: 973-80.
36. Champsaur M, Lanier LL. Effect of NKG2D ligand expression on host immune responses. Immunol Rev; 235: 267-85.
37. Biron CA. Activation and function of natural killer cell responses during viral infections. Curr Opin Immunol 1997; 9: 24-34.

38. Nichols PH, Ramsden CW, Ward U, Sedman PC, Primrose JN. Perioperative immunotherapy with recombinant interleukin 2 in patients undergoing surgery for colorectal cancer. Cancer Res 1992; 52: 5765-9.
39. Nichols PH, Ramsden CW, Ward U, Trejdosiewicz LK, Ambrose NS, Primrose JN. Peri-operative modulation of cellular immunity in patients with colorectal cancer. Clin Exp Immunol 1993; 94: 4-10.
40. Sedman PC, Ramsden CW, Brennan TG, Giles GR, Guillou PJ. Effects of low dose perioperative interferon on the surgically induced suppression of antitumour immune responses. Br J Surg 1988; 75: 976-81.
41. Romano F, Cesana G, Berselli M, et al. Biological, histological, and clinical impact of preoperative IL-2 administration in radically operable gastric cancer patients. J Surg Oncol 2004; 88: 240-7.
42. Elias D, Farace F, Triebel F, et al. Phase I-II randomized study on prehepatectomy recombinant interleukin-2 immunotherapy in patients with metastatic carcinoma of the colon and rectum. J Am Coll Surg 1995; 181: 303-10.
43. Lin CY, Bai DJ, Yuan HY, et al. Perioperative cimetidine administration promotes peripheral blood lymphocytes and tumor infiltrating lymphocytes in patients with gastrointestinal cancer: Results of a randomized controlled clinical trial. World J Gastroenterol 2004; 10: 136-42.
44. Enesel MB, Acalovschi I, Grosu V, et al. Perioperative application of the Viscum album extract Isorel in digestive tract cancer patients. Anticancer Res 2005; 25: 4583-90.
45. Mels AK, Statius Muller MG, van Leeuwen PA, et al. Immune-stimulating effects of low-dose perioperative recombinant granulocyte-macrophage colony-stimulating factor in patients operated on for primary colorectal carcinoma. Br J Surg 2001; 88: 539-44.
46. Krebs P, Barnes MJ, Lampe K, et al. NK-cell-mediated killing of target cells triggers robust antigen-specific T-cell-mediated and humoral responses. Blood 2009; 113: 6593-602.
47. Kirstein JM, Graham KC, Mackenzie LT, et al. Effect of anti-fibrinolytic therapy on experimental melanoma metastasis. Clin Exp Metastasis 2009; 26: 121-31.
48. Savory LJ, Stacker SA, Fleming SB, Niven BE, Mercer AA. Viral vascular endothelial growth factor plays a critical role in orf virus infection. J Virol 2000; 74: 10699-706.
49. Le Boeuf F, Diallo JS, McCart JA, et al. Synergistic interaction between oncolytic viruses augments tumor killing. Mol Ther; 18: 888-95.
50. Patel R, Belanger S, Tai LH, Troke AD, Makrigiannis AP. Effect of Ly49 haplotype variance on NK cell function and education. J Immunol; 185: 4783-92.

Running Title: Oncolytic virus inhibits surgery induced NK cell dysfunction

FIGURE LEGENDS

Figure 1. Surgical stress increases lung tumor metastases by impairing NK cells. Quantification of lung tumor metastases at 3d from **(a)** NK intact and NK depleted mice subjected to surgical stress, **(b)** NK-deficient mice subjected to surgery, **(c)** NK-deficient mice receiving adoptively transferred purified NK cells or non-NK cells from surgically stressed and control mice. Data are representative of three similar experiments with n=5-6/group (*, p =0.01;**, p =0.0109; n.s., not significant).

Figure 2. Defective *in vitro* killing of tumor cells by surgically stressed NK cells. The ability of purified $DX5^+$ NK cells from surgically stressed and untreated controls to kill tumor cells **(a)** YAC-1, **(b)** B16F10lacZ, **(c)** RMA-S, **(d)** EL-4 labelled with α-Thy1.2/ isotype control/no Ab. The data are displayed as the mean percent (+/- SD) of chromium release from triplicate wells for the indicated effector:target (E:T) ratios. Data are representative of three similar experiments.

Figure 3. Defective killing of tumor cells and enhanced virus susceptibility by surgically stressed NK cells *in vivo*. The ability of NK cells from surgically stressed and untreated controls to reject **(a)** $\beta 2m^{-/-}$ splenocytes, **(b)** MHC-I-deficient RMA-S tumor cells. **(a,b)** Data are pooled from 3 independent experiments (*, p <0.0001; **, p =0.003; ***, p =0.0008).

Figure 4. Surgically stressed NK cells display abnormal NK cell migration and markers. The mean percentage (a) or total number (b) of NK cells ($CD122^+$, $TCR\beta^-$) is shown from the spleen, blood or lung of surgically stressed and untreated mice. **(c)** $CFSE^+$ cells from peritoneal lavage, blood and lungs from surgically stressed and untreated mice are shown. **(d)** MFI of the indicated cell surface marker was performed on $CD122^+$, $TCR\beta^-$ gated splenocytes from surgically stressed and untreated mice. Data are representative of at least three similar

Running Title: Oncolytic virus inhibits surgery induced NK cell dysfunction

experiments where n=5-6/group (*, p =0.005; **, p =0.038 ***, p =0.0008; ^, p =0.00138; #, p =0.0092; ##, p =0.025; n.s., not significant).

Figure 5. Novel anti-cancer OV as perioperative therapy against immune suppressive effects of surgery. **(a,b)** Quantification of lung tumor metastases at 3d from the indicated treatment groups (*, p <0.001; **, p =0.0005). **(c,d)** Quantification of lung tumor metastases at 3d from NK intact and NK depleted mice subjected to surgery with and without OV (***, p =0.0001; #, p =0.0034). **(e,f)** *In vitro* killing by indicated treatment groups. **(g-j)** % gated IFNγ expression from NK cells isolated from the spleen of indicated treatment groups. **(g,i)** Each dot plot is taken from 1 representative mouse/group. **(h,j)** Bar graphs represent data from three similar experiments. N=5/group (+, p =0.04; ++, p =0.012; +++, p= 0.0007). **(k)** Rejection of $\beta 2m^{-/-}$ splenocytes by indicated treatment groups (^, p <0.0001). All data are representative of at least 3 similar experiments.

Figure 6. Defective *in vitro* killing and OV activation of human NK cells. The ability of human PBMC to kill K562 tumor cells **(a,b)** Perioperative blood collection program - preoperative, POD1, POD3, POD28(±14) **(c, d)** Neoadjuvant JX-594 clinical trial – healthy donor control, PreOV, PostOV D1, PostOV D3, PostOV D14. The data are displayed as the mean percent (+/- SD) of chromium release from triplicate wells for 100:1 (E:T) ratio.

Figure 1. Surgical stress increases lung tumor metastases by impairing NK cells

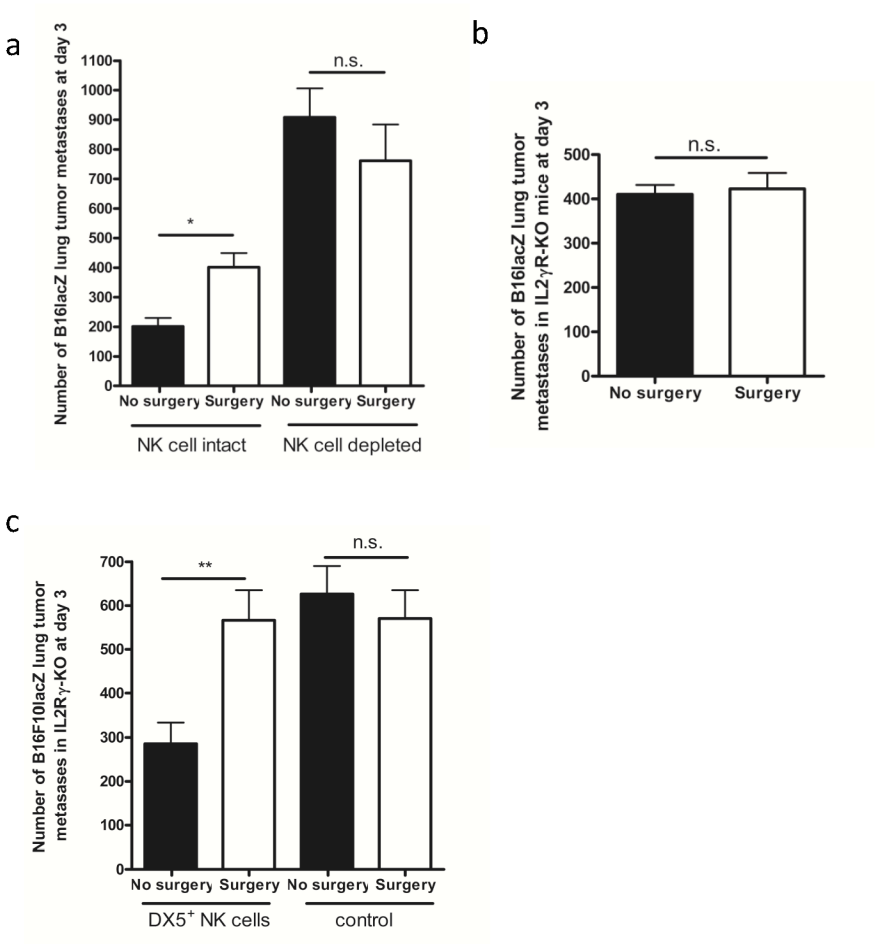

Figure 2. Defective killing of tumor cells by surgically stressed NK cells *in vitro*

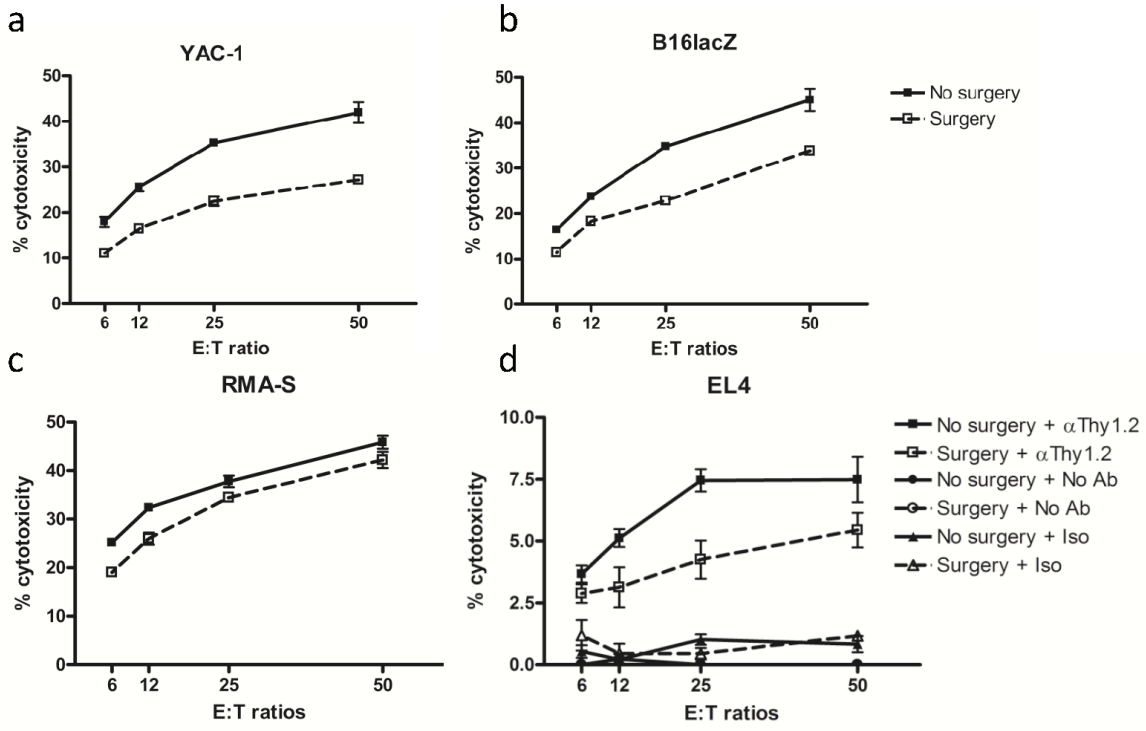

Figure 3. Defective killing of hematopoietic and tumor cells by surgically stressed NK cells *in vivo*

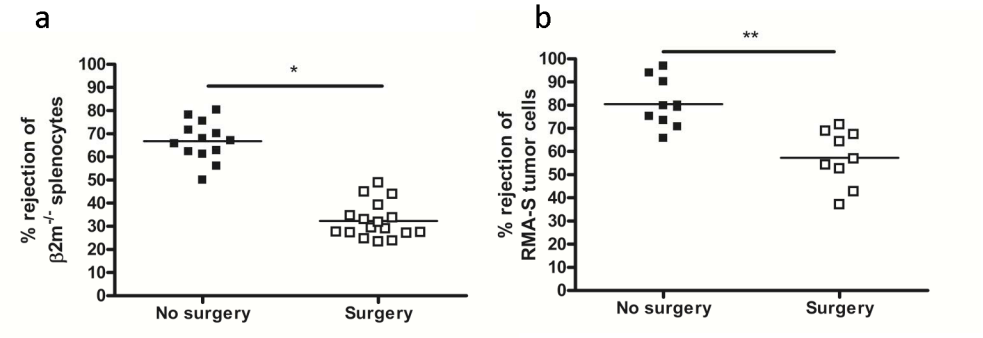

Figure 4. Surgically stressed NK cells display abnormal NK cell markers and migration

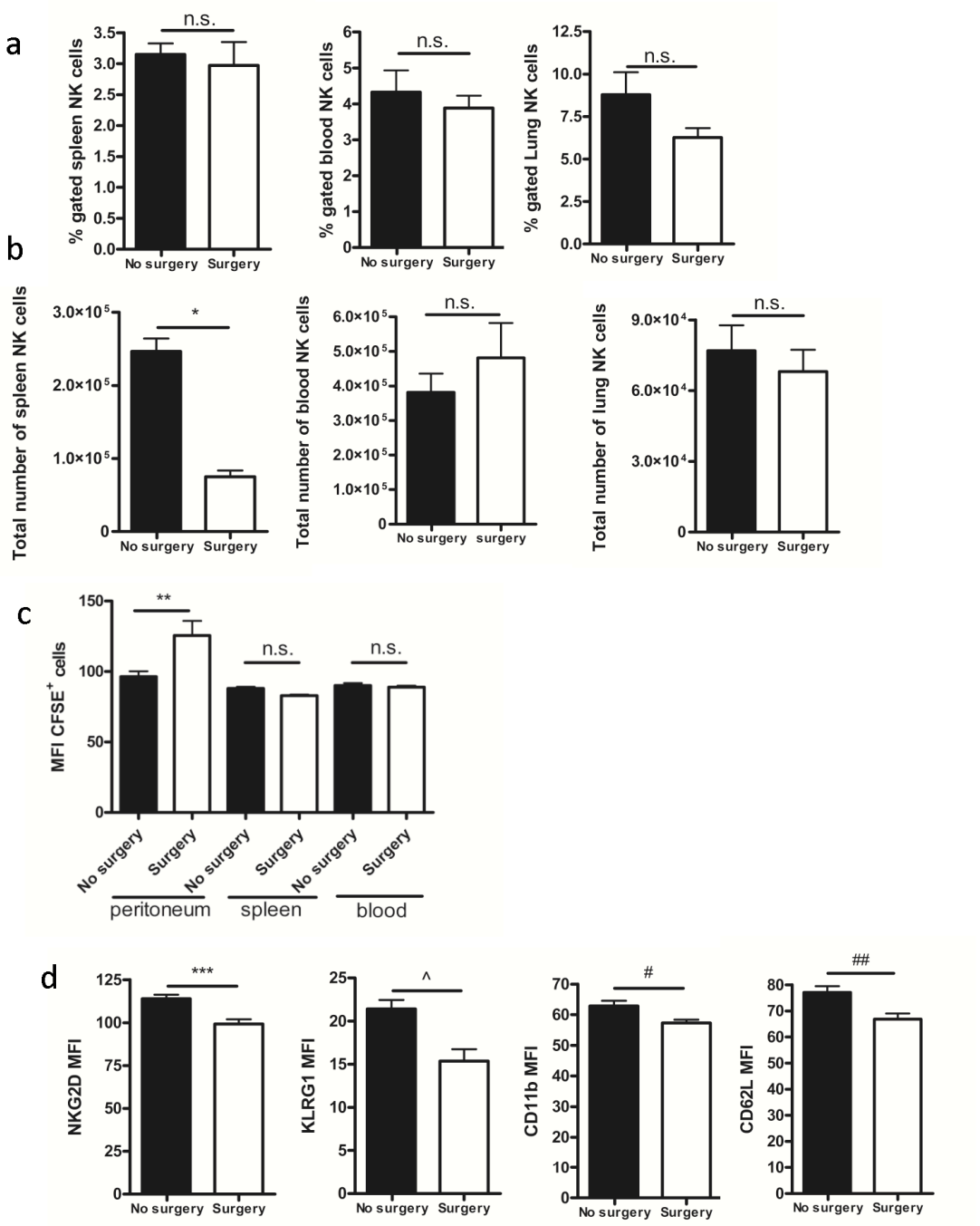

Figure 5. Novel anti-cancer oncolytic virus as perioperative therapy against immune suppressive effects of surgery

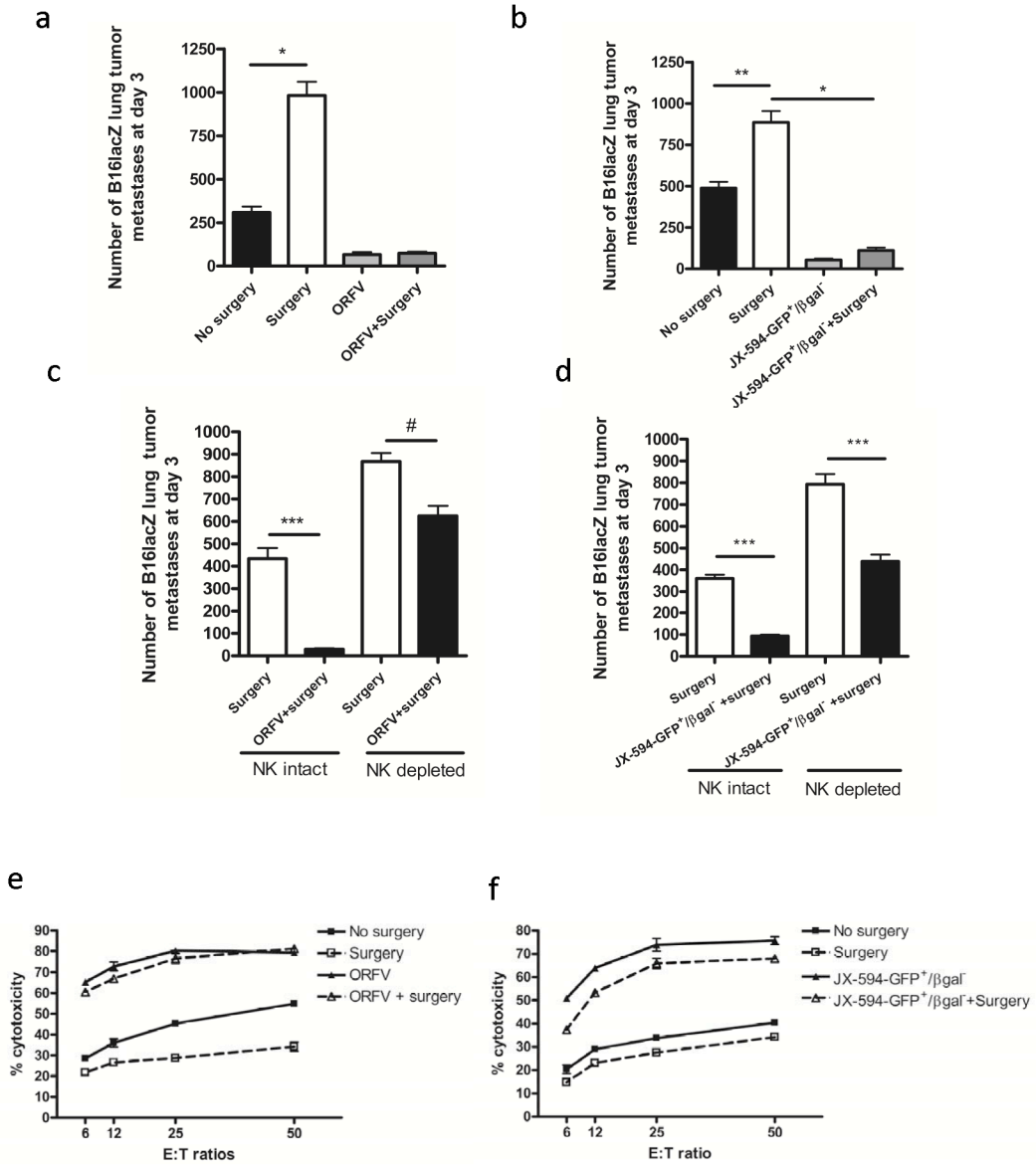

Figure 5. cont'd. Novel anti-cancer oncolytic virus as perioperative therapy against immune suppressive effects of surgery

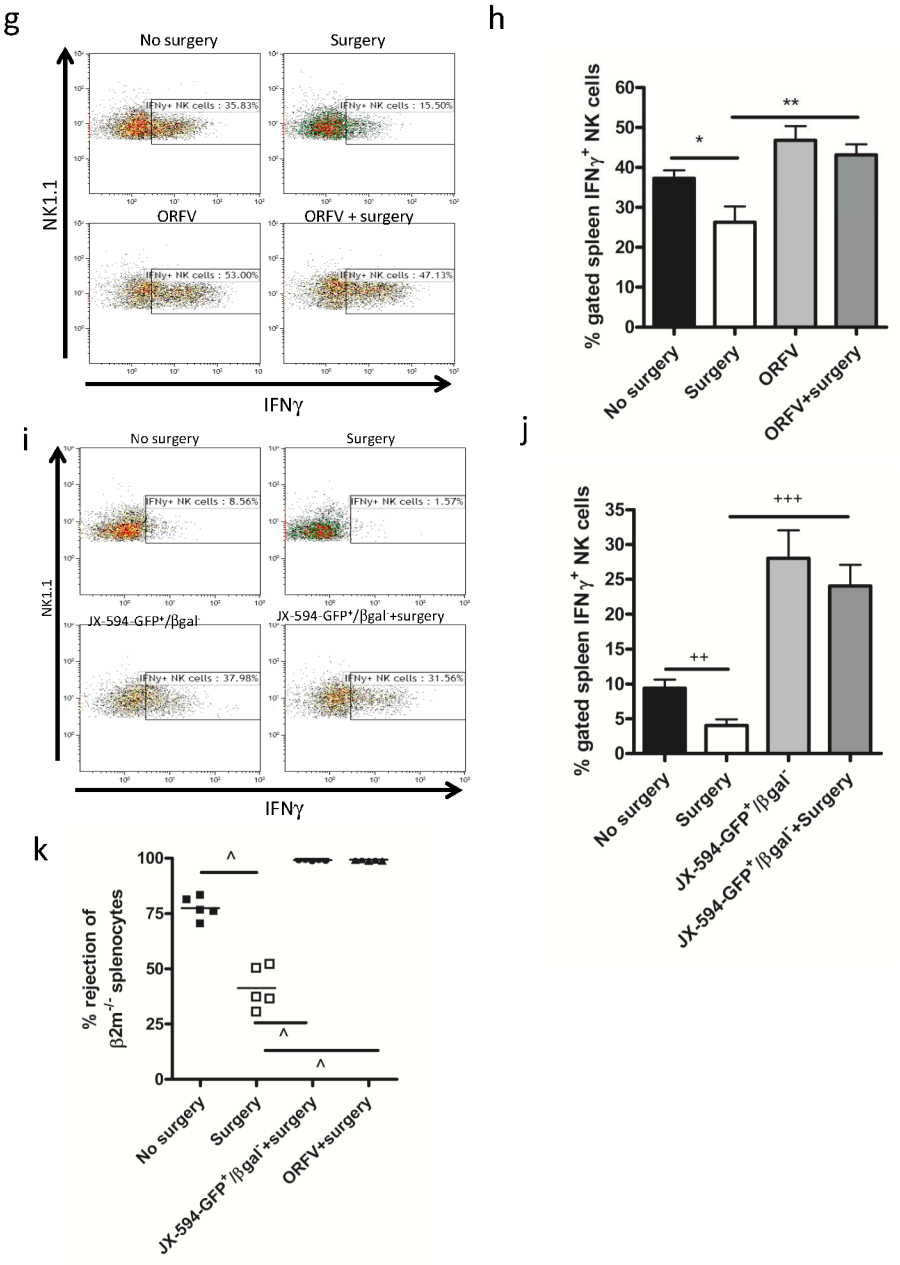

Figure 6. Defective human NK cell killing post-surgery and OV activation of human NK cells

a

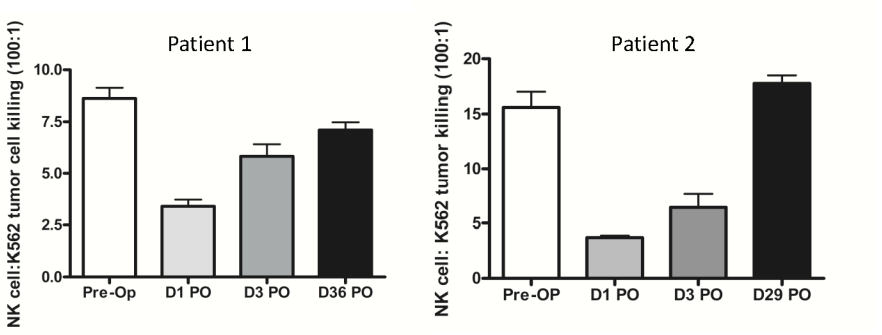

b

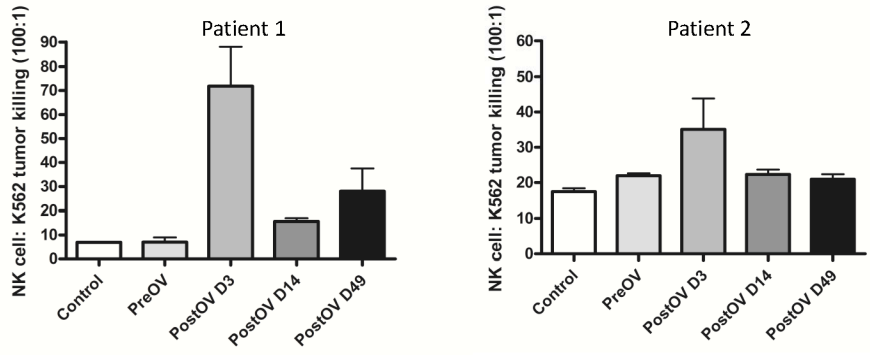

APPENDIX II: HARNESSING OV-MEDIATED ANTITUMOUR IMMUNITY IN AN INFECTED-CELL VACCINE

Chantal G Lemay, Julia L Rintoul, Agnieszka Kus, Jennifer M Paterson, Vanessa Garcia, Theresa J Falls, Lisa Ferreira, Byram W Bridle, David P Conrad, Kenneth Garson, Barbara C Vanderhyden, Vera A Tang, Jean-Simon Diallo, Rozanne Arulanandam, Fabrice Le Boeuf, David F Stojdl, Brian D Lichty, Harold L Atkins, Kelley A Parato, John C Bell* and Rebecca C Auer*

Contribution:

Assisted in the planning, and executing of the multi-colour flow cytometry experiments. In particular, all those experiments that involved intra-cellular staining. I also contributed intellectually in the development of this project. Finally, I contributed to the assembly of the manuscript, proofreading the manuscript, and assisting in the response to reviewers.

Accepted: *Molecular Therapy, March 2012*

Harnessing oncolytic virus-mediated anti-tumour immunity in an infected cell vaccine

Chantal G Lemay[1,2], Julia L Rintoul[1,2], Agnieszka Kus[1,2], Jennifer M Paterson[1,2], Vanessa Garcia[1,2], Theresa J Falls[2], Lisa Ferreira[2], Byram W Bridle[3], David P Conrad[1,2], Vera A Tang[2], Jean-Simon Diallo[1,2], Rozanne Arulanandam[1,2], Fabrice Le Boeuf[1,2], Kenneth Garson[2], Barbara C Vanderhyden[2], David F Stojdl[2], Brian D Lichty[4], Harold L Atkins[1,2], Kelley A Parato[2], John C Bell[1,2]* and Rebecca C Auer[1,2]*

[1]Department of Biochemistry, Microbiology and Immunology, University of Ottawa, [2]Ottawa Hospital Research Institute, Centre for Innovative Cancer Therapeutics, Ottawa, Ontario, Canada; [3]Department of Pathobiology, University of Guelph, Guelph, Ontario, Canada. [4]Department of Pathology and Molecular Medicine, Centre for Gene Therapeutics, McMaster University, Faculty of Health Sciences, Hamilton, Ontario, Canada.

** Contributed Equally*

Short title: OV-infected cell as a tumour vaccine

Corresponding author: John C. Bell

ABSTRACT

Treatment of permissive tumours with the oncolytic virus (OV) VSV-Δ51 leads to a robust anti-tumour T cell response, which contributes to efficacy; however, many tumours are not permissive to *in vivo* treatment with VSV-Δ51. In an attempt to channel the immune stimulatory properties of VSV-Δ51 and broaden the scope of tumours which can be treated by an OV, we have developed a potent oncolytic vaccine platform, consisting of tumour cells infected with VSV-Δ51. We demonstrate that prophylactic immunization with this infected cell vaccine (ICV) protected mice from subsequent tumour challenge, and expression of GM-CSF by the virus (VSVgm-ICV) increased efficacy. Immunization with VSVgm-ICV in the VSV-resistant B16-F10 model induced maturation of dendritic and natural killer (NK) cell populations. The challenge tumour is rapidly infiltrated by a large number of IFNγ-producing T and NK cells. Finally, we demonstrate that this approach is robust enough to control the growth of established tumours. This strategy is broadly applicable because of VSV's extremely broad tropism, allowing nearly all cell types to be infected at high MOIs *in vitro,* where the virus replication kinetics outpace the cellular IFN response. It is also personalized to the unique tumour antigen(s) displayed by the cancer cell.

INTRODUCTION

The current standard of care for cancer treatment is associated with severe off-target effects due to poor selectivity of the agent for cancer cells. New targeted therapeutics often target only one gene or pathway in a cell, allowing for resistance to easily evolve[1]. Likewise, cancer immunotherapies, though making great strides in recent years, are still focused on identifying one or very few tumour associated antigens that can be targeted. However, tumours can rapidly evolve immune evasion and immune suppression mechanisms countering these therapies, leading to treatment failure[2, 3]. As well, tumours are antigenically heterogeneous[4, 5] as a result of high genetic instability[6]. In theory, a vaccine presenting the spectrum of tumour antigens could allow for the *in vivo* selection of the optimum epitope(s) to target.

Oncolytic viruses have emerged as a promising anti-cancer treatment platform, able to specifically replicate in and kill cancer cells while leaving normal cells unharmed. Though engineered for tumour-specific lysis, the multi-modal nature of this platform is currently being revealed. Many of these viruses can be delivered systemically to reach distant tumour beds[7], be targeted to tumour vasculature to induce tumour vascular shutdown[8, 9], and be engineered to carry genetic payloads. Importantly, pre-clinical and clinical evidence for oncolytic virus-mediated anti-tumour immunity is emerging [10]. Recent results from a phase II clinical trial with OncoVex^{GM-CSF}, an oncolytic HSV expressing GM-CSF, have demonstrated that patients treated with this platform have a very different tumour immune landscape, demonstrating significantly lower regulatory T cells and higher $CD8^+$ effector T cells in the tumour [11].

Previous research by our lab has demonstrated that a Vesicular Stomatitis Virus harbouring a deletion in the M protein at position 51 (VSV-Δ51) is very sensitive to interferon [12] and neutralizing antibody[13], which act to clear virus from the host. Anti-tumour immune stimulation may be important for the ongoing tumour destruction once the virus is cleared, and offers the potential to restore immune surveillance mechanisms that can lead to complete responses and prevent recurrence. Wild Type VSV (VSVwt) has been observed to induce anti-tumour immune responses in models expressing exogenous antigens [14] and has now been demonstrated to be a potent boost in an elegant prime/boost oncolytic vaccination model[15, 16]. Strategies that allow us to exploit the anti-tumour immunity induced through virus replication and lysis will be vital to using the full potential of these viruses. Herein we describe an infected cell vaccine (ICV) platform that presents a multitude of tumour antigens in the context of a robust oncolytic virus infection. We demonstrate that this leads to potent immune stimulation and ultimately activates both natural killer (NK) cells and T cells for tumour debulking and long-term cancer surveillance. In addition, no prior knowledge on the tumour antigens is required to make this vaccine.

RESULTS

T cells are required for VSV-mediated long-term tumour regression

Many oncolytic virus platforms have been observed to induce anti-tumour immune responses[17-20]. We examined the role of the T cell compartment in oncolytic VSV-Δ51 treatment of cancer. A VSV-sensitive clone of colon carcinoma tumours (CT26.LacZ) was established in immunocompetent and athymic nude mice. When tumours were palpable, mice were treated with six intravenous (IV) doses of VSV-Δ51-GFP, UV-inactivated VSV, or PBS. In the immune competent mice, only those treated with VSV-Δ51-GFP had measurable responses, with 60 percent of the mice demonstrating complete tumour clearance (**Figure 1a,b**). The athymic nude mice initially respond to VSV treatment, demonstrating stable tumour sizes, but showed marginal long term efficacy, with only 1 out of 10 mice having a durable response (**Figure 1c,d**). This suggests that the T cell compartment is required for long-term tumour eradication following systemic VSV therapy in this model.

Subsequently, immune competent mice demonstrating long-term complete responses were used as splenocyte donors in an adoptive cell transfer. Naive immune competent mice that received splenocytes from VSV-treated and cured mice were not susceptible to CT26.LacZ tumour growth, but were susceptible to syngeneic 4T1 growth (**Figure 1e**). Splenocytes from naive mice and CT26.LacZ tumour-bearing, but untreated mice were not able to protect against subsequent tumour challenge. Therefore, a specific and long-lived anti-tumour immune response is generated through treatment with oncolytic VSV.

UV-inactivated VSV was not able to induce any efficacy in the CT26 subcutaneous model (**Figure 1a**). This leads us to reason that VSV replication in the tumour cells is required for immune stimulation. CT26.LacZ tumours are very sensitive to VSV and demonstrate robust infection by immunohistochemistry at 24hrs following IV administration (**Figure 1f**). Conversely, B16-F10 cells do not demonstrate any VSV replication in IV-treated tumours (**Figure 2a**) and B16-F10 tumour bearing mice have no response to VSV-treatment (**Figure 2b,c**), further demonstrating the importance of replication in efficacy. Previous research by *Breitbach et al*[8] demonstrates that after intravenous administration, UV inactivated VSV is undetectable in tumour sections using the methods described in the current manuscript. The viral proteins found in the tumor sections in figures 1 and 2 must result from productive virus replication and spread and not simply tumour specific accumulation of viral particles.

VSV infection is a potent immune stimulator in a prophylactic ICV

We have so far demonstrated that VSV replication in a permissive tumour can elicit a therapeutic anti-tumour T cell response. We postulated whether we could generate a sufficiently robust therapeutic response in VSV-resistant B16F10 cells by infecting them *ex vivo* and presenting this cocktail as an infected cell vaccine (ICV). This would bypass the necessity for *in vivo* replication to mount an anti-tumour immune response. Though B16-F10 cells are not readily permissive to VSV following IV delivery, we can achieve complete infection by infecting the cells *in vitro* at a high multiplicity of infection (MOI) (**Supplementary Figure S1a**).

As a means of determining the immunogenicity of such a vaccine, γ-irradiated tumour cells were infected and assessed for their ability to provide protection against a

future tumour challenge (**Figure 3a**). This VSV-infected cell vaccine (VSV-ICV) was administered intraperitoneally (IP) to mice on days 0 and 7, with a tumour challenge on day 14 (**Figure 3b**).

The immunization of mice with γ-irradiated B16-F10 cells infected with VSV-Δ51-GFP was able to completely protect 30% of mice tested (9 protected/29) from later live cell challenge (**Figure 3c**). Control groups immunized with PBS or γ-irradiated B16-F10 cells demonstrate complete susceptibility to the tumour challenge. These results were also verified in a different mouse strain with the parental CT26.wt cell line (**Supplementary Figure S2**). Like the B16-F10 cells, and unlike the clone CT26.LacZ, the parental CT26.wt cells are not permissive to *in vivo* VSV infection.

GM-CSF expression by VSV enhances immune activation by the VSV-ICV

Granulocyte-monocyte colony stimulating factor (GM-CSF) is a potent immunostimulating cytokine able to increase monocyte and macrophage migration and activation[21]. To increase the immune stimulation properties of our vaccine, GM-CSF was cloned into the VSV-Δ51 genome and expression was confirmed by western blot (data not shown). The infected cell vaccine made with VSV-Δ51-GMCSF (VSVgm-ICV) prevented B16-F10 tumour engraftment in over 95 percent of mice tested (21 protected/22) (**Figure 3c**). Due to the heightened efficacy of this approach, we chose the VSV-Δ51-GMCSF virus for further characterization. The VSV-Δ51-GMCSF virus was tested as a direct oncolytic alongside VSV-Δ51-GFP in the B16-F10 subcutaneous model and it demonstrated no increased efficacy (**Supplementary Figure S1b**).

Replication beyond the infected cells of the vaccine is not required for full ICV efficacy

We examined whether virus replication and spread or tumour cell integrity were important for ICV efficacy. UV-inactivated VSV lacks the ability to express any gene products and was unable to confer any protection (**Figure 3d**). G-Less VSV is a recombinant that lacks the gene encoding the glycoprotein, but is grown in cells expressing VSV G. This virus infects cells and expresses N, M, L, and P genes. It can package new virions, though these are not infectious[22]. This virus was able to protect the same proportion of mice as the VSV-ICV in this experiment (**Supplementary Figure S3**). These viruses are compared to VSV-Δ51-GFP because neither UV-inactivated nor G-Less virus expresses GM-CSF. To determine the importance of cellular integrity to the efficacy of the vaccine, vaccine preparations were attempted in two other methods. γ-irradiated B16-F10 cells were first freeze/thawed multiple times before being mixed with VSV-Δ51-GMCSF (irrB16 --> F/T + VSVgm). Compared to the regular VSVgm-ICV, this preparation was not able to protect any of the 6 mice treated. Alternatively, the VSVgm-ICV was made as per usual but freeze/thawed multiple times before injection (VSVgm-ICV --> F/T). This preparation protected only 4 out of 7 mice.

Taken together, these results indicate that in two VSV-resistant cancer models tumour cells infected with VSV-Δ51 can stimulate an anti-tumour immune response that is capable of protecting mice from a later tumour challenge. In addition, the expression of GM-CSF from infected cells greatly increased the immunization capabilities of the ICV in the B16-F10 model. Interestingly, it seems that cellular integrity is important in conferring immunological protection from this vaccine but virus need only have basal replication within the cells constituting the vaccine, as

demonstrated by the VSV_{GLess}-ICV. Whether it's simply transcription or genome replication that is required is not presently clear.

VSVgm-ICV induces rapid innate immune activation

We next examined the activation of early innate cells following VSVgm-ICV treatment. Splenocytes were harvested at 24hrs post treatment and dendritic cells (DCs) evaluated for markers of activation. Mice treated with either VSVgm alone or VSVgm-ICV had a higher proportion of activated DCs. This is demonstrated by a higher frequency of cells expressing MHC II and CD86, as well as higher expression levels of these activation markers (**Figure 4a-c**).

In addition, splenic lymphocytes were examined for early activation through CD69 expression early after treatment with the VSVgm-ICV. CD69 is a marker of early lymphocyte activation and is not found on naive lymphocyte populations [23, 24]. Lymphocytes from VSVgm-ICV-treated mice demonstrate dramatically higher degrees of early activation than control animals (**Figure 4d**). In keeping with this finding, at 24hrs post treatment, a higher frequency of blood NK cells from VSVgm or VSVgm-ICV-treated mice express IFNγ and more of the cytokine is expressed per cell (**Supplementary Figure S4a,b**). However, not surprisingly, NK cells are no longer expressing IFNγ in the blood on the day of tumour challenge (**Supplementary Figure S4c,d**).

VSVgm-ICV increases tumour infiltration by activated T and NK cells

To understand what cell types are responsible for tumour rejection in the B16-F10 model following VSVgm-ICV treatment, we implanted the challenge flank tumour in matrigel, thereby allowing us to easily resect and disaggregate the tumour (**Figure 5a**).

Mice were injected with Brefeldin A 6hrs before tumour harvest. This allows us to determine the expression profiles of tumour infiltrating cells while they are in the tumour environment. We determined that T cells are 10 times more numerous in the tumour following vaccination with the VSVgm-ICV than with irradiated cells alone or VSVgm (**Figure 5c**). This difference is even larger when compared to the PBS treated mice, with 30 times more T cells in the treated tumour. Indeed, over 8% of the tumour cellular content is T cells, equal to a ratio of one T cell for every 12.5 tumour cells (**Supplementary Figure S5a**). Importantly, there is also a much greater number of $CD3^+$ $IFN\gamma^+$ cells in the tumour following VSVgm-ICV than in any control group (**Figure 5b,d and Supplementary Figure S5b**).

In addition to a significant increase in T cells in the challenge tumour, VSVgm-ICV-immunized mice have 4- to 13-fold more NK cells (**Figure 5e**). Importantly, there are more NK cells producing either IFNγ or Granzyme B (**Figure 5g**), and there are more NK cells expressing both IFNγ and Granzyme B (**Figure 5f**).

A VSVgm-ICV reduces tumour burden in the therapeutic setting

Having demonstrated that a VSVgm-ICV can protect mice from a tumour challenge, we sought to examine the vaccine's potency in more relevant therapeutic models, through the treatment of mice that have already been inoculated with tumours. C57BL/6 mice bearing B16-F10 subcutaneous tumours were treated IP with VSVgm-ICV, irrB16, VSVgm, or PBS control (**Figure 6a**). Animals treated with the VSVgm-ICV have a dramatic delay in tumour growth (**Figure 6b**). In contrast, treatment with oncolytic VSV-Δ51-GMCSF has similar tumour growth to PBS-treated animals.

Treatment with γ-irradiated B16-F10 cells leads to marginally delayed tumour growth compared to the other control groups, though this is not statistically significant.

A systemic dissemination model was also undertaken to examine the effectiveness of this vaccine. Mice were given B16-F10 cells intravenously, leading to tumour seeding mostly in the lung, though macroscopic tumours can also occur in the thymus, kidneys, and ovaries. Treatments were initiated the following day and all mice were euthanized on day 22 to examine tumour burden (**Figure 6c**). Treatment with VSVgm-ICV demonstrated undetectable tumour burden at the time of sacrifice in 80 percent of mice and no other tumours were found in any of the animals (**Figure 6e,d**). In contrast, control-treated mice demonstrate heavy tumour burden, with one PBS-treated mouse found dead before scheduled euthanizing, in addition to 3 other PBS-treated mice, 1 VSVgm-treated mouse, and 1 irrB16-treated mouse having large growths in locations other than the lung. Lung weights demonstrate that the VSVgm-ICV-treated mice have a much lower tumour burden than controls, identical to non-tumour bearing mouse lungs. As a more stringent test of the VSVgm-ICV's therapeutic potential, treatments were started on days 3 or 4 after tumour seeding. In both cases 2 of 4 VSVgm-ICV treated mice had no visible lung tumours at the time of sacrifice, whereas all irrB16-treated mice had significant tumour burden (**Supplementary Figure S6**). Treatments beginning later than day 4 were not attempted and so it remains to be seen if efficacy can be achieved while delaying treatments further.

A spontaneous model of ovarian cancer also demonstrated therapeutic benefit from the VSVgm-ICV (**Supplementary Figure S7**). These transgenic mice develop spontaneous bilateral ovarian tumours driven by the SV40 Tag. The vaccine was made

with the 6048R cell line that had been previously established from one such tumour. Though normal ovary weights were not quantified, one VSVgm-ICV-treated mouse had normal appearing ovaries and these weighed 0.05g in total.

These results highlight the potency of this vaccine platform; able to initiate anti-tumour immune responses that can single-handedly slow the progression of highly aggressive and VSV-resistant tumours.

DISCUSSION

Several recent studies have reported the very important role the immune system plays in tumour clearance. Indeed the quantity and quality of $CD8^+$ T cells found in the tumour is one of the strongest favourable prognostic markers in many cancer types[25]. Not surprisingly, cancers evolve multiple mechanisms of immune evasion and suppression[26].

Oncolytic viruses are emerging as promising clinical candidates that target tumours at multiple fronts. Importantly, many have been observed to stimulate anti-tumour immune responses when replicating in susceptible tumours[10]. However, not all tumours are permissive to these viruses. We sought to optimize and test an OV vaccine that could be used with all tumour types, regardless of *in vivo* permissivity; harnessing the anti-tumour immune response generated when an immunogenic virus replicates in tumour cells.

We observed that the efficacy obtained with VSV-Δ51 in the permissive CT26.LacZ colon cancer model is largely dependent on an intact T cell compartment and that mice cured with this OV treatment generate a robust anti-tumour immune response (**Figure 1**). However, this efficacy does not translate to tumour models that are resistant to the viral doses achieved in systemic delivery of VSV (**Figure 2**). We propose that the deficit in efficacy due to the lack of *in vivo* replication could be overcome by infecting γ-irradiated tumour cells *in vitro,* and then injecting this ICV into the mouse. Indeed an ICV using VSV-Δ51-GFP was able to protect 30% of mice from future B16-F10 tumour challenge in a prophylactic setting (**Figure 3c**). Interestingly,

cloning the cytokine GM-CSF into the viral genome greatly increased the potency of the ICV. The VSVgm-ICV protects 95% of mice from future tumour challenge. GM-CSF enhances the recruitement and activation of antigen presenting cells[21]. However, further studies are required to fully elucidate the role of GM-CSF in this vaccine.

Though UV-inactivated VSV does not lead to sufficient immune stimulation, a G-Less VSV was able to recapitulate the tumour protection achieved with fully replication competent virus (**Figure 3d**). Therefore a basal level of viral transcription/replication is required, though it need not replicate beyond the initially infected cells that constitute the vaccine. We also observed a requirement for cellular integrity, thus, it is reasonable to hypothesize that this vaccine does not simply present viral danger signals in the context of tumour antigens. Instead, we speculate that viral infection of cells initiates critical immunogenic processes that, coupled with tumour-associated antigens, lead to robust immune activation. In addition, viral infection of an intact cell is quite immunogically relevant, offering persistent toll-like receptor ligation required for a robust immune response[27].

Treatment with the VSVgm-ICV leads to rapid innate immune activation seen in the spleen and blood (**Figure 4, and Supplementary Figure S4**). In many cases, VSVgm leads to the same level of early immune activation as does the vaccine. VSV injected IP will productively infect the first cells it encounters; therefore initiating similar immune activation due to viral infection. However, no anti-tumour immune responses were detected at late timepoints with VSVgm alone (**Figure 5 and 6**) and importantly no auto-immune sequelae have ever been observed with VSVgm treatment, whether IP or IV (data not shown).

Though the VSVgm-ICV is demonstrated to activate NK cells 24hrs after prophylactic vaccination, they do not likely play a role in challenge tumour rejection as tumour implantation occurs after NK cells have returned to baseline (**Supplementary Figure S4**). Importantly, NK cell activation following VSVgm-ICV should have a significant role in a therapeutic setting, through the early debulking of the existing tumour and through the induction of inflammation at the tumour site. Though seemingly related to the vaccination, we believe that the NK cell infiltration and activation observed in the challenge tumour following VSVgm-ICV is in fact a consequence of activated T cell infiltration (**Figure 5**). Previous research indicates that T cells can activate NK cells in this manner[28]. NK cells have been demonstrated to be important mediators of early tumour debulking and in cytokine secretion, which further amplifies Th1 responses[29-31]. Certainly, the large quantity and activated nature of the T cells observed infiltrating the B16-F10 challenge tumour only 3 days after implantation indicates that the VSVgm-ICV initiates an effective Th1 T cell response.

The activity of this vaccine is highlighted by its impact in therapeutic models of cancer (**Figure 6 and Supplementary Figures S6 and S7**). Importantly, therapy could be delayed to 4 days after systemic dissemination, while still providing a therapeutic benefit. In some cases, the vaccine is delivered in a completely separate anatomical compartment and yet leads to significant tumour clearance. Further studies will focus on better understanding the critical immunological components that lead to this efficacy.

The concept of using virally infected cells as a cancer vaccine has been previously investigated in both mouse models and human patients [32-35] with some success, though few have investigated the immunological basis for this efficacy. Clinical trials using NDV-infected autologous and allogeneic melanoma cells demonstrated impressive 10 and 15-year survival data[36, 37]. However, many of these approaches used inactivated virus, replication-defective, or non-lytic strains. Of note, Livingston *et al* used VSVwt to infect melanoma cell lines to create a vaccine, though observed very limited responses. However, in this case the infected cells were swelled, homogenized, enucleated, and the virus UV-inactivated before treatment[38]. The results we have presented in this manuscript suggest that intact cells and replication competent lytic virus is much more immunogenic. We used an oncolytic strain of VSV so as to minimize toxicity, while allowing us to keep actively, yet locally, replicating virus as part of the vaccine. In addition, in virus-permissive tumour models, there might be an added benefit of tumour debulking and local inflammation in the tumour microenvironment provided by the oncolytic virus.

Though others have also achieved therapeutic efficacy in the B16-F10 tumour model, the VSVgm-ICV achieves this while requiring no previous knowledge about the relevant tumour antigens[15] or the immunosuppressive mechanisms employed by the tumour. Importantly, the ICV is relatively simple to prepare, requiring no long-term *ex vivo* manipulations[39, 40].

The infected cell vaccine platform would be best coupled to a debulking treatment that might also stimulate the immune system. Local tumour irradiation may help with

tumour debulking and has been demonstrated to increase inflammation in the tumour environment[41], leading to enhanced immunotherapeutic responses[42, 43]. An ideal scenario might include first surgically removing the tumour, using this tumour bulk to create the VSV-ICV, and then treating the patient to reduce metastatic recurrence.

The infected cell vaccine is a promising immunotherapeutic platform that achieves the stimulation of both innate and adaptive immune cells. The potency of the ICV is highlighted by the significant impact it has on the progression of an aggressive and immunosuppressive tumour. In addition, the use of autologous tumour leads to a personalized vaccine that can potentially present the full range of a patient's unique tumour antigens. Recently , Castle et al[44] have shown that the B16-F10 tumour cell line has acquired over 500 somatic mutations that could, in principle, encode numerous novel immunogenic epitopes. Despite this, γ-irradiated B16-F10 cells, on their own, are ineffective in stimulating anti-tumour immunity, probably due to the lack of danger signals. Here we show that infection of B16-F10 cells makes them a very potent vaccine platform that has the capacity to induce both a protective and therapeutic immune response. Since the B16-F10 cell line expresses a vast array of potential neo-antigens, perhaps many of these could now be made visible to the immune system when presented as an ICV. It is possible that because of this, the ICV has the potential to induce a broadly active T cell response against a spectrum of neo-antigens. Currently we have no data to support this notion, however studies are underway to determine the number and nature of mutant epitopes that the cellular immune system recognizes in B16-F10 cells following infected cell vaccination. It remains possible that our ICV approach simply focuses a robust response on a single or limited number of tumour antigens.

MATERIALS & METHODS

Cell lines and mice. CT26.WT and CT26.LacZ (also known as CT26.CL25) colon carcinoma, 4T1 breast cancer, and B16-F10 melanoma cells were purchased from the American Type Culture Collection and the B16-F10.LacZ were a gift from Dr. Ann F Chambers. All were cultured in HyQ Dulbecco's modified Eagle medium (High glucose) (HyClone) supplemented with 10% fetal calf serum (CanSera, Etobicoke, Canada). 6048R cells (gift from Dr. Vanderhyden) were grown in αMEM with 10% FBS, 2.08 ug/mL EGF (R&D systems, Minneapolis, MN), 1x of ITSS (Roche, Montreal, CA), Gentamicin, and Penicillin/Streptomycin (Invitrogen, Burlington, CA).

Female 6-week old Balb/C, C57BL/6, and CD1 Nude mice were purchased from Charles River Laboratories (Wilmington, MA). Female 8-week old FVB/N MISIIRTAg transgenic mice (line tg4568- a gift from Dr. Vanderhyden) were generated using the transgene described by Connolly *et al*[45]. These mice develop bilateral ovarian tumours of epithelial origin with full penetrance and typically endpoint at 14 weeks of age. All experiments were conducted with the approval of the University of Ottawa Animal Care and Veterinary Service. Tumour area is calculated by multiplying the width by the length of the tumour.

Virus. VSV-Δ51-GFP and VSV-Δ51-GMCSF were grown in Vero cells and purified by centrifugation or sucrose gradient banding and centrifugation. VSV-GLess was grown on 293G cells. Virus stocks were aliquoted in PBS, kept at -80˚C, used once, and then discarded. VSV-Δ51-GMCSF was cloned using PCR primers to murine GMCSF and amplified off the pcDNA4.1-GMCSF vector. GM-CSF was cloned into the VSV-Δ51 vector at the XhoI and NheI sites between the G and L genes.

Direct treatment model and immunohistochemistry. Subcutaneous tumours were established by injecting $3x10^5$ CT26.LacZ or B16-F10 cells in PBS on the hind flank of the mouse. Tumours were allowed to grow until palpable, 6 treatments were then administered intravenously for two weeks, every Monday, Wednesday, and Friday, unless otherwise stated. VSV-Δ51 was used at $5x10^8$ pfu/100μL. To analyze VSV replication in CT26.LacZ and B16-F10 tumours following intravenous delivery, Balb/c or C57BL/6 mice were implanted with tumours subcutaneously and tumours were allowed to grow until reaching a sufficient size to dissect. Mice were then injected IV with $5x10^8$ pfu/100uL. 48 hours after injection, mice were euthanized, tumours were excised, and frozen in Shandon Cryomatrix freezing medium (TermoElectron, Waltham, MA) in liquid nitrogen. 5μm sections were stained by immunohistochemistry with rabbit anti-serum raised against VSV (gift of Dr. Earl Brown) at a 1/5000 dilution for 30min. Secondary antibody and ABC reagents were used as directed from the Vectastain ABC kit and Horseradish peroxidase activity was assessed using a Diaminobenzene-HRP kit (KPL Biosciences, Guelph, Canada). Nuclei were counterstained with hematoxylin. Images were obtained using an Epson Perfection 2450 Photo Scanner.

Re-challenge and splenocyte transfer. Mice were treated as in the direct oncolysis model with 6 doses of VSV at $5x10^8$ pfu/100uL intravenously once tumours were palpable. Mice that had complete responses were kept for at least 3 months to ensure long term responses. Splenocytes were harvested and purified by Lympholyte-M gradient from mice that were naive, had a tumour but received no treatment, or cured by VSV treatment. $5x10^7$ of these

isolated splenocytes were transferred to naive mice intravenously, and these mice were then challenged 48 hours later with $3x10^5$ CT26.LacZ cells on the right hind flank or 4T1 cells on the left flank. Tumour outgrowth was monitored.

Infected cell vaccine. Tumour cells were harvested from tissue culture and aliquoted in eppendorf tubes at $2x10^7$ cells / 200uL in PBS. These were γ-irradiated for 30Gy (CT26.wt), 45Gy (6048R), or 60Gy (B16-F10) in a Pantak HF320 X-Ray machine. Virus or PBS was added to the tubes at $2x10^8$ pfu in 200uL of PBS and incubated at 37˚C for 2 hours. The mixture was then injected in mice, 100uL intraperitoneally; therefore giving each mouse $5x10^6$ γ-irradiated cells and $5x10^7$ pfu of virus per dose. For Figure 3f, the "irrB16 → F/T + VSVgm" sample was γ-irradiated, then subjected to 3 freeze/thaw cycles in a dry ice bath and 42˚C water bath. Cells were then mixed with VSVgm before injection into the animal. Conversely, for the "VSVgm-ICV → F/T" sample, the ICV was made as usual and following the 2 hour infection the mixture was subjected to 3 freeze/thaw cycles before injection as detailed above. In the prophylactic model, mice were immunized on days -14 and -7, and then challenged with $1x10^5$ live tumour cells subcutaneously on day 0. For the therapeutic model, mice were given $1x10^5$ B16-F10 cells subcutaneously on day 0 or $7x10^4$ B16-F10 cells intravenously, and then vaccinated on days 1, 8, and 20 intraperitoneally. For the 3 and 4 day B16-F10 IV model, mice were treated on days 3, 10, and 22 or 4, 11, and 23, and then euthanized on day 28 to determine lung tumour burden.

In subcutaneous models, tumour measurements were determined with callipers until end point was reached. In intravenous model, endpoint was reached when mouse demonstrated severe respiratory distress, had a mass larger than 15mm, or pre-determined experimental

endpoint was reached. Lungs were removed and fixed in 10% formalin for at least 3 days. These were then blotted dry and weighed. Lungs were then paraffin embedded and slices were analyzed by hematoxylin and eosin staining. Pictures were taken on the Aperio ScanScope (Axiovision Technologies, Toronto, Ontario, Canada) and analyzed using Aperio ImageScope software.

Flow Cytometry. Spleens and blood were harvested from mice at indicated timepoints, red blood cells were lysed using ACK lysis buffer, and resuspended in RPMI+10% FBS. For examination of DC maturation, cells were stained with cell surface antibodies for CD11c-PE-Cy7 (clone N418, eBioscience), CD86/B7-1 (clone GL1, eBioscience), and MHC class II-FITC (clone M5/114.15.2, eBioscience). For early lymphocyte activation, splenocytes were stained with CD3-PerCP (clone 17A2, R&D systems), DX5-PE (BD Bioscience), and CD69-FITC (clone H1.2F3, BD Biosciences). All flow cytometry was performed on a Beckman Coulter CyAn and data analyzed with Kaluza v1.1 software. For the examination of NK cell activation splenocytes were re-stimulated for 1.5 hours with PMA and Ionomycin, during the last hour GolgiPlug (BD Biosciences) was added. These cells were then stained with CD3-PerCP (clone 17A2, R&D systems), DX5-PE, Granzyme-B-PE-Cy7 (clone 16G6, eBioscience), and IFNγ-FITC (clone XMG1.2, eBiosciences) and examined by flow cytometry.

Examination of cellular infiltrate of matrigel challenge tumour. Following the regular prophylactic immunization schedule mice were challenged with $3x10^5$ B16-F10 cells resuspended in 300uL of matrigel (BD Biosciences). 6 hours before euthanasia, mice were treated IV with 0.25mg Brefeldin A (Sigma) as previously published[46]. Mice were

euthanized and matrigel plugs were excised from the flank and disaggregated using a cocktail of collagenase type IV (Cooper Biomedical), Dispase, and DNase I (Invitrogen) resuspended in HBSS. This mixture was then washed and stained with surface antibodies: anti-CD3-PE (clone 17A2, BD Biosciences) or anti-NK1.1-PE (clone PK136, BD Biosciences). Cells were then permeabilized and fixed (BD Cytofix/Cytoperm, BD Biosciences) and stained with intracellular antibodies: IFNγ-FITC (clone XMG1.2, eBiosciences) and Granzyme B-PE-Cy7 (16G6, eBioscience).

Statistical Analysis. All statistical analyses were determined using GraphPad Prism 5.0 software. Where applicable, data are presented as mean + SEM and significance of variance was determined by T-test with Welch's correction, unless otherwise stated.

ACKNOWLEDGEMENTS

CGL and JLR are supported by CIHR Doctoral awards: Frederick Banting and Charles Best Canada Graduate Scholarship. JCB is supported by the Terry Fox Foundation, the Ontario Institute for Cancer Research, the Ottawa Regional Cancer Foundation, the Ottawa Hospital Foundation, and the Canadian Institute for Health Research. The authors disclose no conflicts of interest with regards to this research.

REFERENCES

1. Jones S, Zhang X, Parsons DW, Lin JC, Leary RJ, Angenendt P *et al.* Core signaling pathways in human pancreatic cancers revealed by global genomic analyses. *Science* 2008; **321**(5897)**:** 1801-6.

2. Alpizar YA, Chain B, Collins MK, Greenwood J, Katz D, Stauss HJ *et al.* Ten years of progress in vaccination against cancer: the need to counteract cancer evasion by dual targeting in future therapies. *Cancer immunology, immunotherapy : CII* 2011; **60**(8)**:** 1127-35.

3. Singer K, Gottfried E, Kreutz M, Mackensen A. Suppression of T-cell responses by tumor metabolites. *Cancer immunology, immunotherapy : CII* 2011; **60**(3)**:** 425-31.

4. Hand PH, Nuti M, Colcher D, Schlom J. Definition of antigenic heterogeneity and modulation among human mammary carcinoma cell populations using monoclonal antibodies to tumor-associated antigens. *Cancer research* 1983; **43**(2)**:** 728-35.

5. Gerlinger M, Rowan AJ, Horswell S, Larkin J, Endesfelder D, Gronroos E *et al.* Intratumor heterogeneity and branched evolution revealed by multiregion sequencing. *The New England journal of medicine* 2012; **366**(10)**:** 883-92.

6. Braun S, Hepp F, Sommer HL, Pantel K. Tumor-antigen heterogeneity of disseminated breast cancer cells: implications for immunotherapy of minimal residual disease. *International journal of cancer. Journal international du cancer* 1999; **84**(1)**:** 1-5.

7. Breitbach CJ, Burke J, Jonker D, Stephenson J, Haas AR, Chow LQ *et al.* Intravenous delivery of a multi-mechanistic cancer-targeted oncolytic poxvirus in humans. *Nature* 2011; **477**(7362)**:** 99-102.

8. Breitbach CJ, Paterson JM, Lemay CG, Falls TJ, McGuire A, Parato KA *et al.* Targeted inflammation during oncolytic virus therapy severely compromises tumor blood flow. *Molecular therapy : the journal of the American Society of Gene Therapy* 2007; **15**(9)**:** 1686-93.

9. Liu TC, Hwang T, Park BH, Bell J, Kirn DH. The targeted oncolytic poxvirus JX-594 demonstrates antitumoral, antivascular, and anti-HBV activities in patients with hepatocellular carcinoma. *Molecular therapy : the journal of the American Society of Gene Therapy* 2008; **16**(9)**:** 1637-42.

10. Melcher A, Parato K, Rooney CM, Bell JC. Thunder and lightning: immunotherapy and oncolytic viruses collide. *Molecular therapy : the journal of the American Society of Gene Therapy* 2011; **19**(6)**:** 1008-16.

11. Kaufman HL, Kim DW, DeRaffele G, Mitcham J, Coffin RS, Kim-Schulze S. Local and distant immunity induced by intralesional vaccination with an oncolytic herpes virus encoding GM-CSF in patients with stage IIIc and IV melanoma. *Annals of surgical oncology* 2010; **17**(3)**:** 718-30.

12. Stojdl DF, Lichty BD, tenOever BR, Paterson JM, Power AT, Knowles S *et al.* VSV strains with defects in their ability to shutdown innate immunity are potent systemic anti-cancer agents. *Cancer cell* 2003; **4**(4)**:** 263-75.

13. Power AT, Wang J, Falls TJ, Paterson JM, Parato KA, Lichty BD *et al.* Carrier cell-based delivery of an oncolytic virus circumvents antiviral immunity. *Molecular therapy : the journal of the American Society of Gene Therapy* 2007; **15**(1)**:** 123-30.

14. Diaz RM, Galivo F, Kottke T, Wongthida P, Qiao J, Thompson J *et al.* Oncolytic immunovirotherapy for melanoma using vesicular stomatitis virus. *Cancer research* 2007; **67**(6)**:** 2840-8.

15. Bridle BW, Stephenson KB, Boudreau JE, Koshy S, Kazdhan N, Pullenayegum E *et al.* Potentiating cancer immunotherapy using an oncolytic virus. *Molecular therapy : the journal of the American Society of Gene Therapy* 2010; **18**(8)**:** 1430-9.

16. Bridle BW, Boudreau JE, Lichty BD, Brunelliere J, Stephenson K, Koshy S *et al.* Vesicular stomatitis virus as a novel cancer vaccine vector to prime antitumor immunity amenable to rapid boosting with adenovirus. *Molecular therapy : the journal of the American Society of Gene Therapy* 2009; **17**(10)**:** 1814-21.

17. Prestwich RJ, Errington F, Ilett EJ, Morgan RS, Scott KJ, Kottke T *et al.* Tumor infection by oncolytic reovirus primes adaptive antitumor immunity. *Clinical cancer research : an official journal of the American Association for Cancer Research* 2008; **14**(22)**:** 7358-66.

18. Gauvrit A, Brandler S, Sapede-Peroz C, Boisgerault N, Tangy F, Gregoire M. Measles virus induces oncolysis of mesothelioma cells and allows dendritic cells to cross-prime tumor-specific CD8 response. *Cancer research* 2008; **68**(12)**:** 4882-92.

19. Gujar SA, Marcato P, Pan D, Lee PW. Reovirus virotherapy overrides tumor antigen presentation evasion and promotes protective antitumor immunity. *Molecular cancer therapeutics* 2010; **9**(11)**:** 2924-33.

20. Sobol PT, Boudreau JE, Stephenson K, Wan Y, Lichty BD, Mossman KL. Adaptive antiviral immunity is a determinant of the therapeutic success of oncolytic

virotherapy. *Molecular therapy : the journal of the American Society of Gene Therapy* 2011; **19**(2)**:** 335-44.

21. Sivendran S, Glodny B, Pan M, Merad M, Saenger Y. Melanoma immunotherapy. *The Mount Sinai journal of medicine, New York* 2010; **77**(6)**:** 620-42.

22. Roberts A, Buonocore L, Price R, Forman J, Rose JK. Attenuated vesicular stomatitis viruses as vaccine vectors. *Journal of virology* 1999; **73**(5)**:** 3723-32.

23. Lindsey WB, Lowdell MW, Marti GE, Abbasi F, Zenger V, King KM *et al.* CD69 expression as an index of T-cell function: assay standardization, validation and use in monitoring immune recovery. *Cytotherapy* 2007; **9**(2)**:** 123-32.

24. Pitsios C, Dimitrakopoulou A, Tsalimalma K, Kordossis T, Choremi-Papadopoulou H. Expression of CD69 on T-cell subsets in HIV-1 disease. *Scandinavian journal of clinical and laboratory investigation* 2008; **68**(3)**:** 233-41.

25. Galon J, Costes A, Sanchez-Cabo F, Kirilovsky A, Mlecnik B, Lagorce-Pages C *et al.* Type, density, and location of immune cells within human colorectal tumors predict clinical outcome. *Science* 2006; **313**(5795)**:** 1960-4.

26. Stewart TJ, Abrams SI. How tumours escape mass destruction. *Oncogene* 2008; **27**(45)**:** 5894-903.

27. Yang Y, Huang CT, Huang X, Pardoll DM. Persistent Toll-like receptor signals are required for reversal of regulatory T cell-mediated CD8 tolerance. *Nature immunology* 2004; **5**(5)**:** 508-15.

28. Fehniger TA, Cooper MA, Nuovo GJ, Cella M, Facchetti F, Colonna M *et al.* CD56bright natural killer cells are present in human lymph nodes and are activated by T cell-derived IL-2: a potential new link between adaptive and innate immunity. *Blood* 2003; **101**(8)**:** 3052-7.

29. Vivier E, Raulet DH, Moretta A, Caligiuri MA, Zitvogel L, Lanier LL *et al.* Innate or adaptive immunity? The example of natural killer cells. *Science* 2011; **331**(6013)**:** 44-9.

30. Smyth MJ, Hayakawa Y, Takeda K, Yagita H. New aspects of natural-killer-cell surveillance and therapy of cancer. *Nature reviews. Cancer* 2002; **2**(11)**:** 850-61.

31. Martin-Fontecha A, Thomsen LL, Brett S, Gerard C, Lipp M, Lanzavecchia A *et al.* Induced recruitment of NK cells to lymph nodes provides IFN-gamma for T(H)1 priming. *Nature immunology* 2004; **5**(12)**:** 1260-5.

32. Heicappell R, Schirrmacher V, von Hoegen P, Ahlert T, Appelhans B. Prevention of metastatic spread by postoperative immunotherapy with virally modified autologous tumor cells. I. Parameters for optimal therapeutic effects. *International journal of cancer. Journal international du cancer* 1986; **37**(4)**:** 569-77.

33. Bohle W, Schlag P, Liebrich W, Hohenberger P, Manasterski M, Moller P *et al.* Postoperative active specific immunization in colorectal cancer patients with virus-modified autologous tumor-cell vaccine. First clinical results with tumor-cell vaccines modified with live but avirulent Newcastle disease virus. *Cancer* 1990; **66**(7)**:** 1517-23.

34. Liebrich W, Schlag P, Manasterski M, Lehner B, Stohr M, Moller P *et al.* In vitro and clinical characterisation of a Newcastle disease virus-modified autologous tumour cell vaccine for treatment of colorectal cancer patients. *European journal of cancer* 1991; **27**(6)**:** 703-10.

35. Sivanandham M, Shaw P, Bernik SF, Paoletti E, Wallack MK. Colon cancer cell vaccine prepared with replication-deficient vaccinia viruses encoding B7.1 and interleukin-2 induce antitumor response in syngeneic mice. *Cancer immunology, immunotherapy : CII* 1998; **46**(5)**:** 261-7.

36. Cassel WA, Murray DR. A ten-year follow-up on stage II malignant melanoma patients treated postsurgically with Newcastle disease virus oncolysate. *Medical oncology and tumor pharmacotherapy* 1992; **9**(4)**:** 169-71.

37. Batliwalla FM, Bateman BA, Serrano D, Murray D, Macphail S, Maino VC *et al.* A 15-year follow-up of AJCC stage III malignant melanoma patients treated postsurgically with Newcastle disease virus (NDV) oncolysate and determination of alterations in the CD8 T cell repertoire. *Molecular medicine* 1998; **4**(12)**:** 783-94.

38. Livingston PO, Albino AP, Chung TJ, Real FX, Houghton AN, Oettgen HF *et al.* Serological response of melanoma patients to vaccines prepared from VSV lysates of autologous and allogeneic cultured melanoma cells. *Cancer* 1985; **55**(4)**:** 713-20.

39. Kottke T, Errington F, Pulido J, Galivo F, Thompson J, Wongthida P *et al.* Broad antigenic coverage induced by vaccination with virus-based cDNA libraries cures established tumors. *Nature medicine* 2011; **17**(7)**:** 854-9.

40. Kottke T, Diaz RM, Kaluza K, Pulido J, Galivo F, Wongthida P *et al.* Use of biological therapy to enhance both virotherapy and adoptive T-cell therapy for cancer. *Molecular therapy : the journal of the American Society of Gene Therapy* 2008; **16**(12)**:** 1910-8.

41. Demaria S, Bhardwaj N, McBride WH, Formenti SC. Combining radiotherapy and immunotherapy: a revived partnership. *International journal of radiation oncology, biology, physics* 2005; **63**(3)**:** 655-66.

42. Chakraborty M, Abrams SI, Coleman CN, Camphausen K, Schlom J, Hodge JW. External beam radiation of tumors alters phenotype of tumor cells to render them susceptible to vaccine-mediated T-cell killing. *Cancer research* 2004; **64**(12)**:** 4328-37.

43. Gulley JL, Arlen PM, Bastian A, Morin S, Marte J, Beetham P *et al.* Combining a recombinant cancer vaccine with standard definitive radiotherapy in patients with localized prostate cancer. *Clinical cancer research : an official journal of the American Association for Cancer Research* 2005; **11**(9)**:** 3353-62.

44. Castle JC, Kreiter S, Diekmann J, Lower M, van de Roemer N, de Graaf J *et al.* Exploiting the mutanome for tumor vaccination. *Cancer research* 2012; **72**(5)**:** 1081-91.

45. Connolly DC, Bao R, Nikitin AY, Stephens KC, Poole TW, Hua X *et al.* Female mice chimeric for expression of the simian virus 40 TAg under control of the MISIIR promoter develop epithelial ovarian cancer. *Cancer research* 2003; **63**(6)**:** 1389-97.

46. Foster B, Prussin C, Liu F, Whitmire JK, Whitton JL. Detection of intracellular cytokines by flow cytometry. *Current protocols in immunology / edited by John E. Coligan ... [et al.]* 2007; **Chapter 6:** Unit 6 24.

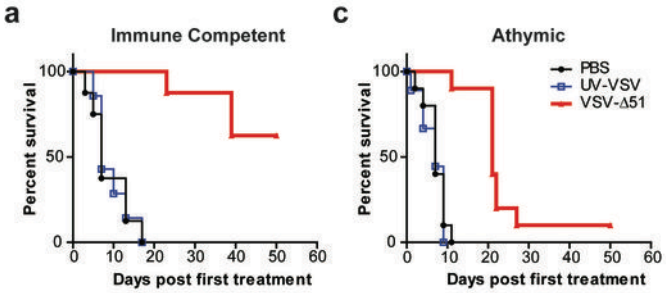

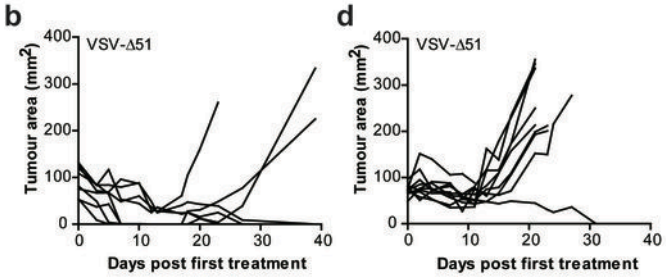

e

	Splenocyte Source		
	Naïve Control	CT26 Bearing	CT26 + VSV Cured
CT26	75	100	0
4T1	100	100	100

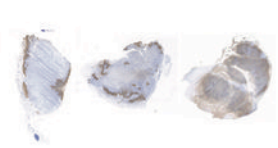

FIGURE LEGENDS

Figure 1. VSV treatment induces a potent anti-tumour immune response, on which treatment is dependent. Balb/C (a, b) or athymic nude (c, d) mice were injected subcutaneously with CT26.LacZ cells. Immune competent Balb/C mice were treated starting on day 14 post tumour implantation and nude mice were treated on day 10 to reflect a slightly faster onset of tumour development. Mice were injected 6 times with 5x108 pfu of VSV-D51-GFP IV or equivalent amount of UV-inactivated VSV-D51 or phosphate buffered saline (PBS). (a) Kaplan-Meier survival analysis of VSV-D51-GFP treatment in Balb/C mice. N=8 per group. Statistical significance verified by the log rank test, where $p<0.0001$. (b) Tumour area growth over time plotted only for VSV-D51-GFP treated mice. (c) Kaplan-Meier survival analysis of VSV-D51-GFP treatment in nude mice. N=10 for each group. Statistical significance verified by the log rank test, where $p<0.0001$. (d) Tumour area growth over time plotted only for VSV-D51-GFP treated mice. (e) Splenocytes were harvested from either naïve mice, CT26.LacZ tumour-bearing mice, or CT26.LacZ tumour-bearing mice cured with 6 doses of VSV-D51-GFP. These splenocytes were injected IV into naïve Balb/C mice, which were challenged subcutaneously 48 hours later with CT26.LacZ cells. (f) Balb/C mice bearing CT26.LacZ subcutaneous tumours were injected IV with 5x108pfu of VSV-D51. Two days later, mice were euthanized; tumours were harvested, and frozen. Sections were stained by IHC for VSV.

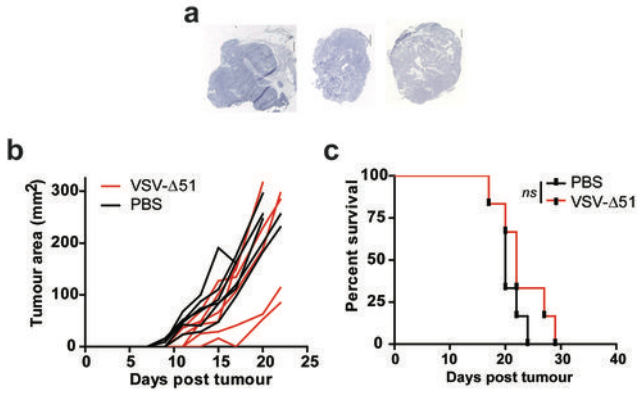

Figure 2. VSV replication is poor in B16-F10 tumours and leads to no efficacy. (**a**) C57BL/6 mice bearing B16-F10 subcutaneous tumours were injected IV with $5x10^8$pfu of VSV-Δ51. Two days later, mice were euthanized, and tumours were harvested and frozen. Sections were stained by IHC for VSV. (**b**) C57BL/6 mice bearing B16-F10 subcutaneous tumours were injected 3 times a week starting on day 6 with 6 doses of VSV-Δ51 IV. Tumour area growth over time plotted for PBS (in black) and VSV-Δ51 treated (in red). N=6 per group. (**c**) Kaplan-Meier survival analysis with statistics examined by log rank test where $p>0.2$.

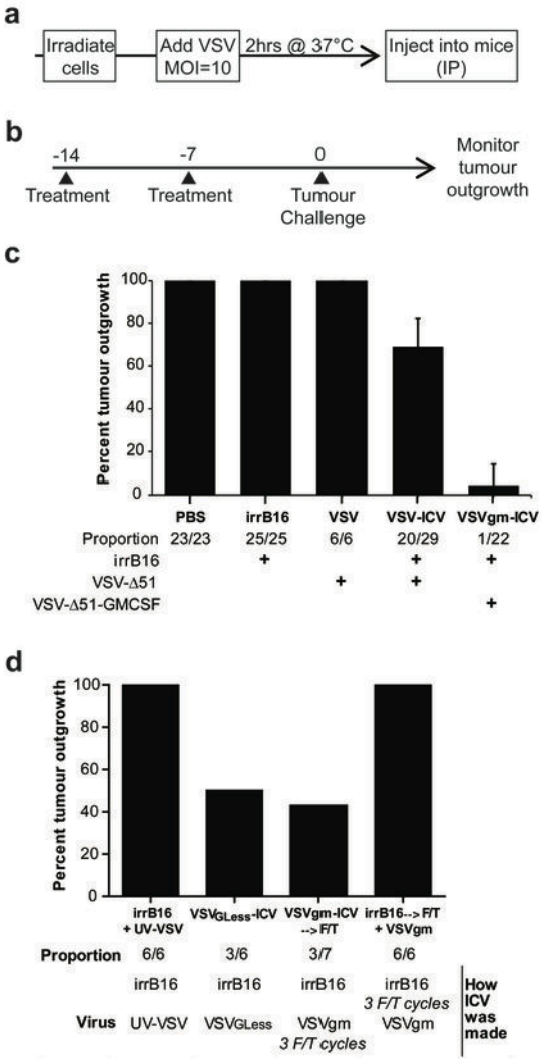

Figure 3. VSV acts as a potent adjuvant in a prophylactic B16-F10 infected cell vaccine. (**a**) Schematic representing preparation of infected cell vaccine. (**b**) Prophylactic ICV treatment timeline in days. (**c-d**) C57BL/6 mice were immunized with various control or vaccine preparations according to the timeline in panel (b). They were then challenged with $1x10^5$ B16-F10 cells subcutaneously and tumour outgrowth was monitored. (**c**) Shown is the weighted mean + weighted standard deviation of final tumour outgrowth for each group, averaged from results from multiple experiments. The total number of mice tested, with the fraction exhibiting tumour growth is listed below the graph. (**d**) Shown is the percent outgrowth from the one experiment in which that condition was tested.

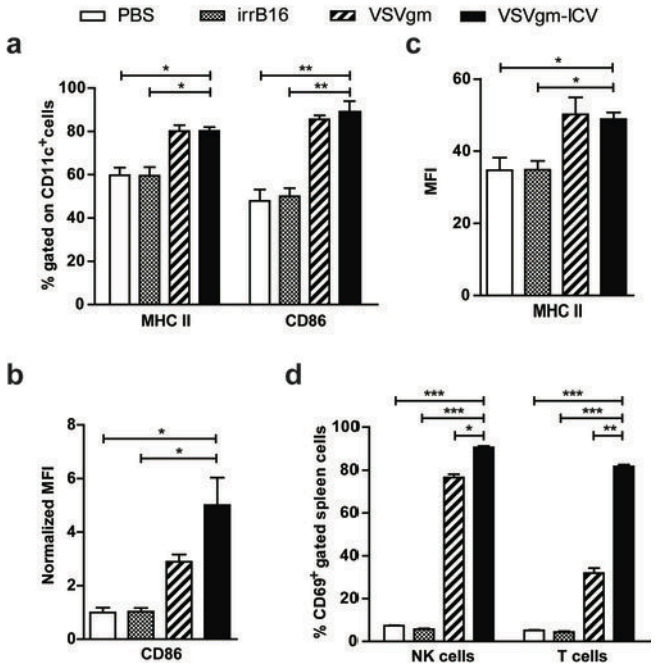

Figure 4. The VSVgm-ICV leads to dendritic cell and lymphocyte early activation in the spleen within 24hrs of vaccination.
C57BL/6 mice were immunized with the VSVgm-ICV or relevant controls IP and euthanized 24hrs later. Splenocytes were stained and examined by flow cytometry for dendritic cell markers of activation. (**a**) Percent of $CD11c^+$ cells that express MHC II and/or CD86. (**b**) Mean fluorescence intensity of MHC II staining on $CD11c^+$ cells. (**c**) Mean fluorescence intensity of CD86 staining on $CD11c^+$ cells normalized to PBS levels. N=3 mice per group, except for VSVgm-ICV that had 4 mice. (**d**) C57BL/6 mice were immunized with the VSVgm-ICV or relevant controls IP and euthanized 15hrs later. Splenocytes were stained and examined by flow cytometry for NK and T cells markers in addition to CD69. Percent of indicated cells that express CD69. All data presented as mean + SEM with 3 mice per group. *P* values, * $P<0.05$, ** $P<0.005$, *** $P\leq0.0001$

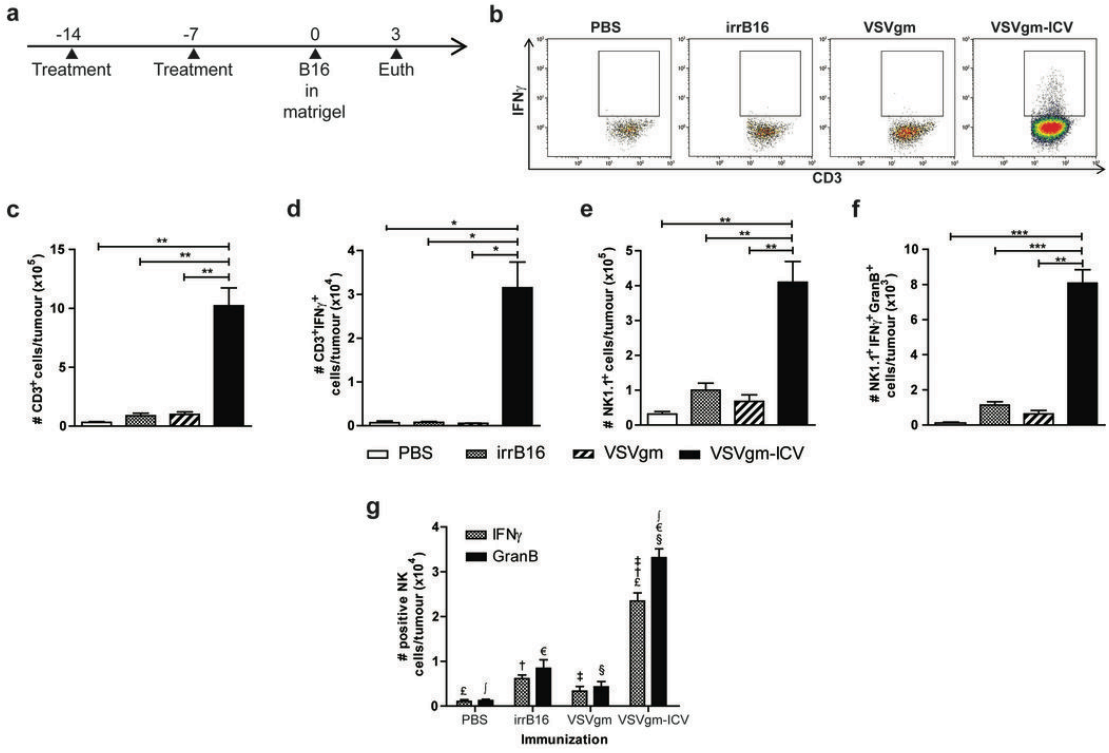

Figure 5. Prophylactic immunization with the VSVgm-ICV leads to robust activated T cell and NK cell infiltration of the challenge tumour.
(**a**) C57BL/6 mice were prophylactically immunized as described earlier with VSVgm-ICV or controls. B16-F10 cells in matrigel were subcutaneously injected on day 0. On day 3, mice were injected IV with brefeldin A, then 6hrs later were euthanized. Tumours were resected on day 3 for enzymatic disaggregation and flow cytometric analysis. (**b**) Representative dot plots demonstrating $CD3^+$ cells expressing IFNγ. (**c**) The total number of $CD3^+$ cells per tumour in each group. (**d**) The total number of $CD3^+$ $IFN\gamma^+$ cells per tumour in each group. (**e**) The total number of $NK1.1^+$ cells per tumour in each group. (**f**) The total number of $NK1.1^+IFN\gamma^+GranzymeB^+$ cells per tumour in each group. (**g**) The total number of $NK1.1^+IFN\gamma^+$ cells and $NK1.1^+GranzymeB^+$ cells per tumour in each group. *P* values, £, †, ‡, ∫, §, and € are all *P≤0.005.* All data are presented as mean + SEM with 5 mice per group. *P* values, * *P*<0.05, ** *P*<0.005, *** *P*≤0.0005

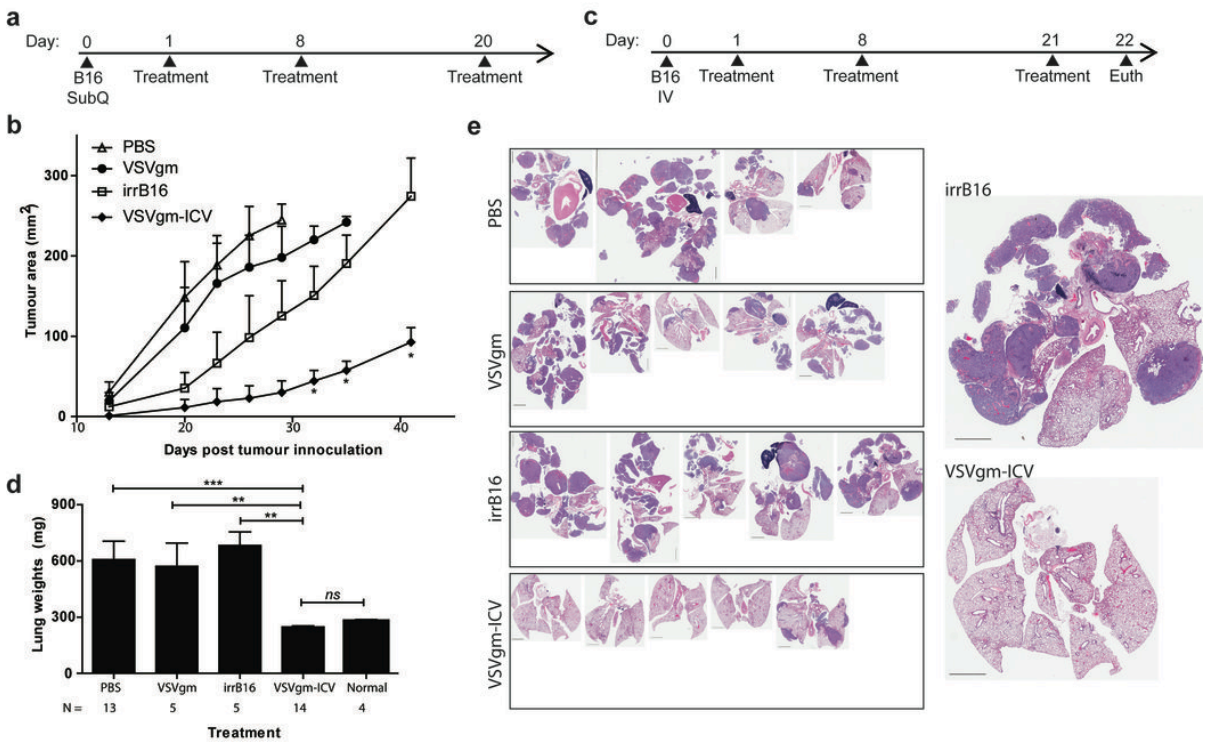

Figure 6. Treatment with the VSVgm-ICV can significantly impact tumour growth in subcutaneous and systemic models.

(**a**) C57BL/6 mice were implanted with B16-F10 subcutaneous tumours and treated according to the presented timeline. (**b**) Tumour area was monitored and is shown in days following tumour implantation as mean + SEM with 5 mice per group, except for the VSVgm only group that had 4. (**c**) C57BL/6 mice were injected IV with B16-F10 cells and treated according to presented timeline with the VSVgm-ICV or controls. Mice were euthanized on day 22, and their lungs were weighed and fixed in 10% formalin. Lungs were then sliced and analyzed by hematoxylin and eosin (H&E) staining. (**d**) Lung weights shown are pooled from 2 separate experiments and presented as mean + SEM with variance analysis by Mann-Whitney test. Normal lungs are those from mice that have not received any lung tumours or treatments. (**e**) H&E staining of all mice in one experiment with representative sections demonstrating tumour burden at endpoint. All lungs are on the same scale, with black bar indicating 2 millimeters. A higher magnification of a representative vaccine and control-treated lung are presented on the right. One PBS mouse had the heart buried in tumour, and so the organ could not be removed. A few control mice had tumours in their thymus and so these organs were kept in the H&Es and weights. *P* values, * $P<0.05$, ** $P<0.005$, *** $P\leq0.0001$

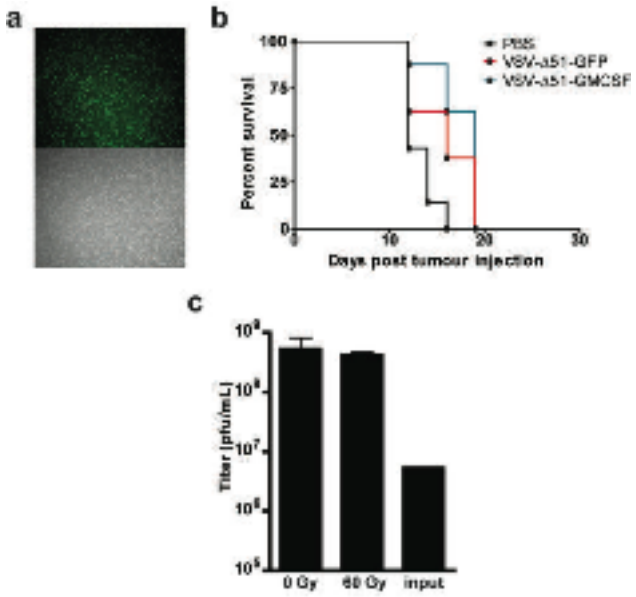

Supplementary Figure S1. VSV infection of B16-F10 cells at a high MOI can overcome replication issues.

(a) B16-F10 cells were infected *in vitro* at an MOI of 10 with VSV-Δ51-GFP. 24hrs later, pictures were taken with a fluorescent microscope. (b) C57BL/6 mice bearing B16-F10 subcutaneous tumours were injected 3 times with VSV-Δ51-GMCSF, VSV-Δ51-GFP, or PBS IV. (c) B16-F10 cells, healthy or 60Gy γ-irradiated, were infected *in vitro* at an MOI of 10 with VSV-Δ51-GFP. 48hrs later supernatants were harvested and titered on Vero cells by plaque assay. Average titer of 3 wells in pfu/mL + SEM.

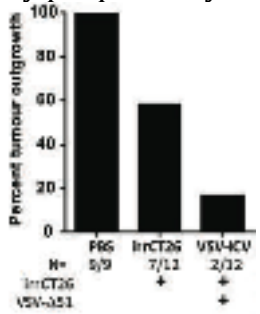

Supplementary Figure S2. VSV acts as a potent adjuvant in a prophylactic CT26.wt infected cell vaccine

Balb/C mice were immunized with a CT26.wt VSV-ICV on days -14 and -7, followed by $3x10^5$ CT25.wt subcutaneously. Tumour outgrowth per group is shown with proportions of mice growing a tumour below. This represents the sum of two independent experiments.

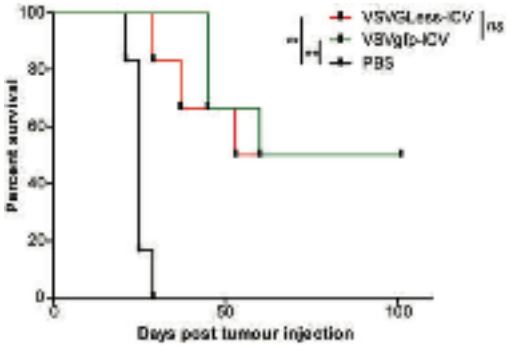

Supplementary Figure S3. The VSV_{GLess}-ICV performs identically as the VSV-ICV. Kaplan-Meier survival curve of mice given prophylactic PBS, VSV-ICV, or VSV_{GLess}-ICV from Figure 3d. Statistical significance verified by Log-Rank test where ** P<0.005.

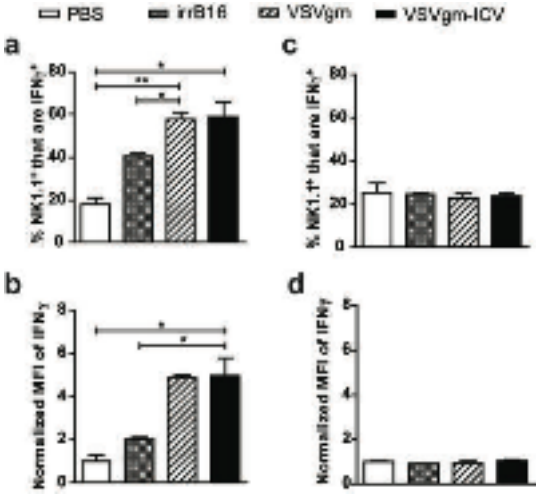

Supplementary Figure S4. Prophylactic immunization with the VSVgm-ICV leads to early NK cell activation; however activation is not maintained until tumour challenge.

(**a-b**) C57BL/6 mice were immunized IP with the VSVgm-ICV or relevant controls and euthanized 24hrs later. Splenocytes were stained and examined by flow cytometry for $CD3^-NK1.1^+$ cells and IFNγ. Data are presented as mean + SEM with 3 mice per group, except for VSVgm-ICV that had 4 mice. (**c-d**) C57BL/6 mice were immunized IP with the VSVgm-ICV or relevant controls on days -14 and -7 and then euthanized on day 1, at which point blood was harvested and stained for $CD3^-NK1.1^+$ cells and IFNγ. Data are presented as mean + SEM with 3 mice per group. (**a,c**) Percent of $CD3^-NK1.1^+$ cells that express IFNγ. (**b,d**) Mean fluorescence intensity of IFNγ staining on $CD3^-NK1.1^+$ cells normalized to PBS levels. P values, * P<0.05, ** P<0.005, *** P≤0.0001

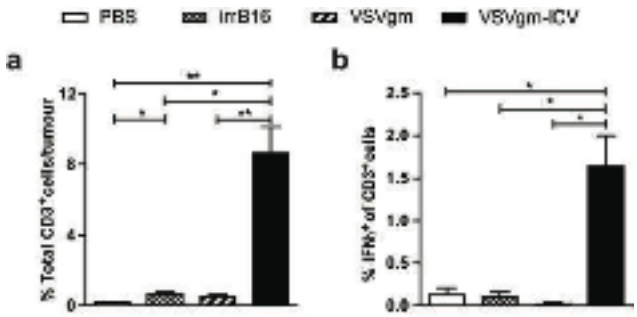

Supplementary Figure S5. A significant increase in the proportion of T and NK cells is observed within the challenge tumour.

Tumours from mice treated in Figure 5 were also analyzed for the proportion of (**a**) $CD3^+$ cells and (**b**) $CD3^+$ cells expressing IFNγ. All data are presented as mean + SEM with 5 mice per group. *P* values, * $P<0.05$, ** $P<0.005$, *** $P\leq0.0001$

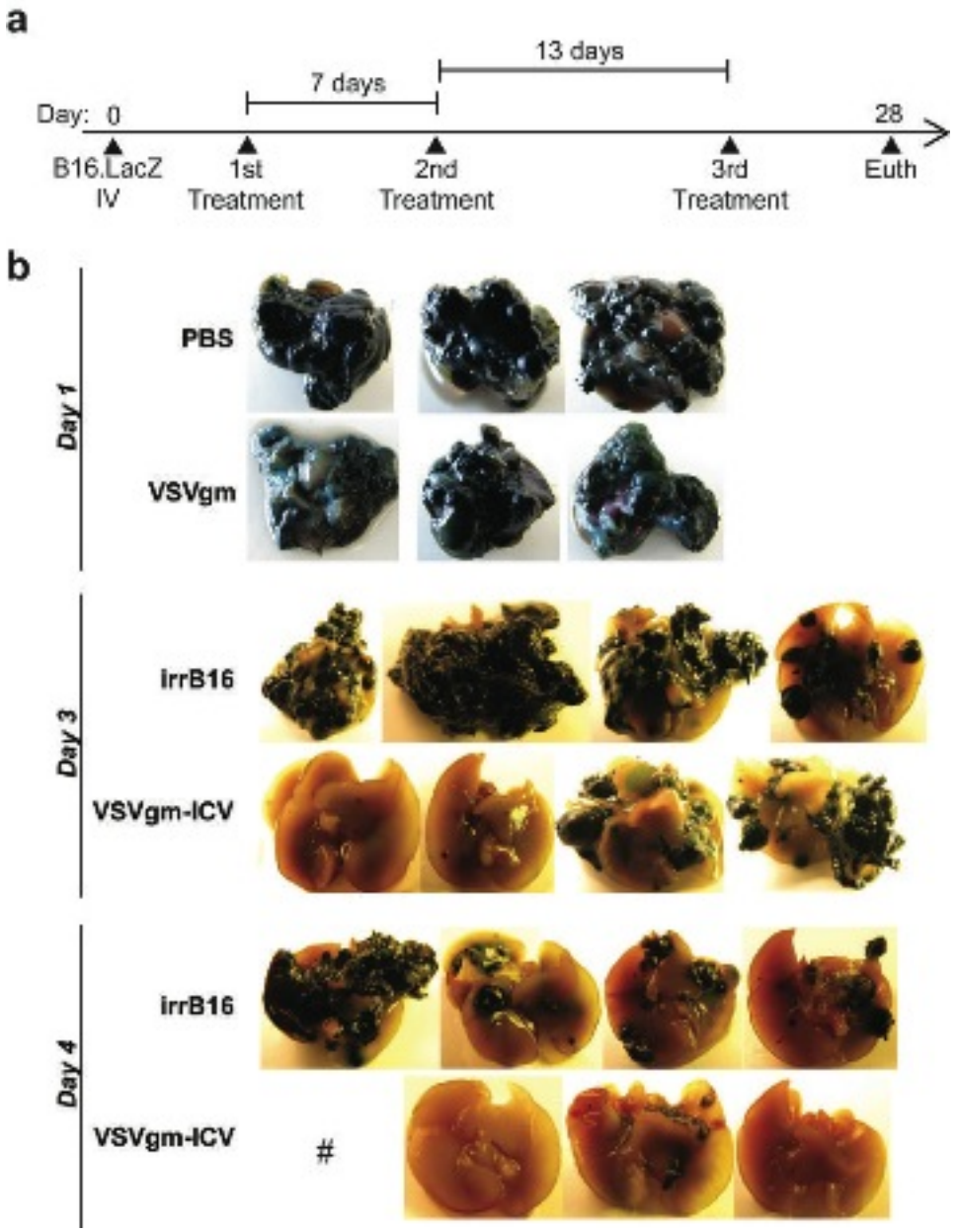

Supplementary Figure S6. Treatment with the VSVgm-ICV reduces tumour burden even when treatment is delayed to day 3 or 4 after tumour inoculation.
(a) $8x10^4$ B16-F10.LacZ cells were administered IV and then mice were treated according to the timeline with PBS, VSVgm, irrB16 cells, or the VSVgm-ICV. (b) Initial day on which treatments began is indicated to the left of the pictures. On day 28, all mice were euthanized, at which point lungs were harvested and stained for β-galactosidase. Pictures were then taken using a macro setting on a digital camera. # Animal found dead of unknown causes before lungs could be harvested.

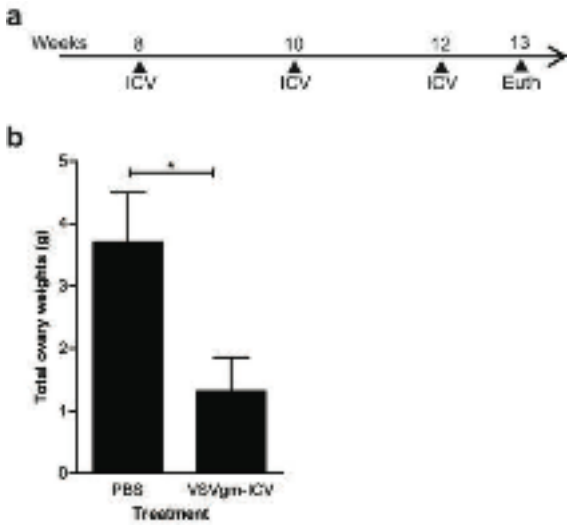

Supplementary Figure S7. The VSVgm-ICV has therapeutic efficacy in the MISIIRTAg spontaneous ovarian cancer model.

(**a**) FVB/N MISIIRTAg transgenic mice were treated on weeks 8, 10, and 12 with either PBS or the VSVgm-ICV IP. At 13 weeks of age, some mice demonstrated severe abdominal masses and all mice were euthanized. (**b**) Ovaries were weighed and total ovary weights per mouse are plotted with *P* value, * $P<0.05$.

APPENDIX III: ORFV: A NOVEL ONCOLYTIC AND IMMUNE STIMULATING PARAPOXVIRUS THERAPEUTIC

Julia L Rintoul, Chantal G Lemay, Lee-Hwa Tai, Marianne M Stanford, Theresa J Falls, Christiano T de Souza, Byram W Bridle, Manijeh Daneshmand, Pamela S Ohashi, Yonghong Wan, Brian D Lichty, Andrew A Mercer, Rebecca C Auer, Harold L Atkins and John C Bell

Contribution:

Planned, executed, and analyzed all of the experiments. I was assisted for flow cytometry experiments by Chantal Lemay and Lee-Hwa Tai. I was assisted for animal experiments by Theresa Falls and Christiano T de Souza. I was assisted in the chromium release assays by Lee-Hwa Tai and Christiano T de Souza. I wrote the manuscript, with input from Chantal Lemay, and John C Bell.

Published: *Molecular Therapy, January 2012*

ORFV: A Novel Oncolytic and Immune Stimulating Parapoxvirus Therapeutic

Julia L Rintoul[1], Chantal G Lemay[1], Lee-Hwa Tai[1], Marianne M Stanford[1], Theresa J Falls[1], Christiano T de Souza[1], Byram W Bridle[2], Manijeh Daneshmand[1], Pamela S Ohashi[3,4], Yonghong Wan[2], Brian D Lichty[2], Andrew A Mercer[5], Rebecca C Auer[1], Harold L Atkins[1] and John C Bell[1]

[1]Department of Biochemistry, Microbiology & Immunology, Faculty of Medicine, University of Ottawa, Ottawa Hospital Research Institute, Centre for Innovative Cancer Research, Ottawa, Ontario, Canada; [2]Department of Pathology and Molecular Medicine, Centre for Gene Therapeutics, McMaster University, Faculty of Health Sciences, Hamilton, Ontario, Canada; [3]The Campbell Family Institute for Breast Cancer Research, Ontario Cancer Institute/Princess Margaret Hospital, University Health Network, Toronto, Ontario, Canada; [4]Department of Immunology, University of Toronto, Toronto, Ontario, Canada; [5]Department of Microbiology and Immunology, University of Otago, Dunedin, New Zealand

Replicating viruses for the treatment of cancer have a number of advantages over traditional therapeutic modalities. They are highly targeted, self-amplifying, and have the added potential to act as both gene-therapy delivery vehicles and oncolytic agents. *Parapoxvirus ovis* or Orf virus (ORFV) is the prototypic species of the *Parapoxvirus* genus, causing a benign disease in its natural ungulate host. ORFV possesses a number of unique properties that make it an ideal viral backbone for the development of a cancer therapeutic: it is safe in humans, has the ability to cause repeat infections even in the presence of antibody, and it induces a potent T_h-1-dominated immune response. Here, we show that live replicating ORFV induces an antitumor immune response in multiple syngeneic mouse models of cancer that is mediated largely by the potent activation of both cytokine-secreting, and tumoricidal natural killer (NK) cells. We have also highlighted the clinical potential of the virus by demonstration of human cancer cell oncolysis including efficacy in an A549 xenograft model of cancer.

Received 1 September 2011; accepted 18 December 2011; advance online publication 24 January 2012. doi:10.1038/mt.2011.301

INTRODUCTION

Biological therapeutics for cancer constitute an exciting alternative or complement to conventional chemo- and radiotherapies. Replicating oncolytic viruses (OVs) are particularly exciting as they have multiple features that can be exploited therapeutically. Although originally selected or engineered to directly infect and destroy cancer cells, there is accumulating evidence that OVs are acting via a number of additional mechanisms including tumor vascular disruption[1,2] and activation of innate[3,4] and/or adaptive antitumor immune responses.[5,6] An example of an OV with potent antitumor immune-stimulating activity is the herpes virus–based OncoVex product that is engineered to express granulocyte–macrophage colony-stimulating factor and has recently completed enrollment in a pivotal phase 2 human clinical trial.[7] The ability to stimulate an innate and adaptive antitumor immune response has been identified as an important component of the therapeutic activity of several different OVs, where some of the OVs have now demonstrated efficacy even in the absence of oncolytic activity.[3,4,8] These data, combined with the early clinical success of OVs,[5,7,9] have highlighted the potential impact of replicating viruses for the treatment of cancer.

Parapoxvirus ovis or Orf virus (ORFV) is the prototypic member of the *Parapoxvirus* genus, and has a worldwide distribution causing acute dermal infections in its natural hosts: goat and sheep.[10] The lesions caused by ORFV infection are initiated and maintained in wounded skin, and are marked by an extensive vascular proliferation and dilation which is caused partly by the expression of vascular endothelial growth factor by the viruses.[11] Although naive to the cancer therapeutic field, the ORFV replicative "niche" is an isolated regenerative wound with an extensive vasculature, much like a tumor microenvironment. In addition, ORFV possesses a number of unique characteristics that have not only led to the development of Parapoxviruses for antiviral vaccine platforms,[12–14] but also suggest that it may be an excellent platform for the development of new cancer biotherapies. In contrast to zoonotic orthopoxviruses,[15] human ORFV infections do not lead to serious disease.[16–18] Additionally, ORFV treatment leads to a potent induction of a T_h-1-dominated immune response involving the accumulation of $CD4^+$ and $CD8^+$ T cells, B cells, natural killer (NK) cells, neutrophils, and dendritic cells (DCs),[19–21] and cytokines including interleukin-1β (IL-1β), IL-8, granulocyte–macrophage colony-stimulating factor, IL-2 and interferon-γ (IFN-γ).[10,22–25] Interestingly, these robust immune responses are associated with the viral particle itself, as numerous data have shown immune stimulation by inactivated ORFV in a number of different species,[12,14,22,26] including humans.[22,27,28] Importantly, the immune stimulation has been compared with other poxviruses, and in all cases the immune stimulatory profile is unique to ORFV.[22,29,30] In addition, in contrast to cytokine therapies, ORFV T_h-1 immune-stimulation is regulated by subsequent upregulation of T_h-2 cytokines like IL-4 and IL-10.[28,29] Lastly, an

ORFV platform may be superior as Parapoxvirus researchers have described reoccurring infections in animals as a result of a very short-lived duration of the ORFV-specific immunity.[15,17] Although antibody production after ORFV infection is normal, antibody appears to play little to no role in protection upon reinfection, and neutralizing antibody is rare.[17,31,32]

We hypothesized that ORFV could be an ideal cancer therapeutic candidate considering its unique immune stimulation profile and its limited pathogenicity in humans. Here, we present data that show that ORFV induces anticancer effects in multiple syngeneic murine models of cancer, where the mechanism of action is largely attributed to potent induction of cytotoxic and cytokine-secreting NK cells. Importantly, although ORFV replicates very poorly in normal human tissues, we show that it has robust replication in a spectrum of human cancer cell lines and is therapeutically active in a human lung cancer xenograft model.

RESULTS

ORFV can reduce tumor burden in multiple mouse models of cancer

Because ORFV has been documented as an efficacious immunotherapy in a number of antiviral models,[12–14] we wanted to first explore the *in vivo* anticancer potential of ORFV in immune-competent mouse models.[33–36] Mice (C57Bl/6 and Balb/c) were challenged with LacZ-expressing cancer cells intravenously (i.v.) on day 0 (**Figure 1a**). Tumor-bearing animals were then treated three times i.v. with phosphate-buffered saline (PBS) as a control, or ORFV at a dose of 10^7 plaque-forming units (p.f.u.). At 10 or 14 days after challenge, lungs were harvested and processed using a β-galactosidase-containing stain solution to visualize lung metastases. Representative images of lungs isolated from the C57Bl/6 mice at day 14 after i.v. B16F10-LacZ tumor challenge illustrate the reduction in lung tumor burden resulting from systemic delivery of ORFV (**Figure 1b**). Lung tumor burden from animals treated with PBS was quantified and compared with mice treated with one (on day 1, 3, or 8) or three doses of ORFV (**Figure 1c**). We found that even one dose of ORFV as late as 8 days after B16F10-LacZ challenge can significantly reduce the tumor burden.

A Balb/c lung model was also tested, and we found that ORFV treatment of CT26-LacZ lung tumor–bearing animals led to nearly 100% reduction in the tumor burden (**Figure 1d**). Quantification of the number of surface lung metastases demonstrated a significant reduction in tumor burden after either one or three doses of ORFV (**Figure 1e**). ORFV treatment of Balb/c mice bearing CT26-LacZ lung tumors led to a significant survival advantage (**Supplementary Figure S1a**), and intravenous ORFV therapy of subcutaneous CT26 tumors led to a significant reduction in tumor burden over time (**Supplementary Figure S1b**). Therefore, systemic ORFV treatment can significantly reduce tumor burden in multiple syngeneic immune-competent models of cancer.

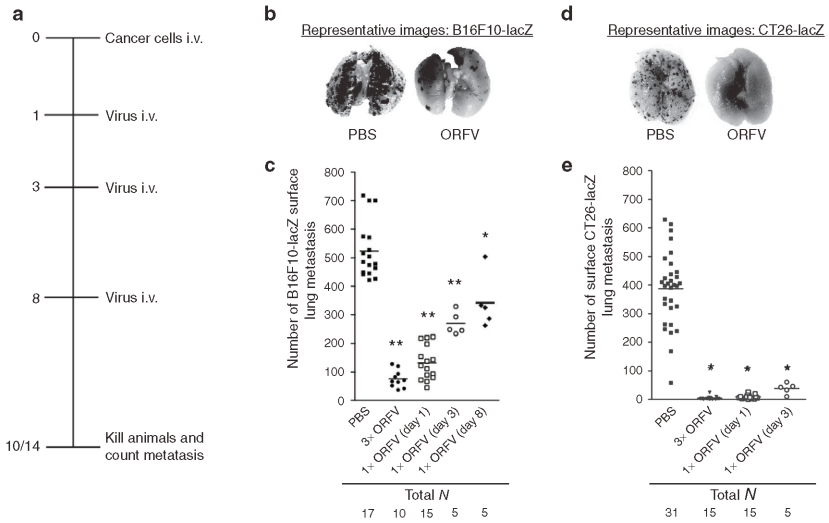

Figure 1 ORFV treatment of syngeneic murine lung models. (**a**) Schematic outlining the treatment schedule for the metastatic lung tumor models. (**b**) C57Bl/6 mice were challenged with 3 × 10^5 B16F10-LacZ cells i.v., and dosed one or three times with ORFV (10^7) as indicated. At day 14 after cell injection, lungs were excised and surface metastases were counted. Representative images of the lungs from animals treated with three doses of ORFV or PBS control are shown. (**c**) The number of surface lung metastases in animals treated as in (**b**); bars represent the mean for each group (*$P < 0.01$, **$P < 0.005$ using an unpaired *t*-test with Welch's correction). (**d**) Balb/c mice were challenged with 10^5 CT26-LacZ cells i.v., and dosed one or three times with ORFV (10^7) as indicated. At day 10 after cell injection, mice were killed, their lungs processed as described above. Representative images of the lungs from animals treated with three doses of ORFV or PBS are shown. (**e**) The number of surface lung metastases in animals treated as in (**d**); bars represent the mean for each group (*$P < 0.005$ using an unpaired *t*-test with Welch's correction). 3× ORFV refers to three doses of virus (10^7) at days 1, 3, and 8 after cell injection; 1× ORFV refers to one dose of virus (10^7) given on the indicated day. i.v., intravenous; ORFV, Orf virus; PBS, phosphate-buffered saline.

ORFV replication is required for full treatment efficacy

The mechanism of ORFV-mediated reduction in tumor burden was analyzed in both models by examining virus amplification *in vitro* in the respective cancer cell lines. Phase-contrast images of B16F10-LacZ cells and CT26-LacZ cells at 48 hours postinfection showed cell rounding, indicative of a virus-induced cytopathic effect (**Figure 2a**). The dose dependency of ORFV-induced

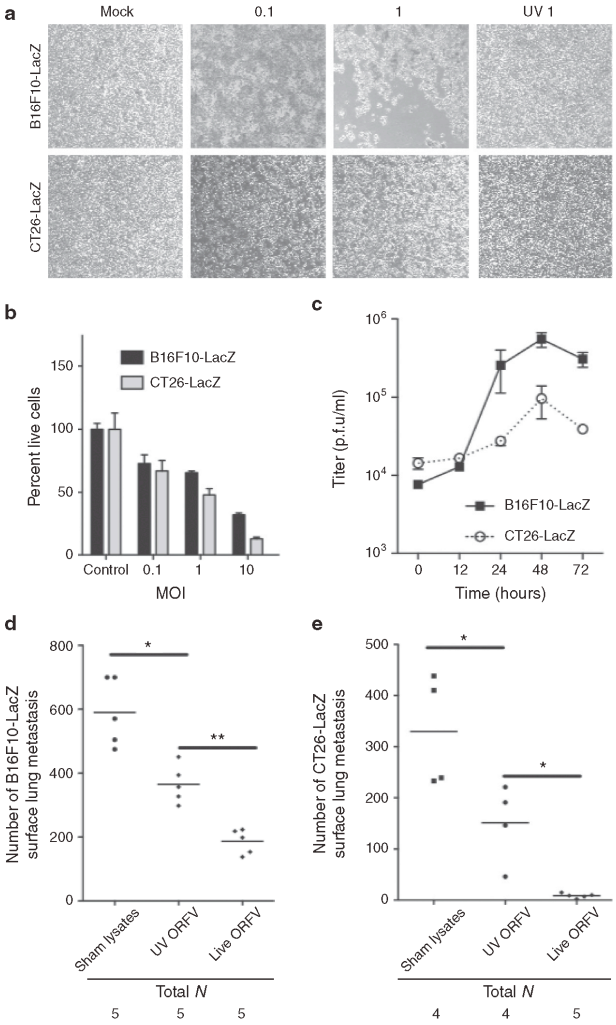

Figure 2 ORFV infection of murine cancer cells. (**a**) Phase-contrast images of mock-infected, ORFV-infected (MOI of 0.1 and 1), or UV-inactivated ORFV-infected (MOI 1) B16F10-LacZ and CT26-LacZ cells at 48 hours postinfection at a magnification of ×40. (**b**) Cytotoxicity assays of B16F10-LacZ and CT26-LacZ cells mock-infected (control) or ORFV-infected at the indicated MOI. Percent live cells was determined at 72 hours postinfection by normalization to mock-infected controls, $N = 4$, mean ± SEM. (**c**) ORFV growth curves were performed on B16F10-LacZ and CT26-LacZ cell lines at an MOI of 0.3. Cells were infected at time 0, and cell lysates collected and processed by plaque assay at time-points postinfection, $N = 2$, mean ± SEM. (**d**) C57Bl/6 mice challenged with 3×10^5 B16F10-LacZ cells intravenously (i.v.), and dosed three times with sham-infected cell lysates, live or UV-inactivated ORFV (10^7). At day 14 after cell challenge, lungs were isolated and metastases counted. Bars represent the mean for each group (*$P < 0.01$, **$P < 0.005$ using an unpaired *t*-test with Welch's correction). (**e**) Balb/c mice challenged with 10^5 CT26-LacZ cells i.v., and dosed three times with sham-infected cell lysate, live or UV-inactivated ORFV (10^7). At day 10 after cell challenge, lungs were isolated and metastases counted. Bars represent the mean for each group (*$P < 0.05$ using an unpaired *t*-test with Welch's correction). MOI, multiplicity of infection; PBS, phosphate-buffered saline; p.f.u., plaque-forming unit; UV, ultraviolet.

cell death was quantified (Figure 2b) and found to be dependent on productive infection as ultraviolet (UV)-inactivated ORFV did not induce cytopathic effect in either cell line (Figure 2a). The amount of infectious ORFV produced by B16F10-LacZ and CT26-LacZ cancer cells was determined by multistep growth curve analysis (Figure 2c) and revealed that both cell lines can support a modest amount of virus replication. To determine whether ORFV replication was important for the *in vivo* efficacy achieved in the C57Bl/6 and Balb/c lung models, UV-inactivated ORFV was compared with live ORFV (Figure 2d,e). Quantification of the number of surface lung metastases in both models indicated that although UV-inactivated virus could significantly reduce lung metastases in these models, replicating ORFV was required to achieve maximum efficacy. Interestingly, despite only modest ORFV replication in murine cancer cell lines, ORFV therapy was as good or better than oncolytic vaccinia, Raccoonpox, and Myxoma virus (MYXV) at reducing lung metastasis in both lung models (**Supplementary Figure S2**), even at a log lower dose (**Supplementary Figure S2b**). From these data, and the observation that UV-inactivated virus has some therapeutic activity, we hypothesized that the activation of innate or adaptive immune responses by ORFV could be contributing to its anticancer activity.

In vivo ORFV infection of lung tumor–bearing animals correlates with clearance of lung metastases

A tissue distribution experiment was performed to determine the kinetics of *in vivo* ORFV infection in relation to the kinetics of lung tumor clearance. Tumor-bearing C57Bl/6 mice were treated with ORFV i.v. at a dose of 10^7 p.f.u. on day 0, and tissues were harvested at three time-points postinfection. ORFV was recovered from the lungs at early time-points, and nearly all virus were cleared by day 5 postinfection (Figure 3a). No virus was recovered from any of the other tissues examined including spleen, liver, kidney, ovary, and brain (data not shown). Lung tumor clearance from ORFV-treated animals was found to occur primarily within the first 48 hours postinfection, evidenced by both the enumeration of lung metastasis (Figure 3b), and representative photographs of the large lobe of lungs from ORFV-treated animals (Figure 3c). The tissue distribution experiment was also performed in Balb/c mice to confirm the correlation between *in vivo* ORFV infection and tumor clearance (**Supplementary Figure S3**). Titer data demonstrate that virus was only recovered from the lungs of animals at day 2 postinfection, and was cleared by day 5 (**Supplementary Figure S3a**), and the clearance of lung metastases occurred primarily within the first 48 hours (**Supplementary Figure S3b,c**). A comparison of the lungs from tumor-bearing, ORFV-treated and untreated Balb/c animals demonstrated no pathological effects from the virus (**Supplementary Figure S4**). We used a LacZ-expressing version of ORFV to determine whether virus replication was restricted to the tumor bed. In these experiments, a B16F10 cell line lacking the LacZ transgene was used to initiate tumor formation in mouse lungs and subsequently tumor-bearing and tumor-free animals were treated with ORFV-LacZ. Significant viral infection and spread was only seen in tumor-bearing animals (Figure 3d).

i.v. delivery of ORFV leads to expansion and activation of innate immune cells in the spleen

To establish the contribution of the immune system in the ORFV-mediated efficacy in the lung models, flow cytometry analysis was performed. Spleens isolated from tumor-bearing Balb/c animals showed dramatic splenomegaly at 5 days postinfection with ORFV (Figure 4a). The splenomegaly was attributed to the expansion in the number of lymphocytes in the spleen (Figure 4b). Flow cytometry analysis demonstrated a trend toward a disproportionate expansion in innate immune cells (DC and NK cells) when compared with adaptive immune cells ($CD8^+$ T cells) in the spleen (Figure 4c). Expression of the early activation marker CD69 on NK cells from Balb/c splenocytes of tumor-bearing animals showed nearly 90% activation at 24 hours postinfection compared with PBS-treated animals (Figure 4d). Splenocytes from tumor-bearing C57Bl/6 animals were analyzed at several time-points postinfection where ORFV induced significantly more CD69 expression on NK cells when compared with PBS-treated animals (Figure 4e).

To determine whether the adaptive immune system was required for the ORFV efficacy, $CD4^+$ or $CD8^+$ T cells were depleted from ORFV-treated animals in a Balb/c CT26-LacZ survival experiment, where ORFV treatment led to a significant extension in overall survival (**Supplementary Figure S5**). We found that neither $CD4^+$ nor $CD8^+$ T cells are required for the ORFV-mediated efficacy in this model. Collectively, these data indicate that ORFV is capable of stimulating an innate immune response, which may be involved in the efficacy achieved in the C57Bl/6 and Balb/c mouse models.

Cell depletion and *ex vivo* cytotoxicity studies implicate NK cells in the efficacy achieved by ORFV

We examined the contribution of NK cells to ORFV therapy using antibody depletion studies. The dose and schedule of the NK cell–depleting antibody was tested in both C57Bl/6 and Balb/c mice (**Supplementary Figure S6a,b**) to ensure that the depletion was sufficient, and would last for the duration of the experiment. In both the C57Bl/6 and Balb/c lung models, NK cell depletion reduced the ability of ORFV to clear lung metastases (Figure 5a,b).

NK cell cytotoxicity assays were performed at time-points postinfection from tumor-naive C57Bl/6 mice treated with live or UV-inactivated ORFV i.v. (Figure 5c,d). At 24 hours postinfection, NK cells isolated from both live and UV-inactivated ORFV-treated animals induced significant cytotoxicity of B16F10-LacZ cells (Figure 5c). NK cells isolated from live ORFV-treated animals induced significantly greater B16F10-LacZ cytotoxicity than those isolated from UV-inactivated ORFV-treated animals. At 72 hours postinfection, only live ORFV treatment resulted in significant NK cell cytotoxicity of target cells (Figure 5d). Thus, systemic ORFV treatment induces a potent cytotoxic NK cell response capable of directly killing B16F10-LacZ target cells.

ORFV induces potent cytokine expression by NK cells isolated from the spleen, blood, and lung

To determine the strength and breadth of the ORFV-mediated activation of NK cells, tissues from tumor-bearing C57Bl/6 animals were analyzed by flow cytometry at 24 hours after ORFV

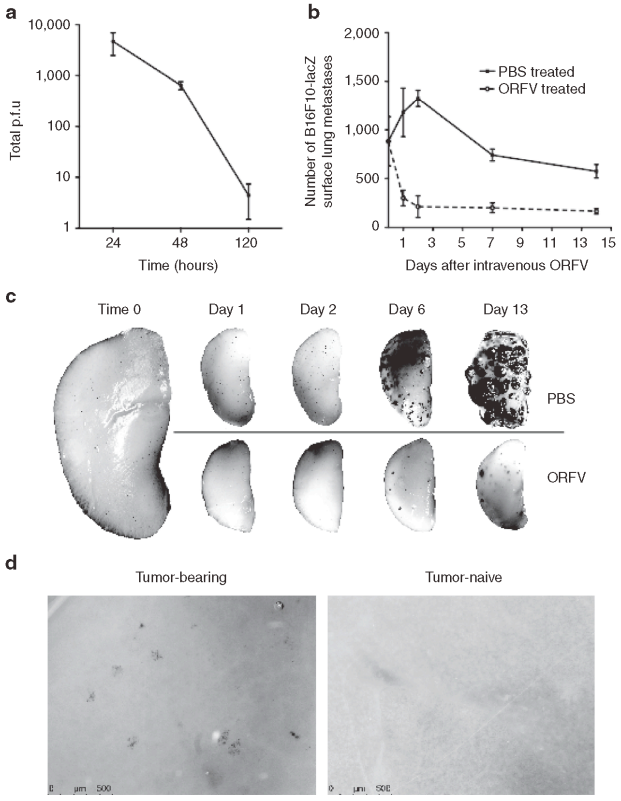

Figure 3 Kinetics of *in vivo* ORFV infection and B16F10-LacZ tumor debulking in C57Bl/6 animals. (**a**) C57Bl/6 mice were challenged with 3 × 10^5 B16F10-LacZ cells intravenously (i.v.) and were treated 24 hours later with ORFV-LacZ (10^7) i.v. Lung tissues were titered for ORFV at the indicated times postinfection; $N = 3$, mean ± SEM. (**b**) C57Bl/6 mice were challenged with 3 × 10^5 B16F10-LacZ cells i.v. and were treated 24 hours later with ORFV (10^7) or PBS i.v. Lung tissues were removed at various times postinfection, and the number of surface lung metastases was enumerated; $N = 3$, mean ± SEM. (**c**) Representative images of the large lobe of lungs isolated from ORFV- or PBS-treated animals are shown at time-points postinfection. (**d**) Representative images of lungs from C57Bl/6 mice with and without B16F10 lung tumors (10^6). At day 4, animals were treated with 10^7 ORFV-LacZ i.v. Virus was detected by β-galactosidase staining at 24 hours postinfection. ORFV, Orf virus; PBS, phosphate-buffered saline; p.f.u., plaque-forming unit.

treatment for both granzyme B and IFNγ expression by NK cells (Figure 6). Importantly, these data were collected after a 5-hour GolgiPlug incubation, in the absence of any *ex vivo* stimulation. Representative histograms of lung-derived lymphocytes are illustrated in Figure 6a, demonstrating increased expression of both IFNγ and Granzyme B from NK cells isolated from ORFV-treated animals compared with PBS-treated animals. Quantification of the percent-gated NK cells secreting either granzyme B or IFNγ from the spleen, blood, and lung illustrates significant expression of both cytokines in all tissues isolated from ORFV-treated animals (Figure 6b,c, respectively). In addition, the overall amount of IFNγ and granzyme B expressed on a per cell basis was quantified (Figure 6d), where ORFV treatment also led to significant increases in the mean fluorescence intensity of both cytokines from the spleen, blood, and lung. Finally, we determined the percent-gated NK cells that were expressing both IFNγ and granzyme B (Figure 6e). These activated NK cells were only detected in ORFV-treated animals, and were identified in all three tissues. These data underline the ability of ORFV to stimulate a potent, diverse, and systemic activation of NK cells.

Tissues from tumor-bearing C57Bl/6 animals treated with PBS or ORFV were also analyzed for CD11c expression, and corresponding expression of co-stimulatory molecules and cytokines at 24 hours after i.v. treatment (**Supplementary Figure S7**). There were significantly more $CD11c^+$ cells in the lung and blood of ORFV-treated animals (**Supplementary Figure S7a**). Dentritic cell (DC) expression of co-stimulatory molecules CD80 and CD86 were elevated in the blood and lung, and spleen, respectively (**Supplementary Figure S7b,c**). ORFV treatment also led to significantly more tumor necrosis factor-α and IL-12 cytokine expression from DCs in the lung

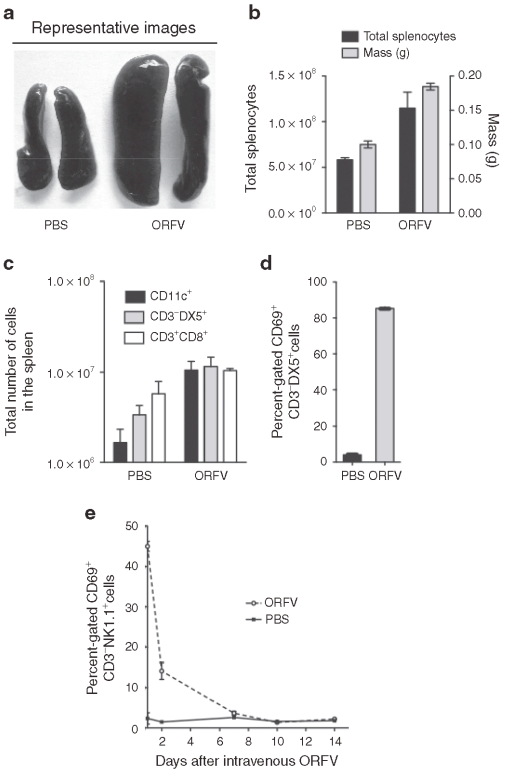

Figure 4 Expansion and activation of innate immune cells in the spleen. (**a**) Spleens isolated from tumor-bearing Balb/c animals treated with ORFV (10^7) or PBS intravenously (i.v.) were photographed at 5 days postinfection. (**b**) The mass and total number of splenocytes illustrated in (**a**) were quantified at 5 days postinfection; $N = 2$, mean ± SEM. (**c**) The total number of dendritic cells ($CD11c^+$), natural killer cells ($CD3^-DX5^+$) and cytotoxic T cells ($CD3^+CD8^+$) were quantified from spleens isolated from tumor-bearing Balb/c mice treated i.v. with ORFV (10^7) or PBS i.v. at 5 days postinfection, $N = 2$, mean ± SEM. (**d**) CD69 expression was quantified from splenic natural killer cells ($CD3^-DX5^+$) isolated from tumor-bearing Balb/c mice 24 hours after ORFV (10^7) or PBS i.v. administration, $N = 2$, mean ± SEM. (**e**) CD69 expression was quantified from splenic natural killer cells ($CD3^-NK1.1^+$) isolated from tumor-bearing C57Bl/6 mice at time-points after i.v. ORFV (10^7) or PBS treatment, $N = 3$, mean ± SEM. ORFV, Orf virus; PBS, phosphate-buffered saline.

(**Supplementary Figure S7d,e**). To rule out virus amplification in murine immune cells, ORFV infection of both DCs and NK cells was also analyzed. At 24 hours postinfection, there was no ORFV amplification in either cell type (**Supplementary Figure S7f**).

ORFV therapy reduces tumor burden in an A549 xenograft model of cancer

To evaluate the clinical potential of the virus, *in vitro* growth curve analysis was performed on a panel of human cancer cells lines, and the fold-increase in virus production was determined (**Figure 7a**).

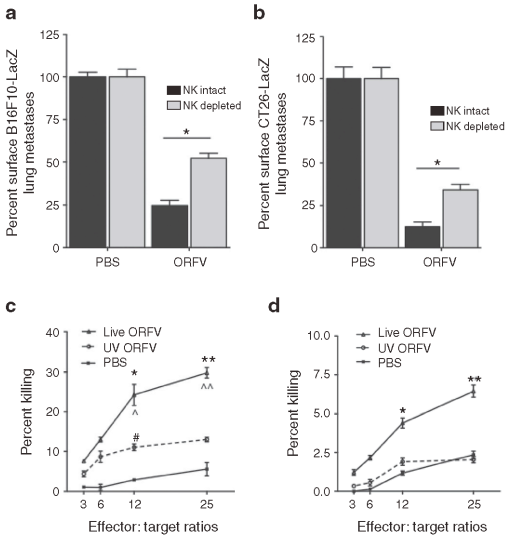

Figure 5 ORFV activation of NK cells is contributing to efficacy achieved in the lung models. (**a**) C57Bl/6 animals treated intravenously (i.v.) with three doses of PBS or ORFV (10^7) were depleted of NK cells using an optimized dose and schedule of anti-asialo i.v. or control IgG antibody. Animals were killed at 14 days after cell injection, lungs were isolated and processed, and the number of surface lung metastases was quantified, $N = 5$, mean ± SEM (*$P < 0.0005$ using an unpaired *t*-test with Welch's correction). (**b**) Balb/c animals treated i.v. with three doses of PBS or ORFV (10^7) were depleted of NK cells using an optimized dose and schedule of anti-asialo i.v. or control IgG antibody. Animals were killed at 10 days after cell injection, lungs were isolated and processed, and the number of surface lung metastases was quantified, $N = 10$, mean ± SEM (*$P < 0.05$ using an unpaired *t*-test with Welch's correction). *Ex vivo* cytotoxicity assays were performed on NK cells isolated from ORFV- or PBS-treated C57Bl/6 mice. Spleens were isolated, pooled, and enriched for NK cells by $DX5^+$ cell sorting. NK cells were then mixed with chromium-labeled B16F10-LacZ target cells in triplicate, at different effector:target ratios. (**c**) Shown is the percent killing of target B16F10-LacZ cells at 24 hours postinfection, $N = 3$, mean ± SEM (*$P < 0.05$, **$P < 0.005$ comparing live ORFV with PBS, $^{\wedge}P < 0.05$, $^{\wedge\wedge}P < 0.01$ comparing live ORFV with UV ORFV, $^{\#}P < 0.05$ comparing UV ORFV with PBS, using an unpaired *t*-test with Welch's correction). (**d**) Shown is the percent killing of target B16F10-LacZ cells at 72 hours postinfection, $N = 3$, mean ± SEM (*$P < 0.05$, **$P < 0.05$ using an unpaired *t*-test with Welch's correction). NK, natural killer; ORFV, Orf virus; PBS, phosphate-buffered saline; UV, ultraviolet.

ORFV was able to productively infect 9 of the 13 cell lines tested with over three-log output in A549 lung adenocarcinoma cells. ORFV growth curve analysis of infected A549 cancer cells and normal human dermal fibroblast cells highlights the preferential cytotoxicity and amplification in cancer cells (**Figure 7b,c**). To test ORFV *in vivo*, CD-1 nude mice were engrafted with A549 cells subcutaneously, and mice were treated intratumorally with five doses of ORFV (10^7) or PBS vehicle control. ORFV was able to significantly reduce A549 tumor burden as illustrated by tumor volume measurements (**Figure 7d**). Collectively, these data highlight the potential of ORFV as a replicating therapeutic for the treatment of human cancer.

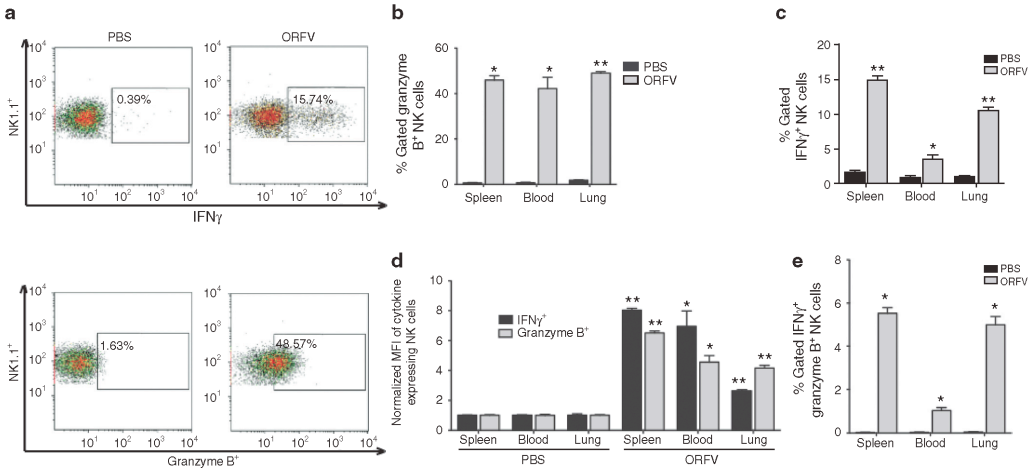

Figure 6 Flow cytometry analysis of ORFV-activated NK cells. (**a**) Tumor-bearing C57Bl/6 animals were treated intravenously (i.v.) with (10^7) ORFV or PBS. At 24 hours postinfection, tissues were harvested from animals, and processed by flow cytometry. Representative histograms of lymphocytes isolated from the lung of animals treated with PBS or ORFV are shown. (**b**) Percent-gated granzyme B expression from NK cells isolated from the spleen, blood, and lung of ORFV- and PBS-treated animals is compared, $N = 4$, mean ± SEM (*$P < 0.005$, **$P < 0.0001$ using an unpaired *t*-test with Welch's correction). (**c**) Percent-gated IFNγ expression from NK cells isolated from the spleen, blood, and lung of ORFV- and PBS-treated animals is compared, $N = 4$, mean ± SEM (*$P < 0.05$, **$P < 0.0005$ using an unpaired *t*-test with Welch's correction). (**d**) The amount of granzyme B and IFNγ expressed on per NK cell basis was determined using the mean fluorescence intensity (MFI). Data are shown as the fold-increase in MFI compared with PBS-treated animals, $N = 4$, mean ± SEM (*$P < 0.01$, **$P < 0.0005$ using an unpaired *t*-test with Welch's correction). (**e**) Percent-gated NK cells expressing both granzyme B and IFNγ were compared for lymphocytes isolated from PBS- and ORFV-treated animals, $N = 4$, mean ± SEM (*$P < 0.005$). IFNγ, interferon-γ; NK, natural killer; ORFV, Orf virus; PBS, phosphate-buffered saline.

DISCUSSION

We have identified and characterized the anticancer properties of a new poxvirus platform and show that ORFV treatment of both immune-competent and xenograft human tumor models leads to significant antitumor activity. Our results implicate NK cells in the ORFV-mediated reduction in tumor burden (Figure 4–6). In addition, we demonstrated by both expression of co-stimulatory molecules, and cytokines (**Supplementary Figure S7**) that ORFV therapy induces the activation of DCs. The exact mechanism by which ORFV stimulates the immune system is not yet known, but both TLR-dependent and independent mechanisms have been described including signaling via CD14.[28,29] It is possible, therefore, that NK cell activation by ORFV is indirect via DC activation, as previous reports have highlighted DC–NK cross-talk mechanisms induced by other OVs.[37]

In earlier studies, inactivated ORFV particles on their own were shown to stimulate a T_h-1-dominated immune response,[12,14,22] and so it was not surprising that UV-inactivated ORFV had a significant impact in the metastatic lung models (Figure 2d,e). Replicating ORFV, however, has a significantly greater impact in the lung models; possibly due to its induction of a more potent cytotoxic NK cell response (Figure 5c,d), coupled with its oncolytic activity in the murine cancer cells (Figure 2c). A number of OVs have been shown to induce potent adaptive antitumor immune responses (reviewed by Melcher *et al.*[38]), but only a select few have been shown to stimulate NK cell responses.[3,4,37] Because cytokine production by NK cells supports T_h-1 immunity,[39] the induction of IFNγ-secreting NK cells suggests that ORFV treatment could also lead to adaptive antitumor immune responses. Interestingly, several reports have now indicated that human[40] and mouse[41] NK cells can be divided into two phenotypically distinct subsets: poorly cytotoxic, cytokine-producing NK cells, and highly cytotoxic, poor cytokine–producing NK cells. Remarkably, we have shown that ORFV is capable of stimulating NK cells of both phenotypes (Figure 5,6).

In our preclinical studies, we observed significant increases in the size of spleens in ORFV-treated mice and this could represent a potential site for an adverse reaction. However, the splenomegaly was transient as immune cell populations returned to their normal proportions within 8 days after treatment. Kinetic studies have found that the ORFV-induced proinflammatory stimulation is balanced with subsequent induction of an anti-inflammatory response.[28,29] We believe that the unique biology of ORFV that allows for self-regulation of inflammatory responses can be exploited for safe and effective therapeutic benefit as we describe herein.

From a clinical perspective, we are encouraged that ORFV efficacy in murine lung tumor models was comparable or better than three other oncolytic poxviruses (**Supplementary Figure S2**), and that ORFV was able to infect a panel of human cancer cell lines (Figure 7a). In the literature, it has only ever been documented that ORFV can productively infect primary cell cultures prepared from bovine testis.[11,42,43] Our findings that a number of human tumor cell lines are permissive for ORFV replication is reminiscent of the earlier studies with MYXV that had documented a restricted host range of the virus, and later found MYXV to

a

Cell line	Cell origin	Fold increase
A549	Lung adenocarcinoma	1090
HeLa	Cervical carcinoma	551
NCI-H460	Lung carcinoma	243
HT1080	Fibrosarcoma	207
PLC/PRF/5	Hepatocellular carcinoma	88
SF295	Glioblastoma	54
SKBR-3	Breast adenocarcinoma	42
SKMEL-3	Melanoma	37
HOP92	Lung carcinoma	32
Ca127	Head and neck squamous cell carcinoma	3
786-0	Renal carcinoma	3
HT29	Colon carcinoma	2
SCC25	Head and neck squamous cell carcinoma	0

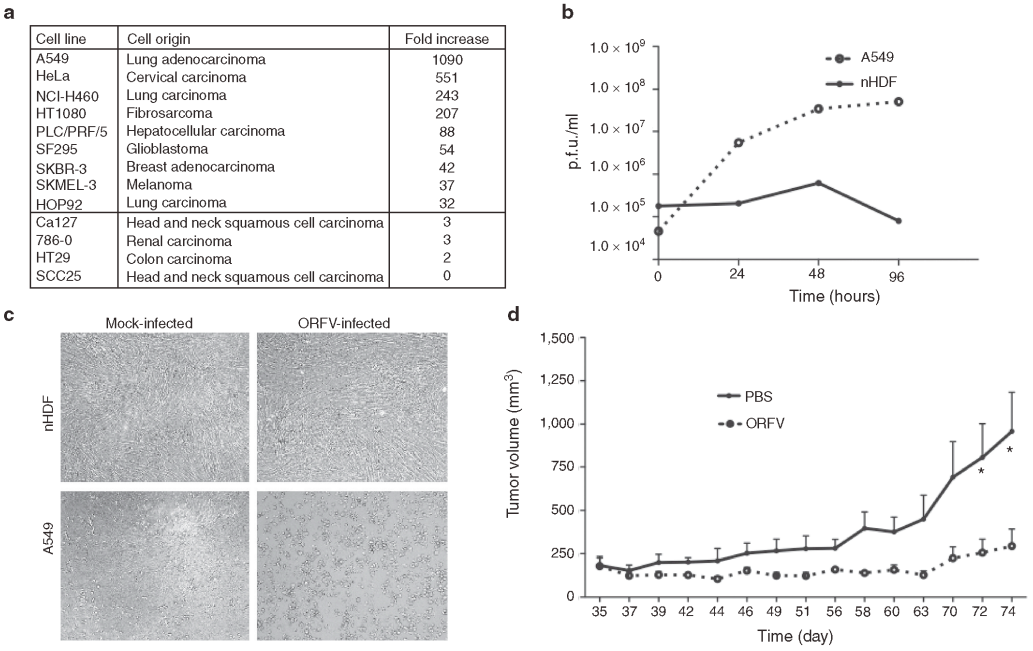

Figure 7 ORFV treatment of human xenograft tumors. (**a**) ORFV growth curves were performed on a panel of human cancer cell lines at an MOI of 1. Cells were infected at time 0, and cell lysates collected and processed for virus by OA3.Ts plaque assay at time-points postinfection. Virus titer was compared with input titers at 72 hours postinfection to calculate the fold-increase in ORFV. (**b**) Representative ORFV growth curves on A549 and nHDF cells at an MOI of 1. (**c**) Phase-contrast images of mock-infected and ORFV-infected A549 and nHDF cells at an MOI of 0.05, at 72 hours postinfection at a magnification of ×40. (**d**) Human A549 cells (2×10^6) were seeded subcutaneously into the right flank of CD-1 nude mice. ORFV (10^7) or PBS treatments were given intratumorally on days 24, 27, 29, 31, and 34 after tumor implantation. Mouse tumor volume was monitored over time, $N = 5$, mean ± SEM (*$P < 0.05$ using an unpaired *t*-test with Welch's correction). MOI, multiplicity of infection; nHDF, normal human dermal fibroblast; ORFV, Orf virus; PBS, phosphate-buffered saline; p.f.u., plaque-forming unit.

replicate well in human cancer cells.[44] Our data suggest, therefore, that like other OVs, ORFV may naturally be selective for cancer cell replication supported by alterations in signal-transduction pathways, like activated AKT for MYXV,[44] and defects in IFN signaling for vesicular stomatitis virus.[45] Indeed, we show here that ORFV can replicate in A549 cells and when engrafted into nude mice, has readily apparent antitumor activity *in vivo* (Figure 7d). These data emphasize ORFV's potential as a multimodality viral therapy for humans, where the virus could have both an oncolytic impact and potentially induce even greater immune responses than those reported here in the murine models.

The potential of ORFV in the activation of NK cells and human cancer cell oncolysis highlight the novel anticancer potential of the virus. Because antibody has been reported to be a barrier to OV therapy,[46] it is advantageous that the majority of the population has had limited exposure to ORFV, and that antibody does not prevent reoccurring infections in animals.[15,17,31,32] These characteristics, combined with the unique biology of the ORFV virion and its limited pathogenicity in humans, make it an attractive platform for the development of new anticancer biotherapeutics.

MATERIALS AND METHODS

Cell lines. Human and murine cell lines were maintained in Dulbecco's modified Eagle's medium (HyClone, Logan, UT) supplemented with 10% fetal calf serum (PAA Laboratories, Etobicoke, Ontario, Canada), and grown at 37°C and 5% CO_2. B16F10-LacZ cells were generated by stable transfection with LacZ complementary DNA, as described earlier.[47] Human tumor cell lines were from the NCI-60 reference panel: A549, HeLa, NCI-H460, HT1080, PLC/PRF/5, SF295, SKBR-3, SMKEL-3, HOP92, Cal27, 786-0, HT29, and SCC25. CT26.CL25 (CT26-LacZ), CT26, B16F10, and OA3.Ts were purchased from ATCC (Manassas, VA). Normal human dermal fibroblast cell cells were purchased from Cascade Biologics (Burlington, Ontario, Canada).

Viruses. Wild-type ORFV strain NZ2 and ORFV-LacZ (vascular endothelial growth factor–deleted LacZ-expressing ORFV) strain NZ2[11,42] were obtained from Dr Andrew Mercer (University of Otago, Dunedin, New Zealand). Oncolytic vaccinia virus, Raccoonpox and MYXV have been described previously.[34]

ORFV production, UV inactivation, and titering. Viral stocks were prepared by the infection of confluent OA3.Ts at a multiplicity of infection of 0.05. Cells and supernatants were harvested following a 5-day infection at 37°C, 5% CO_2 by gentle cell scraping. Cell lysates were collected by centrifugation, and resuspended in 1 mmol/l TRIS pH 9.0, and subjected to three

freeze–thaw cycles. Cell debris was removed by centrifugation, and lysates dounce homogenized before sucrose cushion purification in a JS-13.1 rotor at 11,500 r.p.m. for 1.5 hours at 4°C. Virus stocks were resuspended in PBS. Sham-infected OA3.Ts were processed as described above, and were used as vehicle control treatments. Inactivation of virus was performed on ORFV preparations at a concentration of 10^8 p.f.u./ml in PBS using UV-C irradiation in the Spectrolinker XL-1000 UV crosslinker (Spectronics, Westbury, NY) for 300 seconds. Confirmation of virus inactivation was measured by plaque assay before use. ORFV was titered on confluent monolayers of OA3.Ts using a carboxymethylcellulose overlay. Plaques were visualized following a 7-day incubation at 37°C by removal of overlay, and staining with 1% crystal violet (in 80% methanol). Vascular endothelial growth factor–deleted, LacZ-expressing ORFV plaques were visualized using a β-galactosidase-containing stain solution, as described previously.[48]

Animals. Female 6- to 8-week-old C57Bl/6, Balb/c and CD-1 nude mice were supplied by Charles River Canada (St Constant, Quebec, Canada), and were housed in a level 2 biocontainment facility at the Animal Care and Veterinary Services within the University of Ottawa. All animal experiments were conducted in accordance with the Animal Care and Veterinary Services standard operating procedures.

In vitro *viral infections.* For growth curve analysis, confluent monolayers of cells were infected in a minimal volume for 1 hour at 37°C and 5% CO_2. The viral inoculum was then removed, and replaced with Dulbecco's modified Eagle's medium 10% fetal calf serum. Cells and supernatants were harvested from wells at 0, 12, 24, 48, 72, and 96 hours postinfection. Cell lysates were subjected to three freeze–thaw cycles, and titered on OA3.Ts. Cytotoxicity was assessed in 96-well plates, using alamarBlue (AbD Serotec, Raleigh, NC) after a 72-hour infection period. NK cells were isolated from the spleens of C57Bl/6 mice by negative selection using magnetic sorting and the NK Isolation Kit (Miltenyi Biotec, Auburn, CA). DCs were isolated from C57Bl/6 mice using methods described previously.[37]

In vivo *tumor models.* For murine lung models, 10^5 CT26-LacZ cells were injected i.v. into Balb/c mice. Similarly, a density of 3×10^5 B16F10-LacZ cells was injected i.v. into C57Bl/6 mice. Mice were then treated i.v. with 1–3 doses of 10^7 p.f.u. ORFV in 100 µl of PBS, or control treated (100 µl of PBS or sham-infected lysates), on days 1, 3, and/or 8. At 10 days after CT26-LacZ injection, and 14 days FTER B16F10-LacZ injection, mice were anesthetized with Euthanyl, and lungs were harvested and stained with a β-galactosidase solution.[33] The number of lung metastases was determined by separation of lung lobes, and enumeration under a dissection microscope (Leica, Richmond Hill, Ontario, Canada). For Balb/c CT26-LacZ lung model survival experiments, animals were treated i.v. with three doses of 10^7 p.f.u. ORFV or control (100 µl of PBS), and were monitored for signs of respiratory distress. For the Balb/c CT26 subcutaneous tumor experiment, animals were challenged with 3×10^5 CT26 cells in the right flank, and were treated i.v. with 5 doses of 10^7 p.f.u. ORFV in 100 µl of PBS, or control treated (100 µl of PBS) on days 10, 14, 17, 21, and 24 after tumor implantation. For CD-1 nude xenograft experiments, 2×10^6 A549 cells were injected subcutaneously into the right flank of mice. At 23 days postimplantation, mice were treated intratumorally with five doses of 10^7 ORFV or PBS control. Subcutaneous tumors were measured 2–3 times per week using digital calipers. Animals were killed when tumor burden reached a volume of 1,500 mm^3.

Tissue distribution experiments. To determine the kinetics of the *in vivo* ORFV infection, lung tumor-bearing C57Bl/6 and Balb/c mice were treated with 10^7 p.f.u. of ORFV-LacZ i.v. Organs were then harvested from animals at specified time-points after infection. Tissues were first homogenized, and subjected to three freeze–thaw cycles before OA3.Ts plaque assay, as described above. To allow visualization of plaques at the lowest dilution in the presence of tissue debris, plaques were visualized using an β-galactosidase-containing staining solution.[48] To examine the pathology of lung tissues after ORFV therapy, Balb/c mice ($N = 2$) were challenged i.v. with 10^5 CT26-LacZ cells, followed by i.v. PBS or 10^7 ORFV at 24 hours. At 72 hours, animals were killed, and lungs isolated, fixed, and embedded in paraffin. Hematoxylin-and-eosin-stained sections of lung tissues were examined by a pathologist in a blinded fashion. Images were captured using Aperio ScanScope (Aperio Technologies, Vista, CA) and analyzed using a Aperio ImageScope software.

Flow cytometry. To analyze splenic lymphocyte populations (**Figure 4**) spleens were removed from animals, photographed, weighed, and red blood cells lyzed using ACK lysis buffer (0.15 mol/l NH_4Cl, 10 mmol/l $KHCO_3$, 0.1 mmol/l Na_2EDTA). Splenic lymphocytes were then analyzed for total number of NK, DC, and $CD8^+$ T cells, and CD69 expression by flow cytometry using the following antibodies: CD49b-PE (Clone DX5), CD3-PE (Clone 17A2), CD8-PECy5 (Clone 53-6.7) and CD69-FITC (Clone H1.2F3) from BD Biosciences (Mississauga, Ontario, Canada) and CD11c-FITC (Clone N418; eBioscience, San Diego, CA). NK cell cytokine secretion was examined in lymphocytes isolated from the spleen, blood, and lung of tumor-bearing C57Bl/6 animals (**Figure 6**) following a 5-hour GolgiPlug (BD Bioscience) incubation using the following antibodies: CD3-PerCP (clone 17A2; R&D Systems, Minneapolis, MN), and NK1.1-PE (Clone PK136), Granzyme B-AF700 (Clone GB11), and IFNγ-AF647 (Clone XMG1.2) from BD Bioscience. DC cytokine expression was examined from lymphocytes isolated from the spleen, blood, and lung of tumor-bearing C57Bl/6 animals (**Supplementary Figure S7**) following a 5-hour GolgiPlug (BD Bioscience) incubation using the following antibodies: CD11c-PECy7 (Clone N418), CD80-PE (Clone 16-10A1), CD86-PE (Clone GL-1), TNFα-FITC (Clone MP6-XT22) from eBioscience, and IL-12-APC (Clone C15.6; BD Bioscience). Experiments were performed on a Beckman Coulter CyAn and data analyzed using Kaluza software (version 1.1; Beckman Coulter, Brea, CA).

Cell depletion tumor models. NK cell depletion experiments were performed using an optimized dose and schedule of anti-asialo GM-1 (Cedarlane, Burlington, Ontario, Canada), or Rat IgG1 κ isotype control (BD Bioscience): 25 µl i.v. on days −4, −1, 2, 6, 9, and 13 where cancer cell injection and first ORFV treatment occur on days 0 and 1, respectively. NK cell depletion was confirmed at day 0 (before the beginning of the experiment) in both C57Bl/6 and Balb/c mice (**Supplementary Figure S6**). To allow for similar tumor burden in animals treated with the NK-depleting antibody, the challenge dose of B16F10-LacZ and CT26-LacZ was reduced in the NK-depleted animals to 9×10^4 and 5×10^4, respectively. $CD4^+$ and $CD8^+$ T cells were depleted in Balb/c mice using reagents and dose regimes established previously.[49]

NK cytotoxicity assays. Splenocytes were isolated from tumor naive ORFV- or PBS-treated C57Bl/6 mice at time-points postinfection. Isolated lymphocytes were pooled, and DX5-sorted (DX5 positive selection Kit; Miltenyi Biotec) on an Automacs Pro cell sorter (Miltenyi Biotec). B16F10-LacZ cells were harvested and labeled with Chromium-51 (Perkin Elmer, Waltham, MA) in the form of Na_2CrO_4 at 100 µCi for 60 minutes at 37°C. Sorted NK cells from ORFV- or PBS-treated animals resuspended at a concentration of 2.5×10^6 cells/ml and mixed with target B16F10-LacZ, which were resuspended at a concentration of 5×10^4 cells/ml at different effector-to-target ratios (50:1, 25:1, 12:1, and 6:1). The mixture was incubated for 4 hours before the analysis of chromium release in the supernatant using a gamma counter (Perkin Elmer).

SUPPLEMENTARY MATERIAL

Figure S1. ORFV efficacy in two additional Balb/c tumor models.
Figure S2. ORFV efficacy compared with other oncolytic viruses.
Figure S3. Kinetics of *in vivo* ORFV infection and CT26-LacZ tumor debulking in Balb/c animals.
Figure S4. H&E staining of lung tissues from ORFV- and control-treated Balb/c animals.
Figure S5. *In vivo* ORFV efficacy in the absence of T cells.

Figure S6. Flow cytometry analysis to test for NK cell depletion.
Figure S7. Flow cytometry analysis of ORFV activated dendritic cells.

ACKNOWLEDGMENTS

J.L.R. and C.G.L. are supported by CIHR Doctoral awards: Frederick Banting and Charles Best Canada Graduate Scholarship. L.-H.T. is supported by a Fonds de Reserche Sante Quebec—postdoctoral fellowship. This work was supported by grants from the Terry Fox Foundation (J.C.B. and H.L.A.), Ontario Institute for Cancer Research (P.S.O., H.L.A., R.C.A., J.C.B., B.D.L. and Y.W.), Canadian Cancer Society (B.D.L.), Canadian Institutes of Health Research (J.C.B. and H.L.A.), and from the Health Research Council of New Zealand (A.A.M.). Thanks to Harman Sekhon for his technical expertise and Ellena Whelan for her guidance, and technical expertise. Thanks to Kelley Parato for editing the manuscript.

REFERENCES

1. Breitbach, CJ, Paterson, JM, Lemay, CG, Falls, TJ, McGuire, A, Parato, KA *et al.* (2007). Targeted inflammation during oncolytic virus therapy severely compromises tumor blood flow. *Mol Ther* **15**: 1686–1693.
2. Breitbach, CJ, De Silva, NS, Falls, TJ, Aladl, U, Evgin, L, Paterson, J *et al.* (2011). Targeting tumor vasculature with an oncolytic virus. *Mol Ther* **19**: 886–894.
3. Prestwich, RJ, Ilett, EJ, Errington, F, Diaz, RM, Steele, LP, Kottke, T *et al.* (2009). Immune-mediated antitumor activity of reovirus is required for therapy and is independent of direct viral oncolysis and replication. *Clin Cancer Res* **15**: 4374–4381.
4. Apostolidis, L, Schirrmacher, V and Fournier, P (2007). Host mediated anti-tumor effect of oncolytic Newcastle disease virus after locoregional application. *Int J Oncol* **31**: 1009–1019.
5. Mastrangelo, MJ, Maguire, HC Jr, Eisenlohr, LC, Laughlin, CE, Monken, CE, McCue, PA *et al.* (1999). Intratumoral recombinant GM-CSF-encoding virus as gene therapy in patients with cutaneous melanoma. *Cancer Gene Ther* **6**: 409–422.
6. Bridle, BW, Hanson, S and Lichty, BD (2010). Combining oncolytic virotherapy and tumour vaccination. *Cytokine Growth Factor Rev* **21**: 143–148.
7. Kaufman, HL and Bines, SD (2010). OPTIM trial: a Phase III trial of an oncolytic herpes virus encoding GM-CSF for unresectable stage III or IV melanoma. *Future Oncol* **6**: 941–949.
8. Galivo, F, Diaz, RM, Wongthida, P, Thompson, J, Kottke, T, Barber, G *et al.* (2010). Single-cycle viral gene expression, rather than progressive replication and oncolysis, is required for VSV therapy of B16 melanoma. *Gene Ther* **17**: 158–170.
9. Breitbach, CJ, Burke, J, Jonker, D, Stephenson, J, Haas, AR, Chow, LQ *et al.* (2011). Intravenous delivery of a multi-mechanistic cancer-targeted oncolytic poxvirus in humans. *Nature* **477**: 99–102.
10. Haig, D, McInnes, C, Deane, D, Lear, A, Myatt, N, Reid, H *et al.* (1996). Cytokines and their inhibitors in orf virus infection. *Vet Immunol Immunopathol* **54**: 261–267.
11. Savory, LJ, Stacker, SA, Fleming, SB, Niven, BE and Mercer, AA (2000). Viral vascular endothelial growth factor plays a critical role in orf virus infection. *J Virol* **74**: 10699–10706.
12. Schütze, N, Raue, R, Büttner, M and Alber, G (2009). Inactivated parapoxvirus ovis activates canine blood phagocytes and T lymphocytes. *Vet Microbiol* **137**: 260–267.
13. Weber, O, Siegling, A, Friebe, A, Limmer, A, Schlapp, T, Knolle, P *et al.* (2003). Inactivated parapoxvirus ovis (Orf virus) has antiviral activity against hepatitis B virus and herpes simplex virus. *J Gen Virol* **84**(Pt 7): 1843–1852.
14. Fachinger, V, Schlapp, T, Strube, W, Schmeer, N and Saalmüller, A (2000). Poxvirus-induced immunostimulating effects on porcine leukocytes. *J Virol* **74**: 7943–7951.
15. Czerny, CP, Zeller-Lue, C, Eis-Hübinger, AM, Kaaden, OR and Meyer, H (1997). Characterization of a cowpox-like orthopox virus which had caused a lethal infection in man. *Arch Virol Suppl* **13**: 13–24.
16. Robinson, AJ and Petersen, GV (1983). Orf virus infection of workers in the meat industry. *N Z Med J* **96**: 81–85.
17. Haig, DM and Mercer, AA (1998). Ovine diseases. Orf. *Vet Res* **29**: 311–326.
18. Lederman, ER, Green, GM, DeGroot, HE, Dahl, P, Goldman, E, Greer, PW *et al.* (2007). Progressive ORF virus infection in a patient with lymphoma: successful treatment using imiquimod. *Clin Infect Dis* **44**: e100–e103.
19. Lear, A, Hutchinson, G, Reid, H, Norval, M, and Haig, D (1996). Phenotypic characterisation of the dendritic cells accumulating in ovince dermis following primary and secondary orf virus infections. *Eur J Dermatol* **6**: 135–140.
20. Jenkinson, DM, McEwen, PE, Onwuka, SK, Moss, VA, Elder, HY, Hutchinson, G *et al.* (1990). The pathological changes and polymorphonuclear and mast cell responses in the skin of spcific pathogen-free lambs following primary and secondary challenge with orf virus. *Vet Dermatol* **2**: 1–9.
21. Jenkinson, DM, Hutchison, G and Reid, H (1992). The B and T cell responses to orf virus infection. *Vet Derm* **3**: 57–64.
22. Büttner, M, Czerny, CP, Lehner, KH and Wertz, K (1995). Interferon induction in peripheral blood mononuclear leukocytes of man and farm animals by poxvirus vector candidates and some poxvirus constructs. *Vet Immunol Immunopathol* **46**: 237–250.
23. Haig, DM, Hutchinson, G, Thomson, J, Yirrell, D and Reid, HW (1996). Cytolytic activity and associated serine protease expression by skin and afferent lymph CD8+ T cells during orf virus reinfection. *J Gen Virol* **77 (Pt 5)**: 953–961.
24. Haig, DM and McInnes, CJ (2002). Immunity and counter-immunity during infection with the parapoxvirus orf virus. *Virus Res* **88**: 3–16.
25. Haig, D, Deane, D, Percival, A, Myatt, N, Thomson, J, Inglis, L *et al.* (1996). The cytokine response of afferent lymph following orf virus reinfection of sheep. *Vet Dermatol* **7**: 11–20.
26. Mayr, A, Büttner, M, Wolf, G, Meyer, H and Czerny, C (1989). [Experimental detection of the paraspecific effects of purified and inactivated poxviruses]. *Zentralblatt Veterinarmedizin Reihe B* **36**: 81–99.
27. Yirrell, DL, Vestey, JP and Norval, M (1994). Immune responses of patients to orf virus infection. *Br J Dermatol* **130**: 438–443.
28. Friebe, A, Siegling, A, Friederichs, S, Volk, HD and Weber, O (2004). Immunomodulatory effects of inactivated parapoxvirus ovis (ORF virus) on human peripheral immune cells: induction of cytokine secretion in monocytes and Th1-like cells. *J Virol* **78**: 9400–9411.
29. Friebe, A, Friederichs, S, Scholz, K, Janssen, U, Scholz, C, Schlapp, T *et al.* (2011). Characterization of immunostimulatory components of orf virus (parapoxvirus ovis). *J Gen Virol* **92**(Pt 7): 1571–1584.
30. Sullivan, JT, Mercer, AA, Fleming, SB and Robinson, AJ (1994). Identification and characterization of an orf virus homologue of the vaccinia virus gene encoding the major envelope antigen p37K. *Virology* **202**: 968–973.
31. Czerny, CP, Waldmann, R and Scheubeck, T (1997). Identification of three distinct antigenic sites in parapoxviruses. *Arch Virol* **142**: 807–821.
32. Buddle, BM, Dellers, RW and Schurig, GG (1984). Contagious ecthyma virus-vaccination failures. *Am J Vet Res* **45**: 263–266.
33. Stanford, MM, Shaban, M, Barrett, JW, Werden, SJ, Gilbert, PA, Bondy-Denomy, J *et al.* (2008). Myxoma virus oncolysis of primary and metastatic B16F10 mouse tumors in vivo. *Mol Ther* **16**: 52–59.
34. Evgin, L, Vähä-Koskela, M, Rintoul, J, Falls, T, Le Boeuf, F, Barrett, JW *et al.* (2010). Potent oncolytic activity of raccoonpox virus in the absence of natural pathogenicity. *Mol Ther* **18**: 896–902.
35. Wang, M, Bronte, V, Chen, PW, Gritz, L, Panicali, D, Rosenberg, SA *et al.* (1995). Active immunotherapy of cancer with a nonreplicating recombinant fowlpox virus encoding a model tumor-associated antigen. *J Immunol* **154**: 4685–4692.
36. Epaulard, O, Toussaint, B, Quenee, L, Derouazi, M, Bosco, N, Villiers, C *et al.* (2006). Anti-tumor immunotherapy via antigen delivery from a live attenuated genetically engineered Pseudomonas aeruginosa type III secretion system-based vector. *Mol Ther* **14**: 656–661.
37. Boudreau, JE, Stephenson, KB, Wang, F, Ashkar, AA, Mossman, KL, Lenz, LL *et al.* (2011). IL-15 and type I interferon are required for activation of tumoricidal NK cells by virus-infected dendritic cells. *Cancer Res* **71**: 2497–2506.
38. Melcher, A, Parato, K, Rooney, CM and Bell, JC (2011). Thunder and lightning: immunotherapy and oncolytic viruses collide. *Mol Ther* **19**: 1008–1016.
39. Martín-Fontecha, A, Thomsen, LL, Brett, S, Gerard, C, Lipp, M, Lanzavecchia, A *et al.* (2004). Induced recruitment of NK cells to lymph nodes provides IFN-gamma for T(H)1 priming. *Nat Immunol* **5**: 1260–1265.
40. Cooper, MA, Fehniger, TA and Caligiuri, MA (2001). The biology of human natural killer-cell subsets. *Trends Immunol* **22**: 633–640.
41. Silva, A, Andrews, DM, Brooks, AG, Smyth, MJ and Hayakawa, Y (2008). Application of CD27 as a marker for distinguishing human NK cell subsets. *Int Immunol* **20**: 625–630.
42. Wise, LM, Savory, LJ, Dryden, NH, Whelan, EM, Fleming, SB and Mercer, AA (2007). Major amino acid sequence variants of viral vascular endothelial growth factor are functionally equivalent during Orf virus infection of sheep skin. *Virus Res* **128**: 115–125.
43. Balassu, TC and Robinson, AJ (1987). Orf virus replication in bovine testis cells: kinetics of viral DNA, polypeptide, and infectious virus production and analysis of virion polypeptides. *Arch Virol* **97**: 267–281.
44. Wang, G, Barrett, JW, Stanford, M, Werden, SJ, Johnston, JB, Gao, X *et al.* (2006). Infection of human cancer cells with myxoma virus requires Akt activation via interaction with a viral ankyrin-repeat host range factor. *Proc Natl Acad Sci USA* **103**: 4640–4645.
45. Stojdl, DF, Lichty, BD, tenOever, BR, Paterson, JM, Power, AT, Knowles, S *et al.* (2003). VSV strains with defects in their ability to shutdown innate immunity are potent systemic anti-cancer agents. *Cancer Cell* **4**: 263–275.
46. Willmon, C, Harrington, K, Kottke, T, Prestwich, R, Melcher, A and Vile, R (2009). Cell carriers for oncolytic viruses: Fed Ex for cancer therapy. *Mol Ther* **17**: 1667–1676.
47. Kirstein, JM, Graham, KC, Mackenzie, LT, Johnston, DE, Martin, LJ, Tuck, AB *et al.* (2009). Effect of anti-fibrinolytic therapy on experimental melanoma metastasis. *Clin Exp Metastasis* **26**: 121–131.
48. Chakrabarti, S, Brechling, K and Moss, B (1985). Vaccinia virus expression vector: coexpression of beta-galactosidase provides visual screening of recombinant virus plaques. *Mol Cell Biol* **5**: 3403–3409.
49. Ohashi, PS, Oehen, S, Buerki, K, Pircher, H, Ohashi, CT, Odermatt, B *et al.* (1991). Ablation of "tolerance" and induction of diabetes by virus infection in viral antigen transgenic mice. *Cell* **65**: 305–317.

APPENDIX IV: A SELECTABLE AND EXCISABLE MARKER SYSTEM FOR THE RAPID CREATION OF RECOMBINANT POXVIRUSES

Julia L. Rintoul, Jiahu Wang, Don B. Gammon, Nicholas J. van Buuren, Kenneth Garson, Karen Jardine, Michele Barry, David H. Evans, John C. Bell

Contribution:

Cloning of constructs was performed by myself, and Jiahu. I performed all of the sequencing, PCR, virus manufacturing and titering. Southern blot analysis was performed by Jiahu and myself, with input from Karen. The wetbench work associated Figures 5 and 6 was performed by Don and Nicholas, res

pectively. Kenneth created the plasmid illustrations. Western blotting and immuno-fluorescence was performed by Jiahu. I wrote the manuscript, and revised the manuscript for editorial approval with input from Jiahu, Don, Michele, David and John.

Published: *PLoS ONE, September 2011*

OPEN ACCESS Freely available online

PLoS one

A Selectable and Excisable Marker System for the Rapid Creation of Recombinant Poxviruses

Julia L. Rintoul[1,2◔], Jiahu Wang[2◔], Don B. Gammon[3], Nicholas J. van Buuren[3], Kenneth Garson[2], Karen Jardine[2], Michele Barry[3], David H. Evans[3], John C. Bell[1,2]*

1 Department of Biochemistry, Microbiology and Immunology, Faculty of Medicine, University of Ottawa, Ottawa, Canada, **2** Centre for Cancer Therapeutics, Ottawa Hospital Research Institute, Ottawa, Canada, **3** Department of Medical Microbiology and Immunology, Faculty of Medicine and Dentistry, Li Ka Shing Institute of Virology, University of Alberta, Edmonton, Canada

Abstract

Background: Genetic manipulation of poxvirus genomes through attenuation, or insertion of therapeutic genes has led to a number of vector candidates for the treatment of a variety of human diseases. The development of recombinant poxviruses often involves the genomic insertion of a selectable marker for purification and selection purposes. The use of marker genes however inevitably results in a vector that contains unwanted genetic information of no therapeutic value.

Methodology/Principal Findings: Here we describe an improved strategy that allows for the creation of marker-free recombinant poxviruses of any species. The Selectable and Excisable Marker (SEM) system incorporates a unique fusion marker gene for the efficient selection of poxvirus recombinants and the Cre/loxP system to facilitate the subsequent removal of the marker. We have defined and characterized this new methodological tool by insertion of a foreign gene into vaccinia virus, with the subsequent removal of the selectable marker. We then analyzed the importance of loxP orientation during Cre recombination, and show that the SEM system can be used to introduce site-specific deletions or inversions into the viral genome. Finally, we demonstrate that the SEM strategy is amenable to other poxviruses, as demonstrated here with the creation of an ectromelia virus recombinant lacking the *EVM002* gene.

Conclusion/Significance: The system described here thus provides a faster, simpler and more efficient means to create clinic-ready recombinant poxviruses for therapeutic gene therapy applications.

Citation: Rintoul JL, Wang J, Gammon DB, van Buuren NJ, Garson K, et al. (2011) A Selectable and Excisable Marker System for the Rapid Creation of Recombinant Poxviruses. PLoS ONE 6(9): e24643. doi:10.1371/journal.pone.0024643

Editor: William P. Halford, Southern Illinois University School of Medicine, United States of America

Received December 23, 2010; **Accepted** August 16, 2011; **Published** September 8, 2011

Funding: This work was supported by grants from the National Cancer Institute of Canada, Terry Fox Foundation, Natural Sciences Engineering Research Council, and the Canadian Institutes of Health Research to JB, DE and MB. JLR was supported by a CIHR Doctoral award: Frederick Banting and Charles Best Canada Graduate Scholarship. JW was supported by a Lymphoma Research Foundation of Canada Research Fellowship. DBG was supported by a Ralph Steinhauer Award of Distinction from the Province of Alberta. NJVB was supported by a Doctoral NSERC Canada Graduate Scholarship and an Alberta Heritage Foundation for Medical Research Incentive Award. MB holds a Tier I Canada Research Chair, a Howard Hughes International Scholar Award and an Alberta Heritage for Medical Research Senior Scholar award. The funders had no role in the study design, data collection and analysis, decision to publish, or preparation of the manuscript.

Competing Interests: The authors have declared that no competing interests exist.

◔ These authors contributed equally to this work.

Introduction

Poxviruses comprise a large family of double-stranded DNA viruses that infect a wide range of hosts. Vaccinia virus (VV) is the prototypic member of the *Orthopoxvirus* genus and the best-studied virus in the poxvirus family. Since the eradication of smallpox [1], VV and other poxvirus species have continued to be used for the treatment of human disease [2,3] in part because a greater understanding of poxvirus biology has led to safer and more efficacious poxvirus-based therapeutics. The poxvirus genome is easily genetically modified and can accommodate inserts exceeding 25 kb [4] using strategies that are dependent upon virus-encoded homologous recombination [5,6]. Using these approaches, recombinant VV has since proven to be valuable as a vector for gene therapy in a number of therapeutic applications [4,7,8,9,10,11,12,13,14,15]. Similarly, other members of the poxvirus family have also been explored for their potential as viral vectors for therapeutic purposes [9,10,16,17]. Genetically engineered poxviruses that express immunogens from other infectious agents have shown some promise as novel vaccines against diseases like acquired immunodeficiency syndrome [11], malaria [12], tuberculosis [18], and cancer [7,8,10,13]. As a cancer vaccine, poxviruses have the potential to generate a strong anti-tumoural immune response, especially when genetically modified to express cytokines like IL-2 [14] or cell surface receptors like CD70 that are indicative of oncogenic transformation [15]. Lastly, poxviruses have been successfully engineered as oncolytic agents, offering the advantage of a strong anti-tumoural immune response combined with cancer cell-specific replication [7,16,17,19,20]. A number of these poxvirus candidates have advanced to human clinical trials [10,11,12,13,19], highlighting the therapeutic potential of poxvirus recombinants.

Poxvirus recombinants are typically produced by constructing a plasmid containing the gene(s) of interest flanked by DNA sequences homologous to the desired target locus, followed by transfection of the plasmid into VV infected cells to allow for

recombination of the homologous sequences between the vector and the viral genome [21]. Using traditional approaches, the frequency of recombination is typically less than 0.1% [22], and the isolation of purified recombinant virus is tedious and time-consuming. Recombinant poxviruses are often attenuated, and have reduced growth kinetics and plaque size compared to their wild type counterparts [23]. Historically, the target site of choice has been VV thymidine kinase (Tk), but any non-essential locus can be modified or disrupted in this manner. Recombinants are then isolated and plaque purified. A number of selection methods have been described including selection for Tk-positive or negative phenotypes [21], and resistance to neomycin [24] or mycophenolic acid (MPA) [25]. One can also use plaque assays to identify viruses encoding β-galactosidase [26], β-glucuronidase [27], or fluorescent reporter constructs [28].

Although these methods work well and greatly facilitate the recovery of recombinant viruses, the use of selectable markers inevitably results in the creation of a product that contains genetic information with no therapeutic value. Recombinant poxvirus therapeutics would be considered safer vectors (most notably in the view of regulatory agencies), if the selectable markers were removed from the poxvirus genome [29]. Furthermore, the expression of marker genes from recombinant poxviruses may affect the overall fitness of the virus. Demmin *et al.* have shown that the expression levels of neighboring genes can be affected by the highly active transcription of marker genes incorporated into other large DNA viruses [30].

To facilitate the removal of selectable markers, Falkner and colleagues [31,32] developed transient selection methods wherein a selectable marker is flanked by tandem DNA repeats. The virus is stable while under selection, however the marker is lost through VV dependent homologous recombination once the selection pressure is removed. A similar system was employed by Alejo *et al.*, to create ECTV recombinants [33]. Although these authors describe efficiencies in excess of 90% for removal of the selectable marker, the recombination reaction is a random and lengthy process that relies on poxvirus machinery, and involves more than six rounds of purification. Typically, the efficiency of poxvirus recombination is quite low [22], recombinant viruses are often attenuated and hard to propagate in the presence of wild-type virus [34], and many time-consuming rounds of plaque purification are needed to isolate the desired final viral product. An improved technology is needed that allows for the specific, controlled and efficient removal of selectable markers from recombinant poxvirus genomes.

Here we define a new methodological tool for rapidly producing marker-free recombinant poxviruses. This improved vector development system, which we have termed Selectable and Excisable Marker (SEM), takes advantage of the well-characterized Cre/loxP site-specific recombination system to efficiently excise the reporter gene [35,36]. This strategy avoids the many rounds of passage that are required when using virus recombination systems to excise genes flanked by tandemly duplicated elements [31,32,33]. The SEM system offers the convenience of positive selection of recombinants using both fluorescent and/or drug-based strategies. Since recombinant poxvirus therapeutics are often created with multiple gene knockouts (or knock-ins), the SEM system was designed to be re-usable, therefore eliminating the use of additional reporter genes that would otherwise complicate and lengthen the overall cloning and selection processes. To demonstrate the efficiency and utility of the method, we have applied the SEM strategy to generate viruses with targeted disruptions of different genes using two different poxvirus species. Our results suggest that the SEM vector development system will not only be useful for the creation of novel poxvirus therapeutics, but also for basic virological studies.

Results

Characterization of the components of the SEM system

The Selectable and Excisable Marker system is summarized in **Fig. 1A**. The first generation transfer vector pSEM-1 encoded a foreign gene (firefly luciferase), a selectable marker as a fusion between *yellow fluorescent protein* (*yfp*) and *guanine phosphoribosyltransferase* (*gpt*) genes, and loxP sites in the same orientation flanking the selectable marker, with the target insertion site as the VV Tk locus (**Fig. 1B**). To confirm that the expression of YFP was not disrupted from the creation of the YFP-GPT fusion protein, YFP expression was analyzed by western blot from U2OS cells either mock-transfected (lane 1), or transiently transfected with either pEYFP-C1 as a positive control (lane 2) or plasmids containing the *yfp-gpt* fused gene (pEYFP-gpt or pEYFP-gpt-1loxP) in lanes 3 and 4, respectively (**Figure S1A**). The YFP and YFP-GPT fusion proteins have predicted molecular weights of 26 and 45.5 kDa respectively.

The cellular distribution of Cre from Cre recombinase-expressing cell lines was analyzed by immunofluorescence from parental U2OS cells (control), nuclear Cre cells (Nuc-Cre), and cytoplasmic Cre (Cyto-Cre) cells illustrating that the absence of the nuclear localization sequence in the Nuc-Cre cells leads to accumulation of the enzyme in the cytoplasm (**Fig. 1C**). Cre expression levels were compared among mock-transfected U2OS, U2OS cells transiently transfected with pMC-Cre, and both stable cell lines (**Fig. 1D**). In cells that were transiently or stably expressing Cre-recombinase, anti-Cre western blot analysis identified a band at 35 kDa, corresponding to the Cre enzyme. The expression of Cre in the stable cell lines was 2-fold greater when compared to the transiently transfected cells.

Isolation of a marker-free Tk-deleted, luciferase-expressing VV using the SEM system

(YFP)-based fluorescence activated cell sorting (FACS) was performed on mock infected U2OS cells as a control, and U2OS cells that had been infected with a mixture of parental VV (Wyeth strain), and recombinant VV generated from pSEM-1 expressing the YFP-GPT fusion protein (VV-ΔTk-*yfp-gpt*) (**Fig. 2A**). To ensure the highest possible FACS stringency, a cut-off of 0.5% background fluorescence was maintained by comparing the mock-infected U2OS cells to the recombinant YFP-expressing VV infected U2OS cells (235 positive background cells from 47,421 U2OS cells counted, compared to 3004 positive recombinant VV infected cells, from 49,498 U2OS counted). These sorted cells were then mixed with uninfected U2OS cells, plated into multi-well dishes, and subjected to two more rounds of YFP^+ plaque purification.

To promote fast and simple removal of the *yfp-gpt* cassette from recombinant viruses generated using the SEM system, viruses were passaged on a U2OS cell line expressing a cytoplasmic form of Cre recombinase. VV-ΔTk-*yfp*-gpt-1loxP (control virus) and VV-ΔTk-*yfp-gpt* recombinant VV were passaged on either parental U2OS cells, or U2OS cells stably expressing cytoplasmic Cre recombinase (U2OS-Cre) (**Fig. 2B**). The U2OS cells were monitored for both YFP fluorescence and for luciferase-mediated bioluminescence using the IVIS Imager (Xenogen) and Living Image® v2.5 software. As shown in the top half of **Fig. 2B**, both VV-ΔTk-*yfp-gpt*-1loxP control virus, and VV-ΔTk-*yfp-gpt* viruses express luciferase and YFP when used to infect parental U2OS cells. Infection of U2OS-Cre cells by the VV-ΔTk-*yfp-gpt*-1loxP and

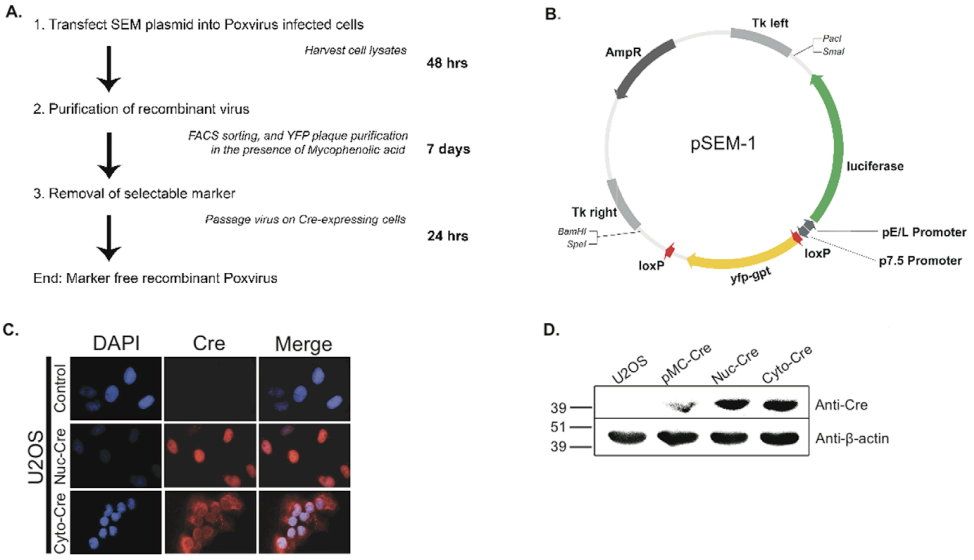

Figure 1. Overview of the poxvirus Selectable and Excisable Marker cloning system. (**A**) Schematic illustrating the Selectable and Excisable Marker poxvirus cloning system. (**B**) First generation poxvirus cloning vector pSEM-1 with labeled open reading frames. (**C**) Immunofluorescence detection of Cre recombinase from U2OS cell lines expressing nuclear or cytoplasmic Cre, or control U2OS cells. (**D**) Western blot analysis of Cre recombinase from U2OS cells mock transfected (U2OS), transiently transfected (pMC-Cre) or stably expressing Cre recombinase targeted to either the nucleus or the cytoplasm (Nuc-Cre and Cyto-Cre respectively).
doi:10.1371/journal.pone.0024643.g001

VV-ΔTk-*yfp-gpt* viruses led to strong luciferase transgene expression, however expression of YFP is only detectable from cells infected with the VV-ΔTk-*yfp-gpt*-1loxP virus. This illustrates the qualitative efficiency by which Cre-expressing U2OS cells excise loxP-flanked markers, as well as the stability of the transgene expression during the recombination reaction. To quantitatively determine the efficiency of the Cre recombination reaction, U2OS cells expressing Cre recombinase were infected with the VV-ΔTk-*yfp-gpt* virus. Virus progeny was then analyzed for the percent YFP positive versus negative virus plaques by U2OS plaque assay. As seen in Figure 2C, both cytoplasmic and nuclear Cre expression from stable cell lines resulted in nearly 100% efficiency for marker gene excision, whereas transient transfection of Cre recombinase was only 44% efficient.

The genomic composition of the VV recombinant viruses was analyzed by PCR of viral DNA before and after removal of the *yfp-gpt* cassette. A schematic of the virus genome at the Tk insertion site is shown (**Fig. 2D**) to illustrate the primer pairs used in the analysis. Primers were designed to amplify regions of DNA at the insertion site (i and iv), surrounding the luciferase transgene (ii), and across the *yfp-gpt* selectable marker (iii). For three of the PCR reactions (primer pairs i, ii, and iv), the amplicons for each of the viruses tested were the same and show that the Cre recombination reaction does not affect the genome structure outside of the 2loxP region (ii), and that the Tk locus was the site of homologous recombination (i, iv) (**Fig. 2E**). Prior to passage on Cre-expressing cells, PCR using primer pair (iii) of DNA from both VV-ΔTk-*yfp-gpt*-1loxP and VV-ΔTk-*yfp-gpt* viruses produced bands at 1900 and 2000 bp, respectively. The 100 bp difference can be attributed to the lack of one loxP site in the VV-ΔTk-*yfp-gpt*-1loxP virus. PCR of DNA from the marker-free recombinant VV-ΔTk' virus using primer pair (iii), produced a much smaller band due to Cre-mediated deletion of the *yfp-gpt* gene.

Genomic analysis and confirmation of identity of 3 independent clones of the VV-ΔTk-*yfp-gpt* and VV-ΔTk' viruses

The genomic composition of the VV-ΔTk-*yfp-gpt* and VV-ΔTk' viruses was analyzed by restriction enzyme digestion, southern blot hybridization and sequencing analysis at the Cre-recombination site (**Fig. 3**). Three independent clones of the VV-ΔTk-*yfp-gpt* virus were compared to the parental VV Wyeth strain, before and after passage on Cre-expressing cells. The DNA fragment containing the Tk insertion site is highlighted (arrow) in the digest of the parental VV Wyeth virus. Interestingly, the *yfp-gpt* cassette included a HindIII restriction site. This led to a unique DNA digest for the VV-ΔTk-*yfp-gpt* clones (**Fig. 3A**). The DNA fragment containing the Tk insertion site is disrupted in digests of the VV-ΔTk-*yfp-gpt* viruses, and is represented by unique bands at ~6000 and ~2800 bp (see arrows, **Fig. 3A**). Digests of the VV-ΔTk' clones resemble the parental VV digest, since the *yfp-gpt* cassette was removed by Cre-recombination. Importantly, the southern hybridization for *yfp* demonstrates that there was only 1 insertion site of *yfp-gpt* during poxvirus homologous recombination (**Fig. 3B**). DNA sequence analysis of the 3 VV-ΔTk' clones was performed to illustrate the consistency of the residual DNA signature following Cre-recombination. A DNAStar sequence alignment of the DNA from each of the 3 VV-ΔTk' clones

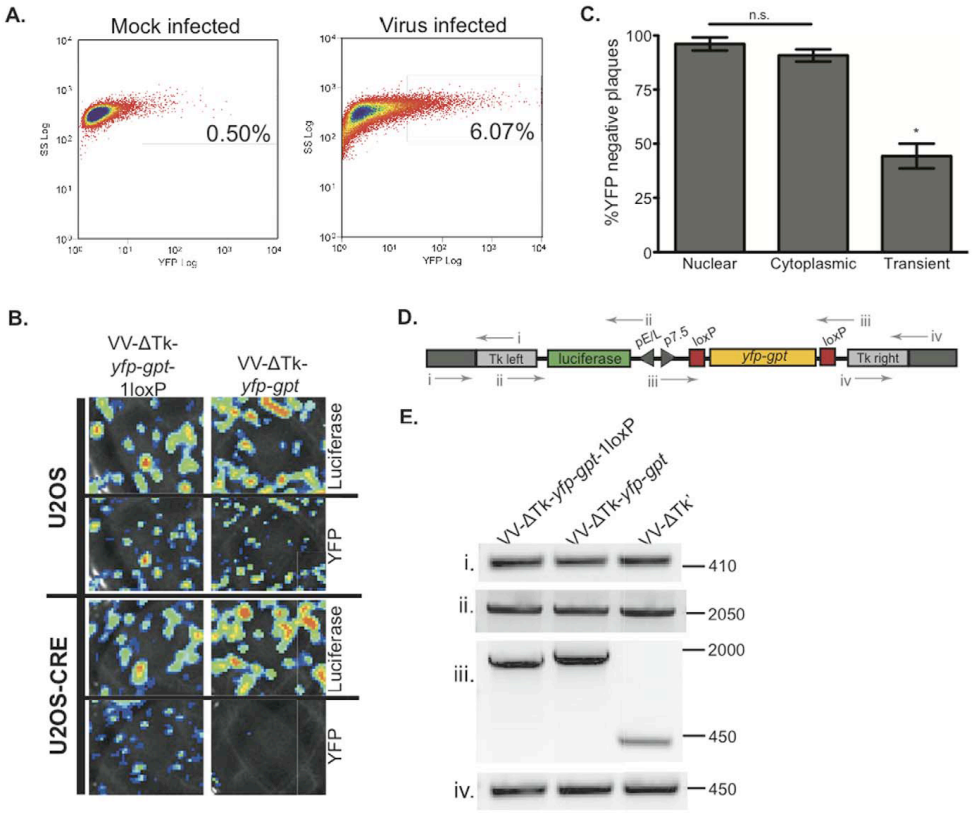

Figure 2. FACS purification of recombinant VV-ΔTk infected cells and Cre-recombinase mediated removal of the selectable marker. (**A**) Dot plot of YFP fluorescence versus side scatter from Fluorescence Activated Cell Sorting (FACS) analysis of U2OS cells mock infected, or infected with a mixture of parental VV and recombinant VV virus expressing YFP. (**B**) Purified recombinant VV-ΔTk-*yfp-gpt*-1loxP (control virus) or VV-ΔTk-*yfp-gpt* virus were used to infect stable cytoplasmic Cre-expressing cells (U2OS-Cre) or parental U2OS cells in 6-well plates, and were monitored for foreign gene expression (firefly luciferase) and marker gene expression (YFP-GPT fusion protein). (**C**) Percent YFP-negative VV-ΔTk' plaques on U2OS cells after passage of virus on Cre cells (nuclear or cytoplasmic stable cell lines or transiently transfected U2OS cells). (**D**) Map of the pSEM-1 plasmid indicating the primer pairs used in the PCR reactions to characterize the genome of recombinant VV-ΔTk viruses shown in panel **E**. (**E**) PCR analysis of DNA extracted from VV-ΔTk-*yfp*-gpt-1loxP (control virus), VV-ΔTk-*yfp-gpt* and VV-ΔTk' viruses. The PCR products span: **i.** across the left Tk flanking region, **ii.** across the luciferase gene, **iii.** across the *yfp-gpt* selectable marker, **iv.** across the right the Tk flanking region. n.s = not-significant, * p = 0.001.

doi:10.1371/journal.pone.0024643.g002

revealed a consensus sequence with no conflicts (**Fig. 3C**). As predicted, the residual DNA signature contained 1 loxP site and remnants from the pSEM-1 vector.

Construction of the second generation SEM cloning vector and the VV-Δ*I4L* viruses

The second generation SEM plasmid, termed pDGloxPKO was designed with multiple cloning sites flanking the *yfp-gpt* cassette. This permits insertion of homologous targeting sequences flanking the selectable marker and/or therapeutic transgene. This vector was also designed such that the *yfp-gpt* cassette and its early/late viral promoter are flanked by loxP sites. To test the importance of loxP site orientation during Cre-recombination, two pDGloxPKO vectors were created with the loxP sites in either the same orientation (pDGloxPKO^{DEL}) (**Figure S2A**), or oriented towards each other (pDGloxPKO^{INV}) (**Figure S2B**). Inserting homologous sequences of DNA from the VV genome flanking the *I4L* gene (I3L and I5L homology) into both pDGloxPKO^{DEL} and pDGloxPKO^{INV} vectors generated pDGloxPKO^{DEL}-Δ*I4L* and pDGloxPKO^{INV}-Δ*I4L*, respectively (**Fig. 4A and 4B**). These vectors were used to create two strains of recombinant VV in which the *I4L* locus is disrupted by vector-derived *yfp-gpt* cassette sequences (see schematic in **Fig. 4C**). Using vector pDGloxPKO^{DEL}-Δ*I4L*, which contains identically oriented loxP sites flanking the

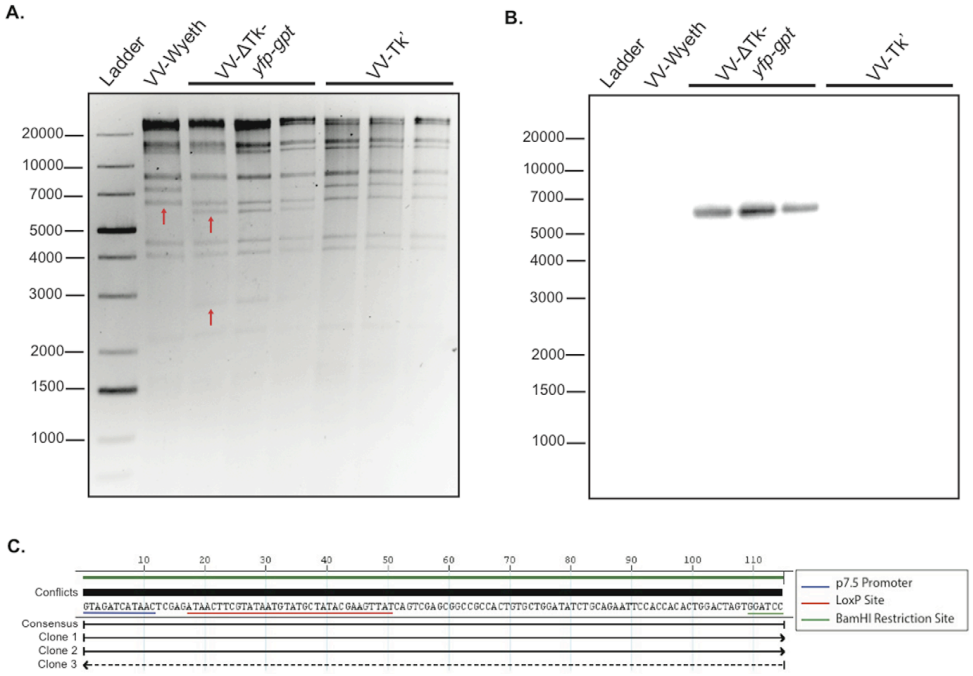

Figure 3. Confirmation of genomic composition of 3 independent recombinant VV-ΔTk viruses. (**A**) An ethidium bromide stained DNA gel of genomic HindIII restriction digests of viral DNA isolated from parental VV (Wyeth Strain), 3 clones of VV-ΔTk-*yfp-gpt* and 3 clones of VV-ΔTk'. Arrows indicate the Tk insertion site (VV-Wyeth), and the unique bands that result from insertion of the *yfp-gpt* cassette (VV-ΔTk-*yfp-gpt*). (**B**) Southern hybridization of the DNA gel in **A** identifying the *yfp* insert present in the genome of the VV-ΔTk-*yfp-gpt* clones, but not in parental VV-Wyeth or the VV-ΔTk' clones. (**C**) DNAStar sequence alignment at the *yfp-gpt* insertion site of DNA isolated from the 3 VV-ΔTk' clones post Cre passage.
doi:10.1371/journal.pone.0024643.g003

yfp-gpt cassette led to the generation of strain VV-Δ*I4L*^{DEL}, whereas using vector pDGloxPKO^{INV}-Δ*I4L* in which the inserted *yfp-gpt* cassette is flanked by loxP sites oriented towards each other generated virus VV-Δ*I4L*^{INV}. The genomic composition of the VV-Δ*I4L*^{DEL} virus post Cre passage was analyzed by sequencing at the excision site of *yfp-gpt* and revealed the Cre/loxP signature remaining in the viral genome post Cre-recombination (**Fig. 4D**). As expected, the virus contains 1 loxP site, and remnants from the pDGloxPKO vector. To exclude the possibility that there were multiple *yfp-gpt* insertion sites, the entire genome of VV-Δ*I4L*^{DEL} virus post Cre passage was sequenced. The sequence of the VV-Δ*I4L*^{DEL} recombinant was compared to the sequence of the parental VV (Western Reserve) using a dotplot analysis (**Figure S3A**). These data illustrate that the VV-Δ*I4L*^{DEL} virus is disrupted only at the *I4L* locus, thereby confirming 1 insertion site at the desired locus.

Cre-mediated recombination of viral DNA is dependent upon loxP site orientation

Both the pDGloxPKO^{DEL} and pDGloxPKO^{INV} plasmids were used to explore the dependence of loxP orientation on Cre-mediated recombination of poxvirus genomes. Previous work has shown that Cre-mediated recombination between identically-oriented loxP sites generates deletions while oppositely oriented loxP sites lead to inversion of DNA sequences [35,36], but it remained to be formally proven that this would also hold-true in virus-infected cells. Recombinant Δ*I4L* viruses were analyzed by PCR for the presence of the *I4L* gene before (BSC-40 passage) and after (U2OS-Cre passage) Cre recombination (**Fig. 5A**). As an additional test of the SEM approach, we have included *F4L*-inactivated recombinants in these experiments, as Δ*F4L* virus backgrounds have been reported to have severe growth kinetics compared to their wild-type counterpart [23]. Referring to the expected amplicon sizes and primer pairs illustrated in **Fig. 4C**, the PCR products generated using primers flanking the *yfp-gpt* cassette (A+D) exhibited sizes indicative of replacement of the *I4L* gene with the *yfp-gpt* cassette in viruses cultured in BSC-40 cells (**Fig. 5A**, left panel). Upon passage in Cre-expressing cells, only those viruses produced using pDGloxPKO^{DEL} vectors (Δ*I4L*^{DEL}, and Δ*I4L*/Δ*F4L*^{DEL}) exhibited the deletion of the *yfp-gpt* cassette (**Fig. 5A**, right panel). This shows that Cre-mediated deletions only occur when the DNA is flanked by identically oriented loxP sites.

The orientation of the *yfp-gpt* cassette in recombinant viruses produced using the pDGloxPKO^{INV}-Δ*I4L* vector were also analyzed by PCR before and after passage through Cre-expressing cells. We used primer pairs designed to amplify the *yfp-gpt* cassette

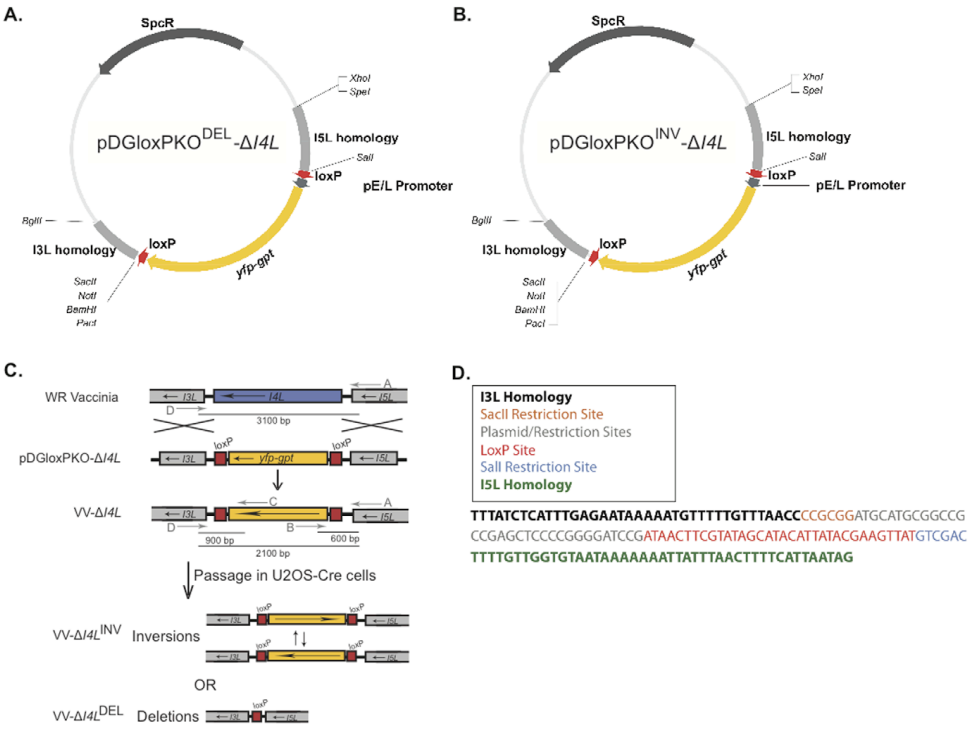

Figure 4. Creation of the VV-Δ*I4L* mutants from the second generation SEM cloning vectors. (**A**) Map of cloning vector pDGloxPKO^{DEL}-Δ*I4L* and (**B**) pDGloxPKO^{INV}-Δ*I4L* with labeled open reading frames. (**C**) Schematic displaying the strategy for knock-out of the *I4L* open reading frame from VV strain WR, and possible outcomes of Cre-recombination of recombinant VV-Δ*I4L* virus generated from either the pDGloxPKO^{DEL}-Δ*I4L* or pDGloxPKO^{INV}-Δ*I4L* vectors. (**D**) DNA sequence analysis of the VV-Δ*I4L*^{DEL} virus post Cre passage.
doi:10.1371/journal.pone.0024643.g004

in the forward orientation (pairs A+B, C+D), and also in the case of *yfp-gpt* inversions (pairs A+C, B+D). The viruses isolated from BSC-40 cells produced PCR products consistent with a single orientation identical to that seen in original plasmid (**Fig. 5B**, left panel). However, upon passage through Cre-expressing cells, the PCR products displayed a pattern characteristic of a mix of two different arrangements of loxP flanked inserts (**Fig. 5B**, right panel).

Western blot analysis was used to confirm deletion of the *I4L* locus of all Δ*I4L* strains. Recombinant Δ*I4L* viruses produced with either pDGloxPKO^{INV}-Δ*I4L* or pDGloxPKO^{DEL}-Δ*I4L* vectors led to inactivation of I4 protein expression and this inactivation was specific since I3, (expressed from the neighbouring gene, *I3L*) levels remained unchanged (**Fig. 5C**). The YFP-GPT protein was only deleted from strains that had been generated with the pDGloxPKO^{DEL}-Δ*I4L* targeting vector *and* passaged in Cre-expressing cells (**Fig. 5C**, right panel), further confirming that deletion events need both identically-oriented loxP sites and exposure to Cre activity. Collectively, these results demonstrate that the SEM vector system can be used to either delete or invert sequences within the viral genome, upon passage of the selected strains in Cre-expressing cells.

The SEM system can be used with other members of the Poxvirus family

The SEM system was also used to create a recombinant ECTV (strain Moscow) lacking the *EVM002* gene using the transfer plasmid pDGloxPKO^{DEL}-Δ*EVM002* (**Fig. 6A**). Referring to the schematic outlined in **Fig. 6B**, ECTV viral recombination with pDGloxPKO^{DEL}-Δ*EVM002* with subsequent MPA drug selection created the primary recombinant ECTV-Δ*EVM002-yfp-gpt*. The virus was passaged through U2OS-Cre cells to obtain the marker-free recombinant virus ECTV-Δ*EVM002*'. The genomic composition of wild type ECTV (ECTV-wt), ECTV-Δ*EVM002-yfp-gpt*, and ECTV-Δ*EVM002*' viruses was confirmed by PCR analysis (**Fig. 6C**). These PCR analyses demonstrate at the genomic level the deletion of the *EVM002* gene, the insertion of the *yfp-gpt* cassette, and its subsequent removal following Cre-mediated recombination. The genomic composition of the ECTV-Δ*EVM002*' was analyzed by sequencing at the excision site of *yfp-gpt* to illustrate the Cre/loxP signature remaining in the viral genome post recombination (**Fig. 6D**). As expected, the virus contains 1 loxP site, and remnants from the pDGloxPKO vector. YFP protein expression from the ECTV viruses was also analyzed by confocal microscopy (**Fig. 6E**). Mock-infected BGMK cells

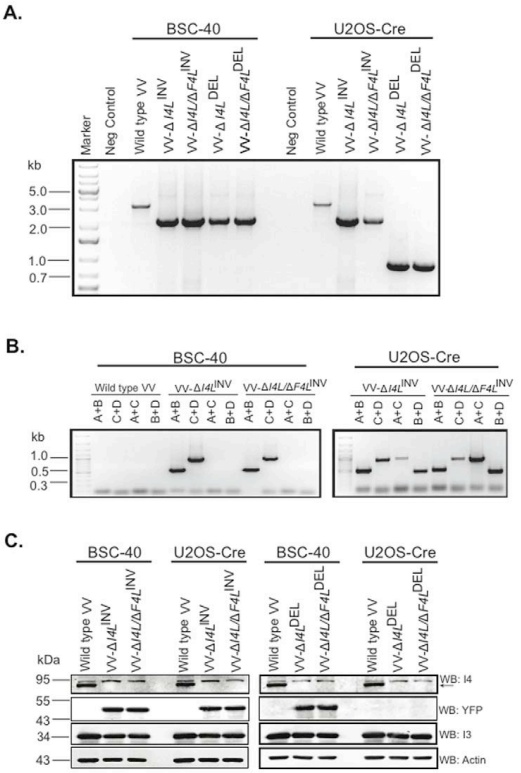

Figure 5. Cre-mediated recombination of vaccinia virus DNA is dependent upon loxP site orientation. (**A**) PCR analysis of the *I4L* locus using primers flanking the *yfp-gpt* cassette of two purified *ΔI4L* strains generated from either the pDGloxPKO^{DEL}-*ΔI4L* or pDGloxPKO^{INV}-*ΔI4L* vectors before (BSC-40) and after (U2OS-Cre) Cre-recombination. (B) PCR analysis of two purified *ΔI4L* strains generated from the pDGloxPKO^{INV}-*ΔI4L* vector with primers amplifying inside and outside the *yfp-gpt* cassette before (BSC-40) and after (U20S-Cre) Cre-recombination. (C) Western blot analysis of two purified *ΔI4L* strains generated from either the pDGloxPKO^{DEL}-*ΔI4L* or pDGloxPKO^{INV}-*ΔI4L* vectors for I4, YFP, I3 (positive control for infection) and actin before (BSC-40) and after (U20S-Cre) Cre-recombination.
doi:10.1371/journal.pone.0024643.g005

were compared to ECTV-wt, ECTV-Δ*EVM002-yfp-gpt*, and ECTV-Δ*EVM002*' infected cells for YFP fluorescence. Only those cells that were infected with recombinant ECTV-Δ*EVM002-yfp-gpt* expressed detectable levels of YFP fluorescence.

Discussion

Poxviruses have been, and will continue to be, important therapeutics for the prevention and treatment of human diseases [2,3,10,11,12,13,19]. Arguably, the application of VV for the eradication of smallpox has been one of the most important medical advances in human history. A variety of poxvirus based vaccine vectors have been developed for both human and veterinary infectious diseases and more recently as agents for the treatment of cancer [2,7,8,10,13,14,15,16,17,19,20]. During therapeutic development it is desirable to use marker genes for both construction of novel vectors but also for pre-clinical and even early phase clinical experimentation. Unfortunately as products mature, there becomes a transition point where marker genes are no longer necessary and, in the view of regulatory agencies, may even compromise the safety of the vector [29].

The SEM system provides a faster, simplified and more efficient means to create marker-free recombinant poxviruses [31,32,35]. As outlined in **Fig. 1A**, the SEM cloning strategy can be summarized in three basic steps: transfection of poxvirus-infected cells with an SEM vector, purification of resulting recombinants through FACS and/or drug selection, and finally removal of the selectable marker by virus passage in Cre-expressing cells. The first generation pSEM-1 vector (**Fig. 1B**) was created to demonstrate the "proof of principle" that it was possible to create marker-free recombinant poxviruses with our system, while stably retaining a functional transgene (in our case luciferase) during the Cre-recombination reaction (**Fig. 2B**). The second generation SEM plasmids (**Figure S2**) broaden the applicability of the SEM system to other poxvirus loci, and other poxvirus genera by the insertion of two multiple cloning sites (MCS) flanking the *yfp-gpt* cassette and loxP sites. Sequences homologous to

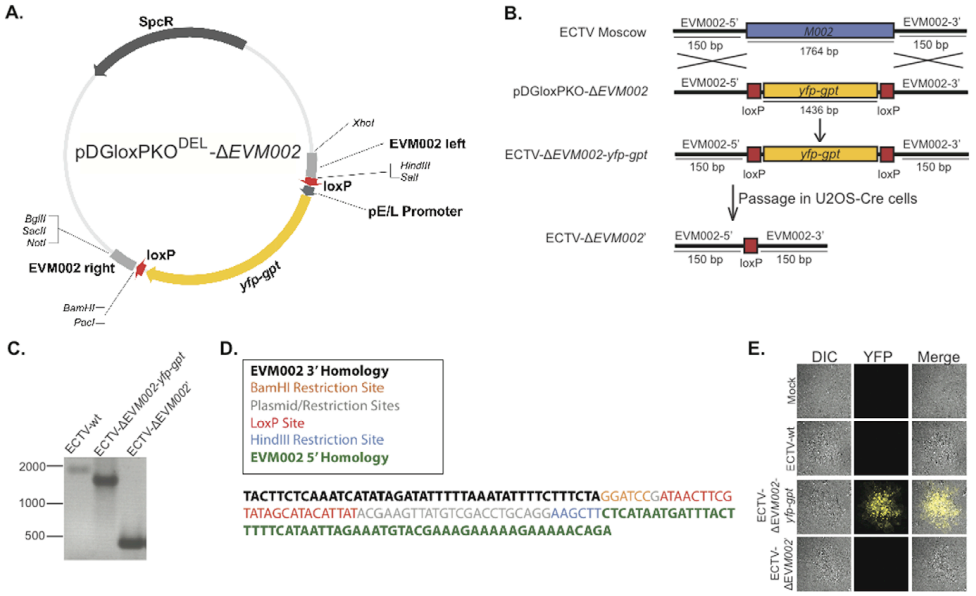

Figure 6. Generation of a recombinant ECTV using SEM. (**A**) Map of pDGloxPKO^{DEL}-Δ*EVM002* with labeled open reading frames. (**B**) Schematic displaying the strategy for knock-out of the *EVM002* open reading frame from ECTV. (**C**) PCR analysis of viral DNA. Primers were used to amplify the regions of pDGloxPKO-Δ*EVM002* homology from wild-type ECTV (ECTV-wt), ECTV-Δ*EVM002-yfp-gpt*, and ECTV-Δ*EVM002'*. (**D**) DNA sequence analysis of the ECTV-Δ*EVM002'* virus (post Cre passage). (**E**) Confocal microscopy was used to detect YFP fluorescence in mock infected BGMK cells or BGMK cells infected with ECTV-wt, ECTV-Δ*EVM002-yfp-gpt*, or ECTV-Δ*EVM002'*. A 40× magnification lens was used to detect differential interference contrast (DIC), and YFP fluorescence.
doi:10.1371/journal.pone.0024643.g006

any poxvirus gene can be added to the pDGloxPKO vector, as we have demonstrated with the ectromelia virus recombinant constructed from pDGloxPKO^{DEL}-Δ*EVM002* (**Fig. 6**).

The most labour-intensive part of traditional poxvirus cloning strategies is the isolation and purification of desired recombinants from a heterogeneous population. To simplify the isolation of pure recombinant poxvirus clones, we have included both drug (*gpt*) and optical (*yfp*) selection strategies in the SEM system. The flexibility and simplicity of this approach ensures that the SEM system will be amenable to any research laboratory. MPA drug selection is relatively inexpensive and historically has shown to be an efficient means to purify poxvirus recombinants [25]. Indeed, we have shown here that MPA selection alone is sufficient to isolate a pure recombinant poxvirus population in as few as three passages (e.g. VV-Δ*I4L*, **Fig. 4** and ECTV-Δ*EVM002*, **Fig. 6**). We have also shown the usefulness of fluorescent sorting strategies to rapidly enrich for the recombinant virus population by subjecting the initial transfection/infection reaction to FACS analysis (**Fig. 2A**). Alternatively, a more traditional approach of using fluorescent microscopy to identify and pick individual plaques expressing YFP can be used. The flexibility of the SEM system in the purification of recombinant poxviruses is particularly important when working with highly attenuated strains. Importantly, we show here that even the double deleted Δ*I4L*/Δ*F4L* VV strains, which have severe replication defects and exhibit a small plaque phenotype [23], can be produced and purified using the SEM system.

We had hypothesized that expression of cytoplasmic Cre-recombinase would maximize recombination efficiency since poxviruses replicate in the cytoplasm. Indeed a single passage of the VV-ΔTk-*yfp-gpt* virus on U2OS cells expressing cytoplasmic Cre is sufficient to eliminate nearly all of the *yfp-gpt* cassette from the viral genome (**Fig. 2B and 2C**). However, infection of U2OS cells stably expressing *nuclear* Cre still led to nearly 100% recombination efficiency (**Fig. 2C**). Not unlike other proteins, the Cre enzyme is initially located in the cytoplasm prior to transport to the nucleus. We speculate that in cells selected for high levels of Cre expression, the amount of enzyme is not limiting for the excision reaction and thus even small amounts, or temporary cytoplasmic expression of Cre from nuclear-cre expressing cells may be sufficient to facilitate recombination. Importantly, despite lower Cre-expression levels achieved from transient transfection of U2OS cells with pMC-Cre (**Fig. 1D**), the recombination frequency was still >40% (**Fig. 2C**). These data illustrate how the SEM system can be used with any transfectable cell line while maintaining the efficiency of the Cre/loxP reaction.

To confirm that the residual DNA signature was consistent for all recombinant viruses post Cre recombination, DNA sequencing was performed at the insertion site (**Figs. 3C, 4D, 6D**). In all cases, one 34 base pair loxP site remains in the viral genome, with some remnants of the respective SEM cloning vectors. We have observed no obvious impact of retention of this 34 base pair sequence on virus replication and indeed this has been studied

extensively in mammalian systems where the retention of loxP sequences has no impact on mRNA stability, promoter activity or genome integrity [37,38]. To further validate the consistency of the recombination events of the SEM system, 3 clones of the VV-ΔTk virus pre (VV-ΔTk-*yfp-gpt*) and post (VV-ΔTk') Cre passage were analyzed by HindIII DNA restriction digest and southern hybridization (**Fig. 3**). As predicted, the DNA signatures are consistent, and the Tk locus is the only site of poxvirus recombination. Since the VV-Δ*I4L* and ECTV-Δ*EVM002*' recombinant viruses were purified as heterogeneous populations (MPA drug selection), the sequence analysis is representative of all recombination events. To confirm that there was only 1 site of *yfp-gpt* integration in the VV-Δ$I4L^{DEL}$ virus, the entire genome of the virus was sequenced. A dotplot comparison of recombinant VV-Δ$I4L^{DEL}$ to parental VV illustrates that the recombination event was targeted to the *I4L* locus (**Figure S3**).

Using the second generation SEM cloning vectors (pDGloxP-KO^{DEL} and pDGloxPKO^{INV}), we have shown for the first time that similar to recombination of cellular DNA [35,36], Cre-mediated recombination between identically-oriented loxP sites generates deletions, while oppositely oriented loxP sites leads to inversions of viral DNA sequences (**Fig. 5**). Interestingly, targeted inversions of the *yfp-gpt* cassette when generating viruses using the pDGloxPKO^{INV}-Δ*I4L* targeting vector identified an additional application for the SEM system. Site-specific inversions may be useful for transcriptional interference studies [39] in which a poxvirus promoter could drive the same mRNA from opposite strands. This approach would allow one to assess the potential strand-specific influence of neighbouring transcriptional processes and read-through transcripts on the efficiency of transcription of the reporter mRNA.

In summary, the SEM strategy provides an efficient means to "surgically" manipulate viral genomes by adding or deleting genes without leaving unwanted marker genes behind. We have demonstrated the applicability of the SEM system to create recombinant viruses in two different species, targeting three different poxvirus loci by deletions and/or insertions, including strains with severe replication defects. By inclusion of fluorescence and drug selection strategies, the SEM system offers both flexibility and simplicity for the purification of recombinant viruses. The *yfp-gpt* cassette was also shown to be useful during Cre-recombination to monitor efficiency, which could be enhanced even further by making use of a reverse *gpt* selection strategy [40]. This system will be especially useful when multiple deletions or transgenes are to be added sequentially to a single vector. Finally, the tools developed in the SEM system may also contribute to basic virology research, like those that involve transcriptional interference studies.

Materials and Methods

Antibodies and reagents

The following primary antibodies were used: rabbit anti-GFP/YFP (Abcam), Cre (Novagen), VV I4 (a gift from Dr. C. Mathews, Oregon State University), mouse anti-β-actin (Sigma-Aldrich) and VV I3 [41]. Secondary antibodies conjugated to horseradish peroxidase (BioRad) or infrared dyes (Li-Cor) were used to detect primary antibodies in immunoblotting. OptiMEM (Invitrogen) was used for transfection experiments.

Cells

The following cells were purchased from American Type Tissue Collection: human osteosarcoma (U2OS), human embryonic kidney, large T antigen transformed (293T), and green monkey kidney (BSC-40) cells. Buffalo green monkey kidney (BGMK) cells were purchased from Diagnostic Hybrid. Cell lines were maintained in Dulbecco's modified Eagle's medium (Hyclone) supplemented with 10% fetal calf serum (Cansera), penicillin (100 U/ml), and streptomycin sulfate (100 μg/ml) at 37°C in 5% CO_2. All cell lines were tested and found clear of mycoplasma contamination.

Plasmids

Plasmids pEYFP-C1, pLPCX, and pLXSN were purchased from Clontech and pGEM-T was purchased from Promega. Plasmid pMC-Cre [42] was a gift from Dr. Klaus Rajewsky (Harvard Medical School), pSEL-eGFP [20] and pSC65-luc [43] were gifts from Dr. David Bartlett (University of Pittsburgh) and pHIT60 and pHIT456 were gifts from Dr. Ian Lorimer (University of Ottawa).

Cloning – pSEM-1 vector

The *gpt* gene was first excised from pSEL-eGFP with *Bse*Y1, repaired, and ligated into a pT7blue-3 cloning vector (Novagen). The *gpt* gene was then excised with *Sal*I and *Bam*HI and ligated, in frame, into *Xho*I/*Bam*HI cut pEYFP-C1. This created pEYFP-gpt bearing a fusion of the two polypeptides. The first loxP sequence was constructed by annealing together two oligonucleotides with the same sequence (loxP, **Table S1**), using the In-Fusion-2 method (Clontech) [44]. The pEYFP-gpt plasmid was then cut with *Nhe*I and recombined with the double-stranded DNA loxP site to obtain ploxP-EYFP-gpt. The second loxP sequence was inserted in a similar way by cutting ploxP-EYFP-gpt at the *Bam*HI site, and inserting the double-stranded oligonucleotide loxP (**Table S1**). The resulting plasmid, p2loxP-EYFP-gpt, contained two loxP sites with the same orientation flanking the gene encoding the YFP-GPT fusion protein.

The pSEM-1 plasmid was assembled by inserting the loxP-*yfp-gpt*-loxP cassette into pSC65-luc. This was accomplished by cutting p2loxP-EYFP-gpt and pSC65-luc plasmids with *Xho*I and *Bam*HI restriction enzymes, and ligating the loxP-*yfp-gpt*-loxP insert into the VV Tk gene in pSC65-luc. Two vectors were created: a negative control vector containing only the first loxP site (pSEM-1ctrl), and a vector containing two loxP sites inserted in the same orientation and flanking the reporter construct (pSEM-1) (**Fig. 1B**).

Cloning – pDGloxPKO vectors

A second series of vectors were assembled using gene synthesis (GeneArt) and contained two multiple cloning sites flanking the loxP sites. To test the importance of loxP orientation, two versions of these plasmids were created with the loxP sites either in the same (pDGloxPKO^{DEL}) or in the opposite orientation (pDGloxP-KO^{INV}) with respect to one another (**Figure S2**).

Cloning – pDGloxPKO-ΔI4L vectors

The PCR and primers I5L (left) plus I5L (right) (**Table S1**) were used to prepare a ~430 bp PCR product encoding sequences flanking the "*I5L*" side of the VV *I4L* locus. Similarly the PCR and primers I3L (left) plus I3L (right) (**Table S1**) were used to produce a ~340 bp PCR product containing sequences flanking the "*I3L*" side of the *I4L* locus. These DNAs were then cloned into the *Spe*I/*Sal*I (*I5L* homology) and *Sac*II/*Bgl*II (*I3L* homology) restriction sites of pDGloxPKO^{INV} and pDGloxPKO^{DEL}. Adding these sequences created vectors pDGloxPKO^{INV}-Δ*I4L* and pDGloxPKO^{DEL}-Δ*I4L* (**Fig. 4**).

Cloning – pDGloxPKODEL-ΔEVM002 vector

The PCR and primers EVM002-5′ (left) plus EVM002-5′ (right) (**Table S1**) were used to prepare a 150 bp product

encoding sequences to the left of the *EVM002* gene. Similarly the PCR and primers EVM002-3′ (left) plus EVM002-3′ (right) (**Table S1**) were used to produce a 150 bp product encoding sequences to the right of the *EVM002* gene in the ectromelia virus (ECTV) genome. These two 150 bp PCR fragments were cloned into pGEM-T vectors (Promega). The fragment encoding sequences located on the left side of the *EVM002* gene was subsequently cloned into the pDGloxPKO^{DEL} vector using the *Xho*I and *Hind*III restriction sites to create pDGloxPKO-*EVM002*-5′. Finally, the EVM002-3′ 150 bp was cloned into pDGloxPKO-*EVM002*-5′ using the *Bam*HI and *Not*I restriction sites to create pDGloxPKO^{DEL}-Δ*EVM002*.

Cloning – Cre plasmids

The gene encoding a form of Cre protein lacking a nuclear localization sequence (NLS) was PCR amplified from pMC-Cre using Taq polymerase and primers NLS-free Cre (left) and NLS-free Cre (right) (**Table S1**). The PCR product was digested with *Xho*I and *Not*I and ligated into pLPCX cut with the same enzymes. This produced plasmid pLPCX-Cyto_Cre. A Cre plasmid was also created with the NLS intact by digesting Cre from pMC-Cre, and inserting the gene into the *Xho*I site of the pLXSN vector to form pLXSN-Nuc_Cre.

U2OS-Cre cells

Retroviral transduction methods were used to produce cells expressing nuclear- or cytoplasmic-localized Cre protein. A stock of transducing particles was first produced by using calcium phosphate to co-transfect 293T cells with 7 μg of plasmid DNA (either pLPCX-Cyto_Cre or pLSXN-Nuc_Cre) along with the retroviral helper plasmids pHIT60 and pHIT456 [45]. Virus-containing supernatants were harvested two days later and the debris removed with a 0.45-μm filter. To perform the transduction experiment, 2.5×10^5 U2OS cells were infected with 2 mL of the virus for 2 hr in the presence of 8 μg/mL of polybrene. Two days later, G418 (800 μg/mL) or puromycin (1 μg/mL) were added and drug-resistant recombinants were harvested a week later. Purified recombinant poxviruses were passaged 1-to-3 times in these cells to remove loxP-flanked genes.

Recombinant viruses

Viruses constructed from the pSEM-1 vector were produced from the VV strain Wyeth [7]. U2OS cells were infected with VV at a multiplicity of infection (MOI) of 0.01 and then transfected with plasmid pSEM-1 or pSEM-1ctrl vectors using Lipofectamine 2000 (Invitrogen). The cells were incubated at 37°C for 4 hr, the medium was replaced, and then the cells cultured for two more days. The dishes were harvested, YFP-positive cells sorted using flow cytometry, and the YFP-positive population purified further by selecting YFP-positive plaques in the presence of MPA for 2 rounds of purification. This produced VV strain VV-ΔTk-*yfp-gpt* with both loxP sites in the same orientation and VV strain VV-ΔTk-*yfp-gpt*-1loxP bearing a single loxP site.

Viruses bearing deletions of the *I4L* gene were produced using pDGloxPKO^{INV}-Δ*I4L* and pDGloxPKO^{DEL}-Δ*I4L* vectors in VV strain Western Reserve (WR), and in Δ*F4L* VV strains [23]. BSC-40 cells were infected for 1 hr (MOI = 2), transfected with plasmid DNA using Lipofectamine 2000, and virus harvested two days later. Recombinant virus were isolated using three rounds of plaque purification on BSC-40 cells in MPA selection media (DMEM supplemented with 10% serum, 50 U/mL penicillin, 50 μg/mL of streptomycin, 200 μM glutamine, 250 μg/mL xanthine, 15 μg/mL hypoxanthine, and 25 μg/mL MPA).

A recombinant ECTV was constructed by infecting BGMK cells with ECTV (strain Moscow) at an MOI = 0.01, followed by transfection with *Xho*I and *Not*I linearized pDGloxPKO-Δ*EVM002* DNA. The virus was harvested two days later and foci were purified twice in the presence of MPA and twice in the absence of MPA selection.

Cell sorting and flow cytometry

U2OS cells were infected with virus at MOI ~0.1 for 6 hr, and sorted for YFP fluorescence on a MoFlo cytometer (DakoCytomation). The top 5% of YFP positive cells (approximately 3,000 cells) were collected and mixed with ~300,000 uninfected U2OS cells and cultured for two days in a 10 cm dish. For flow cytometry, ~10^6 HeLa cells were infected with virus at a MOI = 3 for 4 hr. The cells were suspended in 0.5 mL of PBS containing 1% FBS, and YFP fluorescence determined using a FACScan flow cytometer (Becton-Dickinson) and CellQuest software (Version 3.1).

Luciferase and fluorescence detection using IVIS Imager

The fluorescence and bioluminescence were detected using a 200 Series IVIS Imager (Xenogen) and Living Image® v2.5 software. Cell lysates from Cre cell lines infected with VV-ΔTk-*yfp-gpt* were used to infect U2OS cells which were first imaged for YFP fluorescence prior to incubation with 20 μg of D-luciferin (Molecular Imaging Products Company) added directly to the cultured cells. D-luciferin was incubated with the cells for 20 min at 37°C. Identical program settings (exposure, aperture and pixel binning) were used for all experiments.

Quantification of Cre recombination efficiency

U2OS cells stably expressing nuclear or cytoplasmic versions of U2OS, or U2OS cells transiently transfected with Cre recombinase were infected at an MOI of 0.05 for 2 days. Virus progeny was then analyzed by U2OS plaque assay for YFP expression of individual virus plaques.

Fluorescence microscopy

To detect YFP, 2×10^5 BGMK cells were seeded on coverslips and infected (or mock infected) with virus at a MOI = 0.01 for two days. The cells were fixed with 2% paraformaldehyde, mounted in 50% glycerol containing 4 mg/mL N-propyl-gallate (Sigma-Aldrich), and 250 μg/mL 4,6-diamidino-2-phenylindole (DAPI) (Invitrogen), and visualized using a Zeiss 710 confocal microscope equipped with Zeiss Zen software 2009, light edition. For immunofluorescence microscopy, 5×10^4 Cre-expressing U2OS cells were plated per 1.8 cm^2 well in Nunc Chamber Slides®. The cells were washed three times with PBS and fixed with 4% paraformaldehyde for 10 min at room temperature. The cells were treated for 30 min with blocking buffer (0.2% Triton X-100, 5% normal goat serum in PBS) and then incubated overnight at 4°C with a 1:100 diluted anti-Cre antibody in blocking buffer. The cells were washed with PBS, incubated for 30 min with Cy3 conjugated goat anti-rabbit antibody (Jackson), washed three times, and then mounted on a slide. DNA was stained with 1.5 μg/mL 4,6-diamidino-2-phenylindole (DAPI). Cell images were captured using a Zeiss Axioplan 2 microscope equipped with Axioview 3.1 software.

Virus DNA extraction

DNA was extracted from sucrose cushion purified virus stocks according to methods adapted from Meyer et al. [46]. Briefly, 200 μL of purified virus stock was treated with lysis buffer (1.4 mL

54% sucrose, 15 µL 2-mercaptoethanol, 50 µL if 20 mg/mL, proteinase-K and 250 µL 10% SDS) for 4 hours at 55°C. The samples were then purified by phenol extraction.

Sequencing of viral DNA

Viral DNA from Cre-passaged viruses was subjected to PCR amplification at the site of Cre recombination. Sequencing was performed using the Applied Biosystem DNA analyzers. The entire genome of both parental VV Western Reserve and recombinant VV-Δ*I4L*^{DEL} virus post Cre passage were sequenced from 5 µg of extracted viral DNA at the Genome Québec Innovation Centre (Montréal, Québec) using a high throughput pyrosequencing approach on a Roche 454 GS FLX Titanium sequencer platform. CLC Genomics Workbench 4.6 software was used to assemble the genome sequence. The viral genomes were analyzed and compared using dotplots prepared using the program Gepard [47] with default settings.

DNA restriction digest and southern hybridization

Viral DNA was analyzed using Southern blot. Briefly, 7 µg of DNA was digested overnight with HindIII restriction enzyme (Invitrogen) at 37°C. DNA digests were electrophoresed on a 0.8% agarose gel in 1× TAE buffer at 46 V for 6 hours, then stained with ethidium bromide and photographed. Gels were first denatured for 45 mins, then neutralized for 45 mins prior to transfer over night onto Hybond-N membrane (Amersham), and finally UV cross-linked. A 931 bp *yfp-gpt* probe was labeled with P^{32} α-dCTP (PerkinElmer) using the Multiprime DNA Labeling kit (Amersham). The blot was blocked for 2 hours at 42°C in a formamide pre-hybridization buffer followed by over night hybridization with 5 µCurries of denatured probe. Membranes were washed and exposed to a phospho screen for 18 hours and imaged on a Storm imaging system (Storm 860; Molecular Dynamics) using ImageQuant software, version 5.2.

Western blotting

For immunoblotting, cells were lysed in RIPA buffer with protease inhibitors (Complete®, Roche) for 30 min on ice. The cell lysates were sonicated for 30 seconds, centrifuged at 10,000×*g* and the cell pellets discarded, fractionated by electrophoresis on a Nupage 4–12% Bis-Tris gel (Invitrogen), transferred to Hybond-C extra nitrocellulose membranes (Amersham), and probed with the indicated primary antibodies. Secondary antibodies conjugated to horseradish peroxidase or Li-Cor infrared dyes were used to detect bound antigens.

Statistical Analysis

Data were analyzed by a one-way Anova, followed by a Turkey post-hoc for multiple group comparison at a 99% confidence interval.

Supporting Information

Figure S1 Detection of YFP protein expression by western blot analysis. (**A**) Western blotting of transfected cells. Anti-YFP western blot of U2OS cells mock transfected (1), or transfected with plasmid DNA pEYFP-c1 (2), pEYFP-gpt, (3), or pEYFP-gpt-1loxP (4).
(TIFF)

Figure S2 Plasmid maps of pDGloxPKO^{DEL} and pDGloxPKO^{INV}. (**A**) Map of cloning vector pDGloxPKO^{DEL} and (**B**) pDGloxPKO^{INV} with labeled open reading frames.
(TIFF)

Figure S3 Sequencing analysis of genomic viral DNA from VV-Δ*I4L*^{DEL}. (**A**) Dotplot comparison of sequenced viral genomes of wild type Western Reserve vaccinia virus and recombinant VV-Δ*I4L*^{DEL} virus post Cre passage using default settings available in Gepard [47].
(TIFF)

Table S1 Primers used in the study.
(DOC)

Acknowledgments

Thank you to Mr. Paul Oleynik from the StemCore laboratories for assistance in generating the FACS data. Thank you to Ms. Megan Desaulniers for preparing Western Reserve vaccinia virus, and Ms. Li Qin for preparing genomic viral DNA for sequencing analysis. Thank you to Dr. Christopher Mathews for the anti-VV I4 antibodies. Thank you to Dr. Ian Lorimer for the pHIT60 and pHIT456 plasmids. Thank you to Dr. Klaus Rajewsky for sharing the pMC-Cre plasmid, and Dr. David Bartlett for sharing the pSC65-luc plasmid. Thank you to Dr. John Barrett for his technical expertise. Thank you to Catherine Mathis (Transgene, France) for her expertise and communications regarding Regulatory Guidelines for poxvirus recombinants.

Author Contributions

Conceived and designed the experiments: JLR JW DBG NJVB KG KJ MB DHE JCB. Performed the experiments: JLR JW DBG NJVB KG. Analyzed the data: JLR JW DBG NJVB KG KJ MB DHE JCB. Contributed reagents/materials/analysis tools: JLR JW DBG NJVB KG KJ MB DHE JCB. Wrote the paper: JLR JW JCB.

References

1. Fenner F, Henderson D. A, Arita L, Jezek Z, Ladnyi ID, eds. Smallpox and Its Eradication. Geneva: W.H.O.
2. Gilbert PA, McFadden G (2006) Poxvirus cancer therapy. Recent Pat Antiinfect Drug Discov 1: 309–321.
3. Moroziewicz D, Kaufman HL (2005) Gene therapy with poxvirus vectors. Curr Opin Mol Ther 7: 317–325.
4. Smith GL, Moss B (1983) Infectious poxvirus vectors have capacity for at least 25 000 base pairs of foreign DNA. Gene 25: 21–28.
5. Fenner F, Comben BM (1958) [Genetic studies with mammalian poxviruses. I. Demonstration of recombination between two strains of vaccina virus.]. Virology 5: 530–548.
6. Nakano E, Panicali D, Paoletti E (1982) Molecular genetics of vaccinia virus: demonstration of marker rescue. Proc Natl Acad Sci U S A 79: 1593–1596.
7. Mastrangelo MJ, Maguire HC, Jr., Eisenlohr LC, Laughlin CE, Monken CE, et al. (1999) Intratumoral recombinant GM-CSF-encoding virus as gene therapy in patients with cutaneous melanoma. Cancer Gene Ther 6: 409–422.
8. Erbs P, Findeli A, Kintz J, Cordier P, Hoffmann C, et al. (2008) Modified vaccinia virus Ankara as a vector for suicide gene therapy. Cancer Gene Ther 15: 18–28.
9. Cadoz M, Strady A, Meignier B, Taylor J, Tartaglia J, et al. (1992) Immunisation with canarypox virus expressing rabies glycoprotein. Lancet 339: 1429–1432.
10. Kantoff PW, Schuetz TJ, Blumenstein BA, Glode LM, Bilhartz DL, et al. (2010) Overall survival analysis of a phase II randomized controlled trial of a Poxviral-based PSA-targeted immunotherapy in metastatic castration-resistant prostate cancer. J Clin Oncol 28: 1099–1105.
11. Kanesa-thasan N, Smucny JJ, Hoke CH, Marks DH, Konishi E, et al. (2000) Safety and immunogenicity of NYVAC-JEV and ALVAC-JEV attenuated recombinant Japanese encephalitis virus poxvirus vaccines in vaccinia-nonimmune and vaccinia-immune humans. Vaccine 19: 483–491.
12. Bejon P, Ogada E, Mwangi T, Milligan P, Lang T, et al. (2007) Extended follow-up following a phase 2b randomized trial of the candidate malaria vaccines FP9 ME-TRAP and MVA ME-TRAP among children in Kenya. PLoS One 2: e707.
13. Harrop R, Drury N, Shingler W, Chikoti P, Redchenko I, et al. (2007) Vaccination of colorectal cancer patients with modified vaccinia ankara encoding the tumor antigen 5T4 (TroVax) given alongside chemotherapy induces potent immune responses. Clin Cancer Res 13: 4487–4494.
14. Dasgupta S, Bhattacharya-Chatterjee M, O'Malley BW, Jr., Chatterjee SK (2006) Recombinant vaccinia virus expressing interleukin-2 invokes anti-tumor

cellular immunity in an orthotopic murine model of head and neck squamous cell carcinoma. Mol Ther 13: 183 193.
15. Lorenz MG, Kantor JA, Schlom J, Hodge JW (1999) Anti-tumor immunity elicited by a recombinant vaccinia virus expressing CD70 (CD27L). Hum Gene Ther 10: 1095 1103.
16. Lun X, Alain T, Zemp FJ, Zhou H, Rahman MM, et al. (2010) Myxoma virus virotherapy for glioma in immunocompetent animal models: optimizing administration routes and synergy with rapamycin. Cancer Res 70: 598 608.
17. Evgin L, Vaha-Koskela M, Rintoul J, Falls T, Le Boeuf F, et al. (2010) Potent oncolytic activity of raccoonpox virus in the absence of natural pathogenicity. Mol Ther 18: 896 902.
18. Huygen K, Content J, Denis O, Montgomery DL, Yawman AM, et al. (1996) Immunogenicity and protective efficacy of a tuberculosis DNA vaccine. Nat Med 2: 893 898.
19. Kim JH, Oh JY, Park BH, Lee DE, Kim JS, et al. (2006) Systemic armed oncolytic and immunologic therapy for cancer with JX-594, a targeted poxvirus expressing GM-CSF. Mol Ther 14: 361 370.
20. McCart JA, Ward JM, Lee J, Hu Y, Alexander HR, et al. (2001) Systemic cancer therapy with a tumor-selective vaccinia virus mutant lacking thymidine kinase and vaccinia growth factor genes. Cancer Res 61: 8751 8757.
21. Mackett M, Smith GL, Moss B (1984) General method for production and selection of infectious vaccinia virus recombinants expressing foreign genes. J Virol 49: 857 864.
22. Piccini A, Perkus ME, Paoletti E (1987) Vaccinia virus as an expression vector. Methods Enzymol 153: 545 563.
23. Gammon DB, Gowrishankar B, Duraffour S, Andrei G, Upton C, et al. (2010) Vaccinia virus-encoded ribonucleotide reductase subunits are differentially required for replication and pathogenesis. PLoS Pathog 6: e1000984.
24. Franke CA, Rice CM, Strauss JH, Hruby DE (1985) Neomycin resistance as a dominant selectable marker for selection and isolation of vaccinia virus recombinants. Mol Cell Biol 5: 1918 1924.
25. Falkner FG, Moss B (1988) Escherichia coli gpt gene provides dominant selection for vaccinia virus open reading frame expression vectors. J Virol 62: 1849 1854.
26. Chakrabarti S, Brechling K, Moss B (1985) Vaccinia virus expression vector: coexpression of beta-galactosidase provides visual screening of recombinant virus plaques. Mol Cell Biol 5: 3403 3409.
27. Carroll MW, Moss B (1995) E. coli beta-glucuronidase (GUS) as a marker for recombinant vaccinia viruses. Biotechniques 19: 352 354, 356.
28. Luker KE, Hutchens M, Schultz T, Pekosz A, Luker GD (2005) Bioluminescence imaging of vaccinia virus: effects of interferon on viral replication and spread. Virology 341: 284 300.
29. Committee for the Proprietary Medicinal Products (CPMP). Note for guidance on the quality, preclinical and clinical aspects of gene transfer medicinal products, *The European Agency for the Evaluation of Medicinal Products*, (London, 2001). EMA website. Available: http://www.ema.europa.eu/docs/en_GB/document_library/Scientific_guideline/2009/10/WC500003987.pdf. Accessed 2011 Aug 18.
30. Demmin GL, Clase AC, Randall JA, Enquist LW, Banfield BW (2001) Insertions in the gG gene of pseudorabies virus reduce expression of the upstream Us3 protein and inhibit cell-to-cell spread of virus infection. J Virol 75: 10856 10869.
31. Falkner FG, Moss B (1990) Transient dominant selection of recombinant vaccinia viruses. J Virol 64: 3108 3111.
32. Scheiflinger F, Dorner F, Falkner FG (1998) Transient marker stabilisation: a general procedure to construct marker-free recombinant vaccinia virus. Arch Virol 143: 467 474.
33. Alejo A, Saraiva M, Ruiz-Arguello MB, Viejo-Borbolla A, de Marco MF, et al. (2009) A method for the generation of ectromelia virus (ECTV) recombinants: in vivo analysis of ECTV vCD30 deletion mutants. PLoS One 4: e5175.
34. Gammon DB, Evans DH (2009) The 3′-to-5′ exonuclease activity of vaccinia virus DNA polymerase is essential and plays a role in promoting virus genetic recombination. J Virol 83: 4236 4250.
35. Sauer B, Henderson N (1988) Site-specific DNA recombination in mammalian cells by the Cre recombinase of bacteriophage P1. Proc Natl Acad Sci U S A 85: 5166 5170.
36. Sternberg N, Hamilton D (1981) Bacteriophage P1 site-specific recombination. I. Recombination between loxP sites. J Mol Biol 150: 467 486.
37. Xiang H, Wang J, Boxer LM (2006) Role of the cyclic AMP response element in the bcl-2 promoter in the regulation of endogenous Bcl-2 expression and apoptosis in murine B cells. Mol Cell Biol 26: 8599 8606.
38. Shor B, Cavender D, Harris C (2009) A kinase-dead knock-in mutation in mTOR leads to early embryonic lethality and is dispensable for the immune system in heterozygous mice. BMC Immunol 10: 28.
39. Shearwin KE, Callen BP, Egan JB (2005) Transcriptional interference a crash course. Trends Genet 21: 339 345.
40. Isaacs SN, Kotwal GJ, Moss B (1990) Reverse guanine phosphoribosyltransferase selection of recombinant vaccinia viruses. Virology 178: 626 630.
41. Lin YC, Li J, Irwin CR, Jenkins H, DeLange L, et al. (2008) Vaccinia virus DNA ligase recruits cellular topoisomerase II to sites of viral replication and assembly. J Virol 82: 5922 5932.
42. Gu H, Zou YR, Rajewsky K (1993) Independent control of immunoglobulin switch recombination at individual switch regions evidenced through Cre-loxP-mediated gene targeting. Cell 73: 1155 1164.
43. Chakrabarti S, Sisler JR, Moss B (1997) Compact, synthetic, vaccinia virus early/late promoter for protein expression. Biotechniques 23: 1094 1097.
44. Zhu B, Cai G, Hall EO, Freeman GJ (2007) In-fusion assembly: seamless engineering of multidomain fusion proteins, modular vectors, and mutations. Biotechniques 43: 354 359.
45. Soneoka Y, Cannon PM, Ramsdale EE, Griffiths JC, Romano G, et al. (1995) A transient three-plasmid expression system for the production of high titer retroviral vectors. Nucleic Acids Res 23: 628 633.
46. Meyer H, Damon IK, Esposito JJ (2004) Orthopoxvirus diagnostics. Methods Mol Biol 269: 119 134.
47. Krumsiek J, Arnold R, Rattei T (2007) Gepard: a rapid and sensitive tool for creating dotplots on genome scale. Bioinformatics 23: 1026 1028.

APPENDIX V: SEQUENTIAL THERAPY WITH JX-594, A TARGETED ONCOLYTIC POXVIRUS, FOLLOWED BY SORAFENIB IN HEPATOCELLULAR CARCINOMA: PRECLINICAL AND CLINICAL DEMONSTRATION OF COMBINATION EFFICACY

Jeong Heo, Caroline J Breitbach, Anne Moon, Chang Won Kim, Rick Patt, Mi Kyung Kim, Yu Kyung Lee, Sung Yong Oh, Hyun Young Woo, Kelley Parato, Julia Rintoul, Theresa Falls, Theresa Hickman, Byung-Geon Rhee, John C Bell, David H Kirn and Tae-Ho Hwang

Contribution:

I created the sorafenib resistant cell lines used in Figure 1, by sequential passage of the cells with increasing exposure to sorafenib.

Published: *Molecular Therapy, June 2011*

Sequential Therapy With JX-594, A Targeted Oncolytic Poxvirus, Followed by Sorafenib in Hepatocellular Carcinoma: Preclinical and Clinical Demonstration of Combination Efficacy

Jeong Heo[1], Caroline J Breitbach[2], Anne Moon[2], Chang Won Kim[1], Rick Patt[3], Mi Kyung Kim[1], Yu Kyung Lee[1], Sung Yong Oh[4], Hyun Young Woo[1], Kelley Parato[5], Julia Rintoul[5], Theresa Falls[5], Theresa Hickman[2], Byung-Geon Rhee[6], John C Bell[2,5], David H Kirn[2] and Tae-Ho Hwang[1]

[1]*Pusan National University, Busan, South Korea;* [2]*Jennerex Inc., San Francisco, California, USA;* [3]*RadMD, Doylestown, Pennsylvania, USA;* [4]*Dong-A University, Busan, South Korea;* [5]*Ottawa Hospital Research Institute and University of Ottawa, Ottawa, Ontario, Canada;* [6]*Green Cross Corp., Yongin, South Korea*

JX-594 is a targeted and granulocyte-macrophage colony stimulating factor (GM-CSF) expressing oncolytic poxvirus designed to selectively replicate in and destroy cancer cells through viral oncolysis and tumor-specific immunity. In a phase 1 trial, JX-594 injection into hepatocellular carcinoma (HCC) was well-tolerated and associated with viral replication, decreased tumor perfusion, and tumor necrosis. We hypothesized that JX-594 and sorafenib, a small molecule inhibitor of B-raf and vascular endothelial growth factor receptor (VEGFR) approved for HCC, would have clinical benefit in combination given their demonstrated efficacy in HCC patients and their complementary mechanisms-of-action. HCC cell lines were uniformly sensitive to JX-594. Anti-raf kinase effects of concurrent sorafenib inhibited JX-594 replication *in vitro*, whereas sequential therapy was superior to either agent alone in murine tumor models. We therefore explored pilot safety and efficacy of JX-594 followed by sorafenib in three HCC patients. In all three patients, sequential treatment was (i) well-tolerated, (ii) associated with significantly decreased tumor perfusion, and (iii) associated with objective tumor responses (Choi criteria; up to 100% necrosis). HCC historical control patients on sorafenib alone at the same institutions had no objective tumor responses (0 of 15). Treatment of HCC with JX-594 followed by sorafenib has antitumoral activity, and JX-594 may sensitize tumors to subsequent therapy with VEGF/VEGFR inhibitors.

Received 15 December 2010; accepted 10 February 2011; published online 22 March 2011. doi:10.1038/mt.2011.39

INTRODUCTION

The targeted oncolytic poxvirus JX-594 replicates selectively in cancer cells resulting in virus progeny production, tumor cell necrosis (oncolysis), JX-594 release and subsequent spread within tumor tissues.[1] JX-594 is also engineered to express the granulocyte-macrophage colony stimulating factor (GM-CSF) transgene, a potent activator of dendritic cells,[2] in order to enhance the antitumor immunity that results from oncolysis. In addition, JX-594 and other oncolytic poxviruses and vesicular stomatitis virus have been shown to trigger an acute reduction in tumor perfusion in mouse models.[3,4] Therefore, JX-594 is able to induce direct viral oncolysis followed by tumor vascular shutdown and antitumoral immunity. The Wyeth vaccinia backbone of JX-594 is inherently tumor-selective due to endothelial growth factor receptor (EGFR)-ras pathway dependency (activated in cancer cells)[5,6] and resistance to interferon induction and effects in tumors.[7] The inherent therapeutic index is amplified by the deletion of the vaccinia thymidine kinase (*TK*) gene. As a result, JX-594 replication is also dependent on high levels of cellular TK which is driven by cell cycle abnormalities in cancer.[8] Results from a phase 1 clinical trial of intratumoral JX-594 in patients with refractory liver tumors demonstrated safety, antitumor efficacy and mechanistic proof-of-concept for JX-594 replication, systemic dissemination to distant tumors and expression of biologically active GM-CSF.[9] In this trial, hepatocellular carcinoma (HCC) were found to be highly sensitive to JX-594, resulting in acute vascular shutdown and necrotic (Choi) tumor responses.[10] Noninjected tumors also demonstrated infection and necrosis following trafficking of JX-594 through the blood to distant tumor sites. No liver toxicity was reported. Phase 2 development of JX-594 in patients with advanced HCC was therefore indicated.

The only approved systemic therapy for HCC to date is sorafenib (Nexavar, and Bayer, Leverkusen, Germany). Sorafenib is an oral small molecule multi-kinase inhibitor that has both antiproliferative (*via* B-raf kinase inhibition) and antiangiogenic effects [*via* inhibition of vascular EGFR (VEGFR)] in mice and humans.[11] Sorafenib was evaluated in two phase 3 randomized clinical trials of patients with advanced HCC.[12,13] In both of these trials, objective tumor responses were rare (1–2% objective partial Response

Evaluation Criteria In Solid Tumors (RECIST) responses). The median survival duration was increased by ~3 months. Sorafenib toxicities include rash (hand-foot syndrome), diarrhea, and fatigue; dose reductions and/or discontinuation are common. Therefore, novel therapies are needed for patients with HCC, both as single agents and in combination with sorafenib therapy.

We hypothesized that the combination of the oncolytic poxvirus JX-594 and the small molecule sorafenib could result in superior efficacy to that achievable with sorafenib alone in HCC. These agents have differing and complementary mechanisms-of-action. JX-594 induces acute tumor cell cytolysis, tumor vascular disruption, and necrosis followed by long-term antitumor immunity. In contrast, sorafenib is antiangiogenic and inhibits tumor progression. In addition, the toxicity profiles are not overlapping, and therefore the combination was predicted to have an acceptable toxicity profile. A potential problem with this combination, if given simultaneously, would be that sorafenib could block JX-594 replication through its raf inhibition. We explored simultaneous and sequential combinations *in vitro* and in animal tumor models. Based on promising preclinical data with sequential treatment, clinical proof-of-concept was explored in HCC patients who had completed JX-594 treatment as a single agent on a phase 2 trial. After progression following JX-594, standard sorafenib therapy was evaluated in these patients. In order to assess whether the findings in JX-594 treated patients were typically seen with sorafenib alone, the effect of sorafenib alone was assessed in concurrent and recent historical controls at the same institutions. Finally, a renal cell carcinoma patient was treated with JX-594 followed by sunitinib (Sutent, Pfizer, New York, NY), another small molecule inhibitor of VEGFR with an activity profile similar to sorafenib. Renal cell cancer (RCC) is similar to HCC in that it is a highly vascularized tumor type, and sunitinib shares similar VEGFR inhibition with sorafenib. Therefore, this RCC patient shares similar histologic and treatment features to the three HCC patients.

RESULTS

Sorafenib inhibits JX-594 replication *in vitro*

Based upon our earlier clinical studies[9] we predicted that JX-594 would be able to infect and kill a wide variety of cell lines derived from human HCC. Indeed we found that JX-594, *in vitro*, infects and destroys several different human HCC cell lines. HepG2, SNU423, SNU475, SNU449, and PLC/PRF/5 have been tested and shown to be susceptible to JX-594 infection by burst and/or plaque assay (Figure 1a–e). In addition, the ability of a sorafenib resistant/adapted derivative of PLC/PRF/5 to support JX-594 replication was evaluated. To generate sorafenib resistant/adapted cultures, PLC/PRF-5 cells were grown *in vitro* at increasing doses of sorafenib for a total of 3 months, starting at a sorafenib concentration of 1 µmol/l and increasing up to 6 µmol/l. The resistant/adapted cells supported JX-594 replication at a level comparable to its parental sorafenib sensitive clone (Figure 1a). As discussed earlier, the

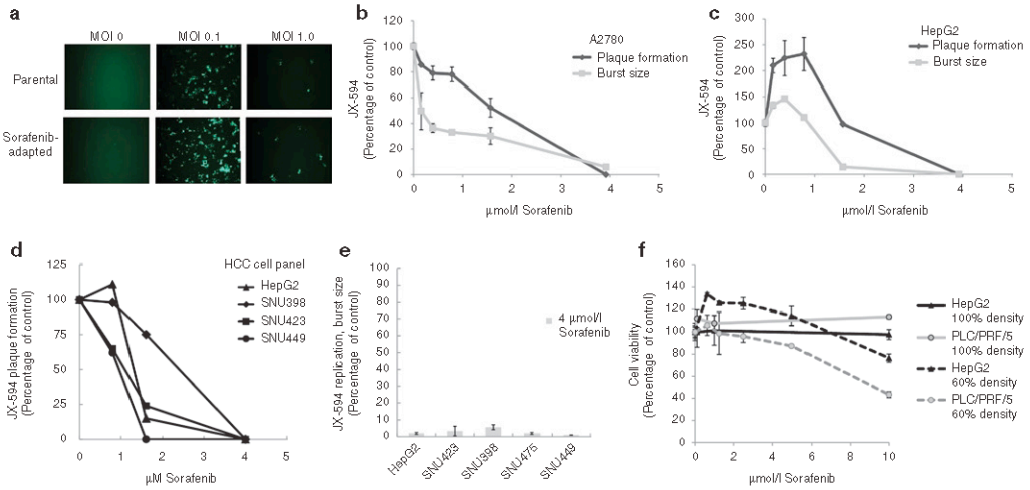

Figure 1 JX-594 replication in liver cancer lines is inhibited in the presence of sorafenib *in vitro*. (**a**) Infectability of PLC/PRF/5 (human hepatoma) cells (parental) and sorafenib-adapted PLC/PRF/5 cells was determined by addition of JX-594 expressing green fluorescent protein at multiplicities of infection (MOI) of 0, 0.1 and 1. Images were taken with a Zeiss Axiovision microscope fluorescent microscope and analyzed using Axiovision acquisition and image storage software 24 hours postinfection. (**b**,**c**) JX-594 replication in the presence of sorafenib was measured by plaque formation and burst assay after incubation with sorafenib for 3 days (plaque formation assay) or 24 hours (burst assay). Results are expressed as percent of no-sorafenib control (replicate mean + SD). (**d**) The ability of JX-594 to form plaques in the absence or presence of increasing concentrations of sorafenib on monolayers of hepatocellular carcinoma (HCC) cell lines. Results are expressed as percent of no sorafenib control. (**e**) JX-594 replication was tested by burst assay using a panel of HCC cell lines infected at MOI of 0.1 for 2 hours, followed by change to media with 4 µmol/l sorafenib. After 48 hours, cells and supernatants were collected for titration by plaque assay on A2780 cells. Results are expressed as percent of no-sorafenib control (replicate mean + SD). (**f**) Cell viability in the presence of sorafenib was determined 24 hours after addition of sorafenib to PLC/PRF/5 and HepG2 cells plated at 60% and 100% densities. Results are expressed as percent of no-sorafenib control (replicate mean + SD).

replication of JX-594 is determined in part by activation of the EGFR/Ras/Raf pathway and so we reasoned that as a Raf kinase inhibitor, sorafenib might theoretically affect virus replication. We therefore tested the ability of JX-594 to infect and replicate tumor cells in the presence of sorafenib. JX-594 was allowed to infect monolayers of A2780 (ovarian cancer cell line) or HepG2 (HCC cell line) in the absence or presence of increasing concentrations of sorafenib, and JX-594 replication was assessed by measuring plaque formation on the original monolayer, and the production of new plaque-forming units (pfu, replicative burst) (**Figure 1b,c**). JX-594 plaque formation and replication were inhibited in a dose-related fashion (**Figure 1b,c**); inhibition was >95% at 4 µmol/l sorafenib. Similar results were found in a subsequent experiments using a broader panel of HCC cell lines (**Figure 1d,e**) and PLC/PRF/5 cells (data not shown), JX-594 plaque formation was inhibited in the presence of sorafenib in a dose-dependent fashion (**Figure 1e**), and JX-594 replication as measured by burst assay was decreased by >90% in all cases by sorafenib concentrations of 4 µmol/l (**Figure 1e**). The concentrations of sorafenib shown to inhibit JX-594 replication (*e.g.*, 4 µmol/l) were shown to be noncytocidal in a sorafenib-alone condition; cells plated at 100% and incubated with sorafenib for 24 hours did not have reduced viability compared to no-sorafenib control. Cells plated at 60% density and incubated with sorafenib for 24 hours also showed no cytotoxicity at 5 µmol/l, while higher concentrations were growth-inhibitory as demonstrated by the 10 µmol/l sorafenib condition that did grow out compared to control at 24 hours (**Figure 1f**). Thus as predicted, the raf kinase inhibitor sorafenib significantly decreased JX-594 replication on viable tumor cells.

Sequential combination of JX-594 and sorafenib results in improved efficacy in two murine tumor models

The data presented above demonstrated that JX-594 efficiently infects HepG2 cells *in vitro* and therefore a murine xenograft model was established using this cell line to evaluate the use of sorafenib in combination with JX-594 *in vivo*. In order to be able to detect additive/synergistic effects when JX-594 and sorafenib were administered simultaneously both agents were given at doses that were suboptimal as single agents in this model. Our pilot experiments showed that doses of 500 µg and 1,000 µg sorafenib/day intraperitoneally in mice resulted in plasma concentrations of ~0.9 mg/l and ~3.1 mg/l (data not shown). Therefore, the doses of sorafenib used in this study were clinically relevant and had detectable effects in this model.

Tumors in control animals treated daily with phosphate-buffered saline (PBS) progressed rapidly, reaching a mean size of 10,000 mm^3 on day 25. Sorafenib or JX-594 dosing alone slowed tumor growth. By the end of study on day 31, the JX-594 group showed significant inhibition versus the PBS control group whereas the sorafenib group did not (P values of 0.0005 and 0.3693, respectively; paired Student's t-test). The regimen of JX-594 followed by sorafenib was statistically superior to PBS (P value 0.0028) and sorafenib alone (P value 0.0101) in terms of tumor growth at the end of study on day 31. In addition, this sequence was superior to sorafenib followed by JX-594 (P value 0.0021) and to simultaneous treatment (P value 0.0052).

The time-to-tumor progression (TTP) was assessed according to Kaplan–Meier analysis (end point reached when tumors reached 5,000 mm^3; log-rank test applied). The regimen of JX-594 followed by sorafenib was statistically significantly superior to all other regimens in terms of TTP. The data was plotted as Kaplan–Meier curves following percent nonprogression over time (**Figure 2a,b**). Animals that died prior to tumors reaching 5,000 mm^3, or did not reach 5,000 mm^3 by the end of study (day 31) were censored when running log-rank (Mantel–Cox) test. The best combination regimen (JX-594 followed by sorafenib) is shown compared to single agents in **Figure 2a**, and to other suboptimal combination regimens in **Figure 2b**. The P values for JX-594 followed by sorafenib versus other groups were as follows: PBS (<0.0001), sorafenib alone (0.0012), JX-594 alone (0.0149), sorafenib followed by JX-594 (0.0001), and sorafenib simultaneously with JX-594 (0.0042). The median TTP for animals in the JX-594 followed by sorafenib group was not reached by the end of the study (day 31). Median TTP times for the other groups were 17 days (PBS), 22 days (JX-594 alone), 27 days (sorafenib alone), 26 days (sorafenib together with JX-594) and 26 days (sorafenib followed by JX-594).

The efficacy of JX-594 in combination with sorafenib was subsequently evaluated in a metastatic B16 melanoma model as it allows for precise quantitation of lung metastases, and the assessment of efficacy in a widely metastatic tumor model in an immunocompetent host. Given the rapidity of tumor progression in this model, it was not feasible to perform sequential therapy. Therefore, JX-594 and sorafenib simultaneous combination therapy was evaluated. Combination therapy resulted in a significant reduction in the mean number of B16 tumors in the lungs compared to PBS ($P < 0.001$), the JX-594 alone group ($P = 0.05$) or the sorafenib alone group ($P = 0.002$) (**Figure 2c**).

Efficacy with modified Choi tumor responses following sequential JX-594 and sorafenib therapy in patients with advanced HCC

Encouraged by the preclinical data above, as well as JX-594 clinical data (objective responses, prolonged survival) as a single agent in HCC, we evaluated the sequential administration of JX-594 followed by sorafenib in patients. Prior to a prospectively designed trial of sequential combination therapy in patients, we elected to study this regimen in pilot fashion to confirm its safety and potential efficacy. Since a JX-594 phase 2 single agent trial was underway in advanced HCC patients who had not received prior sorafenib, we were able to follow patient safety and tumor response on standard sorafenib once tumors progressed following JX-594. Three such patients were identified, and special consent was obtained to obtain serial magnetic resonance imaging (MRI) scans while on sorafenib therapy. These individuals had initially received three intratumoral injections of JX-594 (every 2 weeks) into intrahepatic tumors and were evaluated radiographically at week 8 (by dynamic MRI). After tumor progression following JX-594, these patients were treated with standard sorafenib (the standard treatment in this patient population) and subsequently evaluated for safety and efficacy based on serial dynamic MRI imaging while on sorafenib.

Previous trials with JX-594 have demonstrated reproducible induction of clinically significant tumor necrosis. Therefore, the

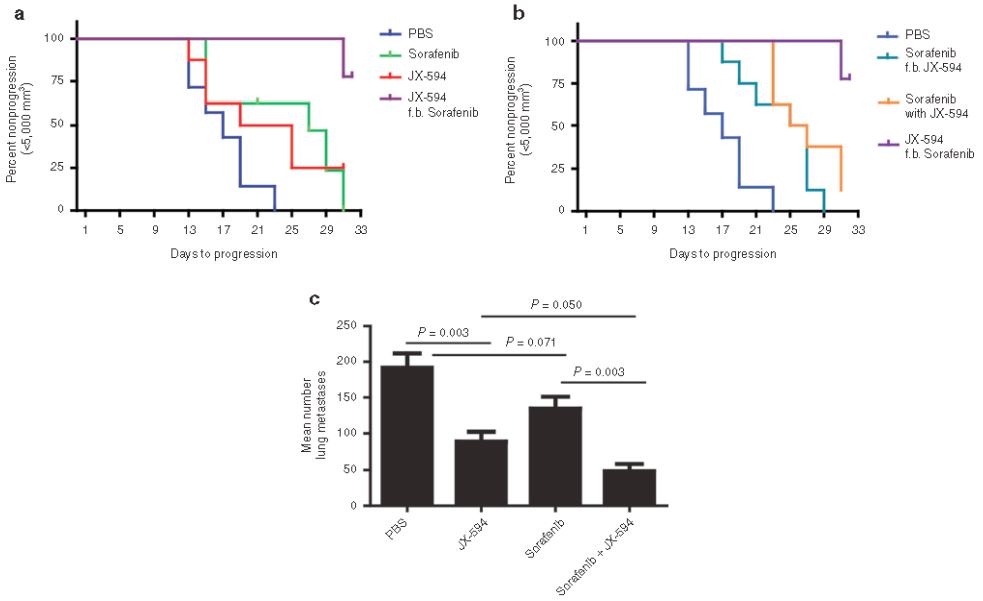

Figure 2 Combination therapy with sorafenib enhances JX-594 efficacy in two murine tumor models. (**a**,**b**) SCID mice with subcutaneous HepG2 tumors of 12–14 mm diameter were randomized to five groups and treated with PBS, daily sorafenib, weekly JX 594, simultaneous sorafenib and JX-594, or sequentially treated with sorafenib for 2 weeks followed by JX-594, or with 2 weekly dose of JX-594 followed by sorafenib. Analysis of time-to-tumor-progression (TTP) was performed. Kaplan–Meier curves show TTP, with 5,000 mm^3 tumor volume considered as progression. (**c**) B16 model of lung metastases: C57 BL/6 mice were injected with 3×10^5 B16-F10-LacZ cells intravenously and 24 hours later were treated with phosphate buffered saline (PBS), sorafenib alone (50 µg/kg per oral dosing daily for 2 weeks) JX594 alone (10^7 plaque-forming units (pfu) intravenously three times per week for 1 week) or in combination ($n = 5$ per group). Three weeks after treatment initiation, mice were killed and lungs were fixed and stained to detect surface B16 tumor nodules.

Choi criteria were deemed an appropriate method to assess antitumor activity of JX-594; Choi criteria are based on both tumor size and tumor enhancement (a measure of tumor perfusion and vascularity after intravenous contrast administration). In addition, the modified RECIST criteria for HCC were also utilized; these criteria were developed for HCC specifically by Lencioni *et al.*, and take into account changes in viable tumor size.[14] While on sorafenib all three patients exhibited rapid and marked tumor necrosis. Tumor necrosis was quantitated through serial measurement of tumor density (*i.e.*, decreased tumor contrast enhancement/ uptake over time) following initiation of sorafenib (**Figure 3a–c**) (**Table 1**). All patients had marked Choi responses[15] and modified RECIST-type responses.[14] Tumor responses on sorafenib occurred as early as 2.5 weeks after sorafenib initiation. In addition, one patient also had noninjected tumors within the liver, and marked tumor response following sorafenib was noted in these tumors as well as the injected tumors, consistent with known spread of JX-594 to noninjected tumors *via* the blood (**Figure 3c**); of note, noninjected tumor infection and responses were described with JX-594 in a phase 1 trial in liver tumor patients.[9] Also noteworthy is that sorafenib alone has not been described to induce Choi or modified RECIST (mRECIST) responses to date, although modest necrosis induction has been described in a minority of patients.[16]

Three-dimensional segmentation analysis of treated tumors reveals significant necrosis induction with JX-594 followed by sorafenib

In order to more fully understand the extent and distribution of tumor volume destruction, a three-dimensional (3D) segmentation analysis of liver tumors was performed in one patient (number 1705). MRI images at baseline, after JX-594 treatment alone (week 8) and post sorafenib initiation (week 13) (**Figure 3a**) were used to reconstruct the entire liver (both normal and tumor tissues) (**Figure 4a**). Necrosis induction was quantified and increasing volume of necrosis and decreasing volume of viable tumor were calculated within each tumors. In this patient, JX-594 treatment alone did not induce significant necrosis. However, following initiation of sorafenib, all three intrahepatic tumors became significantly necrotic (between 50 and 100% of the entire tumor volume) (**Figure 4b**).

Concurrent and historical control patients on sorafenib alone: lack of tumor responses

The relatively acute and extensive vascular disruption and tumor necrosis (captured as modified Choi tumor responses) described here with JX-594 followed by sorafenib has not been reported with sorafenib alone. Nevertheless, in order to assess whether sorafenib

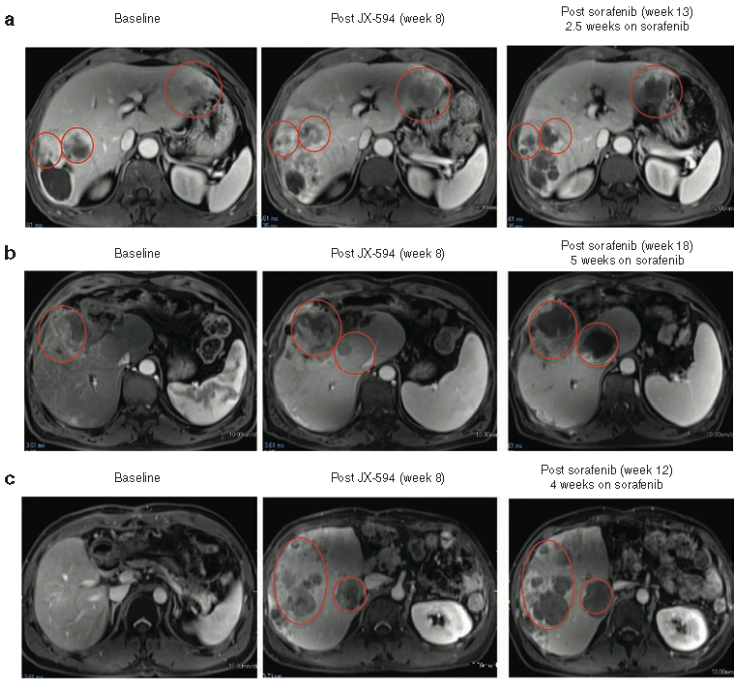

Figure 3 JX-594 treatment of patients with advanced hepatocellular carcinoma cell may sensitize to subsequent sorafenib therapy. (**a**) Patient 1705 was treated with JX-594 at a dose level of 10^8 plaque-forming units (pfu) intratumorally for three treatments every 2 weeks (week 0, week 2, week 4). Sorafenib therapy was initiated at week 10.5. Antitumor response was evaluated by dynamic contrast-enhanced magnetic resonance imaging (MRI) at baseline, after treatment with JX-594 alone and after sorafenib initiation. Red circles indicate target tumors. The darker areas within the target tumors at week 13 represent significant increasing necrosis within the target tumors is seen at week 11, manifested by nonenhancement within these tumors. (**b**) Patient 1702 was treated with JX-594 at a dose level of 10^9 pfu intratumorally for three treatments every 2 weeks (week 0, week 2, week 4). Sorafenib therapy was initiated at week 13. Response was evaluated by dynamic MRI imaging at baseline, after treatment with JX-594 alone and after sorafenib initiation. Red circles indicate target tumors. Mild amount of necrosis is seen in the larger tumor at baseline. The necrosis increases somewhat following JX-594 alone, but significant necrosis is identified following sorafenib therapy. (**c**) Patient 1712 was treated with JX-594 at a dose level of 10^9 pfu intratumorally for three treatments every 2 weeks (week 0, week 2, week 4). Sorafenib therapy was initiated at Week 8. Response was evaluated by dynamic MRI imaging at baseline, after treatment with JX-594 alone and after sorafenib initiation. Red ovals indicate areas of the liver not injected with JX-594. These images demonstrate antitumor activity in noninjected lesions similar to that seen in injected lesions from (**a**) and (**b**). Progressively developing necrosis within these tumors is seen following JX-594 therapy alone and then sorafenib.

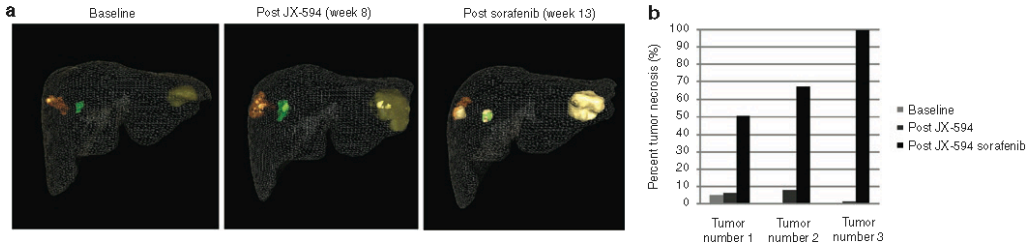

Figure 4 Three-dimensional segmentation analysis reveals significant tumor necrosis induction following JX-594 and sorafenib combination treatment. (**a**) Patient 1705 dynamic magnetic resonance imaging scans collected at baseline, week 8, and week 13 were evaluated using 3D segmentation analysis to assess the volumes of viable and necrotic tumor at each timepoint. Dark orange, green, and yellow indicate viable tumor tissue. Lighter colors within each tumor indicate geographic areas of necrosis. The liver margin is displayed as a wire frame. Note that on the week 13 image, the viable tumor in the largest lesion has been nearly completely replaced by necrosis. (**b**) Percent tumor necrosis (compared to total tumor volume) at baseline, after JX-594 therapy alone and after subsequent sorafenib initiation by tumor.

Table 1 Patient baseline tumor characteristics, treatment, and radiographic response to JX-594 and subsequent sorafenib

Patient number/JX-594 dose (plaque-forming units (pfu))	Baseline tumor(s) max diameter (cm), enhancement	Week 8 response to JX-594 alone (dynamic magnetic resonance imaging (MRI))	Best response to subsequent sorafenib (dynamic MRI)	Sorafenib dosing details	Sorafenib-associated toxicities (possibly or probably related)
1702/(10^9)	7.2 cm total (one tumor); 12% enhancement	Injected tumor: SD (–) Choi response (29% increase enhancement) overall: PD	Overall: (+) Choi response (68% decrease enhancement); SD	400 mg po b.i.d.; decrease to 400 q.d. (2.7 months); discontinue (8 months).	grade 1 hand-foot skin reaction (7 weeks); grade 1 fatigue (4 days); grade 2 esophageal pain (9 days)
1705/(10^9)	8.2 cm total (three tumors); 179% enhancement	Injected tumor: (+) Choi response (36% decrease enhancement) overall: PD	Overall: (+) Choi response (75% decrease enhancement); SD	400 mg po b.i.d.; decrease to 400 q.d. (5.0 months); discontinue (6.5 months)	grade 1 hand-foot skin reaction (5 months); grade 1 diarrhea (5 days)
1712/(10^9)	11.8 cm total (four tumors); 120% enhancement	Injected tumor: (+) Choi response (33% decrease enhancement) overall: PD	Overall: (+) Choi response (89% decrease enhancement); SD	400 mg po b.i.d.; decrease to 400 q.d. (1.7 months); discontinue (2.5 months)	grade 1 hand-foot skin reaction (6 weeks)

Abbreviations: q.d., once daily; b.i.d., twice daily; PD, progressive disease by Response Evaluation Criteria In Solid Tumors (RECIST); po, per oral dosing; SD, stable disease by RECIST.
Choi response criteria: maximum diameter decrease of ≥10% or density decrease of ≥15%.

alone routinely induces modified Choi responses, HCC patients treated with sorafenib alone at the same institutions over the preceding two years (i.e., historical and concurrent) were assessed if they had serial dynamic MRI scans of the liver (baseline and at least one follow-up scan at week 8 or later). Fifteen consecutive control patients were identified. The Barcelona Clinic Liver Criteria (BCLC) stage, tumor stage, age and gender profiles were similar between control patients and those receiving JX-594 followed by sorafenib (Table 1). No modified Choi responses were evident in scans from these patients on sorafenib alone (Table 2). In addition, according to RECIST criteria,[17] while 9 of 15 (60%) patients had progressive disease as their best response on sorafenib alone (40% stable disease), no progressive disease was noted in the JX-594 treated sorafenib patients (three of three with stable disease).

Case report of a patient with RCC treated with JX-594 followed by sunitinib (small molecule inhibitor of VEGFR)

Given the potential for synergistic antitumor activity with JX-594 and sorafenib in patients with HCC, we evaluated sequential therapy with JX-594 followed by sunitinib (also a small molecule with VEGFR inhibitory properties as seen with sorafenib) that is approved for the treatment of RCC. RCC has a high degree of tumor vascularity, and is therefore highly similar to HCC in this feature. Therefore, this clinical situation is analogous to sorafenib therapy in HCC. A patient with metastatic RCC was treated with JX-594 on a phase 1 intratumoral dose escalation trial of JX-594. This patient had widely metastatic cancer, including a 14 cm abdominal mass. According to the prognostic criteria outlined by Patil *et al.*[18] the patient had poor prognosis disease and a life expectancy of <6 months. The patient received four injections of JX-594 into liver metastases, resulting in modified Choi tumor responses within the liver and abdomen, but massive bulky tumor

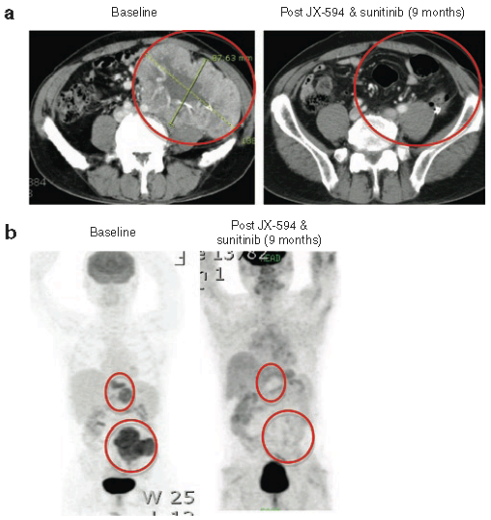

Figure 5 Tumor destruction in patient with advanced, poor prognosis renal cell cancer following JX-594 and sunitinib combination treatment. (**a**) Patient 301 was treated with JX-594 at a dose level of 10^9 plaque-forming units (pfu) intratumorally in liver metastases for four treatments every 3 weeks (week 0, week 3, week 6, and week 9). Sunitinib therapy was initiated at ~week 17. Contrast-enhanced computed tomography scans of patient 301 at baseline and 9 months after JX-594 and sunitinib treatment. A noninjected, large hypervascular mass in the left abdomen shows essentially complete resolution 9 months following JX-594 and sunitinib therapy. (**b**) Whole body positron emission tomography scan of patient at baseline and 9 months after JX-594 and sunitinib treatment shows complete disappearance of fludeoxyglucose-avid tumor following JX-594 and sunitinib.

Table 2 Hepatocellular carcinoma patients receiving sorafenib with (cases) or without (controls) prior JX-594: demographics, radiographic response to sorafenib by Response Evaluation Criteria In Solid Tumors (RECIST) and Choi criteria

Patient number	Age/ gender (F/M)	TNM stage	BCLC stage	Best response by RECIST	Best response by modified Choi
Controls					
1	51/F	4	C	PD	NR
2	48/M	4	C	SD	NR
3	57/M	2	B	SD	NR
4	43/F	3A	B	SD	NR
5	40/M	3A	C	SD	NR
6	63/M	1	A	SD	NR
7	55/M	1	A	PD	NR
8	67/M	3A	C	PD	NR
9	60/F	2	B	PD	NR
10	43/M	1	A	PD	NR
11	50/F	2	B	PD	NR
12	66/M	3A	C	PD	NR
13	56/M	3A	B	PD	NR
14	69/F	3A	C	SD	NR
15	67/M	2	B	PD	NR
Control totals				60% PD, 40% SD	0/15 Responses
JX-594-1	50/M	3A	C	SD	Response
JX-594-2	54/M	3A	C	SD	Response
JX-594-3	39/M	4	C	SD	Response
Cases totals				0% PD, 100% SD	3/3 Responses

Abbreviations: BCLC, Barcelona Clinic Liver Criteria; NR, nonresponder; PD, progressive disease by RECIST; SD, stable disease by RECIST.
Response/Choi response criteria: sum of diameters decrease of ≥10% or density decrease of ≥15%.

masses still remained. Sunitinib was initiated ~8 weeks after the last JX-594 dose. Therapy with full dose sunitinib (50 mg per day) was administered until dose reductions at 4 months (37.5 mg per day) and 7 months (25 mg); the patient remains on low dose sunitinib at this time. Despite the poor prognosis and significant dose reductions, the patient nevertheless exhibited a complete whole body tumor response by computed tomography and positron emission tomography scanning; this included complete disappearance of the large 14 cm. abdominal mass (Figure 5a,b). This patient remains alive and disease-free over 4 years after treatment initiation, despite a baseline life expectancy of <6 months.

DISCUSSION

We hypothesized that JX-594, a multi-mechanistic oncolytic poxvirus, and sorafenib, a small molecule inhibitor of both the B-raf kinase and VEGFR approved for advanced HCC treatment, would have efficacy in combination given their complementary and distinct mechanisms-of-action. Both agents have single agent activity in HCC, and their toxicities are not over-lapping. Here we report that sequential JX-594 followed by sorafenib in animal tumor models was superior to either agent alone, despite inhibition of JX-594 replication by sorafenib if given simultaneously *in vitro*. Relevant syngeneic murine models of HCC are difficult to establish. In addition, JX-594 is derived from the Wyeth strain of vaccinia, a strain which demonstrates markedly lower replication in murine cells compared with human cells. Therefore, the efficacy of the two agents was first evaluated in a xenograft model of human HCC in which JX-594 replication and effects on tumor vasculature could be studied in the presence or absence of sorafenib. We subsequently elected to test the combination therapy in an immunocompetent murine tumor model (B16 lung metastases) that allowed for precise quantification of metastatic tumor burden (note: HCC in humans commonly metastasizes to the lungs). In addition to JX-594 replication and antivascular effects, the induction of potential antitumor immunity may be affected upon addition of sorafenib in this model, making it more relevant to subsequent human studies. The combination of JX-594 and sorafenib was superior to either agent alone in both models. In one model, simultaneous and sequential therapy could be evaluated. As expected in this human tumor model supporting robust viral replication, sequential therapy was superior to concurrent therapy (presumably due to inhibition of viral replication). In a murine tumor model in which viral replication effects are less relevant (JX-594 replication is markedly lower in murine tumor cells versus human tumor cells), concurrent therapy was superior to either agent alone.

Based on the preclinical data above, and single agent activity of both agents in HCC, we evaluated the sequential administration of JX-594 followed by sorafenib in patients. Since a JX-594 phase 2 single agent trial was underway in advanced HCC patients who had not received prior sorafenib, we were able to follow patient safety and tumor response on standard sorafenib once tumors progressed following JX-594. Three such patients were identified, and all three patients exhibited rapid (2.5 weeks) and marked tumor necrosis (up to 100% of the viable tumor mass) and responses on sorafenib. Of note, sorafenib alone has not been described to induce necrotic Choi or mRECIST responses to date, although modest necrosis induction has been described in a minority of patients.[16] Finally, 15 consecutive HCC historical and concurrent control patients on sorafenib alone at the same institutions were retrospectively assessed, and no Choi or mRECIST responses were noted (0 of 15). A fourth JX-594-treated patient (metastatic, poor prognosis RCC) from a separate phase 1 trial was treated with a similar small molecule angiogenesis inhibitor (sunitinib); this patient had a durable complete response lasting over 4 years (still on-going). JX-594 is expected to be cleared within weeks and dramatic responses in injected tumors long after completion of JX-594 therapy have not been observed to date. Therefore based on the data presented here, we hypothesize that JX-594 therapy may sensitize HCC tumors to sorafenib and potentially other VEGFR inhibitors (*i.e.*, a therapeutic class effect). A randomized controlled trial of sorafenib alone versus JX-594 followed by sorafenib is required to validate this hypothesis.

Additional nonclinical and clinical studies should be performed to confirm these findings. Only three patients were evaluated in this study; it is not yet clear whether these patients are representative of the HCC population at large. In addition, while mRECIST and Choi responses have not been reported

with sorafenib alone, it is possible that on future study sorafenib responses will be demonstrated. A phase 2 trial of JX-594 followed by sorafenib has been initiated in patients with advanced HCC. JX-594 treatment is followed by standard sorafenib initiated 1 week after the final JX-594 injection. Promising interim safety and efficacy data has been reported.[19] Of note, objective tumor responses have been reported for patients who have documented resistance to, and tumor progression on, sorafenib monotherapy. A prospective randomized trial will be required to confirm that JX-594 followed by sorafenib leads to superior response rate and survival duration compared to either agent alone in HCC patients; planning for such a trial is underway. In addition, if the ability of JX-594 to resensitize sorafenib-refractory tumors to sorafenib is confirmed, a randomized trial of JX-594 followed by sorafenib versus best supportive care may be indicated in this patient population. Similar trials can be envisioned with other inhibitors of the VEGFR pathway in development.

The potential mechanism(s) involved in JX-594-mediated sensitization of tumors to sorafenib remain to be elucidated. Of note, the effect(s) appear to occur relatively acute and durable, lasting up to 8 weeks or more following the last dose of JX-594 prior to sorafenib. We hypothesize that soluble mediators produced by residual cells within the tumor may be involved. Since sorafenib has effects on both tumor cells and their associated vasculature, it is possible that JX-594 sensitizes either or both of these tumor components to sorafenib. JX-594 replication and transgene expression within tumors may either decrease soluble factor(s) that are protective against sorafenib and/or increase concentrations of soluble sensitizers to sorafenib. It is known that the physiology of vascular endothelium can be affected by persistent epigenetic changes initiated by an acute event.[20,21] We hypothesize that cytokines released during JX-594 infection of tumors could reprogram vascular endothelial cells and render them exquisitely sensitive to the antiangiogenic properties of sorafenib for extended periods of time. Interestingly, it has been shown that the expression of the sorafenib target, VEGFR, is susceptible to epigenetic modulation through DNA methylation.[22] Candidate soluble sensitizers to sorafenib effects include cytokines such as interferons or tumor necrosis factor (*e.g.*, produced by immune cells recruited into tumors by JX-594). Apoptosis inhibitors that could be reduced by intratumoral JX-594 effects may include growth factors for cancer cells (*e.g.*, epidermal growth factor) and/or tumor-associated endothelial cells (*e.g.*, VEGF). Of note, we have also demonstrated that targeted oncolytic vaccinia viruses can selectively infect and replicate within tumor-associated endothelial cells but not in normal vasculature.[4] Other investigators have subsequently reported the ability of other viruses to also selectively infect activated tumor-associated endothelial cells.[23] Finally, it is possible that neovasculature forms following JX-594-mediated tumor necrosis and vascular disruption, and that these newly formed vessels are hypersensitive to sorafenib effects.[24] Other vascular disrupting agents are associated with post-treatment increases in angiogenesis. If VEGF signaling is necessary for this phenomenon, other anti-VEGF pathway inhibitors may also be used in combination with JX-594. A pure VEGF pathway inhibitor that does not also inhibit the EGFR/ras/raf pathway would not have the problem of JX-594 replication inhibition that is associated with sorafenib.

Potential safety concerns with this sequential combination therapy should be considered. First, anti-VEGF/VEGFR therapies can cause bleeding from gastrointestinal or pulmonary sites. The JX-594-mediated lysis of tumors that have invaded vital structures might theoretically lead to bleeding, and anti-VEGF therapy might exacerbate this risk. Bleeding complications have not been reported to date with JX-594, but more clinical experience is needed. More patients must be treated in order to adequately assess potential safety risks.

Vaccinia has previously been shown to be inhibited by tyrosine kinase inhibitors such as imatinib (Gleevec, Basel, Switzerland).[25] In particular, vaccinia and other poxviruses are known to exploit activation of the EGFR pathway for their replication and spread from infected cells.[5] Therefore, it is not surprising that inhibitors of this pathway are able to inhibit vaccinia replication.[6] Raf kinase is downstream of ras and the EGF receptor, and its inhibition blocks this signal transduction pathway. Sorafenib was initially discovered because of its raf kinase inhibitory properties.[26] We demonstrate here that sorafenib has antivaccinia properties (>90% inhibition of replication or cytotoxicity *in vitro*) that may make it a useful inhibitor in the case of poxvirus-mediated toxicity. Potential applications include use as an anti-smallpox agent (in the event or reintroduction of the agent into the population), as has been proposed with imatinib, or in the case of live vaccinia virus vaccine complications. In addition, if future replication-mediated toxicities occur with JX-594, sorafenib might be considered in addition to standard antivaccinia agents such as vaccinia immune globulin and cidofovir.

In summary, targeted, oncolytic poxviruses (*e.g.*, JX-594) are novel class of anticancer agents that can be combined with other agents due to their distinct mechanisms-of-action and nonoverlapping toxicity profiles. In particular, therapeutic potential of small-molecule VEGFR inhibitors or other antiangiogenic agents may be enhanced when combined with JX-594 therapy.

MATERIALS AND METHODS

Cell culture and in vitro evaluations. Human tumor cell lines HepG2 (HCC), PLC/PRF/5 (HCC), and A2780 (ovarian) were obtained from American Type Culture Collection (ATCC, Manassas, VA). Additional HCC lines SNU423, SNU475 and SNU449 were obtained from Korea Cell Bank. For evaluation in matched parental and sorafenib-resistant HCC cells, a sorafenib-resistant subclone of PLC/PRF/5 was derived by serial culturing in the presence of increasing concentrations of sorafenib. Sorafenib (Bayer) was dissolved in dimethyl sulfoxide to a concentration of 100 mg/ml and further diluted to appropriate final concentration in Dulbecco's modified Eagle's medium with 10% fetal bovine serum. Dimethyl sulfoxide in the final solution did not exceed 0.1% (v/v). Cells were cultured *in vitro* for a total of 3 months (starting at a sorafenib concentration of 1 μmol/l and increasing up to 6 μmol/l). For plaque formation assays, A2780 or HepG2 cells were seeded into six-well plates at 4×10^5 cells/well and left overnight. Cells were infected with JX-594 for 2 hours, then the media was removed and 3% Carboxymethylcellulose Dulbecco's modified Eagle's medium overlay containing sorafenib at final concentrations of 0–4 μmol/l was added. Three days later, plates were stained with crystal violet and plaques were counted. In parallel, to assess JX-594 replication by Burst Assay (viral one-step growth curve assay), six-well plates were prepared as above. Forty eight hours after viral inoculation, cells were lysed by three rounds of freezing and thawing followed by sonication to release virus; serial dilutions of the crude viral lysate were subsequently

added to A2780 cells to titer the resulting virus by plaque assay. To assess the direct effects of sorafenib on cell viability, cells were plated in 96 well plates and incubated with sorafenib only. Cell viability was determined by means of colorimetric assay based on live-cell mediated reduction of tetrazolium salt to formazan chromogen (Cell Counting Kit-8; Donjindo Laboratories, Kumamoto, Japan).

Murine tumor models. Mice were housed, cared for and used in experiments as approved by the Animal Care and Veterinary Service at the University of Ottawa or by the Ethical Committee for Animal Study at Pusan National University Hospital. The metastatic B16 melanoma murine tumor model was established in C57BL/6 mice by intravenous tail vein infusion of 3×10^5 B16-F10-LacZ cells. Twenty four hours later animals were treated with sorafenib alone (50 µg/kg per oral dosing daily for 2 weeks), JX-594 alone (10^7 pfu intravenously three times per week for 1 week) or in combination ($n = 5$ per group). Three weeks after treatment initiation, mice were killed and lungs were fixed and stained to detect and quantify surface B16 tumor nodules. For the HepG2 xenograft model, female SCID mice were injected subcutaneously with 4×10^6 HepG2 human HCC cells. Once tumors reached a size of ~12–14 mm maximal diameter (within 30 days) mice were randomized into one of six treatment groups ($n = 8$ per group): (i) PBS alone (daily), (ii) sorafenib alone (400 µg intraperitoneally, daily, days 1–31), (iii) intravenous JX-594 alone (10^7 pfu intravenously, weekly, days 1, 8, 15, 22, 29), (iv) simultaneous treatment with JX-594 and sorafenib (daily sorafenib and weekly JX-594, as above), (v) sorafenib (daily, days 1–14) followed by JX-594 (days 15, 22, 29) and (vi) JX-594 (days 1, 8) followed by sorafenib (daily, days 15–31). Tumor measurements were performed every other day until mice were euthanized. Tumor volumes were calculated with the following formula: SD × SD × LD/2. (SD, short diameter; LD, long diameter). Concentrations of sorafenib in the plasma were determined as described previously.[27–29]

Clinical study approvals, consents, and registration. In order to assess effects of addition of sorafenib, three HCC patients who failed to achieve a durable objective tumor response with JX-594 alone were selected for sorafenib therapy after completion of JX-594 treatment. Patients 1702, 1705, and 1712 were treated under a protocol registered at www.clinicaltrials.gov (NCT00554372). Study protocol and informed consent forms were approved by the United States Food and Drug Administration, Korean Food and Drug Administration, and Institutional Review and Infection Control Committees at Pusan National University Hospital, Busan, South Korea. Patient 301 with RCC was treated under a protocol registered at www.clinicaltrials.gov (NCT00629759). Study protocol and informed consent forms were approved by the Korean Food and Drug Administration and Institutional Review and Infection Control Committees at Dong-A University Hospital, Busan, South Korea. Patients signed informed consent according to Good Clinical Practice (GCP) guidelines.

JX-594 treatment procedures and subsequent sorafenib treatment. HCC patients 1702, 1705, and 1712 (NCT00554372) were enrolled and randomized to receive one of two dose levels (10^8 or 10^9 pfu) (**Table 2**). JX-594 was administered *via* imaging-guided intratumoral injection using a multi-pronged Quadrafuse injection needle (RexMedical, Radnor, PA) in roughly spherical tumors, and by a 21-gauge percutaneous ethanol injection (multi-port; HAKKO Medicals, Tokyo, Japan) needle in irregularly shaped tumors and tumors which could not be safely accessed for injection using the Quadrafuse system. Tumors ($n = 1–5$) were injected every 2 weeks for three cycles. The same tumors injected on cycle 1 were injected thereafter on each cycle. After the planned week 8 radiographic analysis, patients 1702, 1705, and 1712 subsequently initiated standard sorafenib dosing (400 mg per oral twice daily) within 2 weeks. All three patients subsequently underwent dose reductions due to grade 1 hand-foot skin reactions (reduced to 400 mg once daily after 52–148 days) (**Table 1**). Sorafenib was eventually discontinued after an additional 1–5 months.

RCC patient 301 treated under protocol NCT00629759 received four doses (1×10^9 pfu per dose) of JX-594 *via* imaging-guided intratumoral injection using a 21-gauge percutaneous ethanol injection, (multi-port; HAKKO Medicals) needle into three intrahepatic target tumors. Patient 301 subsequently received sunitinib at a dose of 50 mg per oral dosing daily. Subsequent dose reductions were carried out after 4 months (decrease to 37.5 mg per day) and 7 months (decrease to 25 mg per day); the rationale for dose reduction was primarily poor wound healing (**Table 1**).

Tumor response and vascularity assessment. Tumor response was assessed prior to sorafenib initiation (at week 8 after JX-594 initiation), and serially over time after sorafenib initiation. Multiphase dynamic contrast-enhanced MRI was performed on either a 1.5T or 3.0T MR system (Siemens, Erlangen, Germany) and using extracellular gadolinium chelate (OptiMARK; Tyco Healthcare, Princeton, NJ). Patient 301 (NCT00629759) was imaged using multiphase dynamic contrast-enhanced computed tomography scanning on a 16-slice multidetector computed tomography scanner (Somatom Plus; Siemens Medical) using nonionic contrast media (Ultravist; Schering, Ansung, Korea). Changes in tumor contrast enhancement, manifested either by signal intensity at MRI or Hounsfield unit density on computed tomography, (and positron emission tomography signal intensity, where applicable) on serial scans were evaluated by a blinded independent radiologist with expertise in liver cancer assessment. Given the mechanism of tumor destruction previously described for JX-594,[9] we elected to apply modified Choi tumor response criteria to assess changes in tumor density and perfusion. Modified Choi responses were defined as a decrease in tumor density of ≥15% and/or a decrease in maximum diameter of ≥10%.[15]

3D segmentation analysis methods. The software used to create the 3D models was developed by M2S (Lebanon, NH). The input data comprised the arterial phase of dynamic contrast-enhanced MRI scan performed with a 3D spoiled gradient echo pulse sequence. Three tumors were selected for 3D segmentation analysis using software which allows for variable thresholding based on signal intensity. A radiologist with expertise in evaluating HCC on MRI then evaluated the liver lesions for necrosis versus viable tissue, and instructed an imaging specialist to set the thresh holds for each of these two compartments. A 3D model of the whole liver based using the edge-detection capabilities of the software was subsequently generated.

Manufacturing and preparation of JX-594. JX-594 is a Wyeth strain vaccinia modified by insertion of the human *GM-CSF* and *Lac-Z* genes into the vaccinia *TK* gene region under control of the synthetic early late promoter and p7·5 promoter, respectively. Clinical trial material was generated according to Good Manufacturing Practice guidelines in Vero cells and purified through sucrose gradient centrifugation. The genome-to-pfu ratio was ~70:1. JX-594 was formulated in phosphate-buffered saline with 10% glycerol, 138 mmol/l sodium chloride at pH 7.4. Final product quality control release tests included assays for sterility, endotoxin, and potency. Clinical trial material was also tested for GM-CSF protein concentration and was negative (lower limit of detection <14,000 pg/ml). JX-594 was diluted in 0·9% buffered normal saline in a volume equivalent to 25% (NCT00629759) or 50% (NCT00554372) of the estimated total volume of target tumor(s) for intratumoral injection.

Statistical analysis. The difference in tumor volume in mice over time was compared using the paired Student's *t*-test. The statistical analysis for the time-to-tumor progression was performed using Kaplan–Meier estimates and the log-rank test. Differences in the number of lung metastases were assessed using the unpaired *t*-test using GraphPad Prism 5 software (GraphPad, La Jolla, CA).

ACKNOWLEDGMENTS

We thank David Kerr, J Andrea McCart, Peter Forsyth, and John Crowley for serving on the DSMB and reviewing the safety/toxicity data. This study was supported by a grant of the Korea Healthcare technology R&D Project, Ministry for Health, Welfare and Family Affairs, Republic

of Korea (A091047). C.B., A.M., T.H., and D.H.K. are employees of JENNEREX, Inc., and J.C.B., is a consultant and shareholder in Jennerex. JENNEREX, Inc. holds the license for JX-594.

REFERENCES

1. Kim, JH, Oh, JY, Park, BH, Lee, DE, Kim, JS, Park, HE *et al.* (2006). Systemic armed oncolytic and immunologic therapy for cancer with JX-594, a targeted poxvirus expressing GM-CSF. *Mol Ther* **14**: 361–370.
2. Caux, C, Dezutter-Dambuyant, C, Schmitt, D and Banchereau, J (1992). GM-CSF and TNF-alpha cooperate in the generation of dendritic Langerhans cells. *Nature* **360**: 258–261.
3. Breitbach, CJ, Paterson, JM, Lemay, CG, Falls, TJ, McGuire, A, Parato, KA *et al.* (2007). Targeted inflammation during oncolytic virus therapy severely compromises tumor blood flow. *Mol Ther* **15**: 1686–1693.
4. Kim, DH, Wang, Y, Le Boeuf, F, Bell, J and Thorne, SH (2007). Targeting of interferon-beta to produce a specific, multi-mechanistic oncolytic vaccinia virus. *PLoS Med* **4**: e353.
5. Katsafanas, GC and Moss, B (2004). Vaccinia virus intermediate stage transcription is complemented by Ras-GTPase-activating protein SH3 domain-binding protein (G3BP) and cytoplasmic activation/proliferation-associated protein (p137) individually or as a heterodimer. *J Biol Chem* **279**: 52210–52217.
6. Yang, H, Kim, SK, Kim, M, Reche, PA, Morehead, TJ, Damon, IK *et al.* (2005). Antiviral chemotherapy facilitates control of poxvirus infections through inhibition of cellular signal transduction. *J Clin Invest* **115**: 379–387.
7. Stojdl, DF, Lichty, B, Knowles, S, Marius, R, Atkins, H, Sonenberg, N *et al.* (2000). Exploiting tumor-specific defects in the interferon pathway with a previously unknown oncolytic virus. *Nat Med* **6**: 821–825.
8. Hengstschläger, M, Pfeilstöcker, M and Wawra, E (1998). Thymidine kinase expression. A marker for malignant cells. *Adv Exp Med Biol* **431**: 455–460.
9. Park, BH, Hwang, T, Liu, TC, Sze, DY, Kim, JS, Kwon, HC *et al.* (2008). Use of a targeted oncolytic poxvirus, JX-594, in patients with refractory primary or metastatic liver cancer: a phase I trial. *Lancet Oncol* **9**: 533–542.
10. Liu, TC, Hwang, T, Park, BH, Bell, J and Kim, DH (2008). The targeted oncolytic poxvirus JX-594 demonstrates antitumoral, antivascular, and anti-HBV activities in patients with hepatocellular carcinoma. *Mol Ther* **16**: 1637–1642.
11. Wilhelm, SM, Carter, C, Tang, L, Wilkie, D, McNabola, A, Rong, H *et al.* (2004). BAY 43-9006 exhibits broad spectrum oral antitumor activity and targets the RAF/MEK/ERK pathway and receptor tyrosine kinases involved in tumor progression and angiogenesis. *Cancer Res* **64**: 7099–7109.
12. Llovet, JM, Ricci, S, Mazzaferro, V, Hilgard, P, Gane, E, Blanc, JF *et al.*; SHARP Investigators Study Group. (2008). Sorafenib in advanced hepatocellular carcinoma. *N Engl J Med* **359**: 378–390.
13. Cheng, AL, Kang, YK, Chen, Z, Tsao, CJ, Qin, S, Kim, JS *et al.* (2009). Efficacy and safety of sorafenib in patients in the Asia-Pacific region with advanced hepatocellular carcinoma: a phase III randomised, double-blind, placebo-controlled trial. *Lancet Oncol* **10**: 25–34.
14. Lencioni, R and Llovet, JM (2010). Modified RECIST (mRECIST) assessment for hepatocellular carcinoma. *Semin Liver Dis* **30**: 52–60.
15. Choi, H, Charnsangavej, C, Faria, SC, Macapinlac, HA, Burgess, MA, Patel, SR *et al.* (2007). Correlation of computed tomography and positron emission tomography in patients with metastatic gastrointestinal stromal tumor treated at a single institution with imatinib mesylate: proposal of new computed tomography response criteria. *J Clin Oncol* **25**: 1753–1759.
16. Abou-Alfa, GK, Schwartz, L, Ricci, S, Amadori, D, Santoro, A, Figer, A *et al.* (2006). Phase II study of sorafenib in patients with advanced hepatocellular carcinoma. *J Clin Oncol* **24**: 4293–4300.
17. Therasse, P, Arbuck, SG, Eisenhauer, EA, Wanders, J, Kaplan, RS, Rubinstein, L *et al.* (2000). New guidelines to evaluate the response to treatment in solid tumors. European Organization for Research and Treatment of Cancer, National Cancer Institute of the United States, National Cancer Institute of Canada. *J Natl Cancer Inst* **92**: 205–216.
18. Patil, S, Figlin, RA, Hutson, TE, Michaelson, MD, Négrier, S, Kim, ST *et al.* (2010). Prognostic factors for progression-free and overall survival with sunitinib targeted therapy and with cytokine as first-line therapy in patients with metastatic renal cell carcinoma. *Ann Oncol* **22**:295–300.
19. Breitbach, CJH, Cho, M, Jun, W, Woo, W, Yon, K, Hwang, T-H *et al* (2010). Evaluating safety and antitumoral activity of JX-594, a targeted multi-mechanistic oncolytic poxvirus, followed by sorafenib therapy in patients with advanced hepatocellular carcinomaL pilot study for Phase 3. In *International Liver Cancer Association Fourth Annual Conference*, Montreal, Canada.
20. Kim, J, Kim, JY, Song, KS, Lee, YH, Seo, JS, Jelinek, J *et al.* (2007). Epigenetic changes in estrogen receptor beta gene in atherosclerotic cardiovascular tissues and in-vitro vascular senescence. *Biochim Biophys Acta* **1772**: 72–80.
21. El-Osta, A, Brasacchio, D, Yao, D, Pocai, A, Jones, PL, Roeder, RG *et al.* (2008). Transient high glucose causes persistent epigenetic changes and altered gene expression during subsequent normoglycemia. *J Exp Med* **205**: 2409–2417.
22. Kim, JY, Hwang, JH, Zhou, W, Shin, J, Noh, SM, Song, IS *et al.* (2009). The expression of VEGF receptor genes is concurrently influenced by epigenetic gene silencing of the genes and VEGF activation. *Epigenetics* **4**: 313–321.
23. Kottke, T, Hall, G, Pulido, J, Diaz, RM, Thompson, J, Chong, H *et al.* (2010). Antiangiogenic cancer therapy combined with oncolytic virotherapy leads to regression of established tumors in mice. *J Clin Invest* **120**: 1551–1560.
24. Plastaras, JP, Kim, SH, Liu, YY, Dicker, DT, Dorsey, JF, McDonough, J *et al.* (2007). Cell cycle dependent and schedule-dependent antitumor effects of sorafenib combined with radiation. *Cancer Res* **67**: 9443–9454.
25. Reeves, PM, Bommarius, B, Lebeis, S, McNulty, S, Christensen, J, Swimm, A *et al.* (2005). Disabling poxvirus pathogenesis by inhibition of Abl-family tyrosine kinases. *Nat Med* **11**: 731–739.
26. Lyons, JF, Wilhelm, S, Hibner, B and Bollag, G (2001). Discovery of a novel Raf kinase inhibitor. *Endocr Relat Cancer* **8**: 219–225.
27. Jain, L, Gardner, ER, Venitz, J, Dahut, W and Figg, WD (2008). Development of a rapid and sensitive LC-MS/MS assay for the determination of sorafenib in human plasma. *J Pharm Biomed Anal* **46**: 362–367.
28. Zhao, M, Rudek, MA, He, P, Hafner, FT, Radtke, M, Wright, JJ *et al.* (2007). A rapid and sensitive method for determination of sorafenib in human plasma using a liquid chromatography/tandem mass spectrometry assay. *J Chromatogr B Analyt Technol Biomed Life Sci* **846**: 1–7.
29. Afify, S, Rapp, UR and Högger, P (2004). Validation of a liquid chromatography assay for the quantification of the Raf kinase inhibitor BAY 43-9006 in small volumes of mouse serum. *J Chromatogr B Analyt Technol Biomed Life Sci* **809**: 99–103.

APPENDIX VI: POTENT ONCOLYTIC ACTIVITY OF RACCOONPOX VIRUS IN THE ABSENCE OF NATURAL PATHOGENICITY

Laura Evgin, Markus Vaha-Koskela, Julia Rintoul, Theresa Falls, Fabrice Le Boeuf,

John W Barrett, John C Bell and Marianne M Stanford

Contribution:

Assisted in the planning, and executing of the mouse experiments. In particular the tissue distribution experiments, and the lung tumour mouse model experiments. I also contributed to the assembly of the manuscript, proofreading the manuscript, and assisting in the response to reviewers.

Published: *Molecular Therapy, May 2010*

Potent Oncolytic Activity of Raccoonpox Virus in the Absence of Natural Pathogenicity

Laura Evgin[1], Markus Vähä-Koskela[1], Julia Rintoul[1], Theresa Falls[1], Fabrice Le Boeuf[1], John W Barrett[2], John C Bell[1] and Marianne M Stanford[1]

[1]*Department of Biochemistry, Microbiology and Immunology, University of Ottawa, Centre for Cancer Therapeutics, Ottawa Health Research Institute, Ottawa, Ontario, Canada;* [2]*BioTherapeutics Research Group, Robarts Research Institute, London, Ontario, Canada*

A number of oncolytic virus (OV) candidates currently in clinical trials are human viruses that have been engineered to be safer for patient administration by limiting normal cell targeting and replication. The newest OVs include viruses that cause no disease in humans, yet still have natural tumor tropism. Raccoonpox virus (RCNV) is a member of the *Orthopoxvirus* genus of *Poxviridae* and closely related to vaccinia virus, yet has no known pathogenicity in any mammalian species. A screen of cells from the NCI-60 cancer cell panel using growth curves demonstrated greater than a log increase in replication of RCNV in nearly 74% of the cell lines tested, similar to other tested OV poxviruses. In normal cell lines, pretreatment with interferon (IFN)-α/β resulted in significant inhibition of RCNV replication. In both xenograft and syngeneic models of solid tumors, injection of RCNV resulted in significantly slower tumor progression and increased survival of mice. RCNV treatment also prolonged survival in treatment-resistant models of brain tumors and decreased tumor burden by systemic administration in models of lung metastasis.

Received 17 November 2009; accepted 20 January 2010; published online 16 February 2010. doi:10.1038/mt.2010.14

INTRODUCTION

Oncolytic viruses (OVs) are an exciting emerging targeted cancer therapy. Many tumors often sacrifice components of the inflammatory and antiviral defenses in favor of unchecked cellular growth, constituting the "Achilles heel" that OVs exploit for their own replication.

A large number of viruses have been explored for their ability to preferentially replicate in and kill tumor cells.[1] Many of these viruses are responsible for naturally occurring, sometimes benign human infections, and have been genetically modified to increase selectivity to neoplastic tissue.[2] Despite very good safety profiles, many of the OVs tested in the clinic do not demonstrate the robust efficacy seen in preclinical models, illustrating that new selective OV candidates need to be identified.

Poxviruses have an extensive history of use in humans either as vaccines for infectious diseases like smallpox or as vaccine vectors for the prevention and treatment of cancer.[3] Vaccinia virus is a promising new OV candidate and has been engineered to be tumor selective by a variety of strategies including, but not restricted to, removal of the viral thymidine kinase (*TK*)[4] or by deletion of the vaccinia growth factor (*VGF*) gene.[5] A clinical candidate virus, JX-594, also expresses human GM-CSF to increase its immune-stimulating properties.[6] This virus has shown encouraging safety and efficacy in early human clinical studies.[7] Indeed, the safety and efficacy experience in the clinic to date with vaccinia supports the idea that the poxvirus platform is a good starting point for the identification of additional OVs.

Recently, myxoma virus, a leporipoxvirus, and Yaba-like disease virus, a yatapoxvirus, have also shown OV potential.[3,8,9] Myxoma virus cannot naturally infect humans, yet it has the ability to infect many human cancer cell lines[10] and shows efficacy in both immunodeficent brain models and immunocompetent models of other types of tumors.[11,12] The capacity of myxoma virus to replicate productively in human tumor cells is intrinsically linked to the Akt status of the cells,[13] whereas its exclusion from normal human tissue is controlled by interferons (IFNs) and TNF-α.[14]

The finding that myxoma virus has significant efficacy as an OV has led to examination of other nonhuman poxviruses that are more closely related to vaccinia virus. These viruses represent an exciting avenue as they likely require little genetic manipulation to be deemed safe for use in humans. Raccoonpox virus (RCNV) is a member of the *Orthopoxvirus* genus and closely related to vaccinia virus. RCNV was first discovered in a screen of outwardly healthy raccoons in Maryland in 1961.[15] It has no known pathology in any species (including raccoons), which leads many to believe that its "natural" host may still be undiscovered. This virus has been used as a wild mammal vaccine and has been shown to successfully induce immunity, without any concurrent pathology in a number of species, including mice, prairie dogs, cats, and raccoons. In this study, we tested a novel RCNV strain that was isolated from the forepaw of a cat in Canada (this was the first report of RCNV infecting felines).[16] Like vaccinia, RCNV has a large genome and the potential to harbor and express several transgenes. For the

studies presented here, the enhanced green fluorescent protein was inserted into the viral *TK* locus for visualization purposes. We have assessed virus replication in cells from the NCI-60 cell panel, and demonstrate that RCNV is able to replicate several logs in the majority of human tumor cells tested. In normal cells, the replication of RCNV is significantly dampened by pretreatment with IFN. We also demonstrate significant efficacy of RCNV in treatment of both xenograft and syngeneic tumors in animal models, both by direct and systemic delivery of the virus. We believe that RCNV represents an alternative new oncolytic candidate that likely has an excellent safety profile and significant efficacy despite little genetic interference. Its lack of pathology may represent a unique opportunity to treat patient populations that may be contraindicated for the use of other poxviruses.

RESULTS

RCNV replicates and kills human tumor cells *in vitro*

To determine whether RCNV has the ability to infect and kill human tumor cells, a screen of established cancer cell lines from the NCI-60 cell panel was undertaken. Single-step growth curves [multiplicity of infection (MOI) 3] were generated to determine permissiveness, which was defined as greater than one-log increase in virus titers over input, which is within the sensitivity of the plaque assay used to determine titer (Figure 1). Based on this criterion, 74% of cell lines tested were permissive (25 of 34 human tumor cell lines tested). Most (30 of 34 cell lines, 88%) resulted in RCNV titers that were above input virus (1.0, Figure 1a). All murine cancer cells tested showed significant RCNV replication. In addition, RCNV at low MOI (0.1) demonstrated replication in three normal human cell types: umbilical cord vein endothelial cells (HUVECs), dermal microvascular endothelial cells (HMVECs), and astrocytes (HAst) *in vitro* (Figure 1b). However, pretreatment of these cell lines with type I IFN resulted in an up to four-log decrease in RCNV replication. In contrast, pretreatment human cancer cells resulted in negligible (<1 log) decreases in RCNV titer (Figure 1b).

Infection with RCNV correlated with tumor cell death (Figure 2, **Supplementary Figure S1**). In culture, RCNV infection killed the majority of cells rapidly that can be visualized by microscopy (**Supplementary Figure S1**) or demonstrated by Trypan blue exclusion (Figure 2a). Both human and murine tumor cell lines have also been examined for their ability to grow after RCNV infection (Figure 2b,c). Cells were infected at the indicated MOI and 24 hours after infection, cells collected and plated in fresh wells. The ability to grow and form clones was then assessed. In human and primate cell lines, reduction in the ability to form clones correlated with viral dose (Figure 2b). The murine lines CT-26, B16F10, and delayed brain tumor (DBT) were greatly reduced in their ability to form clones after RCNV infection at an MOI of 0.1 (Figure 2c). The 4T1 cells were not as dramatically affected by virus treatment. Thus, most cells infected with RCNV are no longer able to grow *in vitro*, indicating viral destruction of infected cells.

Safety and viral biodistribution of RCNV

RCNV has been used as a vaccine vector in mice, eliciting excellent immunity to *Yersinia pestis* and rabies virus without any adverse effects of the viral vector.[17–27] Prior to our therapy experiments, we confirmed the safety of our strain in adult, immunocompetent mice. In toxicity experiments, a single intraperitoneal (i.p.) injection of up to 5×10^7 plaque-forming units (pfu) or intravenous (i.v.) dose of up to 10^8 pfu of virus did not yield measurable signs of illness in naive immunocompetent (Balb/c) mice. A biodistribution experiment in CD-1 nude mice after i.v. dose of 10^7 pfu of RCNV indicated little virus in any of the organs tested at 6 hours, 72 hours, or 7 days after virus injection (Figure 3a), thereby validating the lack of illness in our safety experiments. A subsequent

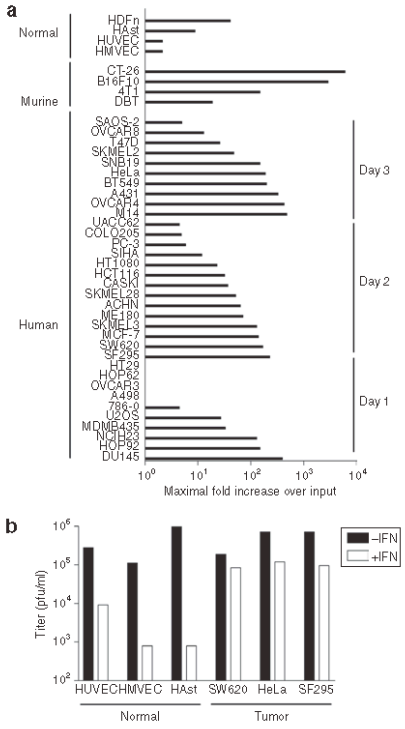

Figure 1 Analysis of RCNV replication in normal and tumor cell lines. (**a**) Human tumor cell lines from the NCI-60 cell panel were screened for replication of RCNV using a single-step growth curve, as were normal cell lines and murine tumor cell lines (as indicated). The lines were infected with RCN-gfp at a multiplicity of infection (MOI) of 3, and the cellular lysates were collected every day for 4 days. The RCNV titer was then determined by titration on BGMK cells. A summary of all of the data is presented, indicating the highest fold increase in titer obtained over the input virus (as determined by collection of cellular lysate at time 0 after infection) on days 1, 2, or 3. (**b**) Comparison of type I interferon pretreatment on RCNV replication in normal and cancerous human cells. Normal human umbilical cord vein endothelial cells (HUVEC), dermal endothelial cells (HMVEC), astrocytes (HAst), SW620, HeLa, and SF295 were pretreated with Intron A (recombinant human IFN-β for HAst) as described in Materials and Methods, and infected with RCN-gfp at an MOI of 0.1. Cellular lysates were collected at 72 hours after infection and titer determined on BGMK cells. pfu, plaque-forming unit; RCNV, Raccoonpox virus.

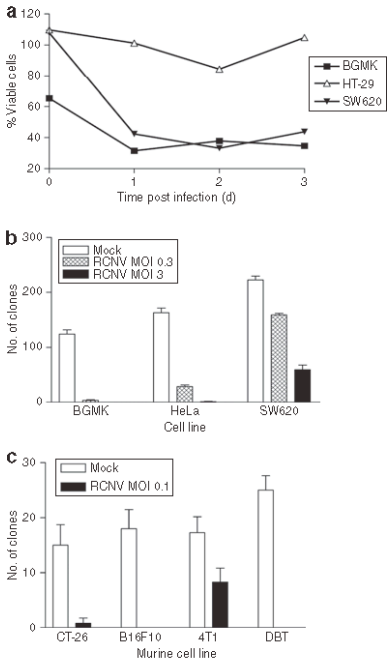

Figure 2 Tumor cell killing by RCNV. (**a**) Cell killing in response to virus infection. The indicated cell lines were seeded in 6-well plates and RCNV added at an MOI of 3. At each of the indicated days after infection, the cells were collected and viability determined by Trypan blue exclusion using a Vi-CELL machine. This viability was then normalized to uninfected control cells. (**b**) Clonogenic assays to determine cell death induced by RCNV. The indicated cell lines were infected at an MOI of 0.3 or 3, and 24 hours after infection, trypsinized and counted. 10^3 viable cells were added in quadruplicate to 12-well plates and allowed to grow into visible colonies, which were visualized using 0.1% crystal violet. (**c**) Murine cells were infected with RCN-gfp at an MOI of 0.1 and clonogenic assay performed as above 3 days after infection. MOI, multiplicity of infection; RCNV, Raccoonpox virus.

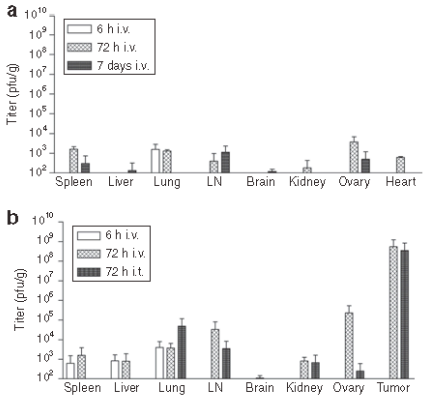

Figure 3 Organ distribution of RCNV in mice. (**a**) Biodistribution experiment was performed in CD-1 nude, naive mice (two per group) and they were injected i.v. with 10^7 pfu RCN-gfp. At either 6 hours, 72 hours, or 7 days, the mice were euthanized and the indicated organs were collected and homogenized, and the viral titer contained in the lysate was measured using BGMK cells. (**b**) Biodistribution of RCNV in immunocompetent, tumor-bearing mice. Mice bearing s.c. CT-26 tumors (10 days after implantation) (two mice per group) were injected either i.v. or i.t. with 10^8 pfu of RCNV. At either 6 or 72 hours after injection, the mice were euthanized and the indicated organs were collected and homogenized, and the viral titer from each individual organ was measured using BGMK cells. The data represented is the average titer from these organs. LN, lymph node; pfu, plaque-forming unit; RCNV, Raccoonpox virus.

biodistribution assay was performed in tumor-bearing immunocompetent animals (Figure 3b). A dose of 10^8 pfu RCN-gfp was injected into CT-26 tumor-bearing Balb/c mice (two per group) by the i.v. or intratumoral (i.t.) route, and at both early (6 hours) and later (72 hours) time points, the organs were collected and RCNV titer determined. At 6 hours after i.v. injection, RCNV could be detected in the spleen, liver, and lung, at relatively low titer (white bars). By 72 hours after injection, RCNV could be detected at low levels in all organs tested, with at least four logs more RCNV detected within the tumor, underlying its proclivity for tumors (hatched and black bars). The titers in all compared organs were very similar regardless of the route of injection, indicating that i.v. delivered RCNV can enter and replicate in tumors. Of note, the highest titers of RCNV in normal tissues were detected in the ovaries of i.v. injected mice. This propensity of orthopoxviruses to enter the ovaries has also been demonstrated using vaccinia virus.[5] In nontumor-bearing animals, RCNV could only be detected in the lungs after 3 days (~2×10^4 pfu/g, data not shown). As RCNV was originally discovered in the lungs of raccoons, this tissue tropism is not unexpected.

RCNV is effective in the treatment of human tumors in a xenograft model

Human colon cancer cell line SW620 was chosen from the screen to examine the efficacy of RCNV treatment of established tumors in nude mice (Figure 4). Tumors were established under the skin and at ~9–12 days postimplantation, we began i.t. injections of RCNV. Treated mice (four mice) received a total of four i.t. injections (time points indicated by arrows) of RCNV (10^7 pfu/dose), whereas the tumors of control mice (five mice) were injected with phosphate-buffered saline (PBS). Mice that received RCNV exhibited no ill effects from virus treatment. Mice that had PBS-treated tumors rapidly grew to end point and one RCNV-treated tumor demonstrated a similar progression to control tumors. Another treated tumor had significant delay in progression and two of four RCNV-treated mice were cured of their tumors ($P = 0.047$).

RCNV is effective in the treatment of syngeneic mouse tumors in immunocompetent animal models

We conducted a similar experiment to those done in the nude mice (Figure 5a) in immunocompetent Balb/c mice bearing syngeneic CT-26 tumors. Repeated intratumoral injections of RCNV into CT-26 tumors improved the survival of mice compared to control animals. In examining individual treated animals, 5 of 11 of the mice were cured of their tumors (Figure 5a, $P = 0.0511$).

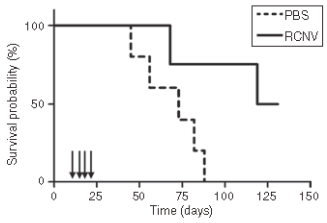

Figure 4 Treatment of human xenograft tumors in nude mice with RCNV. Human SW620 cells (10^6 cells) were injected s.c. into the right flank of naive CD-1 nude mice. At 10 days after implantation, RCN-gfp (10^7pfu) was injected into the tumor. RCNV was also injected at days 14, 17, and 24 after tumor implantation. Mice were followed until end point that was based on high tumor volume ($P = 0.047$). PBS, phosphate-buffered saline; pfu, plaque-forming unit; RCNV, Raccoonpox virus.

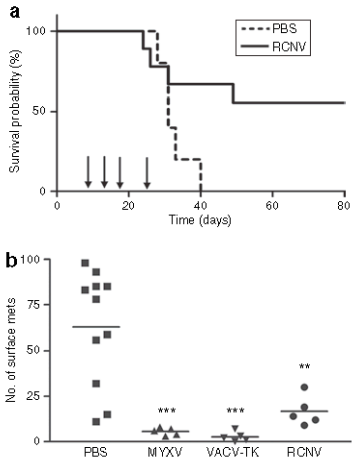

Figure 5 Treatment of syngeneic tumors in immunocompetent mice with RCNV. (**a**) Treatment of syngeneic solid tumors. CT-26 cells (3×10^5 cells) were injected s.c. into the right flank of Balb/c mice. At 10 days after injection, RCNV (10^7 pfu) was injected directly into the tumor. Virus was also injected at days 14, 17, and 24 days after implantation. Tumor volume for each mouse was followed in both the PBS-treated (dashed line) and RCNV-treated groups (solid line) until end point (based on high tumor volume) ($P = 0.0511$). (**b**) Treatment of metastatic CT-26 tumors with oncolytic poxviruses. CT-26-LacZ cells (10^5 cells) were injected i.v. into the tail vein of Balb/c mice. RCNV, MYXV, or VACV (10^7 pfu) was injected i.v. into the mice via the tail vein on days 1, 3, and 8 after cell injection. At day 10, mice were killed, their lungs excised, fixed and stained with an X-gal-containing solution. The lung lobes were then separated and the surface lung metastases counted under a dissecting microscope (**$P < 0.01$, ***$P < 0.001$ by analysis of variance). PBS, phosphate-buffered saline; pfu, plaque-forming unit; RCNV, Raccoonpox virus.

As in the xenograft model, there were no visible signs of illness in RCNV-treated mice, yet several mice failed to respond to treatment. Multiple i.v. injections of RCNV did not result in an increased survival in this model, although at early time points following treatment with RCNV delivered i.v. and i.t., we observed significant ($P = 0.005$) retardation of tumor growth as compared to control tumors (**Supplementary Figure S2a**). This suggests that early doses of virus reach the tumors and retard their progression; however, insufficient virus from subsequent doses is delivered to establish a curative infection in these subcutaneous tumor models.

In contrast, intravenous administration of RCNV to a lung metastasis model with CT-26 did have a significant impact on tumor burden (**Figure 5b**). In addition, the poxvirus OVs MYXV and VACV were also administered, and all viruses demonstrated significant efficacy in this model. In a separate experiment, RCNV was injected i.v. to CT-26 lung tumor–bearing animals, and at 24 hours, we collected the lungs. Both microscopy and titration indicated that RCNV is delivered to the lung and it colocalizes with the tumor tissue (**Supplementary Figure S2b**). This does not rule out a role of immune-mediated destruction of the tumor, yet shows that detectable virus can be found in tumor-bearing lungs.

RCNV can extend survival in treatment-resistant brain tumors in immunocompetent mice

In addition to subcutaneous tumor models, we wanted to assess virus efficacy on malignant glioma, which is both difficult to treat and located in a sensitive organ.[28] A single injection of 10^7 pfu RCNV, MYXV, or VACV was given into the brains of animals harboring intracranial DBT*Fluc* tumors (**Figure 6**). By IVIS, we saw that several tumors injected with RCNV responded to treatment, with the tumor produced IVIS signal either decreasing or remaining steady 10 days after treatment (**Figure 6a**) compared to the rapid increase in signal in the control-treated animals. Overall, treatment with RCNV stabilized disease for a short period of time and showed a trend toward prolonged survival in these mice ($P = 0.0941$) (**Figure 6b**). In comparison, MYXV and VACV, which has provided significant survival advantage in other brain tumor models,[29,30] demonstrated no survival advantage in this particular model (**Figure 6b**). Importantly, RCNV injections were well tolerated with no acute toxicity or neurological symptoms observed during at least 10 days after infection (when mice started dying of tumor burden).

DISCUSSION

RCNV represents a unique OV candidate. It is related to other OV candidates such as vaccinia virus and myxoma virus, and has no known significant pathology in any mammalian species. It was first described in a screen of an outwardly healthy raccoon population, and was not associated with any known illness.[31] RCNV has demonstrated utility as a vaccine vector in wild animal vaccines for rabies virus and sylvatic plague, suggesting its safety in multiple animal species.[17,19,25–27,32–34] RCNV has also been inadvertently introduced into humans by way of a laboratory accident, and even with direct injection by needle-stick, there were a few symptoms beyond an injection site reaction and a small blister, suggesting further safety for eventual use in humans.[35] Our biodistribution experiments also suggest little viral replication in mice after i.v. administration in both naive and tumor-bearing mice (**Figure 3**). It appears therefore that RCNV is a naturally attenuated poxvirus, and we show here that it has inherent oncolytic activity.

In this report, we directly correlate the OV capacity of RCNV to the virus' ability to replicate *in vitro*, in a manner

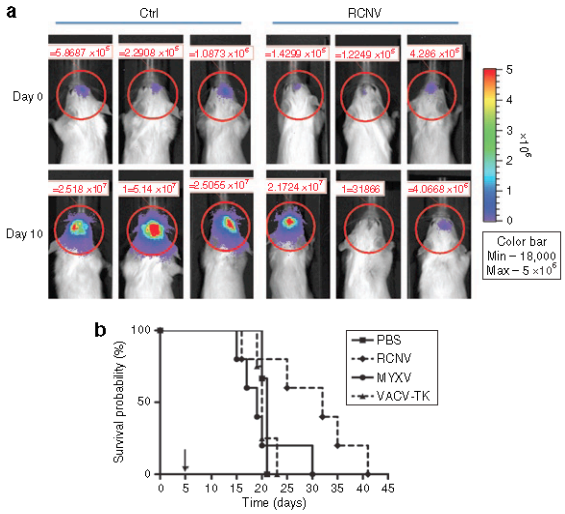

Figure 6 Treatment of syngeneic orthotopic glioma model with RCNV. Intracranial DBT*Fluc* tumors were established in Balb/c mice as described in Materials and Methods. After 5 days, 10^7 pfu RCNV, MYXV, or VACV was injected into the same stereotactic coordinates. (**a**) IVIS imaging of mice at day 0 (at the time of virus injection) and day 10 after injection. (**b**) Kaplan–Meier survival curve shows a trend toward increased survival upon RCNV treatment compared to controls ($P = 0.0941$). PBS, phosphate-buffered saline; pfu, plaque-forming unit; RCNV, Raccoonpox virus.

similar to what has been done to describe the OV capacity of viruses, such as HSV and adenovirus.[36,37] In many other reports, the cellular death induced by the virus is sufficient to argue significant replication. However, poxviruses are known to induce death *in vitro* independent of viral replication (particularly at very high MOI) due to their ubiquitous ability to enter cells and initiate early gene transcription and stimulate death programs.[38] Thus, we have chosen significant viral replication as our indication of oncolytic capacity and then correlated this to specific cellular killing *in vitro*.

RCNV replicates in most tumor cell lines tested, similar to that seen with other OV poxviruses.[10] Comparison of the tumor tropism of RCNV to that of myxoma virus, where a screen of human tumor cell lines has been completed, revealed that cell lines, such as HCT116 (colon cancer), are susceptible to both poxviruses; however, RCNV is able to infect and kill human cancer cell lines such as M14 (melanoma), ACHN (renal), and MCF-7 (breast) that restrict myxoma virus replication. Conversely, cell lines such as PC3 (prostate) are restrictive to RCNV but permissive to myxoma virus.[10] A more systemic comparison of these viruses is required, but the observed differences in the level of susceptibility indicate that these viruses have unique mechanisms of action. In addition, the finding that pretreatment of normal cells with type I IFN largely inhibits RCNV replication is also interesting as it has been shown that myxoma requires the action of both IFN and TNF-α to preclude its replication in normal cells.[14] However, other OV candidates such as VSV and NDV have also demonstrated this differential sensitivity to IFN.[39,40] We believe that the sequencing of RCNV and study of its unique immunomodulatory genes may give additional clues into its tumor tropism.

RCNV treatment significantly delayed the progression of solid tumors in both xenograft and syngeneic tumor models (**Figures 3–6**). However, some tumors did not respond to RCNV despite significant viral titers within the tumor, perhaps due to physical barriers within the tumor as has been shown with other viruses. For instance, extracellular matrix that walls off tumor nests can impede the spread of OVs within tumors[11,41] arguing that strategies that provide widespread infection of tumors is key for effective therapy.

How is RCNV a distinctive oncolytic poxvirus candidate? It appears to have a natural ability to kill certain tumors that are known to be refractory to other poxvirus candidates suggesting that it targets unique tumor-specific signaling pathways. Its apparent safety in a number of mammalian species argues that it could be added to the arsenal of poxviruses under development for treatment of human tumors. An encouraging observation was that RCNV seemed to provide therapeutic activity in a syngeneic brain tumor model (**Figure 6**). This may represent a unique niche for RCNV as it showed no obvious effects on normal brain tissue, yet was able to impact on a highly treatment-resistant brain tumor model. Brain tumors in general are an unmet clinical need that would welcome a new OV strategy.

MATERIALS AND METHODS

Cell lines and viruses

Cell lines: Human tumor cell lines tested were from the NCI-60 reference collection and maintained in media supplemented with a 3:1 mix of fetal calf serum (PAA Laboratories, Etobicoke, Ontario, Canada) and fetal bovine serum (Invitrogen, Burlington, Ontario, Canada), and grown at 37 °C, 5% CO_2. The human tumor cell lines used include the following: DU145, HOP 92, HOP62, NCIH23, 786-0, A498, HT29, SW620, MCF-7,

SKMEL3, ME180, ACHN, SKMEL28, CASKI, HCT116, HT1080, SIHA, PC-3, COLO205, OVCAR3, OVCAR 4, A431, BT549, SNB19, T47D, MDMB435, OVCAR8, SAOS-2, M14, SF295, UACC 62, HeLa, and U2OS. The murine tumor cell lines used include 4T1, B16F10, CT-26, and DBT. B16F10 expressing *LacZ* (B16F10-LacZ) was obtained from Ann Chambers (London Regional Cancer Program, London, Ontario, Canada).[11] CT-26-LacZ cells have been described.[42] DBT cells[28] were kindly provided by Robert C Rostomily, University of Washington, School of Medicine, Seattle, WA. DBT cells expressing firefly luciferase (DBT*Fluc*) were generated by plasmid transfection of DBT cells at no more than five passages, with subsequent maintenance in medium supplemented with 1 mg/ml G418 (Sigma, Oakville, Ontario, Canada). Baby green monkey kidney (BGMK) cells were obtained from Grant McFadden (University of Florida, Gainesville, FL). All remaining cell lines were obtained from ATCC, Manassas, VA. Most cell lines, with the exception of the murine melanoma B16F10/B16F10LacZ cells which are grown in α-MEM (HyClone, Logan, UT), were maintained in Dulbecco's modified Eagle's medium (HyClone). HMVEC-dBlAd (adult dermal blood microvascular endothelial) and HUVEC (umbilical vein endothelial) cells (Lonza, Basel, Switzerland) were maintained in EGM-2 MV or EGM-2 medium, respectively, with appropriate supplements (Lonza) for no more than nine passages.

Viruses. RCNV used in this study was isolated from a cat in Southern Ontario, Canada.[16] This viral isolate was used to create RCN-gfp, a recombinant with the enhanced green fluorescent protein inserted in the *TK* open-reading frame, using the homologous sequence for vaccinia virus *TK*. The viruses myxoma virus (vMyxgfp) and TK$^-$ vaccinia virus (JX-594) were as previously described.[43,44]

Animals. Female 6- to 8-week-old Balb/c, C57BL6, or CD-1 nude mice were supplied by Charles River Canada (St Constant, Quebec, Canada). Mice were housed in groups of up to six mice in microisolator cages within a level 2 biocontainment unit of the Animal Care and Veterinary Services facility (University of Ottawa, Ottawa, Ontario, Canada) in a scheduled 12-hour light/dark environment. All animal protocols were carried out according to standard operating procedures of the Animal Care and Veterinary Services.

Viral growth curves and viability assay. Single-step growth curves were conducted to assess RCNV replication in human tumor cells. Tumor cell monolayers in 6-well plates at 80–95% confluence were infected with RCN-gfp at an MOI of 3, in a volume of 0.5 ml, for 1 hour at 37 °C, 5% CO_2. The virus inoculum was then removed and replaced with growth media. At the indicated time points (0, 24, 48, 72, and 96 hours after infection), adherent cells were dislodged using a cell scraper, and both the cells and corresponding supernatants were collected and frozen at −80 °C. Lysates were then subjected to three freeze–thaw cycles to release the virus from the cells. The RCNV contained in the cellular lysates were determined by titration on BGMK cells. Serially diluted samples from lysates were applied to 95% confluent monolayers of BGMK. Following 1-hour adsorption, the virus inoculum was removed, and replaced with Dulbecco's modified Eagle's medium supplemented with 10% serum and 1.5% carboxymethylcellulose (Sigma). The cells were incubated with virus for 4–5 days. The monolayers were then stained with 1% crystal violet in methanol to allow for visualization of plaques and determination of viral titer.

Replication in the following cell lines was also tested in the presence of Intron A (IFN-α): HUVEC, HMVEC, SW620, SF295, and HeLa. Cell monolayers in 12-well plates were treated with Intron A at a concentration of 200 IU/ml overnight prior to infection. Normal human embryonal astrocytes (ScienceCell, Carlsbad, CA) maintained in 10% fetal bovine serum–Dulbecco's modified Eagle's medium were seeded in 12-well plates at 150,000 cells per well (1 ml) in either the absence or presence of 200 IU/ml recombinant human IFN-β (Betaseron). The cells were inoculated with RCN-gfp at an MOI of 0.1 with 200 IU/ml of Intron A in a volume of 100 µl for 2 hours. The inoculum was then removed and replaced with growth media supplemented with Intron A (200 IU/ml). Seventy-two hours after infection, cell lysates were collected and the virus samples titered (as described above).

Viability/clonogenic assays were performed using the same method as the viral growth curves. The indicated cells were prepared and infected with RCN-gfp at the indicated MOI (or mock-infected) as above. At the indicated time points, cells were collected from the wells as above and the cell viability assessed using Trypan blue exclusion via the Vi-CELL instrument. Cells were then replated at 10^3 viable cells/well in quadruplicate wells of a 12-well plate. Single resuspended cells form clones in 7–14 days in cell culture medium. The monolayers were then stained with 1% crystal violet in methanol to allow for visualization and quantification of clones.

Maximum tolerated dose/biodistribution experiment. To determine the safety of administration of RCNV in mice, increasing doses of RCN-gfp were administered to Balb/c mice by both the intravenous and intraperitoneal routes. Mice (five per group) were injected i.p. with virus with titers ranging from 5×10^4 to 5×10^7 pfu/dose. In a separate experiment, mice (five per group) were injected i.v. with either 10^6, 10^7, or 10^8 pfu of RCN-gfp. The animals were followed for signs of illness for 14 days, examining physical changes such as weight loss, general appearance, lesion formation, and respiratory distress.

The biodistribution of RCNV was determined in naive CD-1 nude mice, tumor-bearing, or naive Balb/c mice. Nude mice (two per group) received a dose of 10^7 pfu of RCN-gfp, and the indicated organs were collected and titered at 6 hours, 72 hours, or 7 days after injection. Mice with CT-26 tumors (10 days postimplantation) (two mice per group) were injected, either i.v. or i.t., with 10^5 pfu of RCNV. Naive mice were injected i.v. as a control. At either 6 or 72 hours after injection, the mice were euthanized and the indicated organs were collected, homogenized, and the viral titer contained in the lysate from each individual organ determined using BGMK cells, as above.

In vivo tumor models

Primary tumor models: A single injection of 10^6 SW620 cells was given subcutaneously to the right flank of nude mice or 3×10^5 CT-26 cells was given subcutaneously to the right flank of Balb/c mice. The mice received four intratumoral injections of RCN-gfp (10^7 pfu in 100 µl PBS) or 100 µl of PBS on days 11, 14, 17, and 24. Tumors were measured (length and width) using calipers beginning on day 11, until end point (when tumors reached a maximum diameter of 15 mm). At end point, the CT-26 tumors were resected, homogenized and the RCNV viral titer determined on BGMK cells.

Metastasis tumor models: 10^5 CT-26-LacZ cells were injected i.v. via tail vein into Balb/c mice. Mice were treated with RCN-gfp, vMyxgfp, or VACV (JX-594) (10^7 pfu in 100 µl PBS) i.v. on days 1, 3, and 8, and end point was 10 days (CT-26) postimplantation. Mice were anesthetized with Euthanyl, and after a terminal bleed via cardiac puncture, lungs were excised and stained with X-gal solution as previously described.[11] The number of metastases on the surface of each lung lobe was determined after physical separation of the lungs. They were counted under a dissecting microscope (Leica, Richmond Hill, Ontario, Canada).

Syngeneic orthotopic glioma model: DBT*Fluc* cells were trypsinized, washed with PBS and suspended in PBS at 1×10^6 cells/10 µl. Mice were kept under continuous 2.5% isoflurane anesthesia during intracranial surgeries and IVIS imaging. Mice were affixed to a stereotactic frame, the scalp was disinfected, and the skull exposed by midline scalpel incision. Cells were injected 1.5 mm lateral and 0.5 mm anterior to the rostral confluence of the sinus[20] at a depth of 3.5 mm over 2 minutes. A fresh batch of cells was used for every five mice.

Mice were imaged 4 days after surgery and divided into groups based on positive tumor (Fluc) signal. Five days postimplantation, a group of

five mice received an intracranial injection of 1×10^7 pfu RCN-gfp in 10 µl PBS (surgeries as above). Another group of five mice received 10^7 pfu vMyxgfp, or 10^7 pfu JX-594 (TK^- vaccinia virus) and three mice serving as controls, received PBS. Animals were imaged at 3- to 4-day intervals over 45 days. Mice reaching end point were killed and the brains stored at −80 °C for titration.

For detection of tumor (Fluc) activity, mice were injected intraperitoneally with 3 mg beetle D-luciferin (Promega, Madison, WI) and imaged 7 minutes later in the IVIS 200 apparatus (Xenogen, Hopkinton, MA) with 1-minute exposure.

Statistical analysis. All statistical analyses were performed using the GraphPad Prism 3.0 software (GraphPad Software, La Jolla, CA). Survival curves were generated by the Kaplan–Meier method, and the log-rank test was used to compare groups.

SUPPLEMENTARY MATERIAL

Figure S1. Representative microscopy of cell lines infected with RCN-gfp.

Figure S2. RCNV treatment in CT-26 solid tumor and lung models.

ACKNOWLEDGMENTS

We thank Grant McFadden of the University of Florida for providing vMyxgfp, and Jan Brun at the Children's Hospital of Eastern Ontario for providing DBT*Fluc* cells. Research support for this project was provided by the Canadian Institute for Health Research and the Ontario Institute for Cancer Research.

REFERENCES

1. Vähä-Koskela, MJ, Heikkilä, JE and Hinkkanen, AE (2007). Oncolytic viruses in cancer therapy. *Cancer Lett* **254**: 178–216.
2. Liu, TC, Galanis, E and Kirn, D (2007). Clinical trial results with oncolytic virotherapy: a century of promise, a decade of progress. *Nat Clin Pract Oncol* **4**: 101–117.
3. Kirn, DH and Thorne, SH (2009). Targeted and armed oncolytic poxviruses: a novel multi-mechanistic therapeutic class for cancer. *Nat Rev Cancer* **9**: 64–71.
4. Puhlmann, M, Brown, CK, Gnant, M, Huang, J, Libutti, SK, Alexander, HR *et al.* (2000). Vaccinia as a vector for tumor-directed gene therapy: biodistribution of a thymidine kinase-deleted mutant. *Cancer Gene Ther* **7**: 66–73.
5. McCart, JA, Ward, JM, Lee, J, Hu, Y, Alexander, HR, Libutti, SK *et al.* (2001). Systemic cancer therapy with a tumor-selective vaccinia virus mutant lacking thymidine kinase and vaccinia growth factor genes. *Cancer Res* **61**: 8751–8757.
6. Liu, TC, Hwang, TH, Bell, JC and Kirn, DH (2008). Translation of targeted oncolytic virotherapeutics from the lab into the clinic, and back again: a high-value iterative loop. *Mol Ther* **16**: 1006–1008.
7. Park, BH, Hwang, T, Liu, TC, Sze, DY, Kim, JS, Kwon, HC *et al.* (2008). Use of a targeted oncolytic poxvirus, JX-594, in patients with refractory primary or metastatic liver cancer: a phase I trial. *Lancet Oncol* **9**: 533–542.
8. Stanford, MM and McFadden, G (2007). Myxoma virus and oncolytic virotherapy: a new biologic weapon in the war against cancer. *Expert Opin Biol Ther* **7**: 1415–1425.
9. Hu, Y, Lee, J, McCart, JA, Xu, H, Moss, B, Alexander, HR *et al.* (2001). Yaba-like disease virus: an alternative replicating poxvirus vector for cancer gene therapy. *J Virol* **75**: 10300–10308.
10. Sypula, J, Wang, F, Ma, Y, Bell, J and McFadden, G (2004). Myxoma virus tropism in human cells. *Gene Ther Mol Biol* **8**: 102–115.
11. Stanford, MM, Shaban, M, Barrett, JW, Werden, SJ, Gilbert, PA, Bondy-Denomy, J *et al.* (2008). Myxoma virus oncolysis of primary and metastatic B16F10 mouse tumors in vivo. *Mol Ther* **16**: 52–59.
12. Lun, XQ, Zhou, H, Alain, T, Sun, B, Wang, L, Barrett, JW *et al.* (2007). Targeting human medulloblastoma: oncolytic virotherapy with myxoma virus is enhanced by rapamycin. *Cancer Res* **67**: 8818–8827.
13. Wang, G, Barrett, JW, Stanford, M, Werden, SJ, Johnston, JB, Gao, X *et al.* (2006). Infection of human cancer cells with myxoma virus requires Akt activation via interaction with a viral ankyrin-repeat host range factor. *Proc Natl Acad Sci USA* **103**: 4640–4645.
14. Wang, F, Gao, X, Barrett, JW, Shao, Q, Bartee, E, Mohamed, MR *et al.* (2008). RIG-I mediates the co-induction of tumor necrosis factor and type I interferon elicited by myxoma virus in primary human macrophages. *PLoS Pathog* **4**: e1000099.
15. Thomas, EK, Palmer, EL, Obijeski, JF and Nakano, JH (1975). Further characterization of Raccoonpox virus. *Arch Virol* **49**: 217–227.
16. Yager, JA, Hutchison, L and Barrett, JW (2006). Raccoonpox in a Canadian cat. *Vet Dermatol* **17**: 443–448.
17. Osorio, JE, Powell, TD, Frank, RS, Moss, K, Haanes, EJ, Smith, SR *et al.* (2003). Recombinant raccoon pox vaccine protects mice against lethal plague. *Vaccine* **21**: 1232–1238.
18. Rocke, TE, Iams, KP, Dawe, S, Smith, SR, Williamson, JL, Heisey, DM *et al.* (2009). Further development of raccoon poxvirus-vectored vaccines against plague (Yersinia pestis). *Vaccine* **28**: 338–344.
19. Mencher, JS, Smith, SR, Powell, TD, Stinchcomb, DT, Osorio, JE and Rocke, TE (2004). Protection of black-tailed prairie dogs (Cynomys ludovicianus) against plague after voluntary consumption of baits containing recombinant raccoon poxvirus vaccine. *Infect Immun* **72**: 5502–5505.
20. Osorio, JE, Frank, RS, Moss, K, Taraska, T, Powell, T and Stinchcomb, DT (2003). Raccoon poxvirus as a mucosal vaccine vector for domestic cats. *J Drug Target* **11**: 463–470.
21. Hu, L, Ngichabe, C, Trimarchi, CV, Esposito, JJ and Scott, FW (1997). Raccoon poxvirus live recombinant feline panleukopenia virus VP2 and rabies virus glycoprotein bivalent vaccine. *Vaccine* **15**: 1466–1472.
22. Lodmell, DL, Esposito, JJ and Ewalt, LC (1993). Rabies virus antinucleoprotein antibody protects against rabies virus challenge *in vivo* and inhibits rabies virus replication in vitro. *J Virol* **67**: 6080–6086.
23. DeMartini, JC, Bickle, HM, Brodie, SJ, He, BX and Esposito, JJ (1993). Raccoon poxvirus rabies virus glycoprotein recombinant vaccine in sheep. *Arch Virol* **133**: 211–222.
24. Hable, CP, Hamir, AN, Snyder, DE, Joyner, R, French, J, Nettles, V *et al.* (1992). Prerequisites for oral immunization of free-ranging raccoons (Procyon lotor) with a recombinant rabies virus vaccine: study site ecology and bait system development. *J Wildl Dis* **28**: 64–79.
25. Fekadu, M, Shaddock, JH, Sumner, JW, Sanderlin, DW, Knight, JC, Esposito, JJ *et al.* (1991). Oral vaccination of skunks with raccoon poxvirus recombinants expressing the rabies glycoprotein or the nucleoprotein. *J Wildl Dis* **27**: 681–684.
26. Lodmell, DL, Sumner, JW, Esposito, JJ, Bellini, WJ and Ewalt, LC (1991). Raccoon poxvirus recombinants expressing the rabies virus nucleoprotein protect mice against lethal rabies virus infection. *J Virol* **65**: 3400–3405.
27. Esposito, JJ, Knight, JC, Shaddock, JH, Novembre, FJ and Baer, GM (1988). Successful oral rabies vaccination of raccoons with raccoon poxvirus recombinants expressing rabies virus glycoprotein. *Virology* **165**: 313–316.
28. Mourad, PD, Farrell, L, Stamps, LD, Chicoine, MR and Silbergeld, DL (2005). Why are systemic glioblastoma metastases rare? Systemic and cerebral growth of mouse glioblastoma. *Surg Neurol* **63**: 511–9; discussion 519.
29. Lun, XQ, Jang, JH, Tang, N, Deng, H, Head, R, Bell, JC *et al.* (2009). Efficacy of systemically administered oncolytic vaccinia virotherapy for malignant gliomas is enhanced by combination therapy with rapamycin or cyclophosphamide. *Clin Cancer Res* **15**: 2777–2788.
30. Lun, X, Yang, W, Alain, T, Shi, ZQ, Muzik, H, Barrett, JW *et al.* (2005). Myxoma virus is a novel oncolytic virus with significant antitumor activity against experimental human gliomas. *Cancer Res* **65**: 9982–9990.
31. Fenner, F (2000). Adventures with poxviruses of vertebrates. *FEMS Microbiol Rev* **24**: 123–133.
32. Rocke, TE, Smith, SR, Stinchcomb, DT and Osorio, JE (2008). Immunization of black-tailed prairie dog against plague through consumption of vaccine-laden baits. *J Wildl Dis* **44**: 930–937.
33. Wasmoen, TL, Kadakia, NP, Unfer, RC, Fickbohm, BL, Cook, CP, Chu, HJ *et al.* (1995). Protection of cats from infectious peritonitis by vaccination with a recombinant raccoon poxvirus expressing the nucleocapsid gene of feline infectious peritonitis virus. *Adv Exp Med Biol* **380**: 221–228.
34. Spatz, SJ, Rota, PA and Maes, RK (1994). Identification of the feline herpesvirus type 1 (FHV-1) genes encoding glycoproteins G, D, I and E: expression of FHV-1 glycoprotein D in vaccinia and raccoon poxviruses. *J Gen Virol* **75 (Pt 6)**: 1235–1244.
35. Rocke, TE, Dein, FJ, Fuchsberger, M, Fox, BC, Stinchcomb, DT and Osorio, JE (2004). Limited infection upon human exposure to a recombinant raccoon pox vaccine vector. *Vaccine* **22**: 2757–2760.
36. Kanerva, A, Zinn, KR, Peng, KW, Ranki, T, Kangasniemi, L, Chaudhuri, TR *et al.* (2005). Noninvasive dual modality *in vivo* monitoring of the persistence and potency of a tumor targeted conditionally replicating adenovirus. *Gene Ther* **12**: 87–94.
37. Toda, M, Iizuka, Y, Kawase, T, Uyemura, K and Kawakami, Y (2002). Immuno-viral therapy of brain tumors by combination of viral therapy with cancer vaccination using a replication-conditional HSV. *Cancer Gene Ther* **9**: 356–364.
38. Taylor, JM and Barry, M (2006). Near death experiences: poxvirus regulation of apoptotic death. *Virology* **344**: 139–150.
39. Krishnamurthy, S, Takimoto, T, Scroggs, RA and Portner, A (2006). Differentially regulated interferon response determines the outcome of Newcastle disease virus infection in normal and tumor cell lines. *J Virol* **80**: 5145–5155.
40. Barber, GN (2005). VSV-tumor selective replication and protein translation. *Oncogene* **24**: 7710–7719.
41. Kim, JH, Lee, YS, Kim, H, Huang, JH, Yoon, AR and Yun, CO (2006). Relaxin expression from tumor-targeting adenoviruses and its intratumoral spread, apoptosis induction, and efficacy. *J Natl Cancer Inst* **98**: 1482–1493.
42. Bronte, V, Tsung, K, Rao, JB, Chen, PW, Wang, M, Rosenberg, SA *et al.* (1995). IL-2 enhances the function of recombinant poxvirus-based vaccines in the treatment of established pulmonary metastases. *J Immunol* **154**: 5282–5292.
43. Kim, JH, Oh, JY, Park, BH, Lee, DE, Kim, JS, Park, HE *et al.* (2006). Systemic armed oncolytic and immunologic therapy for cancer with JX-594, a targeted poxvirus expressing GM-CSF. *Mol Ther* **14**: 361–370.
44. Johnston, JB, Barrett, JW, Chang, W, Chung, CS, Zeng, W, Masters, J *et al.* (2003). Role of the serine-threonine kinase PAK-1 in myxoma virus replication. *J Virol* **77**: 5877–5888.

APPENDIX VII: JULIA RINTOUL, CURRICULUM VITAE

JULIA RINTOUL

SUMMARY OF QUALIFICATIONS

PhD candidate in the lab of Dr. John C. Bell at the Ottawa Hospital Research Institute, Centre for Innovative Cancer Research, with an expected completion date of April 2012. An enthusiastic and self-driven professional with a record of achieving goals and exceeding expectations.

- Diverse experience in quality assurance, project management, and academic research
- Expertise in the areas of biochemistry, virology, immunology and molecular biology.
- Practiced leader, and communicator
- Proven project management skills; focused, results-oriented and highly motivated
- Productive multi-tasking skills with a strong aptitude for managing multiple projects
- Extensive experience in presenting data in large forums
- Ability to clearly articulate complex scientific subjects across a broad audience

EXPERIENCE

Research Experience

- Expertise in poxvirus virology, virus manufacturing, recombinant DNA technology, oncolytic virotherapy, vaccinology, and flow cytometry
- Created a new poxvirus cloning system for clinical applications
- Discovered novel methods for the production of parapoxviruses
- Expertise in designing, implementing and analyzing multi-color flow cytometry experiments
- Experienced in recombinant DNA technology: designed, created and tested 7 recombinant poxviruses
- Skilled at *in vitro* tissue culture and virus manufacturing
- Qualified handler of mice, with expertise in animal surgeries, tissue processing, intraperitoneal injections, cardiac punctures and saphenous bleeds
- Proficiency with most biochemistry techniques, including but not limited to PCR, DNA sequence analysis, western blot, ELISA, and gel electrophoresis

Project Management Experience

- *Jennerex Biotherapeutics, San Francisco, California* (2011-Contract): Consultant - Project Lead for a 12 million dollar breast cancer, Department of National Defense grant submission. This project management role involved coordinating the assembly of required documentation across a large group of collaborators, the outlining and writing of the pre-clinical experimental approach, and the creation of a detailed budget and budget justification.
- *Co-supervised two Master's students* (2010-Present). Invented and directed the Master's thesis projects of two students. The development of these projects has led to a co-authored provisional US patent.
- *Co-supervised two summer students* (2008-2010). Created and managed the students skill development, and progress. Data generated from summer students will be included in future scientific publications.

Industry Experience

- Murphy Goode Estate Winery (Fall 2005): Laboratory Technician, Sonoma County, California
- Jungbunzlauer Canada (Winter 2005): Laboratory Technician, Port Colborne, Ontario
- J.M. Smucker's, Home of Bick's (Summer 2004): Quality Assurance Technician, Dunnville, Ontario

Science Education and Outreach

- *Let's Talk Science Volunteer* (2007-present). Created and conducted interactive science demonstrations and school-related activities, such as science fair judging.
- *Mentor for the Sanofi-Aventis BioTalent Challenge* (2008). Created and managed a project for four high school students. Taught and supervised the students in general lab practices and skills.
- *Scientists Without Borders, Vice President of External Affairs* (2008-2009). Aimed to facilitate up-to-date research in developing nations that lack basic resources. Completed a shipment of laboratory equipment worth $150,000 dollars to Saint John University of Tanzania, Dodoma Tanzania.

ACADEMIC ACHIEVEMENTS

Education

- *Ph.D., Biochemistry – Specialization in Human and Molecular Genetics.* Thesis in the lab of Dr. John C. Bell: "ORFV: A Novel Oncolytic and Immune Stimulating Parapoxvirus Therapeutic" (University of Ottawa 2007-present)

- *B.Sc., Biotechnology – Co-op.* Honors Thesis in the lab of Dr. Jeffrey K. Atkinson: "Ligand Promiscuity of Supernatant Protein Factor: Binding and Transfer of Fluorescent Analogues" (Brock University 2002-2007)

Personal Development

- Foundations of Project Management, February, 2012
- MITACS certificate: The Art of Powerful Conversation, featuring Stuart Knight, June, 2011
- MITACS certificate: Business Conduct Excellence and Dining Etiquette, March, 2011

Publications

- Tai, L-H., de Souza, C.T. **Rintoul, J.L.**, Ly L., Falls, T., Belanger, S., Makrigiannis, A., Bell, J.C., and Auer, R.C. (2012) Preventing postoperative metastases by enhancing natural killer cell function with novel oncolytic virus therapy. (Manuscript in preparation)
- Lemay, C.G., **Rintoul, J.L.**, Kus, A., Falls, T., Garcia, V., Parato, K.A., and Bell, J.C. (2012) An Infected Cell Vaccine (ICV) has potent prophylactic and therapeutic anti-tumour activity. (Accepted, Molecular Therapy)
- **Rintoul, J.L.**, Lemay, C.G., Tai, L-H., Stanford, M.M., Falls, T.J., De Souza, C.T., Bridle, B.W., Daneshmand, M., Ohashi, P.S., Wan, Y., Lichty, B.D., Mercer, A.A., Auer, R.C., Atkins, H., and Bell, J.C. (2012) ORFV: A novel oncolytic and immune stimulating parapoxvirus therapeutic. *Mol Ther*, Jan 24. doi: 10.1038.mt.2011.201.[Epub ahead of print]
- **Rintoul, J.L**., Wang, J. Gammon, D.B., van Buuren, N.J., Garson, K., Barry, M., Evans, D.H., and Bell, J., (2011) A selectable and excisable marker system for the rapid creation of recombinant poxviruses. *PLoS ONE*, 6(9):e24643
- Heo, J., Breitbach, C.J., Moon, A., Kim, C.W., Patt, R., Kim, M.K., Lee, Y.K., Oh, S.Y., Woo, H.Y., Parato, K., **Rintoul, J.**, Falls, T., Hickman, T., Rhee, B.G., Bell, J.C., Kirn, D.H., and Hwang, T.H. (2011) Sequential Therapy with JX-594, a Targeted Oncolytic Poxvirus, Followed by Sorafenib in Hepatocellular Carcinoma: Preclinical and Clinical Demonstration of Combination Efficacy. *Mol Ther*, 19(6):1170-9.
- Breitbach, C.J., De Silva, N.S., Falls, T.J., Aladl, U., Evgin, L., Paterson, J., Sun, Y.Y., Roy, D.G., **Rintoul, J.L**., Daneshmand, M., Parato, K., Stanford, M.M., Lichty, B.D., Fenster, A., Kirn, D., Atkins, H., Bell, J.C. (2011) Targeting Tumor Vasculature With an Oncolytic Virus. *Mol Ther*, 19(5):886-94.
- Evgin, L., Vähä-Koskela, M., **Rintoul, J.L**, Falls, T., LeBoeuf, F., Barrett, J.W., Bell, J.C., and Stanford, M.M. (2010). Potent Oncolytic Activity of Raccoonpox Virus in the Absence of Natural Pathogenicity, *Mol Ther*, 18(5):896-902.

- Nam, T.G., Rector, C.L., Kim, H.Y., Sonnen, A.F., Meyer, R., Nau, W.M., Atkinson, J., **Rintoul, J.**, Pratt. D.A., Porter, N.A. (2007). Tetrahydro-1,8-napthyridinol analogues of alpha-tocopherol as antioxidants in lipid membranes and low-density lipoproteins, 2007 *J Am Chem Soc*, 129(33):10211-10219.

Patents

- BLG File: PAT 6738-0 filed March 15 2011, "Oncolytic Parapoxvirus". Inventors: John Bell, Julia Rintoul, Monica Komar, and Aimee Laporte

Presentations

- Oral presentation: Immunopotentiators for Modern Vaccines (Porto, Portugal – April 2011) "Immune stimulation by parapoxvirus Orf leads to potent NK cell activation, and subsequent anti-tumour activity"
- Oral presentation: 6th International Conference on Oncolytic Viruses (Las Vegas, Nevada – March 2011) "Harnessing Parapoxvirus-Induced Immune Activation As A New Approach For Oncolytic Virus Therapy
- Oral presentation: University of Ottawa Department Seminar (Ottawa, Ontario – February 2011) "Immune stimulation by parapoxvirus Orf leads to potent NK cell activation, and subsequent anti-tumour activity" – **100$ for 1st Prize**
- Oral presentation: Ottawa Hospital Research Institute Research Day (Ottawa, Ontario – November 2010) "Orf virus, the development of a new cancer therapeutic platform"
- Poster presentation: XVII International Poxvirus, Asfivirus, and Iridovirus Conference (Sedona, Arizona – June 2010) "Orf virus as a novel anti-cancer agent"
- Poster presentation: Ontario Institute for Cancer Research Annual Symposium (Alliston, Ontario – March 2010) "Orf virus as a novel anti-cancer agent" – **500$ for 1st prize**
- Poster presentation: 5th Canadian Symposium on Gene Therapy and Vaccines – ATGQ (Grenville-sur-la-rouge, Quebec – May 2010) "Orf virus as a novel anti-cancer agent"
- Poster presentation: Canadian Cancer Immune Therapy Symposium (Niagara Falls, Ontario – April 2010) "Orf virus as a novel anti-cancer agent"
- Poster presentation: University of Ottawa Department Seminar (Ottawa, Ontario – February 2010) "Orf virus as a novel anti-cancer agent" – **100$ for 1st Prize**
- Poster presentation: Ottawa Hospital Research Institute Research Day (Ottawa, Ontario – November 2009) "A novel oncolytiv virus stimulating anti-tumour immunity"
- Poster presentation: Harnessing Immunity to Prevent and Treat Disease (Cold Spring Harbor, New York – November 2009) "A novel oncolytic virus stimulating anti-tumour immunity"

- Poster presentation: Ottawa Hospital Research Institute Research Day (Ottawa, Ontario – November 2008) "The characterization and development of a new oncolytic virus candidate: Orf virus" – **100$ for 2nd Prize**
- Poster presentation: XVII International Poxvirus and Iridovirus Conference (Grainau, Germany – June 2008) "A controllable selection system for poxvirus recombination"
- Poster presentation: 4th Canadian Gene Therapy and Vaccines Symposium (Montreal, Quebec – May 2008) "Characterizing a new oncolytic virus candidate: Orf virus"

Scholarships and Awards

- Frederick Banting and Charles Best Canada Graduate Scholarship – Doctoral Award (35,000$ / annum): Canadian Institute of Health Research – January 2010 to April 2012
- *1000$ Travel Award:* Nominated and selected as the one time recipient of a travel award from the Canadian Cancer Society to attend the Canada Cancer Research Conference (Toronto, Ontario – November 2011)
- *500$ Travel Award*: The top five submitted abstracts were funded with a travel award to attend the 6th International Conference on Oncolytic Viruses (Las Vegas, Nevada – March 2011)
- Frederick Banting and Charles Best Canada Graduate Scholarship – Master's Award (17,500$): Canadian Institute of Health Research – January 2009 to December 2009
- First Runner-up: Canadian Federation of University Women Memorial Fellowship: Canadian Federation of University Women – 2008/2009 competition
- University of Ottawa Excellence Scholarship (6,000$ / annum): University of Ottawa – 2008 to 2012
- Ontario Graduate Scholarship (10,000$): Ontario Ministry of Training, Colleges, and Universities – May 2008 to December 2008
- University of Ottawa Admission Scholarship (6,000$ / annum): University of Ottawa – September 2007 to April 2008
- NSERC Undergraduate Student Research Award, USRA (4,500$): NSERC – Summer of 2007
- Brock University Entrance Scholarship (8,000$ / annum): Brock University – 2002 to 2007